Copyright

by

Christian Preihs

2012

The Dissertation Committee for Christian Preihs Certifies that this is the approved version of the following:

Expanded Porphyrins as Experimental Anticancer Agents and MRI Contrast Agents

Committee:

Jonathan L. Sessler, Supervisor

Michael J. Krische

Jennifer S. Brodbelt

Guangbin Dong

Katherine A. Willets

Christine E. Schmidt

Expanded Porphyrins as Experimental Anticancer Agents and MRI Contrast Agents

by

Christian Preihs, B.Sc.; M.Sc.; M.A.

Dissertation

Presented to the Faculty of the Graduate School of

The University of Texas at Austin

in Partial Fulfillment

of the Requirements

for the Degree of

Doctor of Philosophy

The University of Texas at Austin

December 2012

But man to cover his ignorance in the least things, who can not give a true reason for the grass under his feet, why it should be green rather than red, or of any other color; that could never yet discover the way and reason of nature's working, in those which are far less noble creatures than himself;

Sir Walter Raleigh (1614), Preface to the History of the World

Acknowledgements

First and foremost I would like to thank my advisor, Dr. Jonathan Sessler for his brilliance, generosity, and trust in my abilities.

I would also like to thank all members of the Sessler group, past and present, for their guidance and friendship, especially: Christina Davis, Dr. Christopher Bejger, Dr. Elizabeth Karnas, Gabriela Vargas-Zúñiga, Murat Deliomeroglu and last but certainly not least, Dr. Jung Su Park.

Many thanks to all of our collaborators for their creativity, helpful advice and hard work: Prof. Jinwoo Cheon, Dr. Dongwon Yoo, Heeyeong Jeong, Dr. Jin-sil Choi, Dr. Natalie Barkey, Dr. Masatoshi Ishida and Dr. Jonathan Arambula.

Finally, I want to thank my parents Christa and Joachim Preihs for their unconditional support, guidance and love.

Expanded Porphyrins as Experimental Anticancer Agents and MRI Contrast Agents

Publication No._____

Christian Preihs, Ph.D.

The University of Texas at Austin, 2012

Supervisor: Jonathan L. Sessler

Texaphyrins represent the vanguard of experimental anticancer drugs and also symbolize a well-known example of expanded porphyrins, a class of oligopyrrolic macrocycles with tumor localization properties and powerful metal chelating properties.

Chapter 1 of this thesis describes the unique structural characteristics of this complex synthetic molecule along with the biological relevance and scientific justifications for studying its anticancer properties and powerful MRI contrast ability. This Chapter also serves to underscore the need to improve further and refine the efficacy of texaphyrins as compounds that may be applied in the struggle against cancer.

Chapter 2 details the synthesis of bismuth(III) and lead(II)-texaphyrin complexes that could potentially find use as α-core emitters for radiotherapy. In principle, porphyrins would ostensibly appear to be ideal ligands for use in radiotherapy due to their

tumor-localizing ability. However, Bi(III)- and Pb(II)-porphyrin complexes are extremely rare, most reflecting the vastly challenging synthesis of these compounds as well as their general lack of stability. These limitations provided an incentive for us to use texaphyrins as more versatile ligands to prepare and fully characterize stable bismuth(III) and lead(II) complexes. To be of interest in future medical applications, we needed to prepare these complexes quickly as compared to the relevant time scales set by the half-lives of the isotopes targeted for use in radiotherapy. This goal was successfully realized.

As mentioned above, texaphyrin is able to form stable complexes with a large variety of metals particularly in the lanthanide series. Gadolinium(III) complexes of texaphyrin have been studied in considerable detail. Chapter 3 details the synthesis and conjugation methods used to develop a texaphyrin conjugated dual mode nanoparticle contrast agent. This project has been done in collaboration with the group of Prof. Jinwoo Cheon (Yonsei University, Seoul, Korea), who demonstrated fascinating results with the texaphyrin functionalized nanoparticles. Not only do these conjugates act as improved magnetic resonance contrast agents displaying enhanced signals in both the T_1 and T_2 MRI modes, but also serve to sensitize apoptotic hyperthermia. It is this latter, double effector feature, that has been most extensively studied to date.

Chapter 4 of this dissertation describes work done in close collaboration with Dr. Natalie Barkey and Dr. David Morse (Moffitt Cancer Center, Tampa, FL) where a gadolinium texaphyrin complex was developed that is able to target the melanocortin 1 receptor (MC1R) when encapsulated in a micellar system. As detailed in this Chapter, these collaborateurs demonstrated that these gadolinium-texaphyrin micelles are able to target MC1R-expressing xenograft tumors *in vivo*. This work relied on the supply of a new set of texaphyrin derivatives that were prepared and characterized as part of this dissertation work

Chapter 5 of this disseration introduces sapphyrins, another class of expanded porphyrins with tumor selectivity. This project is based on the hypothesis that a direct linkage of sapphyrin with an anticancer agent based on ruthenium(II) could improve the efficacy of both compounds. Since sapphyrins exhibit limited ability to form stable complexes with transition metals, an appended 1,10-phenanthroline unit was chosen as an efficient N-donor aromatic ligand for ruthenium(II). Therefore, extensive synthetic efforts were made to form this sapphyrin-1,10-phenanthroline construct in an effort to stabilize a mixed sapphyrin-metallo-phenanthroline complex.

Finally, Chapter 6 of this dissertation demonstrates the author's efforts to synthesize a planar rosarin species. Non-aromatic and non-planar rosarins have been known for over two decades. Through structural modification of the compound, namely through linking of both β positions on the bipyrrole unit, a new planar rosarin species has been synthesized exhibiting Hückel antiaromaticity.

Table of Contents

List of Figures

List of Schemes

List of Tables

1. Cancer and Chemotherapeutics

1.1 Cancer – Definition and Biology

The broad term cancer describes a vast group of diseases involving the uncontrolled growth of abnormal cells in the body. Medically known as a malignant neoplasm, cancerous cells may be able to invade neighboring tissues and organs as well as more distant regions of the body through the bloodstream or the lymphatic system (ability to metastasize). In contrast, benign tumors do not grow uncontrollably and are still believed to be incapable of invading neighboring tissues or other body organs. However, this assumption is being reconsidered due to new research results.[1]

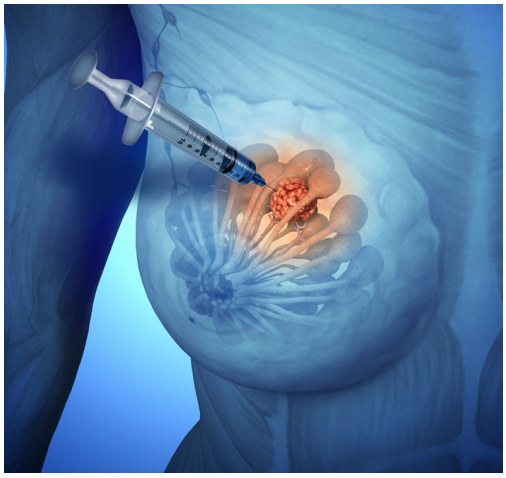

Figure 1.1: Picture showing sampling of breast cancer cells taken for examination (biopsy).[3]

Interestingly, cancer can develop in any body organ and more than 200 different cancer types are known to afflict humans[2] with a risk of developing cancer generally increasing with age.

While only 5-10% of cancers are entirely hereditary, the most common factors that are believed to increase the risk of cancer include radiation, certain infections, tobacco use, environmental pollutants, obesity and lack of physical activity.

Since cancer is fundamentally a disease of failure to regulate tissue growth, a healthy cell has to transform into a cancer cell through alteration of cell growth and differentiating regulating genes.[4] Malignant transformation can occur through the

inappropriate over-expression of normal oncogenes (genes that promote cell growth and reproduction), through formation of novel oncogenes or by the under-expression or disabling of tumor suppressor genes. However, a great number of gene manipulations are required for the transformation of normal cells into cancer cells.[5]

Genetic changes can occur by different mechanisms and at different levels. For instance, large-scale mutations involve the deletion or gain of a portion or an entire chromosome. Small-scale mutations, which may occur in the promoter region of a gene and affect its expression, include mutations, deletions and insertions. Various environmental factors, such as exposure to disruptive substances (carcinogens) or radiation, make mutations more likely to arise and propagate. The self-amplification of mutations may be supported by a more rapid and/or more frequent cell reproduction rate. This often results in a chain reaction caused by initial errors, which compound into more severe errors. Ultimately, this allows the cell to escape control and repair mechanisms that limit normal tissue growth. Once cancer has begun to develop, this ongoing process, also termed clonal evolution, drives progression towards more invasive and potentially lethal stages.

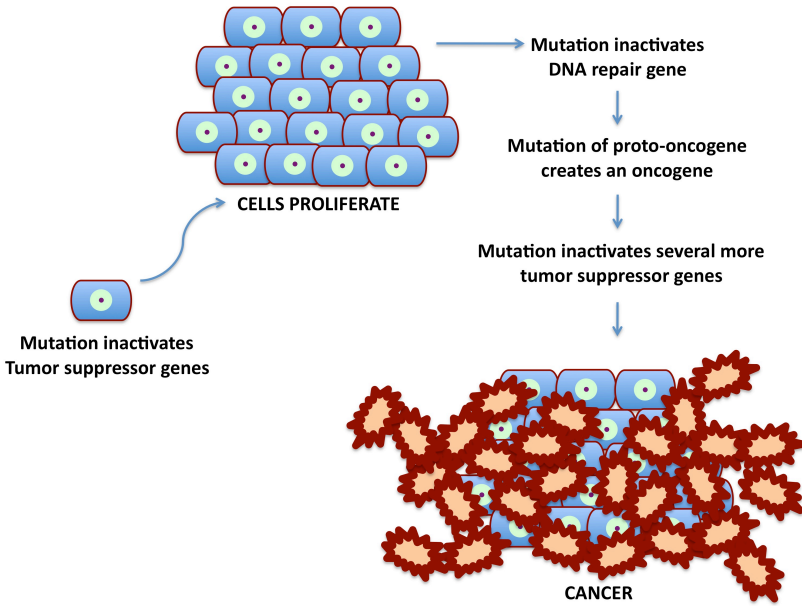

Figure 1.2: Development of cancer after a series of mutations.[6]

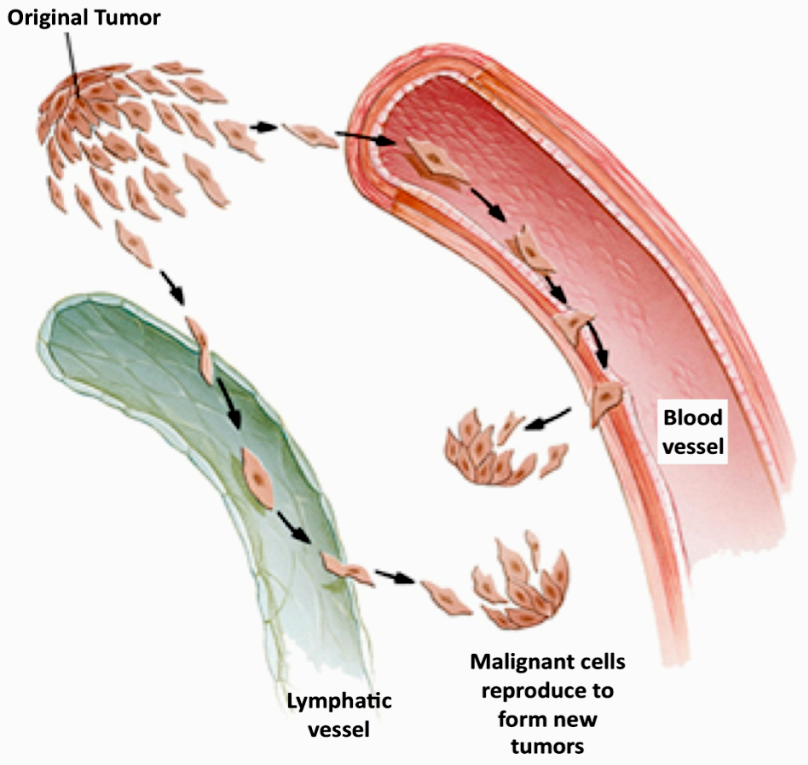

Figure 1.3: Representation of metastasizing malignant cells and their spread through lymphatic or blood vessels.[8]

Metastasis is the spread of a disease from one organ or organ part to another non-adjacent organ or organ part. Some cancer cells acquire the ability to penetrate the walls of lymphatic and/or blood vessels. Others are able to penetrate through the bloodstream through angiogenesis, i.e., a process involving the growth of new blood vessels that is often critical to ensure sufficient oxygen and blood supply to the tumorous tissue. A hypoxic tumor (i.e., tumorous tissue deprived of adequate oxygen supply) is able to stimulate new blood vessel development though the secretion of hormones.[9] Additionally, more recent research describes the hormonal stimulation of a lymphatic drainage system by certain tumor types. This, in turn, increases the severity of the disease due to the

increased likelihood of metastasis formation.[10] Most tumors and other neoplasms are able to metastasize, although to varying degrees.[11] For instance, basal cell carcinoma rarely metastasize.

Important to note is the fact that about 10% of patients presenting to oncology units will have metastases without an original tumor found. In these cases, the primary tumor is referred to as unknown or occult with the patient suffering from cancer of unknown primary origin.[12] In some cases, a primary tumor may appear at later stages. However, it is believed that some primary tumors can regress entirely, leaving their metastases behind.

1.2 Radiotherapy as a Routine Treatment Option

Considerable progress in the medicinal treatment of cancer has been achieved during the last decade, especially in the area of chemotherapy. Even so, a sustained need for novel anticancer agents and improved therapeutic approaches remains, as underscored by the fact that after cardiovascular diseases, cancer is the second leading cause of death in the United States.[13]

The combination of chemotherapy and radiation has led to clinical breakthroughs in the control of several cancerous diseases. However, the challenge to develop better therapies remains. Of particular interest are systems that operate via novel mechanisms of action or which illustrate generalizable approaches to drug development.[14] Separate from this, a range of clinical efforts are being devoted to acquire optimum combinations of proven chemotherapies or, more recently, various noncytotoxic agents.

One treatment option routinely applied in combination with chemotherpeutic agents is radiation therapy (commonly referred to as radiotherapy). It is defined as the

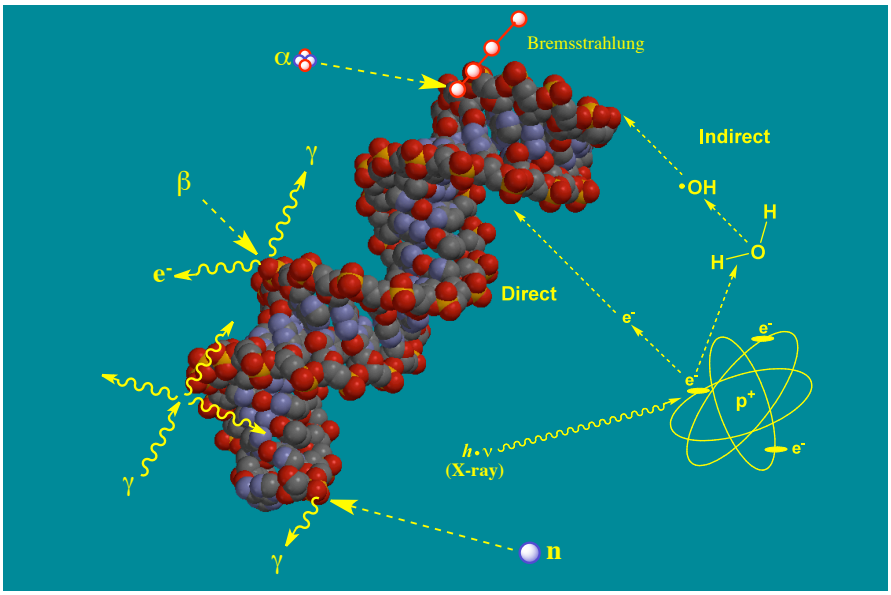

Figure 1.4: Interaction of different ionizing radiation with DNA.

medical use of ionizing radiation as part of cancer treatment. X-rays, γ–rays, and charged particles (e.g. protons or β–particles) as well as uncharged particles (neutrons, α–cores) are used in an effort to damage DNA sequences in cancer cells (Figure 1.4). The reason for the effectiveness of this treatment regimen can be found in the biological characteristics: Cancer cells are undifferentiated, stem cell-like and have a diminished ability to repair sub-lethal damage as compared to most healthy differentiated cells. The DNA damage is inherited through cell division, and as such, accumulated in the cancer cells. This causes them to die or reproduce slower.[15, 16]

Merely five months after the discovery of X-rays by the German physicist Wilhelm Conrad Röntgen in 1895, Émil Herman Grubbé utilized X-ray radiation to treat a breast cancer patient.[15] From that point onward, different radiation sources and treatment methods found their way into various cancer-related therapeutic protocols. However, it was only much later that it was understood how radiation propagated its

cytotoxicity. Today, the three main types of radiation therapy are classified as external beam radiation therapy (EBRT or more common XRT), brachytherapy (sealed source radiation therapy), and systematic radioisotope therapy (unsealed source radiotherapy). The position of the radiation source is a crucial aspect in this classification: external radiation is positioned outside the body, brachytherapy uses sealed radioactive sources that are placed in the area to be treated, and systemic radioisotopes are applied by infusion or oral ingestion. A special case of external beam radiation therapy is particle therapy. Here, particles such as protons or other heavier ionized nuclei are used to treat body areas with cancerous tissues. In this context it is important to note is that photons, used in X-ray or gamma ray therapy, can also be considered particles. However, they are not classified as particle therapy.

In 1923, Petry showed a correlation between radiosensitivity and the presence of oxygen based on a study of the effects of radiation on vegetable seeds.[17] He theorized that a lack of oxygen decreases the cytotoxic effect of ionizing radiation, and in 1955 Thomlinson and Gray established that radioresistant regions in tumor tissues are due to low oxygen tension.[18] This latter observation reflects the fact that solid tumors usually outgrow their blood supply, causing a low-oxygen state known as hypoxia. Shown by modern detection techniques, these hypoxic regions cause limitations in the efficacy of XRT. Oxygenated tissue proves to be two to three times more sensitive towards radiation. However, in the absence of oxygen, DNA is repaired more efficiently. Thus, it appears that hypoxic cells, as found in many solid tumors, are difficult to destroy completely using XRT alone.[19, 20] In this case radiosensitization could allow modulation of the radiation response and thus an improvement in local tumor control. Here, the idea is to administer radiosensitizers that would enhance the effects of radiation at cancerous sites, reduce cytotoxic effects for normal tissues, or both.

1.3 ESTABLISHED CHEMOTHERAPEUTICS AND RADIATION SENSITIZING DRUGS

Traditional chemotherapeutic drugs that are widely used as radiation sensitizers include 5-fluorouracil (5-FU) **1** and gemcitabine **2** (Figure 1.5.).[14] The pyrimidine moiety in 5-FU is an analog of the RNA building block uracil and functions as an antimetabolite. As a chemotherapeutic agent, it has both DNA- and RNA-directed effects.[21] Its presumed radiosensitizing ability is due to the prevention of DNA synthesis through thymidylate synthase inhibition.[22]

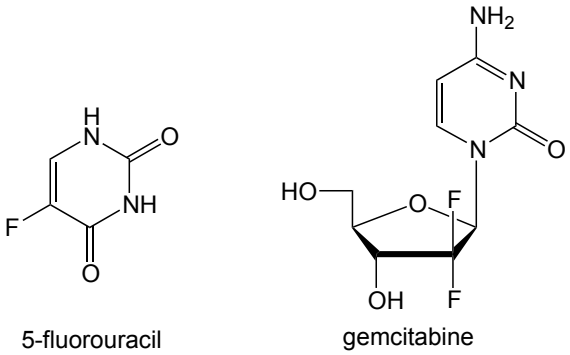

5-fluorouracil **1** gemcitabine **2**

Figure 1.5: Structures of 5-fluorouracil and gemcitabine.

Gemcitabine is a nucleoside analog used as chemotherapeutic and ("off label") as a radiation sensitizer. It is marketed as Gemzar® by *Eli Lilly and Company*. Similarly to 5-FU and other pyrimidine analogs, the triphosphate derivative of gemcitabine (produced *in situ*) is able to replace one of the building blocks of nucleic acids, here cytidine, during DNA replication. Tumor growth is inhibited since only one additional nucleoside can be attached to this intentionally defective nucleoside. This leads to apoptosis or so-called programmed cell death. Apoptosis may also be induced through the inhibition of the enzyme ribonucleotide reductase. The diphosphate analog of gemcitabine binds to the active site and inactivates the enzyme irreversibly. Hence, the cell is unable to produce deoxyribonucleotides required for DNA replication and repair.[23]

Administration of gemcitabine is not without problems, with a wide array of serious side effects having been recorded, including flu-like symptoms, nausea, vomiting, allergic reactions and shortness of breath. However, gemcitabine is exceptionally potent.

In 2006 the FDA approved gemcitabine for use in combination with carboplatin in the treatment of advanced ovarian cancer. Another common regimen involves the administration of gemcitabine in combination with cisplatin.

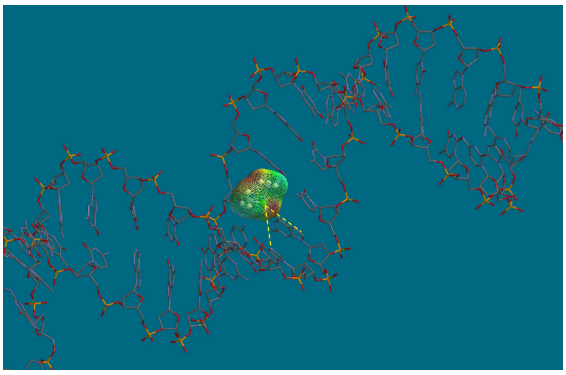

Figure 1.6: Schematic representation of an intrastrand crosslink of cisplatin with DNA.

Cisplatin and other platinated analogues are able to form DNA inter- and intrastrand (Figure 1.6) crosslinks.[24] When removed by repair processes, DNA strand breaks occur and cell reproduction mechanisms are inhibited. Furthermore, cisplatin is believed to cause mutations in DNA-protein kinase (PK) subunits.[24, 25] This particular type of mutation renders cells hypersensitive towards ionizing radiation; cisplatin is thus able to sensitize cells to radiation. A further proposal was put forward attributing cell sensitization to irradiation by inhibition of DNA-PK catalyzed phosphorylation.[25] Since the latter is believed to play a significant role in DNA-repair mechanisms, inhibition of PK would lead to an increased number of defects as a result of precluding in DNA repair actions.[25]

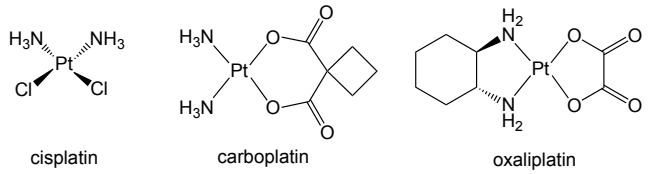

3 **4** **5**

Figure 1.7: Structures of cisplatin, carboplatin and oxaliplatin.

The cisplatin analogues oxaliplatin and carboplatin have also been explored as radiation sensitizers. Oxaliplatin, a recently introduced antineoplastic di-aminocyclohexane platinum derivative with activity against colorectal cancer, has been proposed to sensitize tumor cells more efficiently towards radiation than cisplatin based on preclinical studies.[14, 26]

The diaminocyclohexane unit functions as a carrier and potentiates the formation of the DNA adducts. It is also thought to aid in the inhibition of DNA synthesis. Oxalicarbon is typically administered in combination with 5-FU. Several studies investigating the treatment of metastatic rectal cancer served to demonstrate that this combinatorial regimen improves survival compared to 5-FU alone.[27] In addition to these trials, oxaliplatin has been combined with radiation in advanced but localized rectal cancer in order to improve local control.

Carboplatin, another DNA-modulating agent, was introduced in the late 1980s and has since gained popularity as a chemotherapeutic. Carboplatin demonstrates vastly reduced side effects compared to cisplatin, mostly notably a reduced nephrotoxicity.[28] Carboplatin is also more stable in the bloodstream, and is bound less well by proteins, a feature that may contribute to reduced side effects.

Although 5-FU and most cisplatin analogs represent traditional drugs, they continue to be explored in newer regimens, including those involving radiotherapy. Thus, their importance cannot be overstated.

In addition to the more promising agents discussed immediately above, a vast number of traditional drugs have been explored as potential radiation sensitizers. Although discussion of these is beyond the scope of this dissertation, particularly noteworthy are irinotecan, temozolamide, capecitabine, tirapazamine and the taxanes.[14] Together with 5-FU and cisplatin analogs, these systems when used as radiation sensitizers, have shown promise in terms of therapeutic outcomes. Nevertheless, many clinically relevant questions remain. In fact, just as for the more traditional drugs, cisplatin and 5-FU, controversies still exist considering the optimal dose and treatment schedule that should be used in combination with radiation therapy. Side effects and compatibility issues are also a source of concern.

Given this current state-of-the-art and the rising demand for novel, more effective anticancer-drugs, there is not surprisingly an ongoing search for compounds displaying promise in terms of anticancer treatment. One such class is the porphyrins and their analogs, as discussed below.

1.4 Traditional Porphyrinic Anticancer Agents

Chemotherapeutic agents that are able to localize specifically in cancerous cells have long been desired. In theory, drugs displaying such selective localization will exhibit reduced systemic toxicity and increased efficacy due to a decreased damage to non-target tissues. Therapeutic porphyrinoids, i.e. synthetic pyrrolic heterocycles that contain four central nitrogen atoms, have long been studied as compounds that demonstrate inherent accumulation in tumors.

Porphyrins and related macrocycles have various biological applications and are recognized for performing a great number of biological key functions. When found in naturally occurring systems, these essential redox-active molecules generally coordinate a core metal. Examples of such systems are chlorophyll (core metal: Mg), vitamin B-12 (Co) and heme (Fe). Taken in concert, these prosthetic groups can act as oxidizing agents, electron transporters, catalysts for molecular rearrangements, and oxygen transporters, among other functions.[29-34]

The idea of using porphyrinoids as radia- tion sensitizers derives support from their use in photodynamic therapy (PDT). In the area of PDT, porphyrins have been used as a promising alternative therapy for the treatment of early and localized tumors.[35, 36] It was shown as early as 1924, that porphyrins and porphyrin analogs have the ability to accumulate selectively in tumor tissues, and persist there for long periods of time.[37]

Cohen and Schwartz were the first to assess the radiosensitizing properties of porphyrins. They tested a series of haematoporphyrin analogs and found that the effect varied from radio-sensitization at low porphyrin concentrations to radioprotection at high porphyrin concentrations.[38] Improved local tumor control was achieved in the case of squamous cell carcinoma, rhabdomyosarcoma, fibrosarcoma and carcinoid tumors.[39] The haematoporphyrin derivatives (HPD) used in these studies and more extensively in PDT came to be known as Photofrin®. Photofrin® is actually a purified mixture of porphyrin oligomers (active agent = 2-8 units) and is an agent that has been successfully used over the last two decades for the PDT-treatment of patients with melanoma, early and advanced stage cancer of the lung, digestive tract, and the genitourinary tract. It is solubilized as the anionic polycarboxylate and was the first clinically approved PDT agent. However, Photofrin® engenders a uniformly high level of induced cutaneous phototoxicity. Thus, this first generation system is far from ideal as both, a PDT and as a radiation sensitizer. A recognition of this deficiency spanned efforts that led to a more purified form, termed Photofrin II®. Additionally, it inspired the synthesis and study of other agents whose synthesis and characteristics have been extensively reviewed in the literature.[40-44]

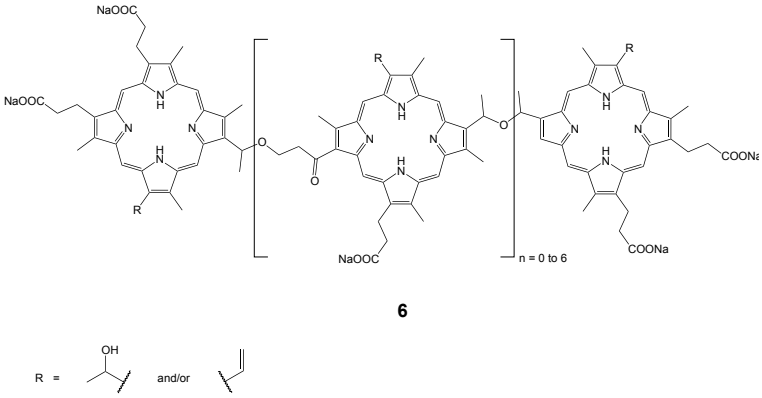

Figure 1.8: Porfimer, the canonical porphyrinic species present in Photofrin®.

The efficacy of radiotherapy prior to surgery for the treatment of maxillofacial tumors is reported to be 40% higher with Photofrin® than without.[45] A radiosensitizing effect of HPD in the case of sarcoma ascites tumors transplanted into mice has been demonstrated by Chen.[46] An interesting note is that Bellnier and Dougherty[47], as well as Moan and Pettersen[48], did not observe significant radiosensitization induced by porphyrins *in vitro*. Such seemingly difficult to rationalize results might reflect the fact that tumors and malignant cells used for *in vitro* investigations are biologically markedly diverse. However, other explanations to this conundrum can be envisioned.

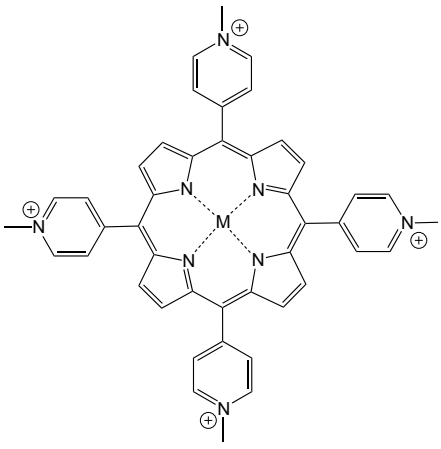

7 M = Co(III)

8 M = Fe(III)

Figure 1.9: Structures of Co(III) and Fe(III) tetrakis(4-*N*-methylpyridyl)porphyrin **7** and **8**.

O`Hara *et al*. investigated metal complexes of tetrakis(4-*N*-methyl-pyridyl)porphyrins. The cobalt(III) complex appears to be the most effective radiation sensitizer; however, it is tumor line dependent.[49, 50] Furthermore, functionalization with nitro groups and/or extra positive charges only resulted in slight increases in sensitization.[50]

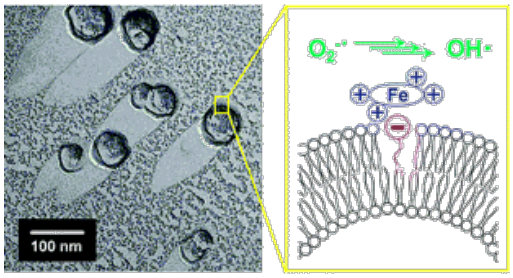

Figure 1.10: TEM picture of an Fe(III)-porphyrin-loaded liposome.[53]

Cationic porphyrins continue to be the focus of attention because of the promise they entail for the use in photodynamic and anticancer therapy.[51, 52] For instance, it has been shown that the strong

electrostatic interactions of a Fe(III)-porphyrin-loaded liposome (see Figures 1.9 and 1.10) could render such systems to stay intact *in vivo*. This could be a potential target for the design and development of an efficient drug delivery system.[53]

It has been hypothesized for many years that the relationship between anemia, hypoxia, and poor outcome, was not merely correlative, but causative, and that correcting the anemia would improve hypoxia and radiation efficacy.[54, 55] Two studies looked at the impact of hypoxia and treatment outcome and demonstrated that patients with hypoxic tumors had a poor prognosis.[54, 55] Based in part on this data, a randomized trial was initiated with the goal of testing the hypothesis that maintaining normal hemoglobin with transfusions would improve the outcome of radiation therapy. Although originally reported as a positive trial, subsequent analysis did not show a difference in disease-free survival.[56]

1.5 Expanded Porphyrins with Anticancer Properties

1.5.1 Sapphyrins

Research in the Sessler group at The University of Texas at Austin has largely focused on two tumor selective compounds belonging to the class of so-called expanded porphyrins, namely texaphyrin and sapphyrin. The latter is an expanded porphyrin that contains an arrangement of five pyrrole subunits, but only four *meso* carbons. Sapphyrin was discovered serendipitously by R. B. Woodward, *et al*. in the 1960's[57] during the course of investigations directed toward the synthesis of vitamin B_{12}. It was the first expanded porphyrin to have been identified and characterized. A decade later, A. W. Johnson successfully prepared sapphyrin, as did the Woodward group in work that was

only reported after Woodward's death. Sessler and coworkers then reported an optimized synthesis of sapphyrins in reasonable yields. This allowed the therapeutic potential of these macrocycles to be explored. Tumor localization[58, 59] was observed and this made sapphyrins attractive as possible anticancer drug candidates. Hydrophilic sapphyrin analogs were prepared and shown to have promise for the treatment of solid tumors.[59] Sapphyrins have also been proposed as potential photosensitizers for PDT.[60] They absorb light in the red portion of the visible spectrum, which is considered to be an attractive feature. This is because tissue and blood cells exhibit a broad relative absorption minimum[61] and are essentially transparent,[62, 63] which limits the penetration of visible photons with $\lambda_{max} \leq 650$ nm. To date, sapphyrins have been found to display efficient photosensitizing effects against superficial squamous cell carcinoma in mice.[64]

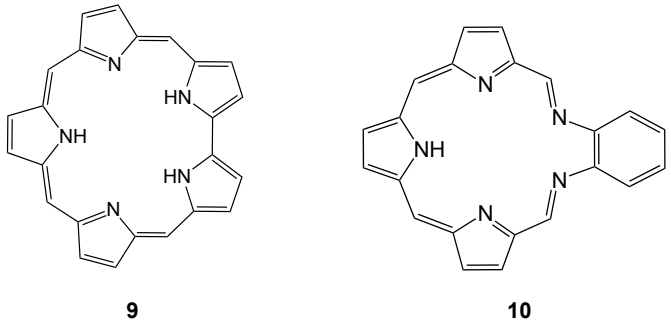

Figure 1.11: Basic structures of sapphyrin **9** and texaphyrin **10**.

1.5.2 Texaphyrins

1.5.2.1 Tumor Localization, Cytotoxicity and MRI Activity

Efforts in the Sessler group to utilize texaphyrins as radiation sensitizers have focused on the synthesis and use of texaphyrin chelating gadolinium, later renamed as motexafin gadolinium (MGd, Xcytrin™). As with other porphyrinic species, texaphyrins

accumulate preferentially in tumor tissues. Although the specific origins of the selective accumulation of MGd in neoplastic tissues remain unknown, it has already been observed that these compounds bind well to, and presumably modify, low density lipoproteins.[65] Once modified, these latter blood components are believed to be taken up by rapidly prolifering cells, such as tumor cells. These cells exhibit a considerably less efficient lymphatic drainage system, which in turn results in a diminished elimination of any (potentially cytotoxic) foreign substances within the cells, including the porphyrinoid.

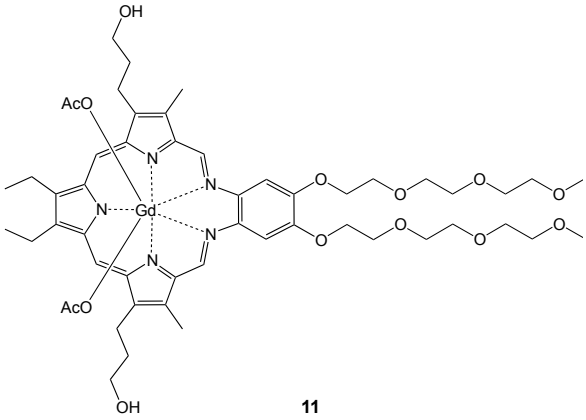

11

Figure 1.12: Motexafin gadolinium (MGd).

MGd was selected for clinical development in the context of radiation therapy by Pharmacyclics, Inc.[66, 67] Ultimately, the drug did not receive approval by the FDA. However, this work has provided insights into the cellular antioxidant system and inspired the discovery and investigation of new molecules capable of ROS generation within cancer.[68] It has also inspired new research involving texaphyrins.

One of the most important "lessons" learned is that MGd produces its observed radiation sensitizing function, at least in part, by acting as a redox mediator.[69] This mechanistic rationale relies on the fact that MGd is easy to reduce in comparison to a porphyrin. Intracellularly, it accepts an electron from an endogeneous electron rich species and catalyzes the oxidation of various reducing metabolites, such as ascorbate, reduced nicotinamide-adenine dinucleotide phosphate (NADPH), thioredoxin reducase, glutathione, and dihydrolipoate. This leads to the formation of a reduced texaphyrin

radical that reacts with oxygen to produce superoxide in a rapid equilibrium process, which in turn regenerates MGd. *In vitro*, and presumably *in vivo*, this superoxide is

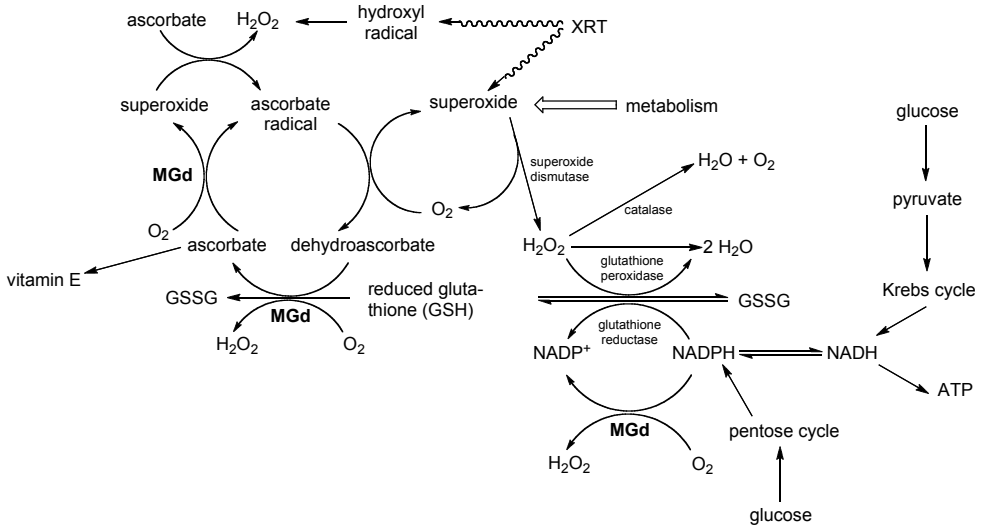

Scheme 1.1: Metabolic processes affected by MGd. This scheme is a modified version of one previously presented.[69]

converted quickly into hydrogen peroxide,[70] a species that is a known to be a potent apoptosis trigger. The rate constant for non-enzymatic disproportionation of superoxide is estimated to be 1 x 10^5 M^{-1} s^{-1} at pH 7.4.[71]

Because MGd, in contrast to other redox active agents, localizes in tumors, the net effect of this catalytic (in MGd) process is (1) the site selective production of ROS and enhancement of cancer cell death and (2) a corresponding decrease in the concentration of reducing metabolites, such as ascorbate and glutathione, that under normal circumstances both ascorbate and glutathione serve to mitigate the effects of oxidative stress and ionizing radiation. Their removal is thus expected to make cells more susceptible to X-ray treatment (XRT). Consistent with this rationale was the observation that the addition of BSO, antimycins A, or diamide, compounds involved in inhibiting

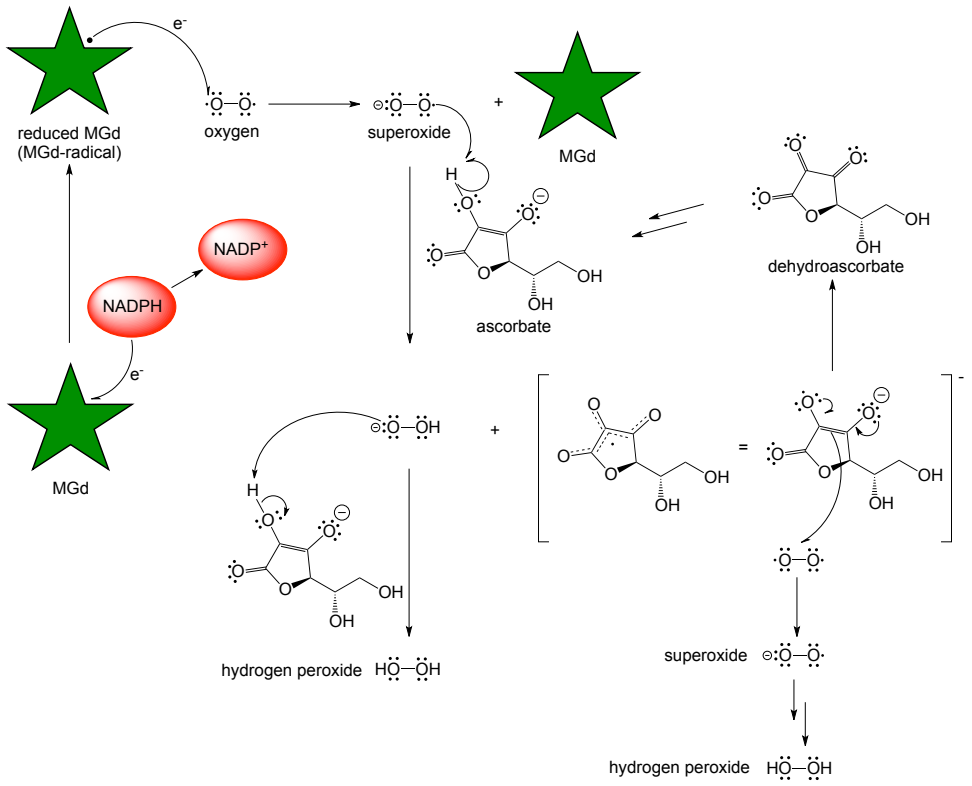

Scheme 1.2: Mechanistic representation of how MGd is thought to act as a redox mediator.

glutathione metabolism or forming reactive oxygen species, enhanced the effects of MGd.

In addition to displaying modest cytotoxicity effects, MGd was also shown to be detectable by magnetic resonance imaging (MRI). This MRI detection reflects the presence of a centrally coordinated paramagnetic metal ion, gadolinium(III)[72] which

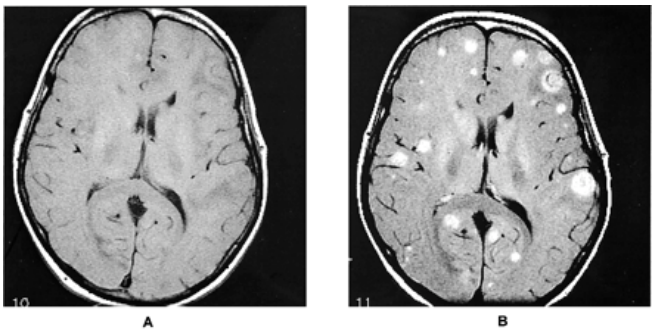

Figure 1.13: T_1 weighted noncontrast brain MRI before (A) and after (B) administration of MGd.[74]

provides for a highly effective spin lattice (T_1) relaxation. Based on MRI analyses, MGd was found to localize well in tumors. In contrast, no appreciable localization in adjacent normal tissue was observed.[73]

Studies initiated by Viala *et al*. provided initial evidence for a cytotoxic benefit for patients with breast cancer treated with MGd. The tumoral response upon administration of MGd can also be tracked in the MR images. The images in question (Figure 1.16) are taken from a 41-year old woman with brain metastases from breast cancer.[75] The results based on Phase IB and II multidose trials provide support for the proposal that MGd is safe and, presumably due to its porphyrinic structure, also localizes well in tumors. In these studies, enhancements in the MR signal intensity were seen only in target lesions, but not in normal brain tissue. This provided further evidence for the selectivity of MGd. The ratio of MGd in tumor cells to that in surrounding normal cells is reported to be up to 9:1.[76] However, this ratio, as inferred from MR images, increases to 50:1 in the case of metastatic brain tumors.[77] The uptake in target lesions was higher after ten daily injections than after the first dose. This finding is best interpreted in terms of an ability to accumulate and persist in brain metastases. Response to treatment at successive MRI examinations can be evaluated as well, since either the gadolinium texaphyrin or the gadolinium(III) cation, originally contained in its core, remains in tumor cells for several months. The administration of a paramagnetic contrast agent for follow-up MR examinations would be entirely redundant.[75]

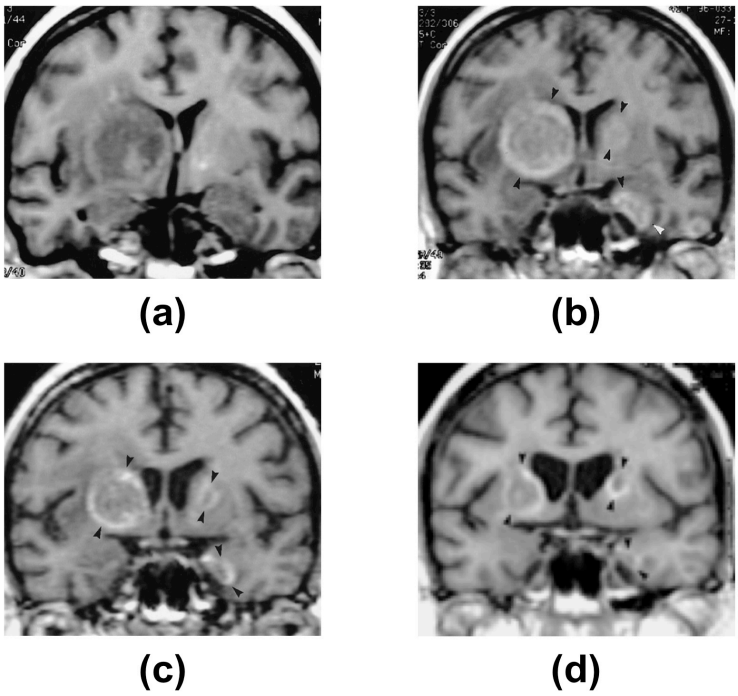

Figure 1.14: T_1 weighted MR images (a-d) of brain metastases and clinical progress inferred after administration of MGd.[75]

(a) MR image after the first injection (2.3μmol/kg) of MGd. No significant enhancement in the target lesions is observed.

(b) MR image after the 10th injection of MGd. Enhancement is localized in the target lesions (arrowheads) and is described as grade 3 (high enhancement).

(c) MR image 56 days after the first injection of MGd. Enhancement (arrowheads) is still visible and is still grade 3. At this stage, the tumor has decreased to 68% of its initial size.

(d) MR image 16 weeks after the first injection of MGd. Enhancement (arrowheads) is still visible and is grade 1 (moderate enhancement).

1.5.2.2 Historical Syntheses of Texaphyrins

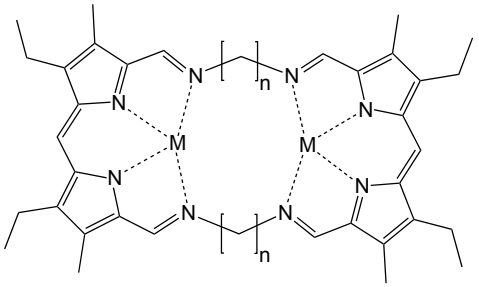

n = 2,3 M = Zn(II), Pb(II), Cu(II)

12

Figure 1.15: Structural representation of Mertes' tetrapyrrolic macrocycles.

The condensation of primary α,ω-diamines and heterocyclic dicarbonyl compounds has been thoroughly investigated and used to prepare a wide range of multidentate Schiff base-type cyclic ligands and their metal complexes.[78-80] Much of the early work was carried out with 2,6-dicarbonyl derivatives of pyridine as the heterocycle of choice. However, the use of pyrroles could give rise to interesting porphyrin analogs. Condensations involving pyrrolic precursors were first carried out by Mertes (a.k.a. Bowman-James), who reported the first "truly" expanded porphyrin tetrapyrrolic macrocycles **12** in the mid-1980s.[79] Unfortunately, these ligands could not be converted to the corresponding fully conjugated species due to the nature of the bridging methylene units,[79] nor were they particularly stable.

Perhaps the most exciting development in the field of expanded porphyrins was made in 1987 when Sessler´s group at the University of Texas at Austin reported the synthesis and crystal structure of a novel tripyrrane-containing porphyrinogen-like macrocycle.[81] Bearing resemblance to the shape of the five-pointed star in the state flag

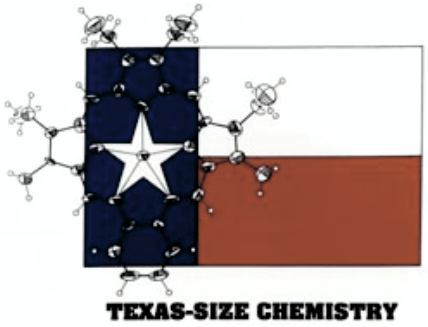

Figure 1.16: Structural representation of texaphyrin and the state flag of Texas.[85]

of Texas, texaphyrins are pentaaza Schiff-base macrocycles that bear a strong, but "expanded" similarity to traditional porphyrins.[82-84] As will be shown in later Chapters of this dissertation, recent efforts have demonstrated an ability of texaphyrins to chelate a variety of metal cations. However, the texaphyrins as prototypical expanded porphyrins were initially characterized in terms of their ability to coordinate "large cations", specifically with those of the trivalent lanthanide series.[82, 86, 87] One reason for this propensity is the fact that the central core of texaphyrins is roughly 20% larger than that of the porphyrins.[88] At the time of this initial publication, texaphyrins were the first expanded porphyrins to be structurally characterized and the first to exhibit metal complexation behavior.

The synthesis of the first texaphyrins hinged on the efficient synthesis of the key symmetric tripyrrane dialdehyde precursor. The synthesis of this important intermediate is shown in Scheme 1.1.

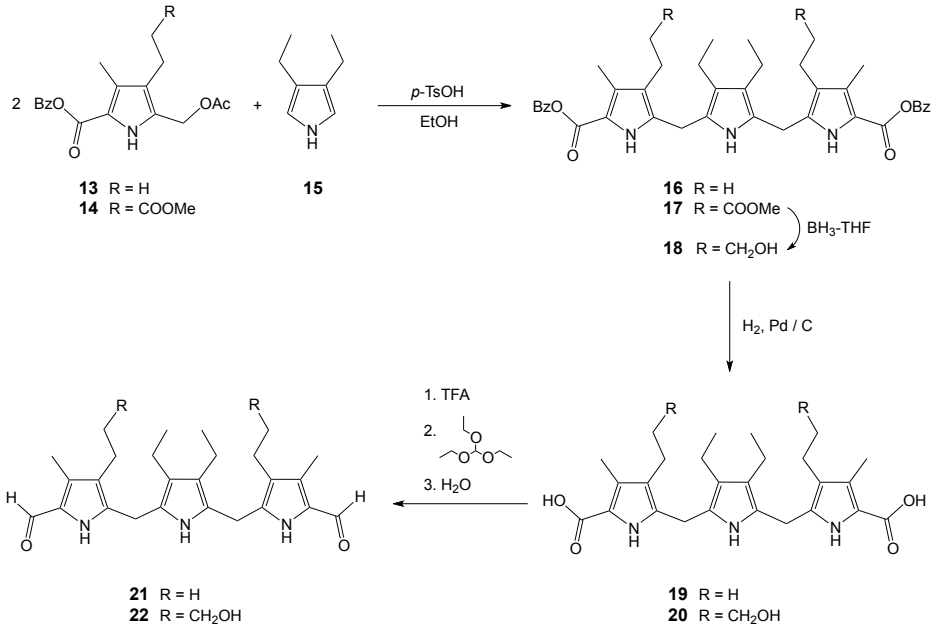

Scheme 1.3: Synthesis of tripyrrane dialdehydes **21** and **22**.

In order to obtain the tripyrrane unit **16**, 3,4-diethylpyrrole was condensed with two equivalents of (acetoxymethyl)pyrrole **13** under acidic conditions. Hydrogenolysis of the benzyl esters with 10% palladium on carbon under one atmosphere of hydrogen, followed by Clezy formylation[89] of the intermediate diacid tripyrrane **19**, provided the desired dialdehyde **21** in 68% yield.[90] Shown also is a related sequence used to obtain the diformyltripyrrane **22** bearing two hydroxylpropyl substituents; this latter species is a key intermediate in the synthesis of MGd **11**.

The nonaromatic form of the texaphyrin ligand, commonly referred to as sp^3-texaphyrin, is synthesiszed by an hydrogen chloride catalyzed 1:1 Schiff base condensation between the tripyrrane dialdehydes **21** and **22** and an appropriately derivatized o-phenylenediamine (Scheme 1.2) under conditions of high dilutions. Here, the term sp^3 refers to the hybridization of the two methylene-type carbon atoms bridging from the three pyrrole units in the scaffold. This procedure is similar to the one employed by Mertes *et al*. for the formation of the so-called "accordion" macrocycle **12**, shown in Figure 1.15.

The protonated form of the texaphyrin porphyrinogens **31**-**41** can be isolated in nearly quantitative yield.

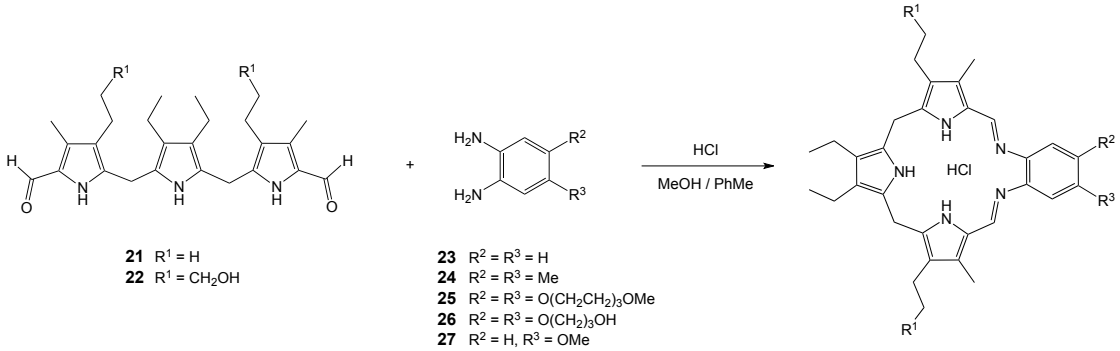

21 $R^1 = H$
22 $R^1 = CH_2OH$

23 $R^2 = R^3 = H$
24 $R^2 = R^3 = Me$
25 $R^2 = R^3 = O(CH_2CH_2)_3OMe$
26 $R^2 = R^3 = O(CH_2)_3OH$
27 $R^2 = H$, $R^3 = OMe$
28 $R^2 = H$, $R^3 = Cl$
29 $R^2 = H$, $R^3 = COOH$
30 $R^2 = H$, $R^3 = NO_2$

31 $R^1 = R^2 = R^3 = H$
32 $R^1 = H$, $R^2 = R^3 = Me$
33 $R^1 = H$, $R^2 = R^3 = OMe$
34 $R^1 = H$, $R^2 = R^3 = O(CH_2CH_2)_3OMe$
35 $R^1 = H$, $R^2 = R^3 = O(CH_2)_3OH$
36 $R^1 = CH_3OH$, $R^2 = R^3 = O(CH_2)_3OH$
37 $R^1 = CH_3OH$, $R^2 = R^3 = H$
38 $R^1 = R^2 = H$, $R^3 = OMe$
39 $R^1 = R^2 = H$, $R^3 = Cl$
40 $R^1 = R^2 = H$, $R^3 = COOH$
41 $R^1 = R^2 = H$, $R^3 = NO_2$

Scheme 1.4: Synthesis of the protonated non-aromatic texaphyrin porphyrinogen **31**-**41**.

Initially, oxidation of the non-aromatic texaphyrin proved quite difficult. In fact, a number of oxidizing agents, including PbO_2, SeO_2, AgO_2, Ph_3CBF_4, Ph_3CPF_6, and DDQ, were tested. However, only decomposition of the ligand was observed.[91]

It was subsequently discovered that stirring this nonaromatic macrocycle in an air-saturated mixture of chloroform and methanol with *N,N,N´,N´*-tetramethyl-1,8-naphthalenediamine ("proton sponge", a nonnucleophilic base) provided the free-base aromatic texaphyrin **42** in 12% yield.[91]

The texaphyrin species **42** can be considered as a 22 π-electron benzannulene that possesses both 18 π- and 22 π-electron delocalization pathways. Consistent with its aromatic character, **42** is observed to be more stable than its precursor **31**. Further evidence of the aromatic nature of **32** was obtained from spectroscopic studies: For instance, a 10 ppm upfield shift of the internal pyrrole NH signal ($\delta = 0.9$) is observed in the ^{1}H NMR spectrum of **42**, as compared to the corresponding signals in **31**.[91, 92] An

identical phenomenon (major changes in chemical shift values) is observed in the case of porphyrins, a finding that was interpreted as texaphyrins having a similar diamagnetic ring current.

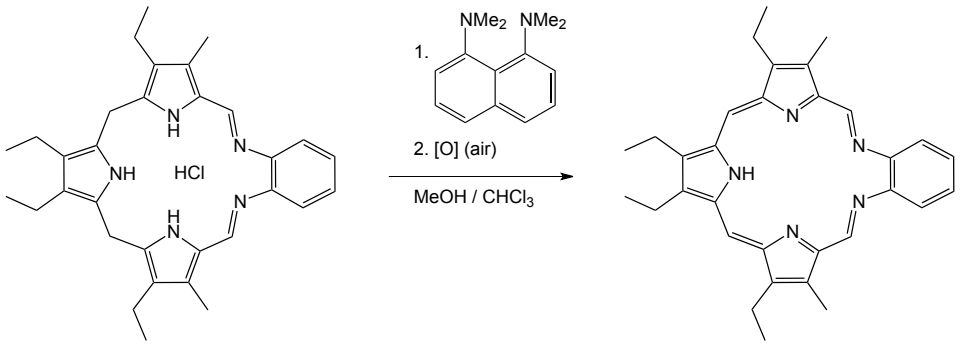

Scheme 1.5: Synthesis of a free base, aromatic texaphyrin.[90, 91]

Even though the discovery of the aromatic texaphyrin was thought to be a major step towards the successful synthesis of this expanded porphyrin, the preparation was severely limited synthetically in terms of reproducibility, generality and yield. Unfortunately, these macrocycles showed no propensity to chelate metals.

However, an important breakthrough occurred, when Dr. Toshiaki Murai, a postdoctoral fellow in Dr. Sessler's group at that time, found that treating the precursor **31** with $CdCl_2$, and base under aerobic conditions furnished a strongly absorbing green substance **43**. It was subsequently characterized as being the cadmium complex of the aromatic ligand.[91-93]

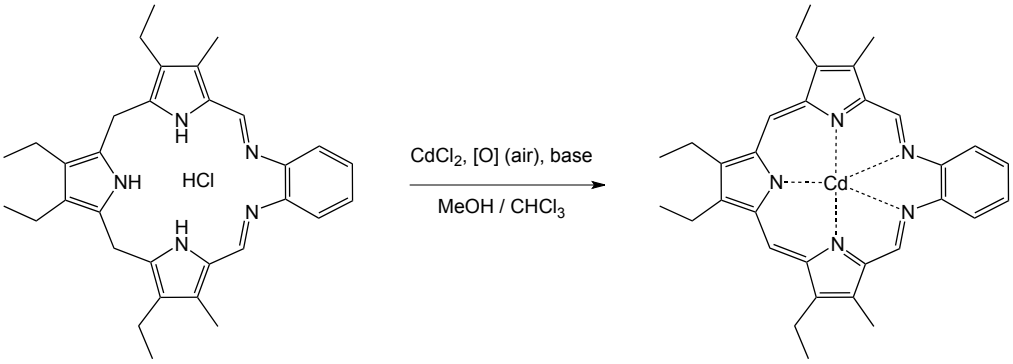

31 **43**

Scheme 1.6: Synthesis of an aromatic texaphyrin-Cd-complex.[91, 92]

Once the sp^3 systems shown in Scheme 1.2 (**31**-**41**) were in hand, they were subjected to complexation attempts particularly with metals in the lanthanide series. The trivalent lanthanide cations have ionic radii ranging from 1.06 Å (for La(III)) to 0.85 Å (for Lu(III)).[94] The reduction in size going from lanthanum to lutetium is due to an effect called the lanthanide contraction.[94] This phenomenon results in the relatively poor shielding of nuclear charges by the 4f electrons. Thus, the 6s electrons are drawn towards the nucleus ultimately leading to a smaller atomic radius. Notably, the general size of lanthanide cations is roughly the same as cadmium(II) (radius = 0.92 Å).[94] This provided an incentive to explore the complexation characteristics of texaphyrins with metals from the lanthanide series.

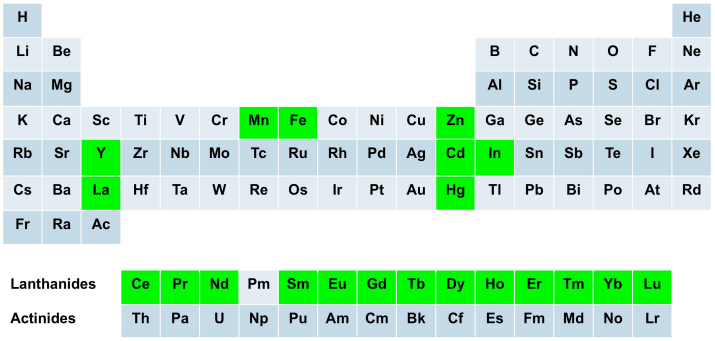

Figure 1.17: "Periodic table of texaphyrin". Stable texaphyrin complexes with all metals shown in green are known.

To date, stable texaphyrin complexes of almost every lanthanide(III) metal have been synthesized. Important to note is the fact that electron donating groups on the phenyl moiety of the macrocycle enhance the metal chelating ability, whereas electron-withdrawing groups have the opposite effect.

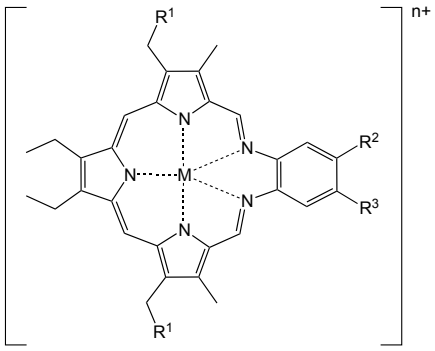

44 $R^1 = R^2 = R^3 = H$, n = 1 for M = Cd
45 $R^1 = R^2 = R^3 = H$, n = 1 for M = Zn, Mn, Hg; n = 2 for M = Nd, Sm, Eu
46 $R^1 = H$, $R^2 = R^3 = Me$, n = 2 for M = Sm, Eu, Gd
47 $R^1 = H$, $R^2 = R^3 = OMe$, n = 2 for M = Ce, Pr, Nd, Sm - Lu
48 $R^1 = R^2 = H$, $R^3 = OMe$
49 $R^1 = R^2 = H$, $R^3 = Cl$
50 $R^1 = R^2 = H$, $R^3 = COOH$
51 $R^1 = R^2 = H$, $R^3 = NO_2$
52 $R^1 = (CH_2)_2OH$, $R^2 = R^3 = O(CH_2)_3OH$, n = 2 for M = La, Ce, Pr, Nd, Sm - Lu

Figure 1.18: Representative stable texaphyrin complexes.[82, 90-96]

The basic strategy of effecting metallation and oxidation has been successfully employed to obtain numerous other texaphyrin complexes with a wide range of relatively large cations, other than lanthanides. In all cases the metal cation is thought to stabilize the macrocycle as a result of a presumed thermodynamic template effect.[80] Thus, once formed these metal complexes are extremely stable, except under acidic aqueous conditions, which readily leads to hydrolysis of the macrocycle.[91]

1.5.2.3 Spectroscopic Features of Texaphyrins

One crucial feature of texaphyrin complexes is their ability to absorb strongly in the >700 nm spectral region.[97, 98] As noted above, this region is of particular interest since it is a spectral region where bodily tissues and blood are maximally transparent.[97]

For instance, the UV-Vis spectrum of MGd **11** is dominated by two absorption bands. The higher energy Soret-like band at 474 nm is analogous to the ~400 nm band of

porphyrins and is characteristic of the absorption bands seen for other vividly pigmented porphyrin-type moieties. The Soret-like band is flanked by N- and Q-like bands at higher and lower energies, respectively, with the lowest energy Q-band for MGd being seen at 740 nm.

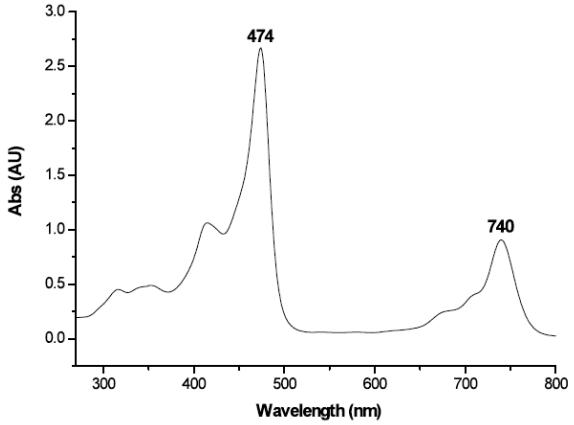

Figure 1.19: UV-visible spectrum of MGd **11**, 25 μM in methanol.

Interestingly, there is a steady shift in the Q-like band from red to the blue (Δ = 15 nm)[99] as the Ln(III) ion in question is changed from lanthanum to lutetium. This shift in the Q-like bands appears to follow the contraction of the metal ions in the lanthanide series. A plot of the wavelength (in nm) of the Q-like band versus the ionic radius of the Ln(III) ion gives a linear relationship.[99]

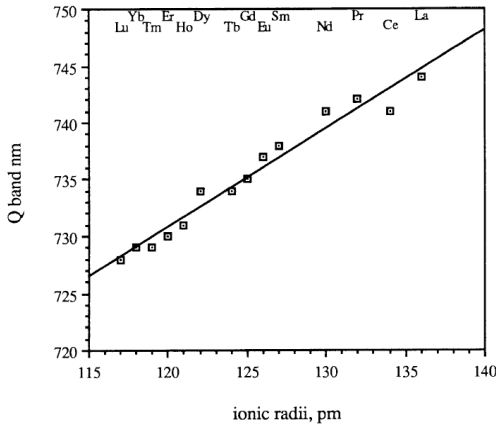

Figure 1.20: Plot of the wavelength (in nm) of the Q-like band versus the ionic radius of several Ln(III) ions.[99]

Another spectral feature of other metallated texaphyrins, especially diamagnetic texaphyrin species, is their ability to fluoresce. The resulting Q-type emission bands, like the Q-type absorption bands, are substantially red-shifted (by >100 nm) compared to typical porphyrins.[88, 97] Further investigations of the spectroscopic properties of various texaphyrin complexes have established that, like the porphyrins, the Q-type band energies correspond to the

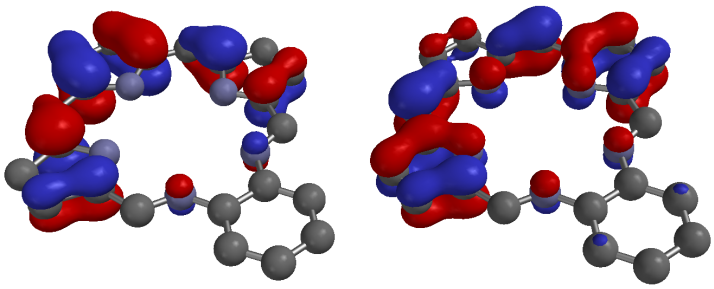

Figure 1.21: Calculated HOMO- (left) and LUMO-surface (right) of an unmetalated and unfunctionalized aromatic texaphyrin species.

relevant π-electron HOMO-LUMO energy gaps.

Since, in texaphyrins, the benzo moiety is an intimate part of the π-system of the macrocycle, any variation to this ring will affect the π-conjugation and allow resonance interactions between the substituent and the main macrocyclic frame. Hence, by varying the nature of these substituents, it is possible to shift the maxima of the Soret-like and Q-type bands to higher or lower energies.

1.6 CONCLUSIONS

The biomedical results obtained to date provide support for the notion that the expanded porphyrins, texaphyrin and sapphyrin could have a role to play in a variety of biomedical application areas. These include but are not limited to use as anticancer agents and isotope delivery vehicles for radiotherapy, site-localizing carriers, and treatments for neurodegenerative diseases. The unique mode of action of texaphyrins, which in some instances involves the manipulation of reactive oxygen species, and their inherent versatility in terms of sites for chemical modification and functionalization, make them attractive scaffolds for further study. The ensuing Chapters will give further insights into

the unique chemistry of this class of expanded porphyrins, and detail synthetic work designed to support collaborative studies that target new biomedical applications. Additionally, a new sapphyrin species will be introduced in an effort to potentially improve its anticancer properties.

Sections of this Chapter are part of a review on texaphyrins (Arambula, J. F.; Preihs, C.; Borthwick, D.; Magda, D.; Sessler, J. L., *Anti-Cancer Agents in Med. Chem.* **2011**, *11*, 222-232.). Dr. Jonathan F. Arambula, Christian Preihs and Dr. Jonathan L. Sessler co-wrote the paper, Derric Borthwick and Darren Magda contributed to corrections and discussions. Other sections of this Chapter were taken from: Preihs, C., M.A. Thesis, The University of Texas at Austin, December 2009.

References

(1) Podsypanina, K.; Du, Y. C.; Jechlinger, M.; Beverly, L. J.; Hambardzumyan, D.; Varmus, H. *Science* **2008**, *321*, 1841-1844.

(2) http://cancerhelp.cancerresearchuk.org/about-cancer/cancer-questions/how-many-different-types-of-cancer-are-there

Retrieved 07-30-2012

(3) http://images.3d4medical.com/Biopsy-82-free-image_RM5524.html

Retrieved 11-19-2012; Figure reprinted with permission from Johnston, N. 3D4Medical.com, 7704 Concerto Lane, San Diego, CA 92127, USA.

(4) Croce, C. M. *N. Engl.. J. Med*. **2008**, *358*, 502-511.

(5) Loeb, K. R.; Loeb, L. A. *Carcinogenesis* **2000**, *21*, 379-385.

(6) Modified figure from:

http://en.wikipedia.org/wiki/File:Cancer_requiresmultiple_mutations_from_NIHen.png

Retrieved 07-31-2012

(7) Merlo, L. M., Pepper, J. W.; Reid, B. J.; Maley, C. C. *Nat. Rev. Cancer* **2006**, 6, 924-935.

(8) Modified figure from: http://uscneurosurgery.com/conditions/spine-center/expertise/metastatic-spine-tumors.php

Retrieved 07-31-2012

(9) Maruyama, K. In *Drug Delivery System*, CAS **1999**, Vol. 14, 433-447.

(10) Shayan, R.; Achen, M. G.; Stacker, S. A. *Carcinogenesis* **2006**, *27*, 1729-1738.

(11) Kunar, V.; Abbas, A. K.; Fausto, N.; Robbins, S. L.; Cotran, R. S. *Robbins and Cotran pathologic basis of disease*, 7th ed., Elsevier Saunders, Philadelphia, **2005**.

(12) Briasoulis, E.; Pavlidis, N. *Oncologist* **1997**, *2*, 142-152.

(13) American Cancer Society, Cancer Facts and Figures **2010**, American Cancer Society, Atlanta **2010**.

(14) Spalding, A. C.; Lawrence, T. S. *Cancer Investigation* **2006**, *24*, 444-456.

(15) Von Sonntag, C. In *The Chemical Basis of Radiation Biology*, Taylor and Francis, London **1987**.

(16) Feldmeier, J. J. In *Radiation Oncology*, G. R. Weiss, Ed., Appleton & Lange, Norwalk **1993**, 74-88.

(17) Petry, E. *Biochim. Z.* **1923**, *135*, 353-383.

(18) Thomlinson, R. H.; Gray, L. H. *British Journal of Cancer* **1955**, *9*, 539-549.

(19) Otto, S. E. In *Pocket guide to oncology nursing*, Mosby-Year Book, Inc., St. Louis **1995**.

(20) Gates, R. A.; Fink, R. M. In *Oncology nursing secrets*, Hanley and Belfus, Inc., Philadelphia **1997**.

(21) Longley, D. B.; Harkin, D. P.; Johnston, P. G. *Nat. Rev. Cancer* **2003**, *3*, 330-338.

(22) Thomas, D. M.; Zalcberg, J. R. *Clin. Exp. Pharmacol. Physiol.* **1998**, *25*, 887-895.

(23) Cerqueira, N. M. F. S. A.; Fernandes, P. A.; Ramos, M. J. *Chemistry: A European Journal* **2007**, *13*, 8507-8515.

(24) Guo, Z.; Sadler, P. J. *Angew. Chem. Int. Ed.* **1999**, *38*, 1512-1531.

(25) Turchi, J. J.; Henkels, K. M.; Hermanson, I. L.; Patrick, S. M. *J. Inorg. Biochem.* **1999**, *77*, 83-87.

(26) Rixe, O.; Ortuzar, W.; Alvarez, M.; Parker, R.; Reed, E. *Biochem. Pharmacol.* **1996**, *52*, 1855-1865.

(27) De Gramont, A.; Figer, A.; Seymour, M.; Homerin, M.; Hmissi, A. *J. Clin. Oncol.* **2000**, *18*, 2938-2947.

(28) Natarajan, G. et al. *Biochem. Pharmacol.* **1999**, *58*, 1625-1629.

(29) Jiang, X.; Pandey, R. K.; Smith, K. M. *Tetrahedron Letters* **1995**, *36*, 365-368.

(30) Ghiggino, K. P.; Bennett, L. E.; Henderson, R. W. *Photochemistry and Photobiology* **1988**, *47*, 65-72.

(31) Derat, E.; Cohen, S.; Shaik, S.; Altun, A.; Thies, W. *J. Am. Chem. Soc.* **2005**, *127*, 13611-136121.

(32) Benfrey, O. T.; Morris, P. J. T. Eds. *Robert Burns Woodward Artist and Architect in the World of Molecules*, Chemical Heritage Foundation, Philadelphia **2001**, 256-277, 302-242.

(33) Alberts, B.; Johnson, A.; Lewis, J.; Raff, M.; Roberts, K.; Walter, P. In *Molecular Biology of the Cell*, 4th Ed., Gardland Science, New York **2002**.

(34) Sanchez-Alcazar, J. A.; Khodjakov, A.; Schneider, E. *Cancer Research* **2001**, *61*, 1038-1044.

(35) Kalka, K.; Merk, H.; Mukhtar, H. *J. Am. Acad. Dermatol.* **2000**, *42*, 389-413.

(36) Luksiene, Z.; Juzenas, R.; Moan, J. *Cancer Letters* **2006**, *235*, 40-47.

(37) Hausmann, W. *Biochem. Z.* **1909**, *14*, 275-278.

(38) Schwartz, S.; Absolon, K.; Vermund, H. *Univ. Minnesota Med. Bull.* **1955**, *27*, 7-13.

(39) Schwartz, S.; Keprios, M.; Modelevsky, G.; Freyholtz, H.; Walters, R.; Larson, L. In *M. Doss (Ed.), Diagnosis and Therapy of Porphyrins and Lead Intoxication*, Springer, Berlin **1978**.

(40) Sternberg, E. D.; Dolphin, D. *Tetrahedron* **1998**, *54*, 4151-4202.

(41) Pandey, R. K.; Sihiau, F.-Y.; Dougherty, T. J.; Smith, K. M. *Tetrahedron* **1991**, *47*, 9571-9584.

(42) Lou, Y.; Chang, C. K.; Kessel, D. *Photochem. and Photobiol.* **1996**, *63*, 528-534.

(43) Dougherty, T. J.; Gomer, C. J.; Henderson, B. W.; Jori, G.; Kessel, D.; Korbelik, M.; Moan, J.; Peng, Q. *J. Nat. Cancer Inst.* **1998**, *90*, 889-905.

(44) Pandey, R. K.; Zheng, G. In *Porphyrin Handbook* **2000**, *6*, 157-230.

(45) Zhao, F.-Y.; Zhang, K.-H.; Huang, H.-N.; Sun, K.-H.; Ling, Q.-B.; Xu, B. *Lasers Med. Sci.* **1986**, *1*, 253-256.

(46) Chen, D. Y. *Treat. Laser* **1985**, *5*, 137.

(47) Bellnier, D. A.; Dougherty, T. J. *Int. J. Radiat. Biol.* **1986**, *50*, 659-664.

(48) Moan, J.; Pettersen, E. O. *Int. J. Radiat. Biol.* **1981**, *40*, 107-109.

(49) O´Hara, J.; Douple, E. B.; Abrams, M. J.; Picker, D. J.; Giandomenico, C. M.; Vollano, J. F. *Int. J. Radiat. Oncol. Biol. Phys.* **1989**, *16*, 1049-1052.

(50) James, B. R.; Meng, G. G.; Posakony, J. J.; Ravensbergen, J. A.; Ware, C. J.; Skov, K. A. *Metal-Based Drugs* **1996**, *3*, 85-89.

(51) Ali, H.; van Lier, J. E., *Chem. Rev.* **1999**, *99*, 2379-2450.

(52) Han, F. X. G.; Wheelhouse, R. T.; Hurley, L. H. *J. Am. Chem. Soc.* **1999**, *121*, 3561-3570.

(53) Yuasa, M.; Oyaizu, K.; Horiuchi, A.; Ogata, A.; Hatsugai, T.; Yamaguchi, A.; Kawakami, H. *Mol. Pharmaceutics* **200**4, *5*, 387-389.

Figure reprinted with permission from Yuasa, M.; Oyaizu, K.; Horiuchi, A.; Ogata, A.; Hatsugai, T.; Yamaguchi, A.; Kawakami, H. *Mol. Pharmaceutics* **200**4, *5*, 387-389. Copyright 2004 by the American Chemical Society.

(54) Rudat, V.; Stadler, P.; Becker, A.; Vanselow, B.; Dietz, A. *Strahlenther. Onkol.* **2001**, *177*, 462-468.

(55) Brizel, D. M.; Dodge, R. K.; Clough, R. W.; Dewhirst, M. W. *Radiother. Oncol.* **1999**, *53*, 113-117.

(56) Fyles, A. W.; Milosevic, M.; Pintilie, M.; Syed, A.; Hill, R. P. *Radiother. Oncol.* **2000**, *57*, 13-19.

(57) Bauer, V. J.; Clive, D. L. J.; Dolphin, D.; Paine III, J. B.; Harris, F. L.; King, M. M.; Loder, J.; Wang, S.-W. C.; Woodward, R. B. *J. Am. Chem. Soc.* **1983**, *105*, 6429-6436.

(58) Kral, V.; Davis, J.; Andrievsky, A.; Kralova, J.; Synytsya, A.; Pouckova, P.; Sessler, J. L. *J. Med. Chem.* **2002**, *45*, 1073-1078.

(59) Wang, Z.; Lecane, P.; Thiemann, P.; Fan, A.; Cortez, C.; Ma, X.; Tonev, D.; Miles, D.; Lin, A.; Hemmi, G.; Naumovski, L.; Miller, R. A.; Magda, D.; Cho, D.-G.; Sessler, J. L.; Pike, B. L.; Yeligar, S. M.; Karaman, M. W.; Hacia, J. G. *Mol. Cancer* **2007**, *6*, 9-20.

(60) Roitman, L.; Ehrenberg, B.; Nitzan, Y.; Kral, V.; Sessler, J. L. *Photochem. Photobiol.* **1994**, *60*, 421-426.

(61) van Gemert, M. G. C.; Welch, A. J.; Amin, A. P. *Lasers Surg. Med.* **1986**, *6*, 76-83.

(62) Wan, S.; Parrish, J. R.; Anderson, R. R.; Madden, M. *Photochem Photobiol.* **1981**, *34*, 679-681.

(63) Eichler, J.; Knop, J.; Lenz, H. *Radiat. Environ, Biophys.* **1977**, *14*, 239-242.

(64) Parmeswaran, D.; Pushpan, S. K.; Srinivasan, A.; Ravi, K. M.; Chandrashekar, T. K.; Ganesan, S. *Photochem. Photobiol.* **2003**, *78*, 487-495.

(65) Sessler, J. L.; Miller, R. A. *Biochem. Pharmacol.* **2000**, *59*, 733-739.

(66) Mehta, M. P.; Shapiro, W. R.; Phan, S. C.; Gervais, R.; Carrie, C.; Chabot, P.; Patchell, R. A.; Glantz, M. J.; Recht, L.; Langer, C.; Sur, R. K.; Roa, W. H.; Mahe, M. A.; Fortin, A.; Nieder, C.; Meyers, C. A.; Smith, J. A.; Miller, R. A.; Renschler, M. F. *Int. J. Radiat. Oncol. Biol. Phys.* **2009**, *73*, 1069-1076.

(67) Patel, H.; Mick, R.; Finlay, J.; Zhu, T. C.; Rickter, E.; Cengel, K. A.; Malkowicz, S. B.; Hahn, S. M.; Busch, T. M. *Clin. Cancer Res.* **2008**, *14*, 4869-4876.

(68) Sessler, J. L.; Hemmi, G.; Mody, T. D.; Murai, T.; Burrell, A.; Young, S. W. *Acc. Chem. Res.* **1994**, *27*, 43-50.

(69) Magda, D.; Lepp, C.; Gerasimchuk, N.; Lee, I.; Sessler, J. L.; Lin, A.; Biaglow, J.; Miller, R. A. *Int. J. Radiat. Biol. Oncol. Phys.* **2001**, *51*, 1025-1036.

(70) Sessler, J. L.; Tvermoes, N. A.; Guldi, D. M.; Hug, G. L.; Mody, T. D.; Magda, D. *J. Phys. Chem. B* **2001**, *105*, 1452-1457.

(71) Rockwell, S.; Donnelly, E. T.; Liu, Y.; Tang, L.-Q. *Int. J. Radiat. Oncol. Biol. Phys.* **2002**, *54*, 536.

(72) Young, S. W.; Sidhu, M. K.; Qing, F. *Invest. Radiol.* **1994**, *29*, 330-338.

(73) Rosenthal, D. I.; Nurenberg, P.; Becerra, C. R.; Frenkel, E. P.; Carbonne, D. P.; Lum, B. L.; Miller, R.; Engel, J.; Young, S.; Miles, D.; Renschler, M. F. *Clin. Cancer Res.* **1999**, *5*, 739-745.

(74) Carde, P.; Timmerman, R.; Mehta, M. P.; Koprowski, C. D.; Ford, J.; Tishler, R. B.; Miles, D.; Miller, R. A.; Renschler, M. F. *J. Clin. Oncol.* **2001**, *19*, 2074-2083.

Figure reprinted with permission from Carde, P.; Timmerman, R.; Mehta, M. P.; Koprowski, C. D.; Ford, J.; Tishler, R. B.; Miles, D.; Miller, R. A.; Renschler, M. F. *J. Clin. Oncol.* **2001**, *19*, 2074-2083. Copyright 2012 by the American Society of Clinical Oncology.

(75) Viala, J.; Vanel, D.; Meingau, P.; Lartigau, E.; Carde, P.; Renschler, M. F. *Radiology* **1999**, *3*, 755-759.

Figure reprinted with permission from Viala, J.; Vanel, D.; Meingau, P.; Lartigau, E.; Carde, P.; Renschler, M. F. *Radiology* **1999**, *3*, 755-759. Copyright 2012 by The Radiological Society of North America.

(76) Miller, R. A.; Woodburn, K.; Fan, Q.; Renschler, M. F.; Sessler, J. L.; Koutcher, J. A. *Int. J. Radiation Oncology Biol. Phys.* **1999**, *45*, 981-989.

(77) Mehta, M. P.; Shapiro, W. R.; Glantz, M. J.; Patchell, R. A.; Weitzner, M. A.; Meyers, C. A.; Schultz, C. J.; Roa, W. H.; Leibenhout, M.; Ford, J.; Curran, W.; Phan, S.; Smith, J. A.; Miller, R. A.; Renschler, M. F. *J. Clin. Oncol.* **2002**, *20*, 3445-3453.

(78) Sessler, J. L.; Burrel, A. K. *Top. Curr. Chem.* **1991**, *161*, 177.

(79) (a) Acholla, F. V.; Mertes, K. B. *Tetrahedron Lett.* **1984**, *25*, 3269-3270. (b) Acholla, F. V.; Takusagawa, F.; Mertes, K. B. *J. Am. Chem. Soc.* **1985**, *107*, 6902-6908.

(80) Curtis, N. F. *Coord. Chem. Rev.* **1968**, *3*, 3-47.

(81) Sessler, J. L.; Johnson, M. R.; Lynch, V. *J. Org. Chem.* **1987**, *52*, 4394-4397.

(82) Sessler, J. L.; Hemmi, G. W.; Mody, T. D.; Murai, T.; Burrell, A. *Acc. Chem. Res.* **1994**, *27*, 43-50.

(83) Mody, T. D.; Sessler, J. L. In *Supramolecular Materials and Technologies*, Reinhoudt DN (ed) Wiley: Chichester **1999**, *Vol. 4*, 245-299.

(84) Mody, T. D.; Fu, L.; Sessler, J. L. In *Progress Inorganic Chemistry*, Karlin KJ (ed) Wiley: Chichester **2001**, *Vol. 49*, 551.

(85) http://sessler.cm.utexas.edu/Sessler_Group_Website/Home.html
Retrieved 08-11-2012

(86) Sessler, J. L.; Mody, T. D.; Hemmi, G. W.; Lynch, V. *Inorg. Chem.* **1993**, *32*, 3175-3187.

(87) Sessler, J. L.; Tvermoes, N. A.; Guldi, D. M.; Mody, T. D. *Phys. Chem.* **1999**, *103*, 787-794.

(88) Mody, T. D.; Sessler, J. L. *J. Porphy. Phthalocy.* **2001**, *5*, 134-142.

(89) Clezy, P. S.; Liepa, A. J. *Aust. J. Chem.* **1972**, *25*, 1979-1990.

(90) Jasat, A.; Dolphin, D. *Chem. Rev.* **1997**, *97*, 2267-2340.

(91) Sessler, J. L.; Murai, T.; Lynch, V.; Cyr, M. *J. Am. Chem. Soc.* **1988**, *110*, 5586-5588.

(92) Sessler, J. L.; Murai, T.; Lynch, V. *Inorg. Chem.* **1989**, *28*, 1333-1341.

(93) Sessler, J. L.; Johnson, M. R.; Lynch, V.; Murai, T. *J. Coord. Chem.* **1988**, *18*, 99-104.

(94) Cotton, F. A.; Wilkinson, G. In *Advanced Inorganic Chemistry*, John Wiley: New York **1980**, *4th ed.*, pp 589, 982.

(95) Maiya, B. G.; Mallouk, T. E.; Hemmi, G. W.; Sessler, J. L. *Inorg. Chem.* **1990**, *29*, 3738-3745.

(96) Sessler, J. L.; Mody, T. D.; Ramasamy, R.; Sherry, A. D. *New J. Chem.* **1992**, *16*, 541-544.

(97) Sessler, J. L.; Dow, W. C.; O'Connor, D.; Harriman, A.; Hemmi, G. W.; Mody, T. D.; Miller, R. A.; Qing, F.; Springs, S.; Woodburn, K. *J. Alloys and Compounds* **1997**, *249*, 146-152.

(98) Harriman, A.; Majya, B. G.; Murai, T. D.; Hemmi, G. W.; Sessler, J. L.; Mallouk, T. E. *J. Chem. Soc., Chem. Commun.* **1989**, 314-316.

(99) Hemmi, G. W. *Dissertation (Ph.D.)*, The University of Texas at Austin **1992**, 41-43.

2. Bismuth- and Lead-Texaphyrins as Potential α-Core Emitters for Radiotherapy

2.1 INTRODUCTION

The chemistry of bismuth has been largely unexplored, until recently when bismuth complexes have gained interest for the treatment of gastric ulcers[1] and in cancer therapy.[2] Whereas medical applications of bismuth salts (e.g. Pepto-Bismol®) have already been explored extensively, the coordination chemistry of this element remains poorly investigated. Trivalent and pentavalent oxidation states for bismuth are the most common ones, with the chemistry of Bi(III) being more extensively developed. Here, research efforts have led to the synthesis and characterization of various complexes with coordination numbers ranging from three to ten.[3-7]

The high affinity of bismuth with nitrogen and oxygen chelates makes this metal an attractive candidate for the formation of complexes with a number of chelators and macrocycles, such as (4,7,10-tris-carboxymethyl-1,4,7,10-tetraaza-cyclododec-1-yl)-acetic acid (DOTA).[8]

Until the early 1980s, merely a few reports on the complexation of bismuth by porphyrins were published, presumably due to their inherent instability.[9-10] Nevertheless, during the past decade, various studies and computational methods led to a better understanding of the coordination of bismuth in porphyrins, both, in organic and aqueous media.[11-14] Prof. Bernard Boitrel and coworkers at the University of Rennes (Frances) were the first to succeed in the synthesis of stable bismuth(III) picket porphyrins (Figure 2.1 (a.)).[15] They also introduced hanging-carboxylate porphyrins (Figure 2.1. (b.))[16] as bismuth(III) chelators. These systems are providing an advanced knowledge of the co-

(a)

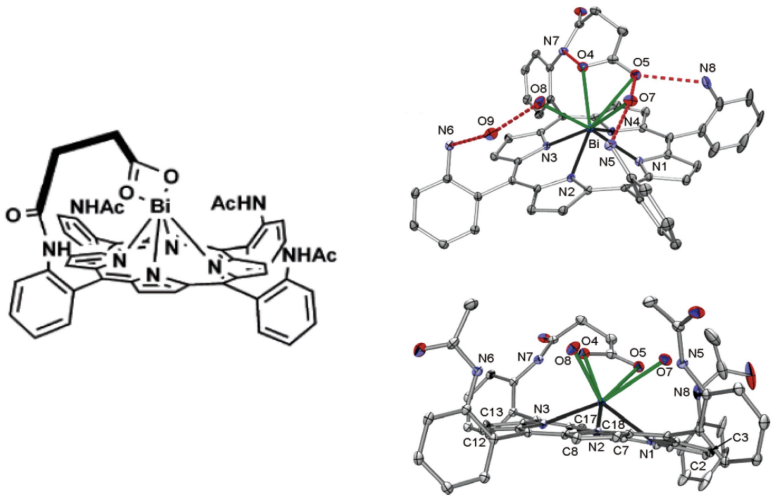

(b)

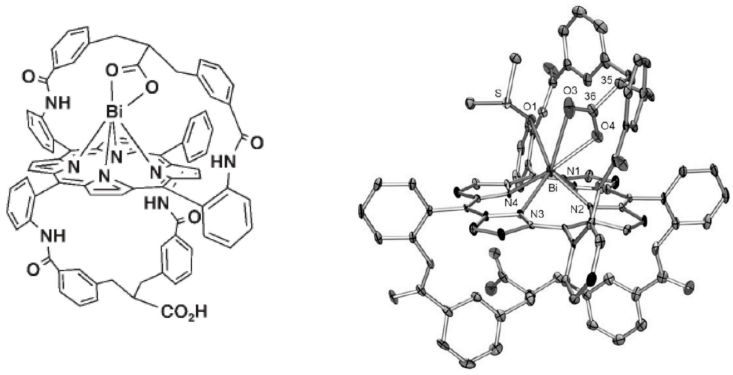

Figure 2.1: Valence bond structures (left) and X-ray crystal structures (right) of (a) Boitrel's picket bismuth(III) porphyrin[15] and (b) Prof. Boitrel's hanging-carboxylate bismuth(III) porphyrin.[16]

ordination behavior of bismuth and, more notably, allowing for the preparation of drug delivery systems bearing alpha-emitting bismuth isotopes for applications in radio-therapy. The bismuth isotopes in question, namely ^{212}Bi and ^{213}Bi, are characterized by very limited half-lives (60.55 min and 45.65 min for ^{212}Bi and ^{213}Bi, respectively). This has prompted lead(II) to be a more suitable metal for the purpose of creating alpha-emitting complexes. The lifetime of ^{212}Pb is longer than that of ^{212}Bi and ^{213}Bi, it exhibits a half-life of 10.64 hours and produces ^{212}Bi as its primary decay product along with a β-particle.

The radiation chemistry of bismuth has provided an incentive to develop a so-called *in situ* generator of ^{212}Bi based on the initial complexation of ^{212}Pb.[16] Such a generator requires a chelator that can rapidly coordinate both, lead(II) and its isoelectric

neighbor bismuth(III). One series of ligands endowed with this ability is the so-called hanging carboxylate porphyrins. Representative structures are shown in Figures 2.1 (b) and 2.2.

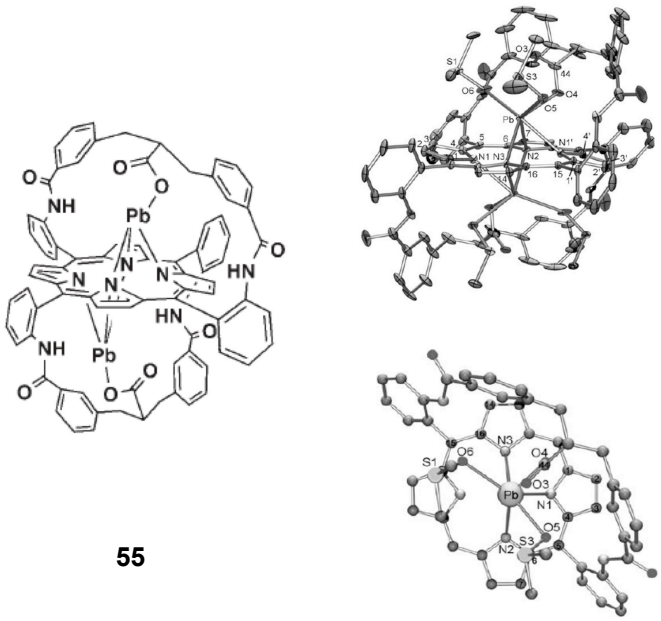

Figure 2.2: Valence bond structures (left) and X-ray crystal structures (right) of Boitrel's hanging-carboxylate lead(II) porphyrin.[16]

However, the stable systems reported to date have been structurally complex and a challenge to produce synthetically. The need for elaborate porphyrins reflects the fact that the lead(II) and bismuth(III) cations do not fit inside the cavity of a tetrapyrrolic porphyrin. Bi(III) or Pb(II) complexes of non-elaborated porphyrins generally suffer from stability problems, with decomplexation reactions having been specifically noted in the case of *tetrakis*(3-pyridyl)porphyrin,[13] *meso*-tetra-*n*-popylporphyrin,[17] and octaethylporphyrin[18]. This is most likely due to the large distance of the metal center from the plane of the four nitrogen atoms in the porphyrin ligand. Moreover, the insertion kinetics for typical unfunctionalized porphyrins are usually very slow, with heating at reflux in solvents such as methanol, dichloromethane, chloroform or toluene generally being required in the case of bismuth. Even more problematic, partial decomplexation is often observed during the course of purifying the resulting complexes. In an effort to overcome these difficulties, a goal of the author was to explore the use of texaphyrin as a ligand for lead and bismuth.

2.2 TEXAPHYRINS AS LIGANDS FOR BISMUTH(III) AND LEAD(II)

2.2.1 Structural Characteristics

As already mentioned in section 1.5.2.2, texaphyrins have a roughly 20% larger core than their tetrapyrrolic congeners,[19] which allows for the complexation of larger cations, in this case bismuth(III) and lead(II). As detailed below, the reduced, sp^3 precursor form of texaphyrin is indeed able to complex these two cations rapidly; Specifically, exposure of the nonaromatic texaphyrin ligands to commercially available bismuth nitrate or lead nitrate in methanol in the presence of triethylamine and molecular

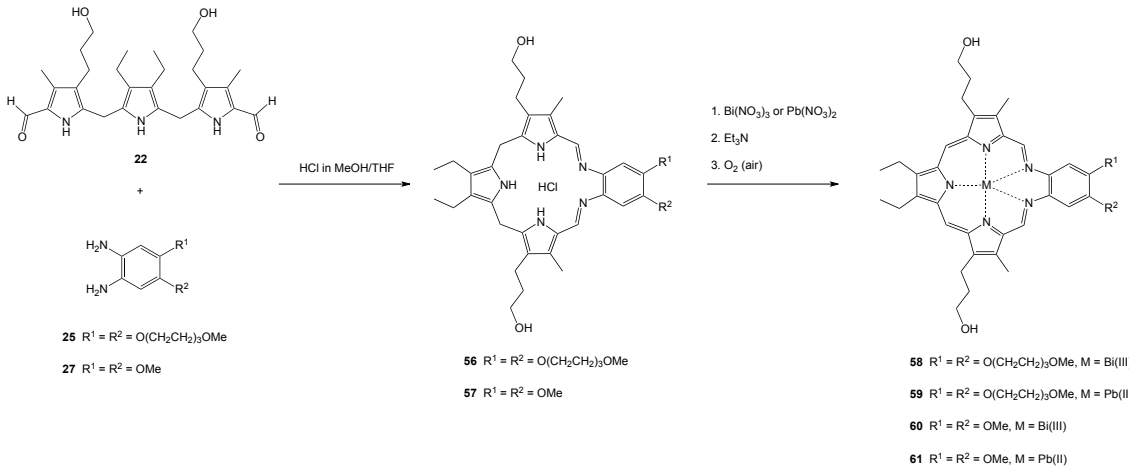

Scheme 2.1: Synthesis and structure of Bi(III) and Pb(II)-texaphyrins. Note that ancillary ligands are not shown. In fact, complex **60** exists in the form of a μ-oxo binuclear complex under most conditions; see text.

oxygen lead to the aromatic complexes **58**, **59**, **60** and **61**, respectively. In doing so, the first discrete binuclear μ-oxo bismuth(III) macrocyclic complex to be described in the literature is formed as judged by X-ray diffraction analysis. The present Bi(III) and Pb(II) species are chemically stable, a feature that coupled with their ability to be produced in a

water soluble fashion, has permitted their characterization and cytotoxicity studies *in vitro* using the A2780 ovarian cancer cell line.

The chemical structures of the target Bi(III)- and Pb(II)-texaphyrin complexes are shown in Figure 2.3. Compounds **58** (MBi) and **59** (MPb) bear appended polyethylene glycol units and were expected to display water solubility sufficient to allow for cell studies.

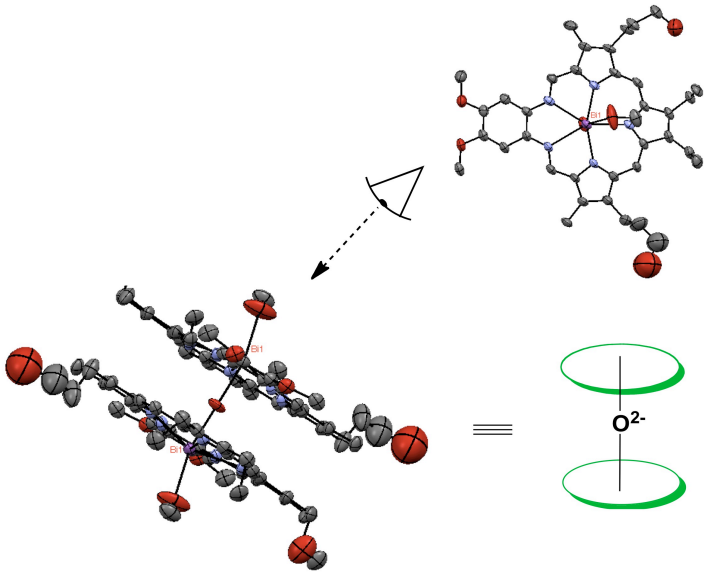

Figure 2.3: Single crystal X-ray structure of **60**. Note that the top structure shows only one individual texaphyrin subunit viewed from the top.

In contrast, complexes **60** and **61**, with appended methoxy functionalities, were designed to allow for the growth of single crystals suitable for X-ray diffraction analysis. While diffraction grade crystals were obtained in the case of **60** (Figure 2.4), to date no crystals of **61** suitable for complete X-ray analysis and refinement could be obtained. However, a preliminary X-ray structure of **61** is shown in Figure 2.5.

Crystals of **60** suitable for X-ray diffraction analysis were obtained by slow evaporation from methanol. The complex exists as a binuclear dimer in the solid state with a μ-oxo atom bridging the Bi(III) centers ligated by the individual texaphyrin subunits. One axial nitrate anion and one methanol molecule are bound to each bismuth(III) metal center. This binding of ancillary ligands is consistent with the oxophilicity of bismuth. The out-of-mean plane distance of the Bi(III) center is roughly 0.3 Å.

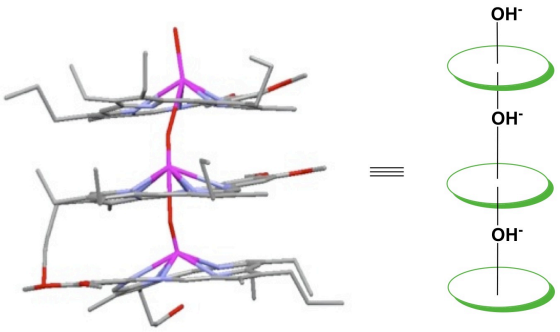

Figure 2.4: Preliminary single crystal X-ray structure of **61**.

The preliminary X-ray structure of **61** is best interpreted in terms of a trimeric fashion with bridged μ-hydroxy groups between the texaphyrin moieties. While representing a unique structure in porphyrin chemistry, this conclusion is not secure due to the fact that an advanced refinement of the structural parameters is not possible.

To the best of our knowledge, the dimeric structure of the bismuth(III) texaphyrin complex **60** (Figure 2.4) is the first structurally characterized binuclear macrocyclic *μ*-oxo bismuth(III) complex, and the first stacked expanded porphyrin system to be prepared with a texaphyrin and a non-transition metal. In contrast to what is true for texaphyrins, however, a number of *μ*-oxo metalloporphyrin complexes are known (albeit not with bismuth). In general, the μ-oxo bridge in these latter complexes can be cleaved by addition of an aqueous acid, such as hydrochloric or hydrobromic acid to yield, as a general rule, the corresponding monomeric species. In the case of **60**, however, such treatments led only to decomposition, presumably through hydrolysis. On the other hand,

the use of non-aqueous conditions (trifluoroacetic acid (TFA) in DMSO-d_6) allowed conversion of the binuclear species **60** to its mononuclear form (Figure 2.6), as inferred from ^{1}H NMR spectroscopic analyses (see Figure 2.7). This process (conversion to the mononuclear form) is fully reversible by addition of triethylamine (TEA), which serves to regenerate the μ-oxo binuclear complex **60**.

The broad signals in the ^{1}H NMR spectrum of **60** provide support to the notion that a dimeric μ-oxo-bridged structure is stable in solution as well. The line broadening in (a) is mainly due to extensive overlap of the signals: Presumably, the two texaphyrin ring systems are able to rotate freely around the μ-oxo axis which makes the corresponding hydrogen atoms rather indistinguishable on the NMR timescale. Upon addition of TFA, spectrum (b), the μ-oxo bond is believed to break with the now mononuclear texaphyrin systems existing independently in solution.

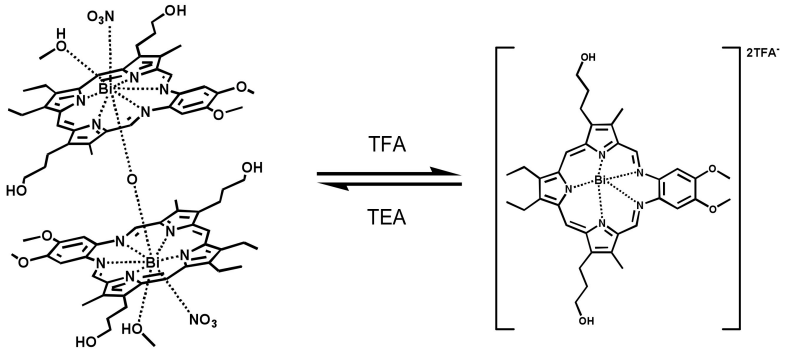

Figure 2.5: Reactions involving the μ-oxo bond in **60** observed upon the addition of trifluoroacetic acid (TFA) and triethylamine (TEA).

(a) No TFA added:

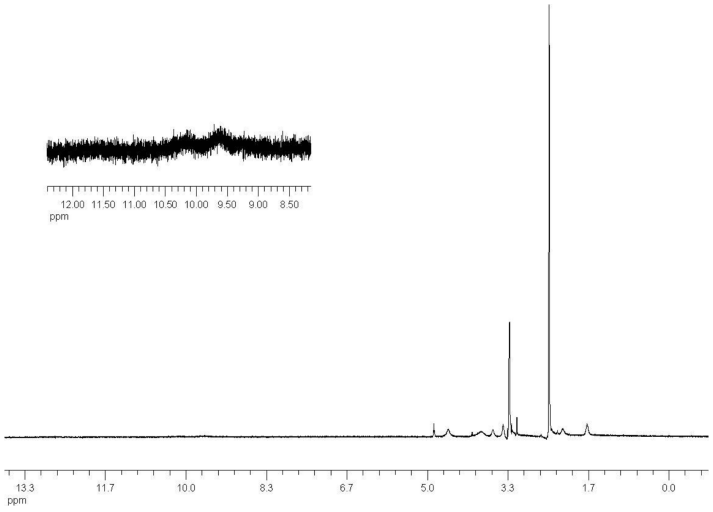

(b) TFA added:

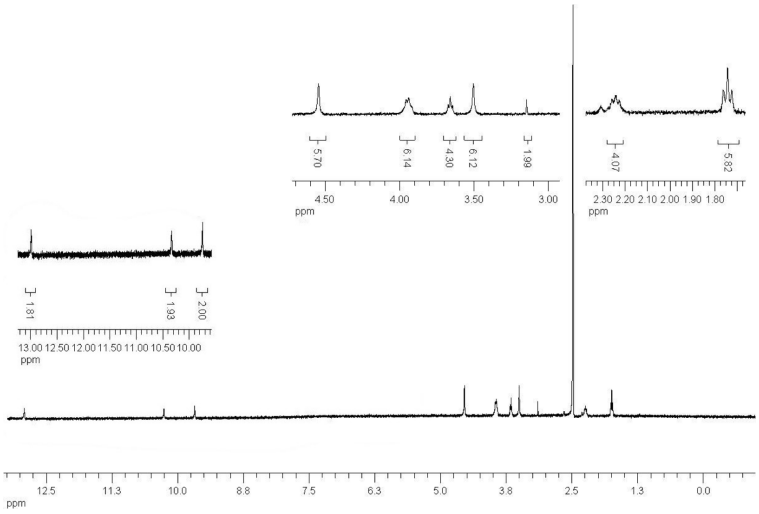

Figure 2.6: ^{1}H NMR spectrum (400 MHz, DMSO-d_6, 25 °C) for **60**. Upon addition of TFA (one equiv), the three signals for the protons on the sp^2 hybridized carbons ('meso' carbons) appear as sharp singlets between 9.5 and 13 ppm.

2.2.2 Kinetics of Metal Insertion

The kinetics of metal insertion were monitored by observing the increase in the absorption at λ_{max} = 478 nm (Soret-like band) as a function of time using commercially available bismuth(III) nitrate or lead(II) nitrate as the cation source. When the reaction was carried out at 75 °C in methanol, the spectral changes associated with the insertion of Bi(III) were completed within 34 minutes (Figure 2.8), leading us to infer that the insertion reaction is also complete. The insertion of Pb(II) was complete after approximately 98 minutes. In other words, the insertion time for Bi(III) is about 50% of the half-life of ^{212}Bi and the insertion time for Pb(II) is about 14% of the half-life of ^{212}Pb. This leads us to infer that texaphyrin may have a role to play as a ligand for the complexation of ^{212}Bi or ^{212}Pb under conditions of α-particle therapy.

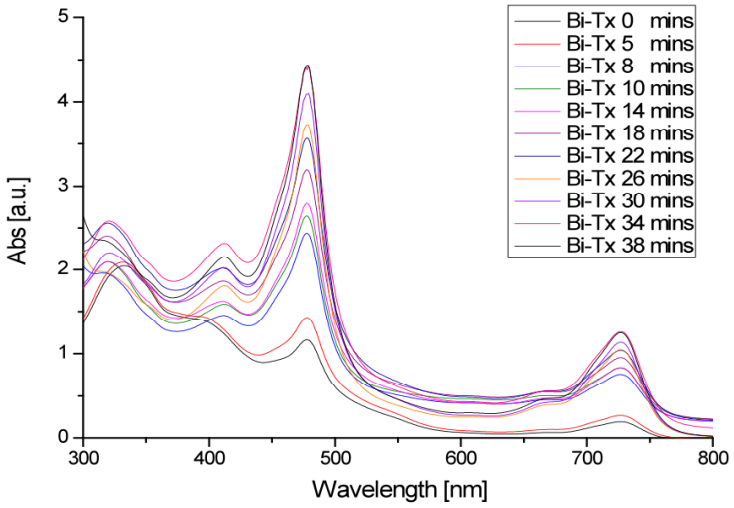

Figure 2.7: Changes in the UV-Vis spectrum of **60** produced when the sp^3 precursor was treated with Bi(III) nitrate in methanol at 75 °C under aerobic conditions. Note that the spectrum recorded at 34 minutes is identical to that recorded at 38 minutes.

2.2.3 Cytotoxicity Studies

In accord with design expectations, the water-soluble texaphyrin derivatives coordinating bismuth (**58**, MBi) and lead (**59**, MPb) displayed high levels of stability in buffered aqueous solution as judged by HPLC analyses. No appreciable decomposition products were observed in solutions of **58** and **59** at pH values ranging from 6 to 7.5. These complexes were thus deemed suitable for biological testing. To determine the inherent cytotoxicity of **58** and **59** towards potential tumor targets, cell proliferation assays were conducted using an A2780 ovarian cancer cell line that was recently found to display sensitivity towards MGd.[20] As shown in Figure 2.9, both MBi **58** and MPb **59** gave IC_{50} values of 2.2 and 2.9 μM, respectively. While such values are not particularly noteworthy *per se*, they are of interest in that they reflect a two to three fold increase in cytotoxicity relative to MGd (IC_{50} = 6.3 μM in this cell line).

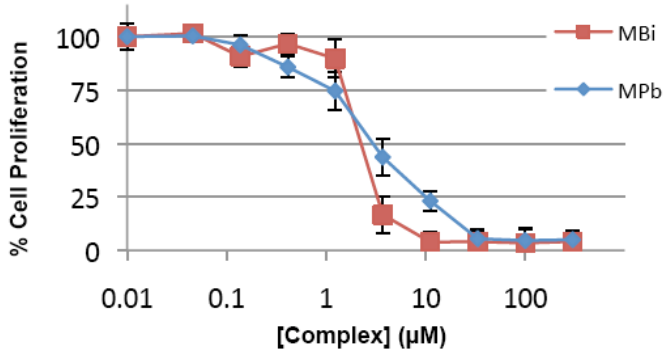

Figure 2.8: Cell proliferation versus complex concentration for MBi and MPb (complexes **58** and **59** of this study) using the A2780 ovarian cancer cell line.

At this point, it is unknown whether the observed cytotoxicity is due to the redox mediation typically noted for texaphyrin complexes[21, 22] or due to heavy metal toxicity, or some combination thereof. However, we favor the former rationale. This is because, in this particular cellular assay, the cytotoxicity (antiproliferative activity) of the free metal salts (i.e. $Bi(NO_3)_3$ and $Pb(NO_3)_2$) was significantly lower than that of the corresponding

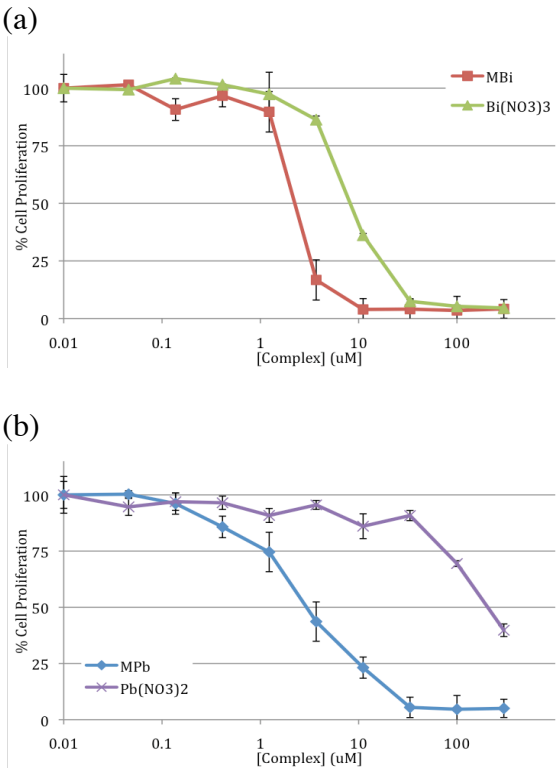

Figure 2.9: Toxicity studies of (a) MBi **58** in comparison with $Bi(NO_3)_3$ and (b) MPb **59** in comparison with $Pb(NO_3)_2$.

metal complexes. Bismuth(III) nitrate has an IC_{50} value of 7.9 μM, and under the conditions of our experiments the IC_{50} value for lead(II) nitrate was found to be between 100 and 300 μM. An accurate value for the latter could not be determined due to solubility limits of the metal salts.

2.3 Conclusions

In summary, we have shown that both the bismuth(III) and lead(II) metal cations form stable complexes with texaphyrins. A single crystal X-ray crystallographic analysis of the bismuth(III) complex **60** reveals that it forms a binuclear μ-oxo sandwich complex that can be cleaved to its corresponding monomer by addition of TFA under non-aqueous conditions. The water-soluble complexes functionalized with polyethylene glycol groups, **58** and **59**, show cyototoxic activity in A2780 ovarian cancer cell lines. On the basis of the present studies and appreciating the tumor-selective properties of texaphyrins, we suggest that this class of ligands would make good complexants for ^{212}Bi, ^{213}Bi, or ^{212}Pb and thus warrant further study as candidates for radiotherapy. The present study also serves to underscore how new coordination modes, namely μ-oxo Bi(III)

complexes, can be stabilized using texaphyrins as opposed to, e.g., porphyrins. This provides an incentive to study further the fundamental coordination chemistry of this and other new porphyrin analogues.

All compounds were synthesized, purified and characterized by the author. All X-ray quality single crystals were grown by the author. All cytotoxicity studies were performed by Dr. Jonathan F. Arambula at The University of Texas MD Anderson Cancer Center under supervision of Dr. Zahid H. Siddik. All crystal structures were solved and refined by Dr. Vincent M. Lynch of the Department of Chemistry and Biochemistry at The University of Texas at Austin. Dr. Jonathan L. Sessler supervised the project.

Sections of this Chapter were taken from Preihs, C.; Arambula, J. F.; Lynch, V. M.; Siddik, Z. H.; Sessler, J. L., *Chem. Commun.* **2010**, *46*, 7900-7902.

References

(1) Baxter, G. F. *Chem. Ber.* **1992**, *28*, 445-448.

(2) Kozak, R. W.; Waldmann, T. A.; Atcher, R. W.; Gansow, O. A. *Trends Biotechnol.* **1985**, *4*, 259-264.

(3) Kumar, K.; Magerstädt, M.; Gansow, O. A. *J. Am. Chem. Soc., Chem. Commun.* **1989**, 145-146.

(4) Hancock, R. D.; Cukrowski, I.; Baloyi, J.; Mashishi, J. *J. Chem. Soc., Dalton Trans.* **1993**, 2895-2899.

(5) Luckay, R.; Reibenspies, J. H.; Hancock, R. D. *J. Chem. Soc., Chem. Commun.* **1995**, 2365-2366.

(6) Hancock, R. D.; Maumela, H.; de Sousa, A. S. *Coord. Chem. Rev.* **1996**, *148*, 315-347.

(7) Wullens, H.; Devillers, M.; Tinant, B.; Declercq, J.-P. *J. Chem. Soc., Dalton Trans.* **1996**, 2023-2029.

(8) Brechbiel, M. W.; Pippin, C. G.; McMurry, T. J.; Milenic, D.; Roselli, M.; Colcher, D.; Gansow, O. A. *J. Chem. Soc., Chem. Commun.* **1991**, 1169-1170.

(9) Treibs, A. *Justus Liebigs Ann. Chem.* **1969**, *728*, 115-148.

(10) Buchler, J. W.; Lay, K. L. *Inorg. Nucl. Chem. Lett.* **1974**, *10*, 297-300.

(11) Barbour, J.; Belcher, W. J.; Brothers, P. J.; Rickard, C. E. F.; Ware, D. C. *Inorg. Chem.* **1992**, *31*, 746-754.

(12) Michaudet, L.; Fasseur, D.; Guilard, R.; Ou, Z.; Kadish, K. M.; Dahoui, S.; Lecomte, C. *J. Porphyrins Phthalocyanins* **2000**, *4*, 261-270.

(13) Chacko, G.-P.; Hambright, P. *Inorg. Chem.* **1994**, *33*, 5595-5597.

(14) Boitrel, B.; Breede, M.; Brothers, P. J.; Hodgson, M.; Michaudet, L.; Rickard, C. E. F.; Al Salim, N. *Dalton Trans*. **2003**, 1803-1807.

(15) Halime, Z.; Lachkar, M.; Furet, E.; Halet, J.-F.; Boitrel, B. *Inorg. Chem*. **2006**, *45*, 10661-10669.

(16) Halime, Z.; Lachkar, M.; Roisnel, R.; Furet, E.; Halet, J.-F.; Boitrel, B. *Angew. Chem. Int. Ed*. **2007**, *46*, 5120-5124. Figures reprinted with permission from Halime, Z.; Lachkar, M.; Roisnel, R.; Furet, E.; Halet, J.-F.; Boitrel, B. *Angew. Chem. Int. Ed*. **2007**, *46*, 5120-5124. DOI: 10.1002/anie.200700543, article first published online: 30 May 2007. Copyright 2007 WILEY-VCH Verlag GmbH & Co. KGA, Weinheim, Germany.

(17) Barkigia, K. M.; Fajer, J.; Adler, A. D.; Williams, G. J. B. *Inorg. Chem*. **1980**, *19*, 2057-2061.

(18) Sayer, P.; Gouterman, M.; Connell, C. R. *Acc. Chem. Res*. **1982**, *15*, 73-79.

(19) See Reference (88) in Chapter 1.

(20) Arambula, J. F.; Sessler, J. L.; Fountain, M. E.; Wei, W.; Magda, D.; Siddik, Z. H. *Dalton Trans*. **2009**, *48*, 10834–10840.

(21) Magda, D.; Sessler, J. L.; Gerasimchuk, N.; Miller, R. A. In *Medicinal Inorganic Chemistry*, Sessler, J. L.; Doctrow, S.; McMurry, T.; Lippard, S. J. Eds. American Chemical Society Symposium Series 903, Oxford University Press, **2005**.

(22) Evens, A. M.; Lecane, P.; Magda, D.; Prachand, S.; Singhal, S.; Nelson, J.; Miller, R. A.; Gartenhaus, R. B.; Gordon, L. I. *Blood*, **2005**, *105*, 1265–1273.

3. Gadolinium Texaphyrin Functionalized Magnetic Nanoparticles

3.1. Development of Dual Mode MRI Contrast Agents

Achieving high accuracy and precision are the main challenges in a variety of imaging techniques used in disease diagnostics such as positron emission tomography (PET), computed tomography (CT), optical microscopy and magnetic resonance imaging (MRI). As discussed in Chapter 1 of this dissertation, MRI is a powerful technique for producing tomographic images of biological targets in a noninvasive manner and with a high spatial resolution. Basic MRI scans often involve so-called T_1 weighted scans, a term that refers to a set of standard scans that depict differences in the spin-lattice relaxation time of various tissues within the body. In the body, T_1 weighted scans work well for differentiating fat from water, with water appearing darker and fat brighter. In contrast, T_2 weighted scans depict differences in the spin-spin relaxation time and result in fatty tissues appearing darker in the MRI image and regions with high water concentrations appearing brighter. Typically, T_1 contrast agents are comprised of

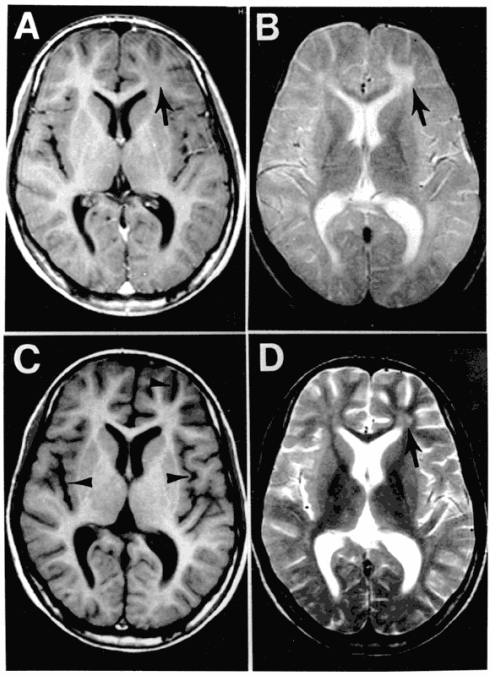

Figure 3.1: Representation of T_1 and T_2 MRI modes (taken from a patient suffering from complications from measles).
(A) and **(C)** are T_1 weighted images, **(B)** and **(D)** are T_2 weighted images. Note the hypointense (dark) signal on the T_1-weighted image (arrow in A) and a hyperintense (bright) signal on the T_2-weighted image (arrow in B).[1]

paramagnetic materials, such as manganese oxide nanoparticles or gadolinium complexes.[2, 3] T_2 contrast agents commonly consist of superparamagnetic nanoparticles (e.g., iron oxide).[3-5] Unfortunately, such single mode contrast agents are far from ideal, particularly when accurate imaging of small biological targets is required.[6, 7] Therefore, multimodality imaging techniques combining the imaging results from two or more devices, have been employed in an effort to increase the accuracy of disease diagnosis and improve therapeutic outcome.[8-11] Clinically, the best example of multimodality imaging is seen in the rapid evolution of PET-SPECT (Single-photon emission computed tomography) and PET-CT scanner hybrids. Hence, the PET modality has developed into perhaps the most used multimodal imaging method.[12]

However, the implementation of multimodal imaging techniques is far from ideal. For instance, discrepancies resulting from different penetration depths and spatial/time resolutions of multiple imaging devices can lead to inaccuracies and unintentional errors in disease diagnostics.

Therefore, the development of dual imaging strategies and devices that employ a single instrumental system represent an attractive target since they overcome the inherent disadvantages associated with more classic multimodal imaging techniques.

Prof. Jinwoo Cheon (Yonsei University, Seoul, Korea) and coworkers were the first to develop magnetic nanoparticles that can act as dual-mode MRI contrast agents. In their seminal studies they use a so-called "magnetically decoupled" core-shell design, which is described in greater detail below. This leads to the generation of two different T_1 and T_2 imaging modes that are utilized simultaneously, potentially leading to more accurate MR imaging.[13]

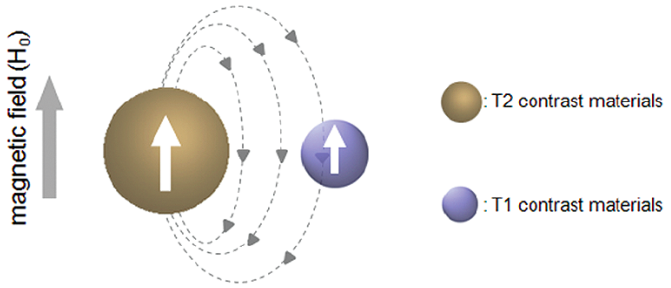

Figure 3.2: Electronic spins of paramagnetic T_1 contrast materials affected by a magnetic field from superparamagnetic T_2 contrast materials when they are in close proximity.[13]

The difficulties associated with the efficient design of T_1 and T_2 dual-mode MRI contrast agents is at least in part due to the fact that, in the case of a direct contact of the T_1 active and the T_2 active compounds, the magnetic field generated by the super-paramagnetic T_2 contrast material perturbs the relaxation process of the paramagnetic T_1 contrast material. This phenomenon induces the quenching of the T_1 signal.[13] Therefore, a rational design of a T_1 and T_2 dual mode MRI contrast agent requires the physical insertion of a separating layer between the T_1 contrast material and the T_2 contrast material. One example of such a sophisticated design is shown in Figure 3.3.[13] Here, the T_2 contrast material ($MnFe_2O_4$) is located in the core of the nanoparticle, while the T_1 contrast material ($Gd_2O(CO_3)_2$) is located on the shell. A silicon dioxide layer with varying thicknesses is able to isolate both materials sufficiently from each other. In applying this strategy, Prof. Cheon and coworkers have been able to develop

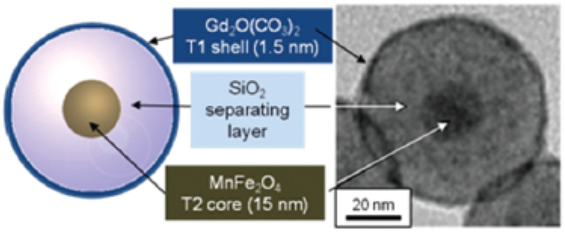

Figure 3.3: Schematic and transmission electron microscope (TEM) image of core-shell type dual mode contrast agents.[13]

nanoparticles that function as the first efficient dual mode MRI contrast agents (DMCA) with enhanced contrast effects in both T_1 and T_2 modes.[13]

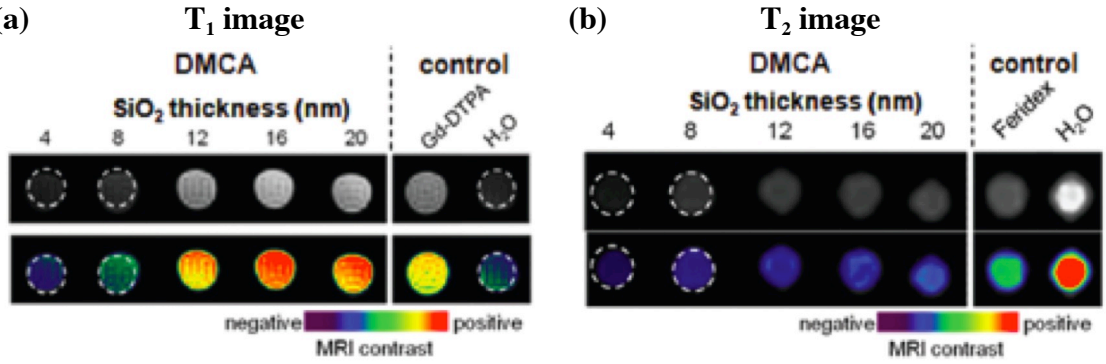

Figure 3.4: (a) T_1 and (b) T_2 weighted MR images and their color-coded images of DMCA with varying SiO_2 thickness by using a 4.7 Tesla MRI machine. Contrast agents: 200 μM (Gd) for the T_1 image, 100 μM (Mn + Fe) for the T_2 images. The images of Gd-DTPA (DTPA = diethylenetriamine-pentacetate) and Feridex (ferumoxides) were taken together for the purpose of comparison. In the color-coded image, positive and negative contrasts are indicated by the red and blue colors, respectively.[13]

This project was undertaken with the initial goal of using texaphyrin macrocycles as T_1 contrast material in Prof. Cheon's DMCA systems. In doing so it was demonstrated that texaphyrin functionalized magnetic nanoparticles are efficient dual-mode MRI contrast agents but can also effectively sensitize cancer cells to make them highly vulnerable to apoptotic magnetic hyperthermia at low temperatures. These findings will be discussed in subsequent sections. Before the discussion of these experimental results, the concept of magnetic hyperthermia as an experimental anticancer treatment method will be introduced.

3.2 MAGNETIC HYPERTHERMIA AS EXPERIMENTAL ANTICANCER TREATMENT

Temperature control is an important self-defense tool for many higher organisms. For example, one response mounted by humans in an effort to fight injury including viral and bacterial infections, involves an increase in body temperature. This reaction produces the well-recognized symptoms of fever.[14, 15] Today, the idea of using artificial temperature control for disease treatment is being realized with the aid of various techniques, such as ultrasound, near-infrared light, and magnetic fields by increasing localized temperature in a targeted region, i.e. hyperthermia.[16-21] Magnetic nanoparticles have attracted considerable attention for hyperthermia applications due to their unique ability to generate heat effectively when exposed to an alternating magnetic field (AMF). More

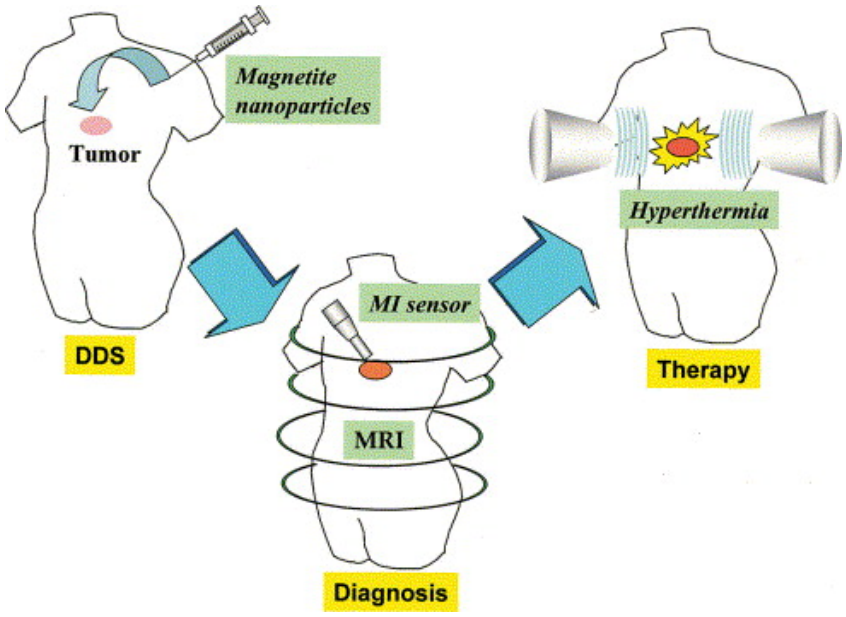

Figure 3.5: Schematic illustration of a therapeutic strategy involving the use of magnetic nanoparticles as a tool for cancer diagnosis via MRI enhancement (or as magnetoimpedance (MI) sensors). Therapy via hyperthermia can then be induced by exposure to an alternating magnetic field (AMF).[22]

importantly, this can be achieved without limitations in penetration depth.[23-34] Hyperthermia, the artificially induced heat treatment of a disease, uses temperatures ranging between 42 ºC and 47 ºC. Generally speaking, temperatures below 45 ºC induce apoptotic cell death.[35, 36] As compared to necrosis, i.e. the premature death of cells in living tissue, apoptosis is a far more benign form of "programmed" cell death.[37] Nonliving cells produced as the result of apoptotic process are cleaned by phagocytosis without affecting neighboring normal cells. In contrast, necrosis, such as that produced by harsh and high temperature hyperthermia, is considered relatively harmful since it can be correlated with inflammatory disease and metastasis.[38, 39] Unfortunately, effective hyperthermia under apoptotic conditions is often difficult to achieve due to the fact that cells typically acquire resistance to induced thermal stress.[40-42] In fact, repeated exposure to high temperatures with a high concentration of magnetic nanoparticles is usually necessary to reach a sufficient level of therapeutic efficacy. Regrettably, these conditions favor necrotic cell death rather than apoptosis. Because cancer cells are more susceptible to heat, initial heat damage in cancer cells can be observed at temperatures of approximately 43 °C. While healthy cells and normal tissue remain mostly undamaged at these temperatures,[43, 44] the goals of selective, cancer focused hyperthermia at this and other relatively low temperatures defines a recognized but unmet goal.

3.3 Use of Texaphyrin Functionalized Magnetic Nanoparticles With Dual-Mode MRI Activity For ROS Production and Hyperthermia Treatment

In collaboration with Prof. Jinwoo Cheon we introduced a new design concept for a double effector magnetic nanoparticle system for high performance apoptotic mild hyperthermia. Double effector nanoparticles are composed of two functional components, which serve as sources of reactive oxygen species (ROS) and efficient heat production.

We demonstrate that ROS-generating magnetic nanoparticles can effectively sensitize cancer cells to make them highly vulnerable to subsequent apoptotic magnetic hyperthermia at low temperatures (Scheme 3.1).

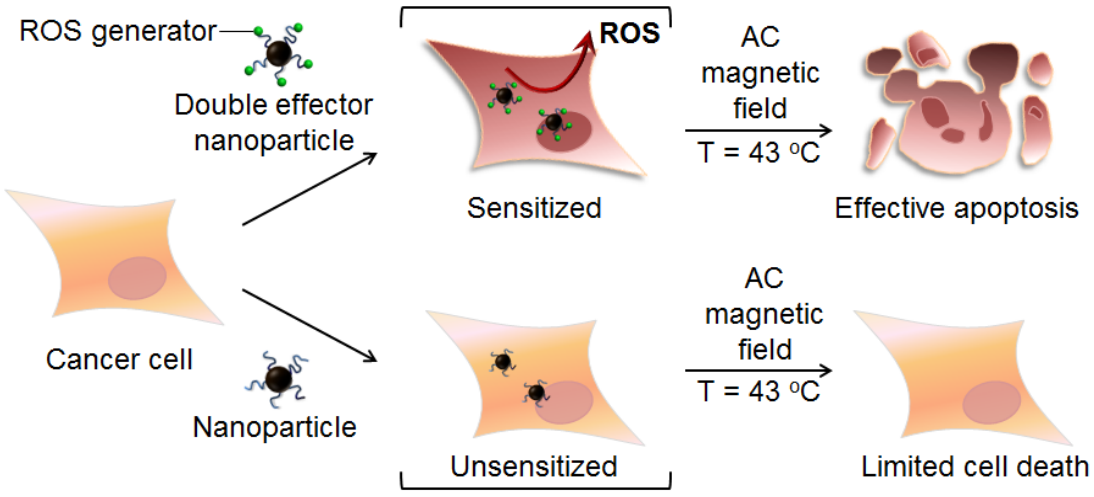

Scheme 3.1: Double effector nanoparticles for apoptotic magnetic hyperthermia. Double effector nanoparticles generate reactive oxygen species (ROS). ROS sensitize cancer cells to hyperthermia even at relatively low temperatures (~43 °C). This sensitization strategy is effective for apoptotic hyperthermia, both *in vitro* and *in vivo*. Conventional unsensitized hyperthermia results in only marginal efficacy.

3.3.1 Preparation of Texaphyrin Functionalized Nanoparticles

The synthesis of these double effector nanoparticles starts with the synthesis of a texaphyrin species with an appended amine functionality. Generally, the hydroxy functionality in **11** is rather unreactive towards a variety of functionalization reactions. However, the conversion of the alcohol to an amine via Mitsunobu reaction can be carried out efficiently.[45] Prior to the Mitsunobu reaction, one OH-group has to be protected using 4,4'-dimethoxytrityl chloride as a protecting group. The Mitsunobu

reaction and deprotection using acetic acid then yields the amine functionalized texaphyrin **63**. While this texaphyrin species is considerably less stable than **11** and prone to hydrolysis, it is also more reactive towards functionalization of the appended amino group. The texaphyrin species **63** obtained can be linked (via *in situ* reaction with disuccinimidyl suberate) to nanoparticles bearing amine functionalities on the surface (Scheme 3.2).

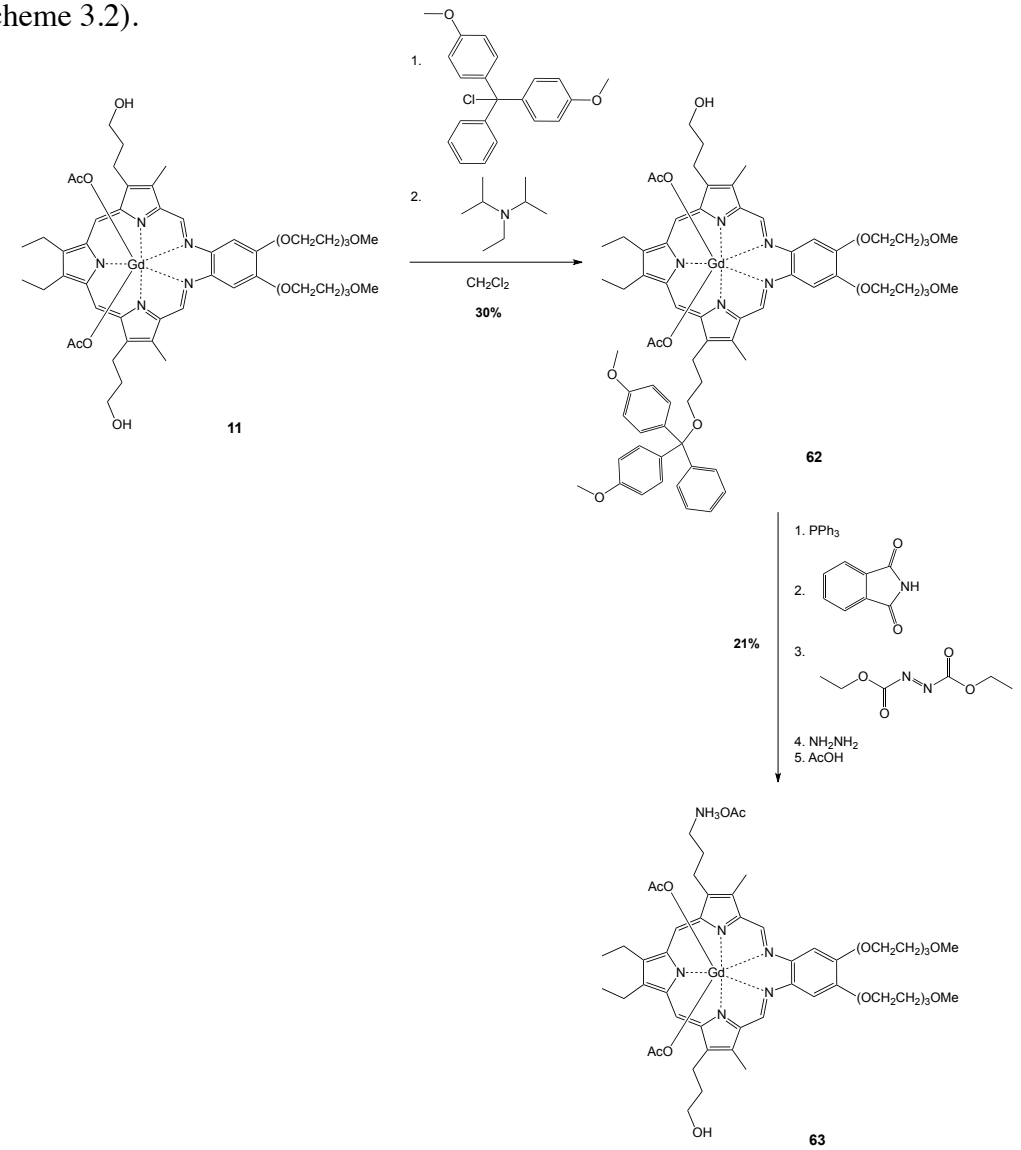

Scheme 3.2: Synthesis of amine functionalized texaphyrin **63**.

With the amine functionalized texaphyrin **63** in hand, the next step involves the functionalization of the magnetic nanoparticles. For this conversion, it turned out to be advantageous to first react the amine functionality on the texaphyrin scaffold with disuccinimidyl suberate, a compound frequently used in bioconjugation methods as a protein cross-linking agent. However, due to instability of the resulting NHS-appended texaphyrin, this reaction has to be performed in situ with **64** instantly reacting with the nanoparticles.

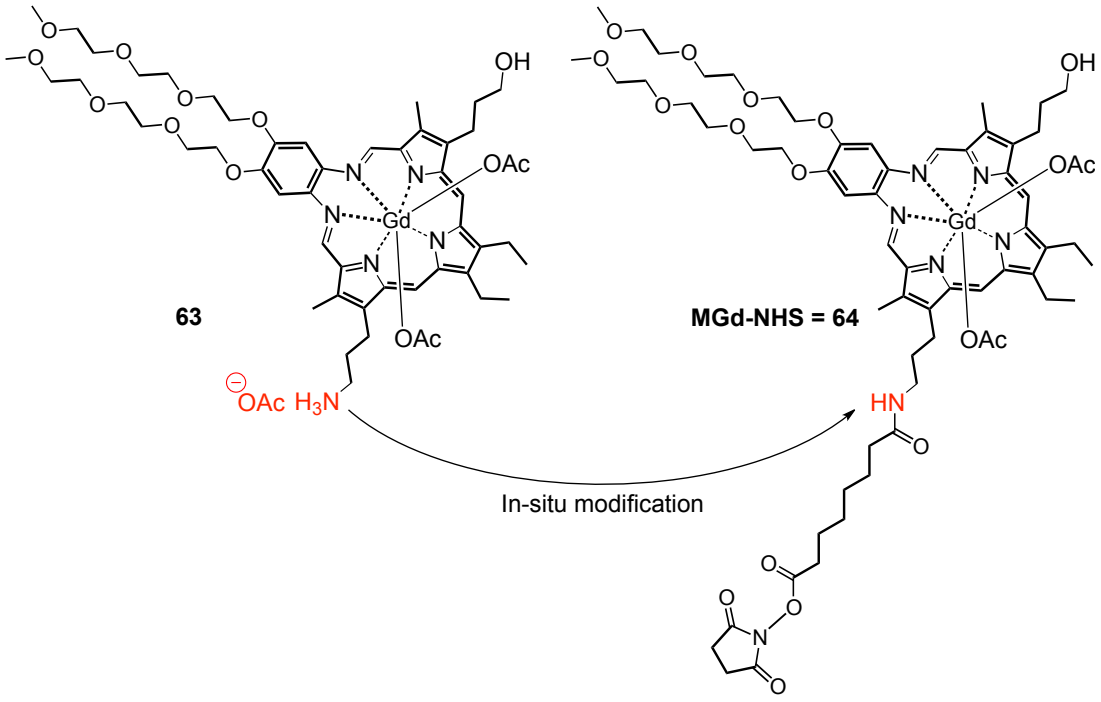

Scheme 3.3: *In situ* preparation of MGd-NHS **64**.

After multiple ineffective functionalization attempts, it was concluded that a long linker between the nanoparticle surface and the texaphyrin unit is necessary for a successful conjugation step. The nanoparticles used in this study contain a zinc doped iron oxide core (T_2 active material) coated with a layer of silicon dioxide functioning as a separating layer. Further functionalization of the hydroxy functionalities on the SiO_2 layer

with 3-aminopropyltrimethoxysilane (APTMS) followed by reacton with succinic anhydride results in the formation of terminal COOH-groups on the surface. Conjugation of the latter groups via EDC/Sulfo-NHS (N-hydroxysulfosuccinimide) with poly(ethylene glycol) bis(amine) then results in the formation of terminal amines that can be subjected to the final conjugation step with **64** (Scheme 3.4).

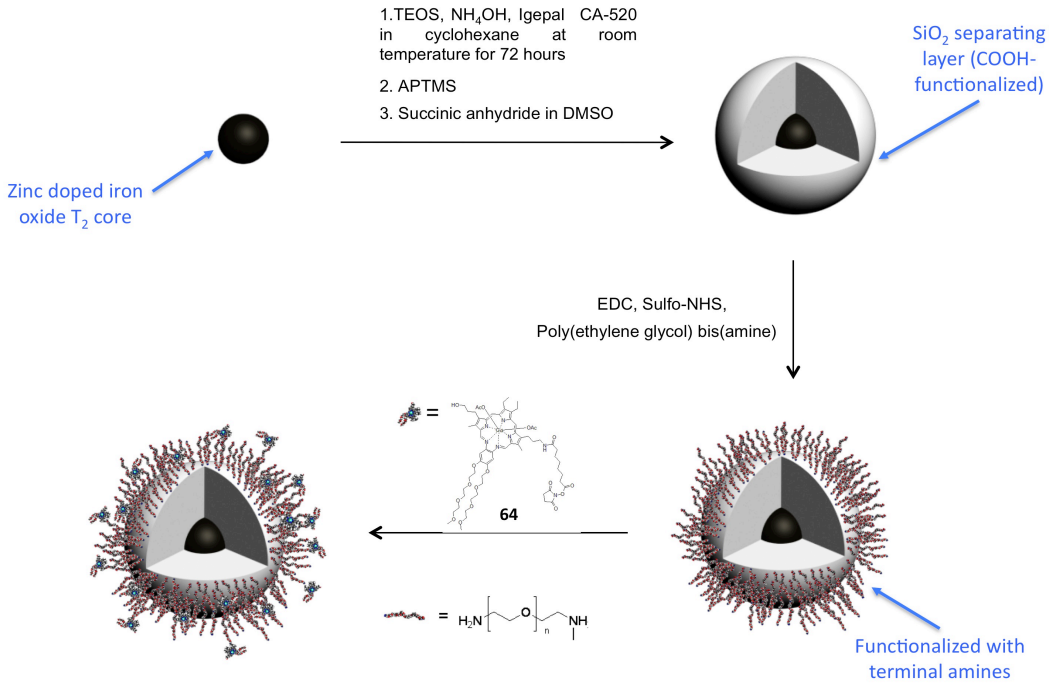

Scheme 3.4: Funtionalization of nanoparticles with texaphyrin **64**.

The presence of the gadolinium texaphyrin (GdTx) units on the magnetic nanoparticles (MNPs) was confirmed by UV-Vis absorption spectroscopy, which revealed the presence of spectral features ascribable to both the gadolinium

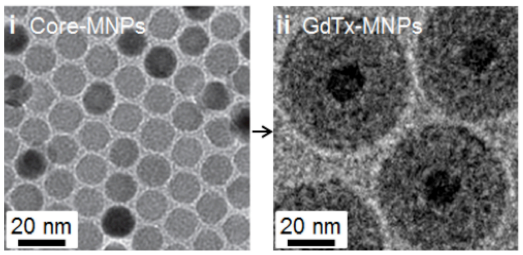

Figure 3.6: TEM images of (i) core-MNPs and (ii) GdTx-MNPs

texaphyrin and magnetic nanoparticles in the spectrum.

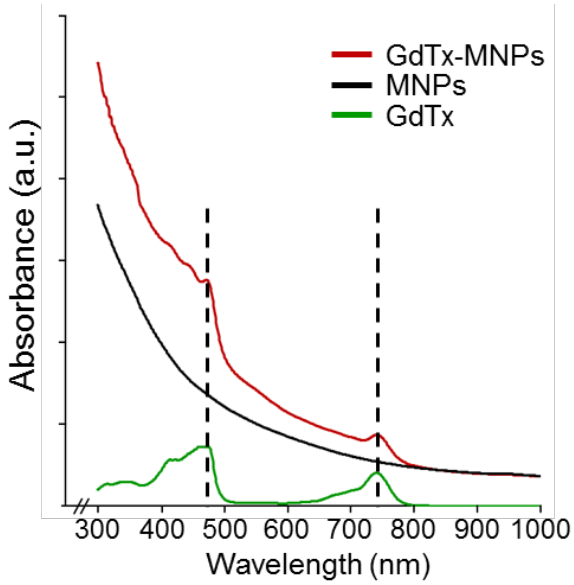

Figure 3.7: UV-Vis absorption spectra of gadolinium texaphyrin (green), magnetic nanoparticles (black), and GdTx-MNPs (red). The spectrum of the latter corresponds to a linear combination of the individual spectra of the gadolinium texaphyrin and the magnetic nanoparticles.

3.3.2 *In vitro* Experiments with GdTx-MNPs

In accord with what is expected for a magnetic nanoparticle containing appended gadolinium texaphyrin moieties, an MRI phantom study reveals both T_1 and T_2 contrast enhancements, a finding that provides support for the notion that conjugation had been successfully achieved.[13] Simultaneous T_1 bright and T_2 dark contrast effects are ascribable to the gadolinium texaphyrin (T_1 active material) and magnetic nanoparticle (T_2 active material) portions of the constructs, respectively (Figure 3.8). In contrast, MR images associated with the control groups display either only bright T_1 contrast or dark T_2 contrast, but not both.

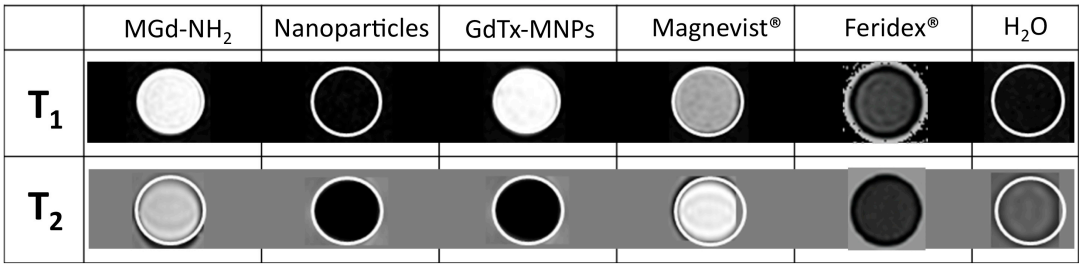

Figure 3.8: MRI contrast images of several contrast materials (T_1 and T_2 modes shown).

The internalization of GdTx-MNP conjugates into cancer cells and the generation of reactive oxygen species (ROS) was examined using optical methods (Figure 3.9). This was done by monitoring the oxidation of 2′,7′-dichloro-fluorescein diacetate (DCFA, Molecular Probes) and its ensuing conversion to 2′,7′-dichlorofluorescein (DCF).[46] After the addition of GdTx-MNPs to MDA-MB-231 cells (a breast cancer cell line), a weak red fluorescence signal is observed, which is ascribed to the gadolinium texaphyrin portion of the internalized GdTx-MNPs (Figure 3.9 (ii)). In analogy to what proved true for MGd, the internalized

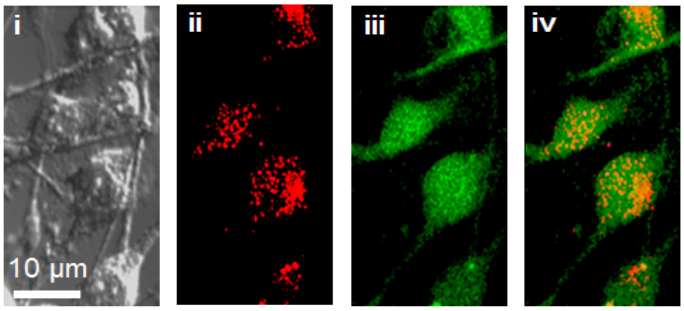

Figure 3.9: Intracellular uptake of GdTx-MNPs and their ROS generation in MDA-MB-231 cells. Confocal microscopic images of MDA-MB-231 cells treated with GdTx-MNPs. **(i)** Differential interference contrast (DIC) image of GdTx-MNPs treated MDA-MB-231 cells, **(ii)** Internalized GdTx-MNPs are shown in a red fluorescence of GdTx, **(iii)** ROS generation is manifest by green fluorescence, which results from oxidation of 2',7'-dichlorofluorescein diacetate (DCFA) to 2',7'-dichloro-fluorescein (DCF). (iv) Overlay of red and green fluorescence gives a yellow color.

GdTx-MNPs are expected to react with cellular metabolites, such as ascorbate present in cancer cells to generate ROS. The initial product of these electron transfer processes is superoxide, which is eventually transformed into hydrogen peroxide (see section 1.5.2.1, Figure 1.14). In the present instance, support for the proposed ROS came from the observation of a green fluorescence that has spread within the cells (Figure 3.9 (iii)). GdTx-MNPs and the proposed ROS generation in the same cell are inferred from an overlay of red and green fluorescence resulting in a yellow color (Figure 3.9 (iv)).

GdTx-MNPs display a high specific loss power (=heating power) value (471 Wg^{-1}), which is four times higher than the commercially available iron oxide nanoparticle, Feridex (an FDA approved MRI contrast agent, Figure 3.10 (a)). As a consequence, it only takes approximately 60 seconds to warm an aqueous medium from 37 ºC to 43 ºC with 0.2 mg/mL of MNPs whereas approximately 250 seconds are required to generate the same degree of warming using an equivalent amount of Feridex® under otherwise identical conditions (Figure 3.10 (b)). The reduced number of GdTx-MNPs required for adequate heat generation is considered a useful feature that may permit lower dosage levels when translated into a clinical setting.

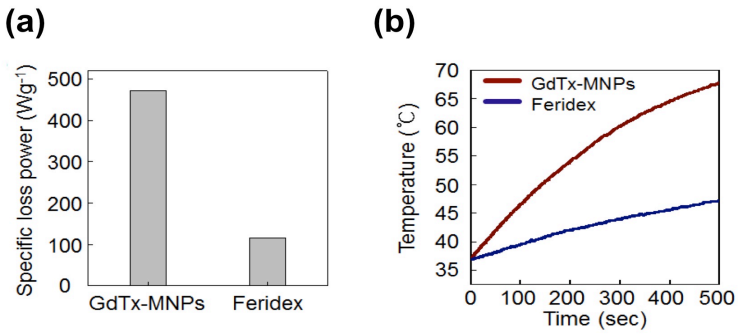

Figure 3.10: (a) Specific loss power value of GdTx-MNPs in comparison with that of Feridex in a 500 kHz AC magnetic field at 30 kAm^{-1}.
(b) Heat profile of 0.2 mg/mL of GdTx-MNPs and Feridex under an AC magnetic field for 500 seconds.

The dual effector nature of the GdTx-MNPs, namely an ability to produce both reactive oxygen species and heat, was initially tested *in vitro*. Towards this end MDA-MB-231 cells (1.0×10^4 cells/well) and 0.2 mg/mL of GdTx-MNPs were coincubated for five hours at a GdTx-concentration of 100 μM. Next, an AC magnetic field was applied. A schematic representation of the experimental setup is shown in Figure 3.11.

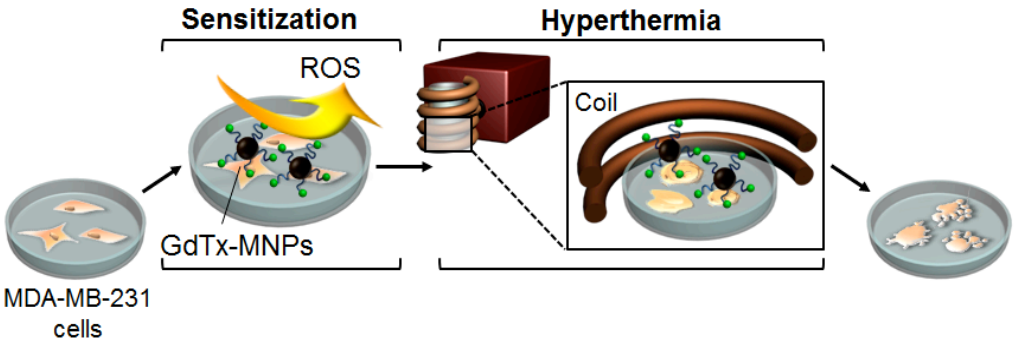

Figure 3.11: Schematic illustration of the *in vitro* experiment. Briefly, GdTx-MNPs treated MDA-MB-231 cells are incubated for five hours and then an AC magnetic field is applied to effect hyperthermia.

The temperature of the medium was found to increase to 43 ºC (±1 ºC). It was then maintained at this temperature for up to 60 min (Figure 3.12 (a)). Cell viability was then measured by CCK-8 assay. In the case of the bare MNPs, cell viability was found to decrease monotonically from 100% to 98%, 90%, 83%, and 75% (blue line, Figure 3.12 (b)) as the time of the hyperthermia treatment is increased (i.e., 0, 10, 20, 30, and 60 min). GdTx-MNPs also reduced the cell viability from 93% to 76%, 66%, 42%, and 36% as the treatment time increased (0, 10, 20, 30, and 60 min) (red line, Figure 3.12 (b)). However, these functionalized MNPs proved more effective.

The slight loss in cell viability observed before magnetic hyperthermia (t = 0) (red line, Figure 3.12 (b)) is caused by surface coated GdTx, an agent that is known for its weak, but noticeable cytotoxic effect through the generation of ROS.[47] We ascribe the

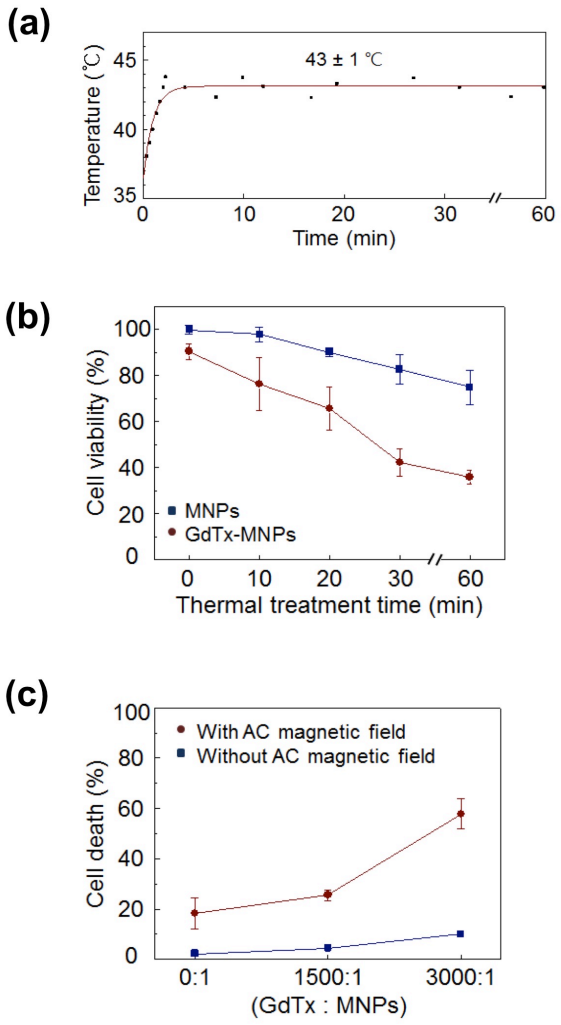

Figure 3.12: (a) Temperature profile. After warming, a temperature of 43 ºC (±1 ºC) is maintained by applying an AC magnetic field of 3.7 kAm^{-1} at 500 kHz. (b) Time dependence of the magnetic hyperthermia treatment effect. Here, 0.2 mg/mL of MNPs and GdTx-MNPs containing 100 μM of GdTx are used. (c) Dependence of the magnetic hyperthermia efficacy on GdTx loading level.

significant enhancement in hyperthermia effects seen with the GdTx-MNPs to ROS mediated sensitization. Although ROS itself show little anti-cancer effect, ROS production dysregulates cancer cell redox homeostasis and induces oxidative stress. These effects, in turn, are expected to render the cells more susceptible to magnetic heat treatment. The dual effect is the most significant at 30 min of thermal treatment where 57% of the cancer cells are eliminated by the GdTx-MNPs after applying an AC magnetic field. In contrast, only 17% of cancer cells are nonviable with MNPs. The amount of GdTx can be correlated with ROS concentration. As the relative GdTx loading level is increased from 0 to 1500 and 3000 (i.e., the number of GdTx molecules conjugated to a given MNP increases), cell death markedly increases from 17% to 21%, and 57%

under magnetic hyperthermia conditions (red line, Figure 3.12 (c)). In contrast, the number of non-viable cells increases only from 0% to 3% and then 7% as the loading level is raised in the absence of an applied AC magnetic field (blue line, Figure 3.12 (c)). This result provided support for the notion that the dominant role of GdTx is as a sensitizer for hyperthermia, rather than as direct cytotoxin.

GdTx-MNPs, under conditions of mediated hyperthermia could potentially kill cancer cells via a number of pathways, including apoptosis and necrosis. In order to determine the predominant cell death pathway induced by the GdTx-MNPs, standard annexin V-fluorescein isothiocyanate (annexin V-FITC) and propidium iodide (PI) staining studies were carried out (Figure 3.13). These assays detect changes in plasma membrane integrity and the release of DNA. Apoptosis initially induces the inversion of phosphatidylserine, which allows for binding to annexin V-FITC, while PI is unable to enter into the

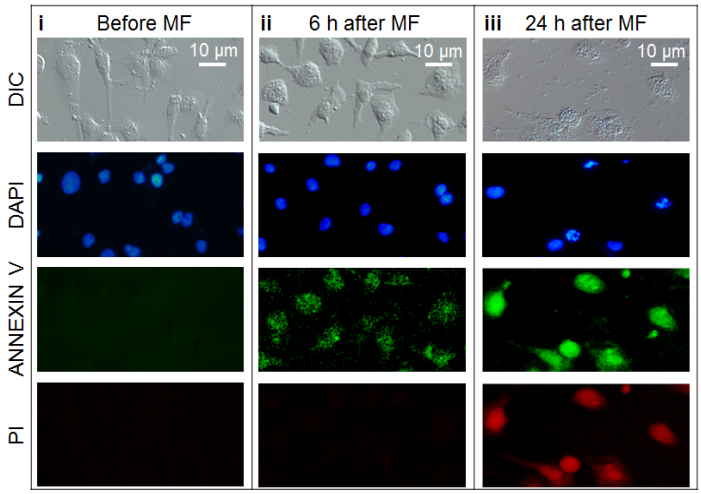

Figure 3.13: Monitoring of the MDA-MB-231 cell death pathway induced by magnetic hyperthermia using GdTx-MNPs. Microscopic images of MDA-MB-231 cells before (i), 6 hours (ii) and 24 hours (iii) after magnetic field application. In these experiments, the nuclei are stained with DAPI (4',6-diamidino-2-phenyl-indole) (blue), and membrane inversion followed by membrane rupture is detected by annexin V-FITC (fluorescein isothio- cyanate) (green) and propidium iodide (red, PI), respectively.

cells to bind to DNA, at least at this initial stage. Before AC magnetic field application, neither annexin V-FITC nor PI-stained cells are detected (Figure 3.13 (i)). At six hours post-hyperthermia treatment, only annexin V-FITC stained cells are detected, a result consistent with the conclusion that the cause of cell death is primarily apoptosis (Figure 3.13 (ii)). If necrosis were occurring, a red fluorescence signal would be observed early on as the result of PI-DNA interactions following membrane rupture. At 24 hours post-hyperthermia treatment, both annexin V and PI stained cells are observed, a finding that presumably reflects membrane rupture, a classic hallmark of late stage apoptosis. (Figure 3.13 (iii)). These results are thus fully consistent with the notion that GdTx-MNPs hyperthermia occurs predominantly through apoptosis.

3.3.3 *In vivo* Experiments with GdTx-MNPs

The Cheon group further tested the efficacy of GdTx-MNPs induced magnetic hyperthermia *in vivo*. MDA-MB-231 breast cancer cells were xenografted to the right hind leg of nude mice in several experimental groups (n = 3). GdTx-MNPs (75 μg), dispersed in normal saline (50 μL), was directly injected into the tumor (100 mm^3). Then, the mouse was placed in a water-cooled magnetic induction coil (Figure 3.14 (a)) and an AC magnetic field (500 kHz at 30 kAm^{-1}) was applied to maintain a constant temperature at the tumor (43 ± 1 ºC) for 30 min. After a single hyperthermia treatment, the tumor size was monitored for 14 days. In the mice making up the untreated control group, the tumor size increased approximately sevenfold by day 14 (Figure 3.14 (b) and (c)). However, for the group receiving hyperthermia treatment with GdTx-MNPs, the tumor was absent after eight days (Figure 3.14 (b) and (c)). For comparison, another group of mice was subjected to hyperthermia treatment after administration of pure MNPs at an identical

dosage. Although the size of the tumor regresses initially, a significant amount of tumor mass remains at day eight ($V/V_{initial} = 0.6$) and the tumor starts to regrow at day 12.

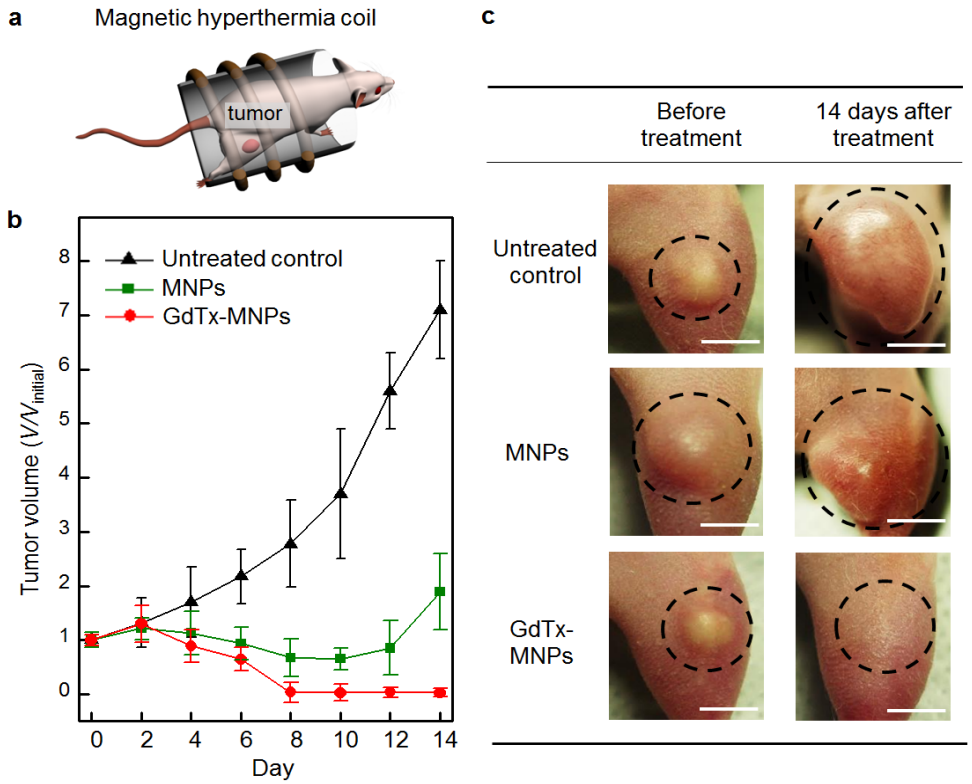

Figure 3.14: *In vivo* magnetic hyperthermia

(a) Schematic representation of the in vivo magnetic hyperthermia study. Magnetic nanoparticles (75 μg) were directly injected into the tumor tissue (tumor volume, 100 mm^3, n = 3) of a mouse and subjected to an AC field for 30 min at 43 ± 1 ºC.
(b) Plot of tumor volume ($V/V_{initial}$) versus the number of days after treatment. In the group treated with GdTx-MNPs hyperthermia (one treatment at 43 ºC for 30 min, red line), the tumor is completely eliminated by day 8, whereas the MNPs hyperthermia group (green line) shows only initial reduction in tumor volume, followed by regrowth.
(c) Images of xenografted tumors (MDA-MB-231) on nude mice before treatment (left column) and 14 days after treatment (right column). Note the different outcomes for untreated control and the mice subjected to hyperthermia with MNPs and GdTx-MNPs. Each scale bar indicates 5 mm.

3.4 CONCLUSIONS

This study, based on the use of double effector nanoparticles, has demonstrated a new approach to achieving apoptotic magnetic hyperthermia. Until now, attempts to use low temperature magnetic hyperthermia for cancer therapy have been challenging due to the development of thermal tolerance. The dramatic reduction in tumor burden seen *in vivo* and the high degree of efficacy seen *in vitro* are ascribed to the sensitization effect arising from ROS, which are thought to play a key role in enhancing the treatment efficacy. The efficient heat generation produced by GdTx-MNPs is also advantageous because lower concentrations of nanoparticles are required to achieve the same biological effect at low temperatures (43 ºC). The pathway of cell death involves predominantly apoptosis, a mode of action that is considered beneficial for ultimate clinical use. Prior to the present study, low temperature hyperthermia and high therapeutic efficacy had proved incompatible. However, the use of the present double effector nanoparticle system allows these seemingly disparate goals to be realized. More broadly, we have shown that it is possible to achieve efficient apoptotic hyperthermia at low temperature.

Important to note is that this project was done in close collaboration with Prof. Jinwoo Cheon's research group at Yonsei University (Seoul, Korea), which the author visited in October 2011. The texaphyrin precursors shown were synthesized by the author at The University of Texas at Austin. While the idea of using GdTx-MNPs for hyperthermia treatment was developed during the author's visit to Yonsei University, all MRI, confocal microscopy, *in vitro* and *in vivo* experiments were carried out by Dr. Dongwon Yoo and Ms. Heeyeong Jeong. Drs. Jinwoo Cheon and Jonathan L. Sessler supervised the project. A manuscript summarizing this project has been published: Yoo, D.; Jeong, H.; Preihs, C.; Choi, J.-S.; Shin, T.-H.; Sessler, J. L.; Cheon, J. *Angew. Chem., Int. Ed.* **2012**, *51*, 1-5. Parts of this Chapter have been taken from this manuscript.

References

(1) http://commons.wikimedia.org/wiki/File:Bonthius1b.gif

By Bonthius, D.; Stanek, N.; Grose, C.; CDC [Public domain, no permission required], via Wikimedia Commons; Retrieved 09-03-2012

(2) Lauffer, R. E. *Chem. Rev.* **1987**, *87*, 901-927.

(3) Na, H. B.; Song, I. C.; Hyeon, T. *Adv. Mater.* **2009**, *21*, 2133-2148.

(4) Arbab, A. S.; Liu, W.; Frank, J. A. *Expert Rev. Med. Devices* **2006**, *3*, 427-439.

(5) Jun, Y.-w.; Lee, J.-H.; Cheon, J. *Angew. Chem., Int. Ed.* **2008**, *47*, 5122-5135.

(6) Caravan, P. *Chem. Soc. Rev.* **2006**, *35*, 512-523.

(7) Bulte, D. L.; Kraitchman, W. M. *NMR Biomed.* **2004**, *17*, 484-499.

(8) Massoud, T. F.; Gambhir, S. S. *Gene. Dev.* **2003**, *17*, 545-580

(9) Nahrendorf, M.; Zhang, H.; Hembrador, S.; Panizzi, P.; Sosnovik, D. E.; Aikawa, E.; Libby, P.; Swirski, F. K.; Weissleder, R. *Circulation* **2008**, *117*, 379-387.

(10) Cheon, J.; Lee, J.-H. *Acc. Chem. Res.* **2008**, *41*, 1630-1640.

(11) Gao, J. H.; Gu, H. W.; Xu, B. *Acc. Chem. Res.* **2009**, *42*, 1097-1107.

(12) Mosley, M.; Donnan, G. *Stroke* **2004**, *35*, 2632-2634.

(13) Choi, J.-s.; Lee, J.-H.; Shin, T.-H.; Song, H.-T.; Kim, E. Y.; Cheon, J. *J. Am. Chem. Soc.* **2010**, *132*, 11015-11017. Figures reprinted with permission from Choi, J.-s.; Lee, J.-H.; Shin, T.-H.; Song, H.-T.; Kim, E. Y.; Cheon, J. *J. Am. Chem. Soc.* **2010**, *132*, 11015-11017. Copyright 2010 American Chemical Society.

(14) Raison, C. L.; Miller, A. H. *Mol. Psychiatry* **2012**, 1–23, *and references therein*.

(15) Kluger, M. J. In *Fever: Its Biology, Evolution, and Function*, Princeton University Press, Princeton **1979**.

(16) Su, Y.; Wei, X.; Peng, F.; Zhong, Y.; Lu, Y.; Su, S.; Xu, T.; Lee, S.-T.; He, Y. *Nano Lett*. **2012**, *12*, 1845-1850.

(17) Barreto, J. A.; O'Malley, W.; Kubeil, M.; Graham, B.; Stephan, H.; Spiccia, L. *Adv. Mater*. **2011**, *23*, H18-H40.

(18) Kuo, W.-S.; Chang, C.-N.; Chang, Y.-T.; Yang, M.-H.; Chien, Y.-H.; Chen, S.-J.; Yeh, C.-S. *Angew. Chem., Int. Ed*. **2010**, *49*, 2711-2715.

(19) Hu, K.-W.; Liu, T.-M.; Chung, K.-Y.; Huang, K.-S.; Hsieh, C.-T.; Sun, C.-K.; Yeh, C.-S. *J. Am. Chem. Soc*. **2009**, *131*, 14186-14187.

(20) Fortin, J.-P.; Wilhelm, C.; Servais, J.; Ménager, C.; Bacri, J.-C.; Gazeau, F. *J. Am. Chem. Soc*. **2007**, *129*, 2628-2635.

(21) Hiraoka, M.; Nagata, Y.; Mitsumori, M.; Sakamoto, M.; Masunaga, S. *AIP Conf. Proc*. **2004**, *716*, 102-105.

(22) Ito, A.; Shinkai, M.; Honda, H.; Kobayashi, T. *J. Biosci. Bioeng*. **2005**, *100*, 1-11.

Figure reprinted with permission from Ito, A.; Shinkai, M.; Honda, H.; Kobayashi, T. *J. Biosci. Bioeng*. **2005**, *100*, 1-11. Copyright 2005 The Society for Biotechnology, Japan. Published by Elsevier B.V. All rights reserved.

(23) Colombo, M.; Carregal-Romero, S.; Casula, M. F.; Gutiérrez, L.; Morales, M. P.; Böhm, I. B.; Heverhagen, J. T.; Prosperi, D.; Parak, W. *J. Chem. Soc. Rev*. **2012**, *41*, 4306-4334.

(24) Noh, S.-h.; Na, W.; Jang, J.-t.; Lee, J.-H.; Lee, E. J.; Moon, S. H.; Lim, Y.; Shin, J.-S.; Cheon, *J. Nano Lett*. **2012**, *12*, 3716-3721.

(25) Bae, K. H.; Park, M.; Do, M. J.; Lee, N.; Ryu, J. H.; Kim, G. W.; Kim, C.; Park, T. G.; Hyeon, T. *ACS Nano* **2012**, *6*, 5266-5273.

(26) Guardia, P.; Di Corato, R.; Lartigue, L.; Wilhelm, C.; Espinosa, A.; Garcia-Hernandez, M.; Gazeau, F.; Manna, L.; Pellegrino, T. *ACS Nano* **2012**, *6*, 3080-3091.

(27) Lartigue, L.; Innocenti, C.; Kalaivani, T.; Awwad, A.; del Mar Sanchez Duque, M.; Guari, Y.; Larionova, J.; Guerin, C.; Montero, J.-L. G.; Barragan-Montero, V.; Arosio, P.; Lascialfari, A.; Gatteschi, D.; Sangregorio, C. *J. Am. Chem. Soc.* **2011**, *133*, 10459-10472.

(28) Lee, J.-H.; Jang, J.-t.; Choi, J.-s.; Moon, S. H.; Noh, S.-h.; Kim, J.-w.; Kim, J.-G.; Kim, I. S.; Park, K. I.; Cheon, *J. Nature Nanotechnol.* **2011**, *6*, 418-422.

(29) Ho, D.; Sun, X.-L.; Sun, S.-H. *Acc. Chem. Res.* **2011**, *44*, 875-882.

(30) Yoo, D.; Lee, J.-H.; Shin, T.-H.; Cheon, J. *Acc. Chem. Res.* **2011**, *44*, 863-874.

(31) Cole, A. J.; Yang, V. C.; David, A. E. *Trends Biotechnol.* **2011**, *29*, 323-332.

(32) Riehemann, K.; Schneider, S. W.; Luger, T. A.; Godin, B.; Ferraro, M.; Fuchs, H. *Angew. Chem., Int. Ed.* **2009**, *48*, 872-897.

(33) Shi, D.; Cho, H. S.; Chen, Y.; Xu, H.; Gu, H.; Lian, J.; Wang, W.; Liu, G.; Huth, C.; Wang, L.; Ewing, R. C.; Budko, S.; Pauletti, G. M.; Dong, Z. *Adv. Mater.* **2009**, *21*, 2170-2173.

(34) Sonvico, F.; Mornet, S.; Vasseur, S.; Dubernet, C.; Jaillard, D.; Degrouard, J.; Hoebeke, J.; Duguet, E.; Colombo, P.; Couvreur, P. *Bioconjugate Chem.* **2005**, *16*, 1181-1188.

(35) O'Neill, K. L.; Fairbairn, D. W.; Smith, M. J.; Poe, B. S. *Apoptosis* **1998**, *3*, 369-375.

(36) Harmon, B. V.; Corder, A. M.; Collins, R. J.; Gobé, G. C.; Allen, J.; Allan, D. J. Kerr, J. F. R. *Int. J. Radiat. Biol.* **1990**, *58*, 845-858.

(37) Kanduc, D.; Mittelman, A.; Serpico, R.; Sinigaglia, E.; Sinha, A. A.; Natale, C.; Santaroce, R.; Di Corcia, M. G.; Lucchese, A.; Dini, L.; Pani, P.; Santacroce, S.; Simone, S.; Bucci, R.; Farber, E. *Int. J. Oncol.* **2002**, *21*, 165-170.

(38) Golstein, P.; Kroemer, G. *Trends Biochem. Sci.* **2007**, *32*, 37-43.

(39) Bonfil, R. D.; Bustuoabad, O. D.; Ruggiero, R. A.; Meiss, R. P.; Pasqualini, C. D. *Clin. Expl. Metastasis* **1998**, *6*, 121-129.

(40) Beckham, J. T.; Wilmink, G. J.; Opalenik, S. R.; Mackanos, M. A.; Abraham, A. A.; Takahashi, K.; Contag, C. H.; Takahashi, T.; Jansen, E. D. *Laser Surg. Med.* **2010**, *42*, 752-765.

(41) Huang, L.; Mivechi, N. F.; Moskophidis, D. *Mol. Cell. Biol.* **2001**, *21*, 8575-8591.

(42) Nollen, E. A. A.; Brunsting, J. F.; Roelofsen, H.; Weber, L. A.; Kampinga, H. H. *Mol. Cell. Biol.* **1999**, *19*, 2069-2079.

(43) Van der Zee, J. *Ann. Oncol.* **2002**, *13*, 1173-1184.

(44) Fajardo, L. F. *Cancer Res.* **1984**, *44*, 4826-4835.

(45) Wei, W.-H.; Fountain, M.; Magda, D.; Wang, Z.; Lecane, P.; Mesfin, M.; Miles, D.; Sessler, J. L. *Org. Biomol. Chem.* **2005**, *3*, 3290-3296.

(46) See reference (22) in Chapter 2.

(47) Wondrak, G. T. *Antioxid. Redox Signaling* **2009**, *11*, 3013–3069.

4. *In Vivo* MR imaging of Polymer Micelles Targeted to the Melanocortin 1 Receptor

4.1 INTRODUCTION

Rationally-designed, polymer-based micelle carriers represent a promising approach to the delivery of therapeutic and/or diagnostic agents. They offer a variety of potential advantages as drug delivery systems and could serve to (i) enhance the solubility of lipophilic drugs, (ii) increase circulation times, and (iii) lower the toxicity of the agent in question. Micelles with diameters ranging between 20 and 200 nm are particularly attractive targets due to the fact that particles of this size can escape renal clearance. This generally translates into longer circulation times and can lead to improved accumulation behavior in tumor tissues as the result of enhanced permeability and retention (EPR) effects.[1, 2] The latter describes the property by which certain sizes of molecules, such as nanoparticles, macromolecular drugs and liposomes, tend to accumulate in tumor tissues much more than they do in normal tissues. A few reasons for this phenomenon are explained in Chapter 1 of this dissertation; they include an increased blood supply, as well as a generally less effective lymphatic drainage system, in cancer cells. It has also been suggested that selective accumulation in tumors relative to normal tissues can be enhanced through the use of tumor-specific cell-surface targeting groups, and that binding events may be used to trigger release mechanisms. Such strategies are appealing since they could serve not only to enhance tumor uptake relative to normal tissues, but also to reduce toxicity in peripheral organs.[1-3]

Despite the advantages offered by micelle delivery systems, to date no micellar system has been described that achieves the full promise of targeting *in vivo*. Of

additional concern is the fate of micelle delivery systems in biological media.[4] Previously described micelle delivery systems have suffered from an inherent instability *in vivo*, generally undergoing collapse in the presence of serum lipids and proteins.[4] Micelles can be stabilized for *in vivo* use through crosslinking of individual acyl chains. To date, numerous crosslinking reactions have been attempted, employing strategies that range from the use of disulfides[5, 6] and other redox-sensitive bonds[7] to temperature-[8] and pH-sensitive[9-11] functional groups. In this Chapter a novel crosslinking procedure is described that relies on the pH-sensitivity of metal-oxygen coordination bonds.[12] This particular form of crosslinking behavior is known to increase blood circulation times and results in the formation of a stable micelle delivery system that is able to selectively dissociate and release its contents at generally slightly lower pH values in tumor microenvironments.[13]

There are a number of micelle-based delivery systems for drugs such as doxorubicin and paclitaxel currently in Phase I and II clinical trials.[1, 2] These systems do provide for increased circulation times and larger area-under-the curve pharmacokinetics relative to the corresponding free drug. Some systems now in preclinical study are also "passively targeted,"[6, 14, 15] meaning they lack any specific surface ligands and rely solely on EPR effects to deliver their payload.[5, 8, 16] A significant disadvantage with passive targeting of micelle delivery systems is an increased probability for nonspecific delivery and accumulation in clearance organs, such as liver and kidney, relative to tumor.[2, 17] Additionally, the significance of EPR in human cancers remains largely unproven and there is increasing evidence that EPR alone may not be enough to ensure the selective delivery of a drug.[17]

Most attempts at micelle targeting have come from the use of ligands such as (Arg-Gly-Asp)-based ligands (RGD) of $\alpha_v\beta_3$ integrin, epithermal growth factor receptor (EGFR), or folate.[7, 18-23] Unfortunately, most of these targeted systems suffer from high

peripheral toxicity,[5, 7, 16, 19, 20] have only seen limited testing *in vivo* (e.g., in animal models lacking tumor xenografts[21, 22]), or have not yet quantitatively demonstrated selective tumor accumulation relative to peripheral organs.[7, 11, 18, 23, 24] It is also noteworthy that various other targeted systems have been reported to provide little improvement in tumor uptake as compared to their untargeted controls.[7, 19, 20] Thus, there remains a need for more specific biological targeting agents, including those that rely on localization strategies that are not EPR dependent. This may be of particular relevance in clinical systems, where it has recently been proposed that human cancers have only a modest EPR as compared to murine xenografts.[17]

One attractive target is the melanocortin 1 receptor (MC1R), which is expressed on over 80% of malignant melanomas.[25] Not surprisingly, MC1R has been investigated as a target for delivery of imaging and therapeutic agents. Indeed, a number of MC1R ligands have been developed for this purpose.[26-29] The best known of these, [Nle^4,DPhe^7]-α-MSH (NDP-α-MSH, **69**),[30] is considered the "gold standard" for *in vitro* assays due to its ease of synthesis, low cost and high MC1R affinity.[29, 31] However, NDP-α-MSH is not selective for MC1R and displays strong nanomolar binding affinities to other competing melanocortin receptor isoforms, e.g. MC4R and MC5R.[32-34] Such off-target binding is undesirable given the presence of these receptors in the kidney, brain and central nervous system.[35-39] Koikov *et al*. has reported the development of a ligand, 4-phenylbutyryl-His-DPhe-Arg-Trp-NH_2, with high selectivity and specificity for MC1R.[28] Dr. Natalie Barkey (Moffitt Cancer Center, Tampa, FL) *et al*. has recently altered this ligand with an alkyne (4-phenylbutyryl-His-DPhe-Arg-Trp-Gly-Lys(hex-5-ynoyl)-NH_2; **68**)[40] for click attachment to a micelle-forming triblock polymer. Moreover, it was demonstrated *in vitro* that micelles decorated with compound **68** retain the high binding affinity (2.9 nM K_i) of the free ligand and display improved target selectivity. In this prior work, the K_i of

targeted crosslinked (XL) micelles for MC1R was found to be four times lower than the corresponding targeted uncrosslinked (UXL) micelles while not binding to either of the undesired targets, MC4R or MC5R.[40] However, the following studies show how these micelles can be used to deliver a T_1 MRI contrast-enhancing agent, namely gadolinium texaphyrin (GdTx).

As described in section 1.5.2 of this dissertation, the ratio of the water-soluble texaphyrin species MGd **11** in tumor cells to that in surrounding normal cells is reported to be 9:1.[41] However, we believe that incorporation of a different, hydrophobic texaphyrin species into a micelle (acting as a drug delivery system) would further improve this ratio. Furthermore, the incorporation of gadolinium into the texaphyrin macrocycle allows the tissue distribution of GdTx to be studied non-invasively via standard magnetic resonance imaging methods. To develop micelles containing GdTx, a triblock polymer micelle system with enhanced stability (IVECT™) was used that was initially developed by Intezyne Technologies Inc. (Tampa, FL).[13, 40]

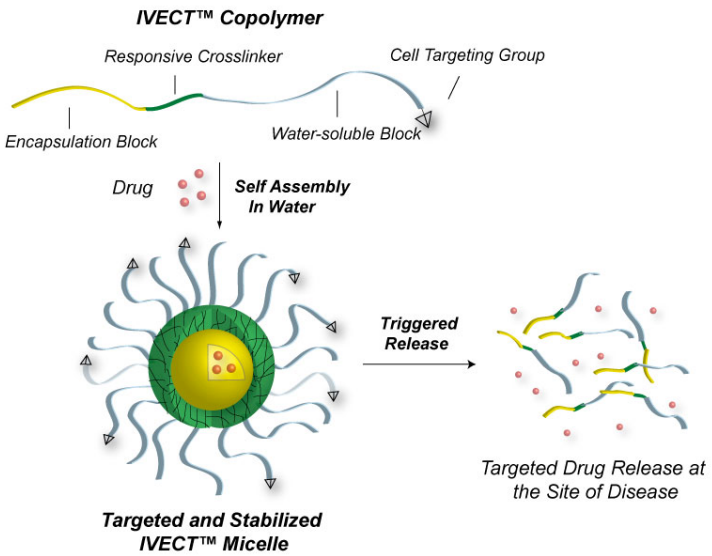

Figure 4.1: Schematic representation of the design and function of targeted IVECT™ micelles.[42]

This triblock polymer is composed of a hydrophobic encapsulation block, a responsive stabilizer block, and a hydrophilic masking block that contains an azide for functionalization via click chemistry. The main advantage of IVECT™ micelles over traditional micelles is the incorporation of the stabilization block, which allows the micelles to be crosslinked via a pH-sensitive Fe(III) metal coordination reaction.[12, 13, 40] They are also biodegradable and designed to release their payload in the acidic microenvironment of tumors.[13] As detailed below, this approach has allowed for the generation of a stabilized IVECT™ micelle system that incorporates GdTx and which both penetrates into xenografted tumors with high selectively and clears from circulation without being retained in the kidney or liver. Tumor penetration, as inferred from MRI studies, was not observed with either untargeted or uncrosslinked micelles. These results provide support for the notion that this approach for tumor-specific targeting is superior to that provided by EPR alone.

4.2 Design and Synthesis of GdTx-Polymer Micelles

For the incorporation of GdTx into the GdTx-polymer micelles a texaphyrin species was chosen that demonstrates low solubility in water but high solubility in a wide range of organic solvents, including apolar solvents such as chloroform or polar solvents such as methanol and dimethyl sulfoxide. The latter was chosen as the solvent for the incorporation step. The synthesis of the GdTx **67** is shown in Scheme 4.1. Briefly, 1,2-veratrole **65** is subjected to dinitration as published previously.[43] Hydrogenation of 1,2-dimethoxy-4,5-dinitrobenzene **66** and condensation with the tripyrrane species **22** in the presence of hydrochloric acid results in the formation of a sp^3 nonaromatic texaphyrin intermediate. Addition of triethylamine as a base in the presence of gadolinium(III)

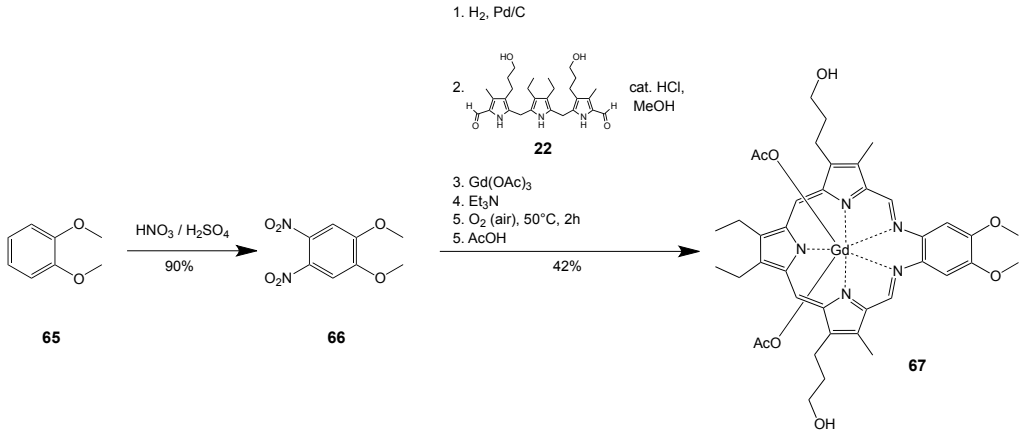

Scheme 4.1: Synthesis of gadolinium texaphyrin (GdTx) species **67**.

acetate tetrahydrate and air leads to the formation of texaphyrin **67**, which can be obtained as a deep green powder after column chromatographic purification.

Single crystals suitable for X-ray diffraction were obtained by treating **67** with sodium nitrate (ligand exchange, Scheme 4.2) and by slow diffusion of ethyl ether into a solution of the texaphyrin in methanol and chloroform.

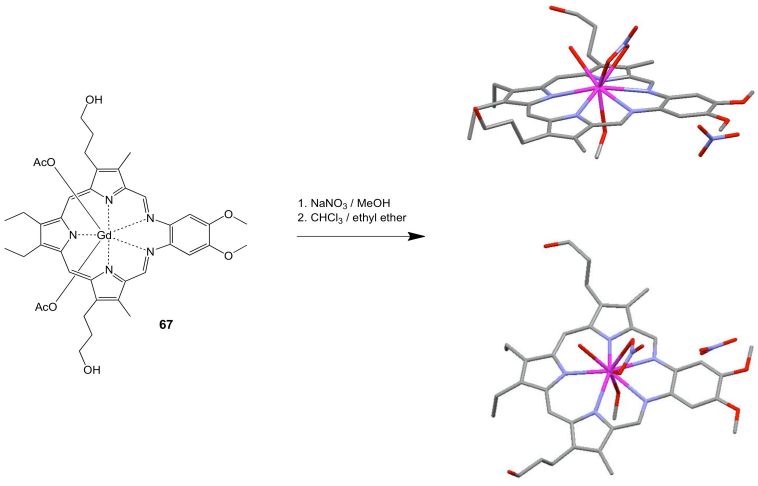

Scheme 4.2: X-ray crystal structure of **67**. These were crystals obtained after ligand exchange. Note that of the two nitrate counterions, only one is coordinated to gadolinium. The other axial ligands are methanol and water.

IVECT™ triblock polymers with a terminal azide were obtained from Intezyne Technologies (Tampa, FL) and either **68**[40] or NDP-α-MSH-lys-hexyne **69** were used as the MC1R-selective ligands, i.e. cell targeting groups (Scheme 4.3). Standard click chemistry was conducted for the design of the micelle construct as previously described.[40]

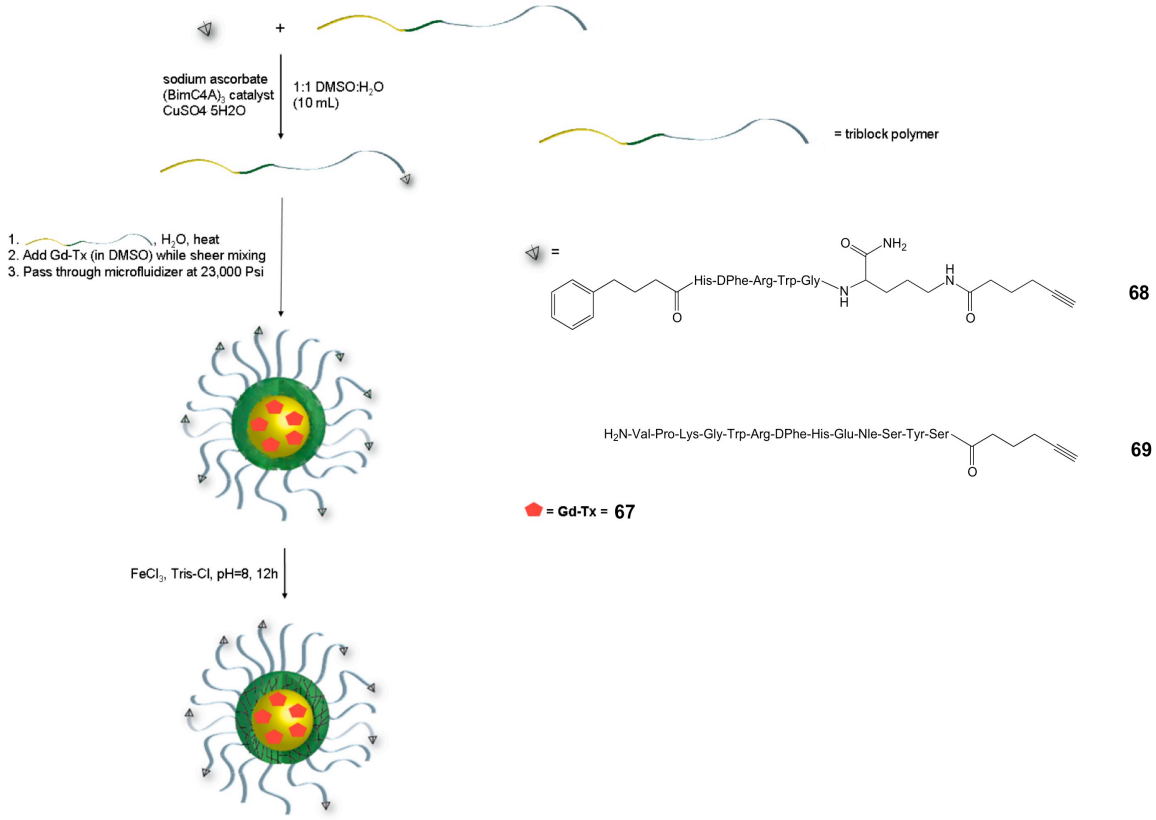

Scheme 4.3: Design of the IVECT™ micelle systems.

NDP-α-MSH **69** was chosen as a model ligand for competition due to its relatively high affinity for MC1R (1.9 nM K_i), and for the ease of synthesis that it provides.[29, 31]

In the percent targeting optimization assays with an alkyne-functionalized NDP-α-MSH **69** there was a clear difference between the binding affinities of the crosslinked

(XL) and uncrosslinked (UXL) micelles. This finding is ascribed to the Fe(III) crosslinking, which serves to stabilize the micelles in biological media. In the absence of crosslinking, the micelles dissociate, in whole or in part, to free monomers, leading to a loss of structural integrity and the premature release of the payload (the encapsulated contrast agent, GdTx **67**, in the present instance).

A second advantage of crosslinking is that it leads to an operational increase in binding avidity, a result that may reflect a benefit of multivalent interactions. The targeted (T) micelles based on texaphyrin **68** that was used in this study also exhibited a stronger avidity to the MC1R receptor when crosslinked (T-XL) as compared to their uncrosslinked counterpart (T-UXL). This finding can be interpreted as further support for the contention that (i) crosslinking stabilizes micelles and (ii) multiple targeting ligands on the micelle surface provide for enhanced binding. *In vitro* europium time-resolved fluorescence (TRF) competition binding assays conducted with both **68**- and **69**-targeted micelles provide support for this central hypothesis.

While *in vitro* MR imaging studies conducted with different GdTx-polymer micelle phantoms showed no apparent contrast effect attributable to the different micelle formulations (UT-UXL, UT-XL, T-UXL and T-XL, see experimental section), the stability, accumulation and MRI contrast properties of these systems could be studied *in vivo*.

4.3 *IN VIVO* STUDIES OF GDTX-POLYMER MICELLES

The above GdTx containing micelles (0.5% GdTx w/w) were further studied *in vivo* using mice xenografted with HCT116 (colon cancer carcinoma) tumor tissue. In accord with the design expectations, these *in vivo* experiments revealed improved MRI contrast enhancements upon administration of the GdTx containing T-XL micelles, with maximal enhancement observed at 24 hours. As can be seen by an inspection of Figure 4.2 and 4.3, this enhancement was not seen with the other micelle systems, supporting the contention that the T-XL micelles provide good systems for effecting tumor localization and imaging. This unique ability of the T-XL micelles to penetrate the tumor appears to result from a combination of the MC1R-specific targeting group and the enhanced stability provided by the Fe(III) crosslinking. If targeting alone were enough to produce effective tumor enhancement, one would also observe a substantial uptake in the

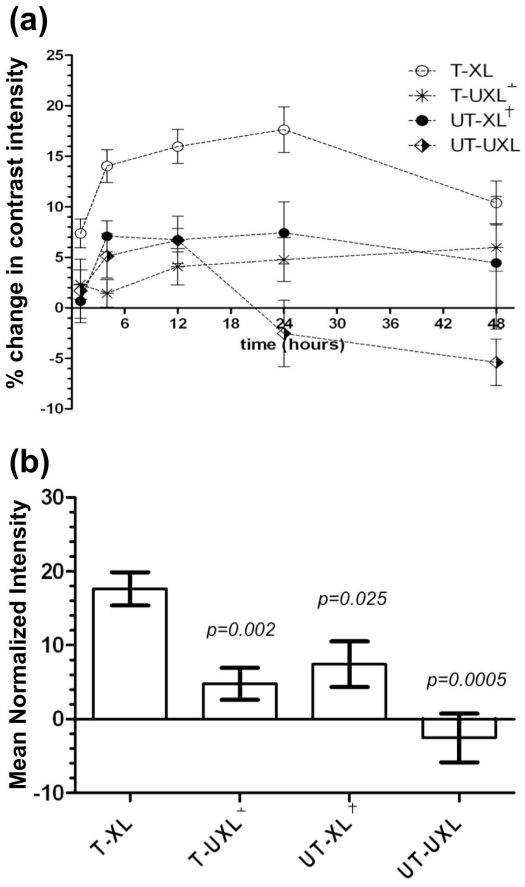

Figure 4.2: Buildup data for GdTx as inferred from contrast enhancement in the tumor ((b) shows mean normalized intensity 24 hours post-injection).
All groups contained three mice except where noted.
⊥One mouse expired between the 24 hours and 48 hours time point.
†One mouse expired upon injection of the micelle agent.

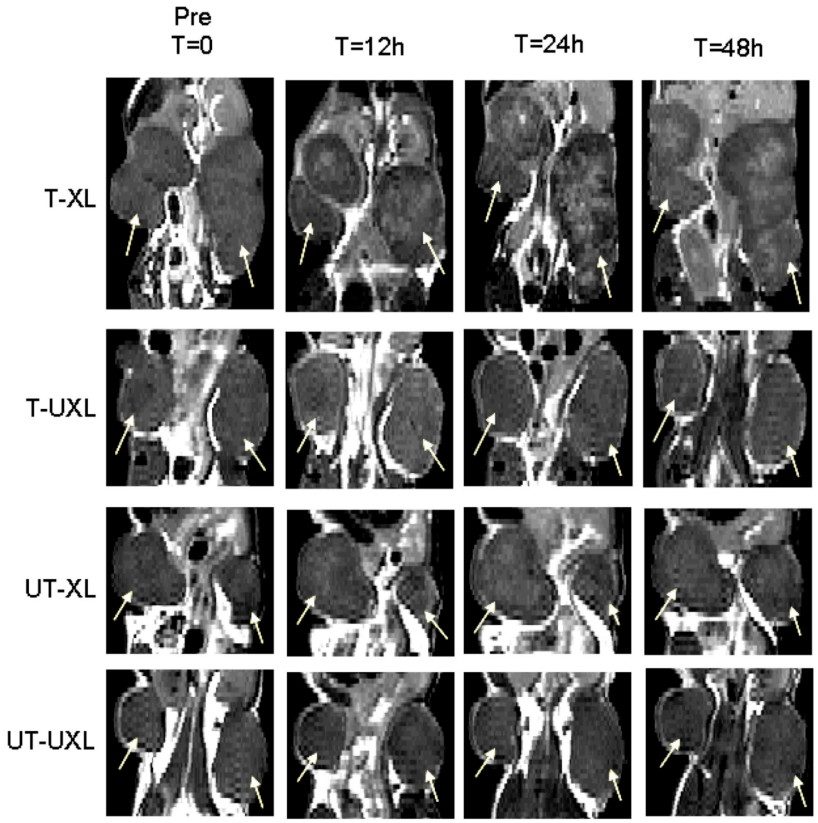

Figure 4.3: T_1 weighted spin echo multi slice (SEMS) images of mice treated with different GdTx micelle formulations. Representative images from each group of mice treated with GdTx micelles at selected time points (0, 12, 24 and 48 hours). White arrows denote location of tumors.

case of T-UXL micelles. Likewise, if crosslinking and EPR alone were enough to affect accumulation, one would observe an increased build-up in the UT-XL group. Finally, it is important to note that the enhancement observed in the T-XL group was not the result of free gadolinium texaphyrin (which is known to accumulate in tumors selectively, see previous sections of this dissertation). If this were the case, one would have observed enhanced uptake in all four micelle groups (i.e., UT-UXL, T-UXL and UT-UXL, in addition to the T-XL system). However, this was not seen. Furthermore, the GdTx

species **67** used in this study alone and without micelles acting as drug delivery systems does not show sufficient solubility characteristics to be used *in vivo*. Thus, the *in vivo* data obtained form the micelle system are consistent with the conclusion that the T-XL micelles containing GdTx **67** allow for functionally acceptable binding avidity, stability, tumor penetration and uptake. Presumably, the crosslinking reaction stabilizes the micelles after administration and during initial time points while they circulate throughout the bloodstream, while the targeting group allows the system to bind to, and be retained within, the tumor cells.

4.4 CONCLUSIONS

The synthesis, characterization and incorporation of a new gadolinium texaphyrin (GdTx **67**) into polymer micelles has been described. The GdTx is characterized by a high inherent T_1 relaxivity. Its encapsulation within the IVECT^{TM} system and the production of crosslinked micelles by reaction with Fe(III) has also been detailed. Moreover, it was demonstrated that the targeted GdTx micelles are selectively retained in target-expressing xenograft tumors *in vivo*. To the best of our knowledge, this is the first example of a targeted micelle that is capable of carrying a payload and which outperforms systems based on EPR in terms of tumor penetration, uptake and retention.

Advantages of the current system include the following: (i) the target, MC1R, is highly expressed in melanoma cells and not in healthy tissues, except for melanocytes; (ii) high short-term stability, and (iii) an ability to accumulate in tumors, rather than various clearance organs. These attributes are reflected in the *in vivo* images that reveal uptake deep within the tumor with peak accumulation at 24 hours for T-XL micelles. In contrast, peak kidney and liver accumulations were seen at one to four hours. These

differences are thought to reflect the benefits of targeting. However, biodegradation of the stabilized micelles may contribute to the effect; to the extent it occurs on short time scales (on the order of hours), it would allow for release of payload (GdTx) within the tumor while concurrently clearing from circulation. While further investigations will be required to detail the full pharmokinetic profile of these new micelles, it is important to appreciate that from an operational perspective they constitute the first examples of micelle systems that are capable of delivering a payload in a tumor selective fashion.

The gadolinium texaphyrin used in this study was synthesized and characterized by the author. The X-ray quality single crystal of complex **67** (obtained after ligand exchange) was grown by the author, the crystal structure was solved and refined by Dr. Vincent M. Lynch of the Department of Chemistry and Biochemistry at The University of Texas at Austin. All micelles described in this Chapter were designed and synthesized by Dr. Natalie Barkey (Moffitt Cancer Center, Tampa, FL) and other coworkers listed below. All *in vitro* and *in vivo* studies were conducted by Dr. Barkey and other coworkers listed below. Drs. Jonathan L. Sessler, Robert J. Gillies and David L. Morse supervised the project. Sections of this Chapter have been taken from the following manuscript: Barkey, N.; Preihs, C.; Cornnell, H. H.; Martinez, G.; Sill, K. N.; Carie, A.; Lloyd, M.; Xu, L.; Lynch, V. M.; Sessler, J. L.; Gillies, R. J.; Morse, D. L. *submitted*.

References

(1) Yokoyama, M. J. *Exp. Clin. Med.* **2011**, *3*, 151-158.

(2) Oerlemans, C.; Bult, W.; Bos, M.; Storm, G.; Nijsen, J. F. W.; Hennik, W. E. *Pharm. Res.* **2010**, *27*, 2569-2589.

(3) Kedar, U.; Phutane, P.; Shidhaye, S.; Kadm, V. *Nanomed.: Nanotech., Biology and Medicine* **2010**, *6*, 714-729.

(4) Kim, S.; Shi, Y.; Kim, J. Y.; Chen, K. P. & J.-X. *Expert Opin. Drug Deliv.* **2010**, *7*, 49-62.

(5) Shiraishi, K.; Kawano, K.; Maitani, Y.; Yokoyama, M. *J. Controlled Release* **2010**, *148*, 160-167.

(6) Li, J.; Huo, M.; Wang, J.; Zhou, J.; Mohammad, J. M. Zhang, Y.; Zhu, Q.; Waddad, Z. Y.; Zhang, Q. *Biomaterials* **2012**, *33*, 2310-2320.

(7) Lee, H.; Hoang, B. Fonge, H.; Reilly, R.; Allen, C. *Pharmaceutical Research* **2010**, *27*, 2343-2355.

(8) Kim, T.; Chen, Y.; Mount, C.; Gambotz, W.; Li, X.; Pun, S. *Pharm. Res.* **2010**, *27*, 1900-1913.

(9) Jia, Z.; Wong, L.; Davis, T. P.; Bulmus, V. *Biomacromolecules* **2008**, *9*, 3106-3113.

(10) Yang, X.; Grailer, J. J.; Pilla, S.; Steebe, D. A.; Dong, S. *Bioconjugate Chem.* **2010**, *21*, 496-504.

(11) Li, Y.; Xiao, W.; Xiao, K.; Berti, L.; Luo, J.; Tseng, H. P.; Fung, G.; Lam, K. S. *Angew. Chem., Int. Ed.* **2012**, *51*, 2864-2869.

(12) Cannan, R. K.; Kibrick, A. *J. Am. Chem. Soc.* **1938**, *60*, 2314-2320.

(13) Rios-Doria, J.; Carie, A.; Costich, T.; Burke, B.; Skaff, H.; Panicucci, R.; Sill, K. *J. Drug Delivery* **2012**, Article ID 951741, 1-8.

(14) Sun, T.-M.; Du, J.-Z.; Yao, Y.-D.; Mao, C. Q.; Dou, S.; Huang, S. Y.; Zhang, P. Z.; Leong, K. W.; Song, E. W.; Wang, J. *ACS Nano* **2011**, *5*, 1483-1494.

(15) Koo, H.; Huh, M.; Sun, I.-C.; Yuk, S. H.; Choi, K.; Kim, K.; Kwon, I. C. *Acc. Chem. Res.* **2011**, *44*, 1018-1028.

(16) Tang, N.; Dy, G.; Wang, N.; Liu, C.; Hang, H.; Liang, W. J. *Natl. Cancer Inst.* **2007**, *99*, 1004-1015.

(17) Christina, A.; Massey, K. A.; Schnitzer, J. E. *Interdisciplinary Reviews: Nanomedicine and Nanobiotechnology* **2011**, *3*, 421-437.

(18) Kessinger, C.; Khemtong, C.; Togao, O.; Tajahashi, M.; Sumer, B.; Gao, J. *Experim. Biol. Med.* **2010**, *235*, 957-965.

(19) Poon, Z.; Lee, J.; Huang, S.; Prevost, R.; Hammond, P. *Nanomedicine* **2010**, *7*, 201-209.

(20) Lee, H.; Fonge, H.; Hoang, B.; Reilly, R.; Allen, C. *Mol. Pharm.* **2010**, *7*, 1195-1208.

(21) Hu, J.; Qian, Y.; Wang, X.; Liu, W.; Liu, S. *Langmuir* **2012**, *28*, 2073-2082.

(22) Liu, T.; Liu, X.; Qian, Y.; Hu, X.; Liu, S. *Biomaterials* **2012**, *33*, 2521-2531.

(23) Xiong, X.-B.; Lavasanifar, A. *ACS Nano* **2011**, *5*, 5202-5213.

(24) Yang, R.; Meng, F.; Ma, S.; Huang, F.; Liu, H.; Zhong, Z. *Biomacromolecules* **2011**, *12*, 3047-3055.

(25) Siegrist W.; Solca, F.; Stutz S.; Giuffrè, L.; Carrel, S.; Girard, J.; Eberle, A. N. *Cancer Res.* **1989**, *49*, 6352-6358.

(26) Cai, M.; Varga, E. V.; Stankova, M.; Mayorov, A.; Perry, J. W.; Yamamura, H. I.; Trivedi, D.; Hruby, V. *J. Chem. Biol. Drug Des.* **2006**, *68*, 183-193.

(27) Mayorov, A. V.; Han, S. Y.; Cai, M.; Hammer, M. R.; Trivedi, D.; Hruby, V. *J. Chem. Biol. Drug Design* **2006**, *67*, 329-335.

(28) Koikov, L. N.; Ebertino, F. H.; Solinsky, M. G. *Bioorg. Med. Chem. Lett.* **2003**, *13*, 2647-2650.

(29) Chen, J.; Giblin, M. F.; Wang, N.; Jurisson, S. S.; Quinn, T. P. *Nucl. Med. Biol.* **1999**, *26*, 687-693.

(30) Sawyer, T.; Sanfilippo, P.; Hruby, V.; Engel, M. H.; Heward, C. B.; Burnett, J. B.; Hadley, M. E. *Procl. Natl. Acad. Sci.* USA **1980**, *77*, 5754-5758.

(31) Chen, J.; Cheng, Z.; Hoffman, T. J.; Jurisson, S. S.; Quinn, T. P. *Cancer Res.* **2000**, *60*, 5649-5658.

(32) Cai, M.; Mayorov, A. V.; Cabello, C.; Stankova, M.; Trivedi, D.; Hruby, V. J. *J. Med. Chem.* **2005**, *48*, 1839-1848.

(33) Handl, H. L.; Vagner, J.; Yamamura, H. I.; Hruby, V. J.; Gillies, R. *J. Anal. Biochem.* **2004**, *330*, 242-250.

(34) Yang, Y.; Hruby, V. J.; Chen, M.; Crasto, C.; Cai, M.; Harmon, C. M. *Biochemistry* **2009**, *48*, 9775-9784.

(35) Rodrigues, A. R.; Pignatelli, D.; Almeida, H.; Gouveiaa, A. M. *J. Mol. Cell. Endocrinol.* **2009**, *303*, 74-81.

(36) Webb, T. R.; Clark, A. J. L. *J. Mol. Endocrinol.* **2009**, *24*, 475-484.

(37) Van der Ploeg, L. H. T.; Martin, W. J.; Howard, A. D.; Nargund, R. P.; Austin, C. P.; Guan, X.; Drisko, J.; Cashen, D.; Sebhat, I.; Patchett, A. A.; Figueroa, D. J.; DiLella, A. G.; Connolly, B. M.; Weinberg, D. H.; Tan, C. P.; Palysha, O. C.; Pong, S.-S.; MacNeil, T.; Rosenblum, C.; Vongs, A.; Tang, R.; Yu, H.; Sailer, A. W.; Fong, T. M.; Huang, C.; Tota, M. R.; Chang, R. S.; Stearns, R.; Tamvakopoulos, C.; Christ, G.; Drazen, D. L.; Spar, B. D.; Nelson, R. J.; MacIntyre, D. E. *PNAS* **2002**, *99*, 11381-11386.

(38) Hall, J. E.; da Silva, A. A.; do Carmo, J. M.; Dubinion, J.; Hamza, S.; Munusmy, S.; Smith, G.; Stec, D. E. *J. Biol. Chem.* **2010**, *285*, 17271-17276.

(39) Jun, D.-J.; Na, K.-Y.; Kim, W.; Kwak, D.; Kwon, E. J.; Yoon, J. H.; Yea, K.; Lee, H.; Kim, J.; Suh, P. G.; Ryu, S. H.; Kim, K. T. *J. Mol. Endocrinol.* **2010**, *44*, 225-236.

(40) Barkey, N. M.; Tafreshi, N. K.; Josan, J. S.; De Silva, C. R.; Sill, K. N.; Hruby, V. J.; Gillies, R. J.; Morse, D. L.; Vagner, J. *J. Med. Chem.* **2011**, *54*, 8078-8084.

(41) See reference (76) in Chapter 1.

(42) Taken from: http://www.intezyne.com/our_technology.asp, Retrieved 09-10-2012. Figure reprinted with permission from: Kevin N. Sill, Chief Science Officer Intezyne Technologies, Tampa, FL, USA. Permission granted on 09-10-2012.

(43) Ehrlich, J.; Bogert, M. T. *J. Org. Chem.* **1947**, *12*, 522-534.

5. Phenanthroline Linked Sapphyrins

5.1 INTRODUCTION

As mentioned in section 1.5.1 of this dissertation, sapphyrins represent another class of expanded porphyrins with promising anticancer activity and which display selective localization in tumorous tissues, including hematological malignancies.[1, 2] Sapphyrins were initially explored in the context of photodynamic therapy where the absorption of light in the 700-800 nm is particularly important. In this spectral region, tissues and blood cells exhibit a broad absorption minimum.[3] This makes them relatively transparent,[3, 4] resulting in a more efficient photosensitizing treatment.

Sapphyrins also attracted interest early on as possible ligands for metal complexation. Because of their basic resemblance to porphyrins, it was initially expected that the sapphyrins would mimic, at least on some level, the rich coordination chemistry displayed by the porphyrins. However, the larger core size (approximately 5.5 Å inner N-N diameter vs. ca. 4.0 Å for porphyrins)[5], the greater number of potentially chelating heteroatom centers, and the fact that pentaazasapphyrins when fully deprotonated are potentially trianionic ligands made sapphyrin a likely candidate for the chelation of larger metals, particularly as a potential ligand for the trivalent lanthanides and actinides. Unfortunately, in spite of extensive effort, this expectation remains largely unrealized.

Complexation attempts with first-row transition elements yielded in only a few poorly characterized metal complexes. For instance, Woodward and his group, who investigated the metal-chelating properties of sapphyrins, found that when dedcamethyl sapphyrin was treated with the acetate salts of Ni^{2+}, Fe^{2+}, Cd^{2+}, Mn^{2+}, Co^{2+}, and Zn^{2+} in the presence of sodium acetate, changes occurred in the visible spectra that could be

interpreted in terms of complexes being formed from each of these salts. However, only the Co^{2+} and Zn^{2+}-containing species could be isolated. Unfortunately, crystals suitable for X-ray diffraction analyses could not be obtained in either case.[6]

Successful metalation of sapphyrin with second- and third row transition metals was finally achieved by Sessler, *et al*. by using the carbonyl salts of rhodium(I) and iridium(I) as the metalating agents, in plane complexation was not observed. Rather, a variety of "sitting-a-top" complexes were obtained.[7] A uranyl complex of a furan-containing analogue of sapphyrin was also obtained by Sessler and coworkers.[8]

Given the inherent limitations associated with the use of sapphyrin as a ligand, we sought to combine it with other chelating groups. Initial efforts along these lines, and the focus of this section centered around the use of phenanthroline. Phenanthroline has a time honored role in inorganic chemistry. It is currently receiving increased attention in the context of DNA recognition.

5.2 Ruthenium Complexes as Potential Anticancer Agents

There is a great interest in understanding the factors that control the binding of metal ions to nucleic acids. This has been fuelled in part by the successful introduction into the clinic of several platinum complexes that exert anticancer activity by forming covalent adducts with the purine bases of DNA (see section 1.3). However, the dose-limiting nephrotoxicity and the development of drug resistance are main drawbacks in the use of platinum based anticancer agents. To date, a varity of other transition metal complexes are being studied for their potential use in chemotherapy and photodynamic therapy. This is part of a broad effort to create metallo drugs that are less toxic and more effective for chemotherapeutic applications. These studies have led to the development of

several experimental ruthenium(II)-based anticancer agents.[9-11] The prototype DNA-binding ruthenium(II)-1,10-phenanthroline complex [Ru-(phen)$_3^{2+}$] (Figure 5.1) was reported by Barton *et al*. in 1984.[12]

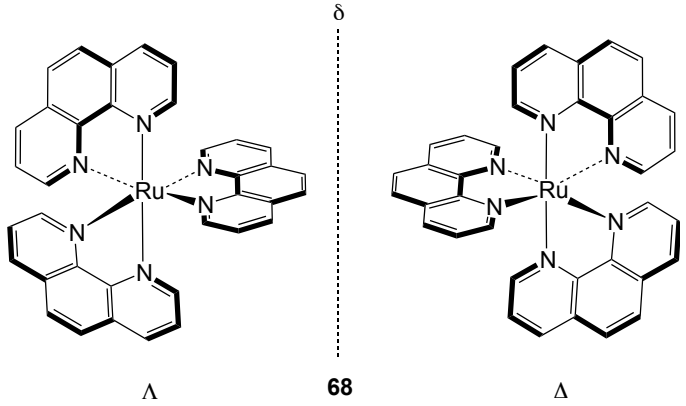

Figure 5.1: Λ and Δ-enantiomer of [Ru(phen)$_3^{2+}$] **68**.

The propeller-shaped molecule binds by partial insertion of one phenanthroline ligand into the base-pair stack.[13] Another analogous compound that has been investigated in terms of its DNA-binding affinity is the Ru(phen)$_2$DPPZ^{2+} (phen = 1,10-phenanthroline; DPPZ = dipyrido[3,2-α:2', 3'-*c*]phenazine).[14] The resulting complex is a mixture of both Δ- and Λ-enantiomer. The latter prefers adenine- and thymine-rich DNA, but with modest selectivity.[15] The Δ-enantiomer prefers guanine- and cytosine-rich DNA and is some six to ten times more selective.[16] Upon binding to DNA, cell division by mitosis is hindered and apoptosis is initiated if DNA-repair mechanisms fail. Another complex, [Ru(phen)$_2$(*p*-MOPIP)]$^{2+}$ (phen = 1,10-phenanthroline, *p*-MOPIP = 2-(4-methoxyphenyl) imidazo[4,5-f][1,10]-phenanthroline), is able to effectively inhibit proliferation of the A375 (skin cancer) cell line with a low IC$_{50}$ (5.9 ± 1.1 mM).[16]

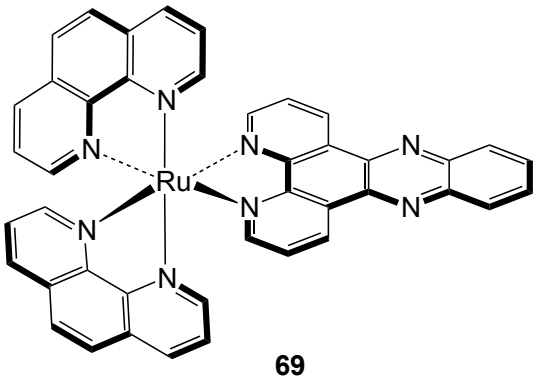

Figure 5.2: Structure of the Λ-enantiomer of Ru(phen)$_2$DPPZ^{2+} **69**.

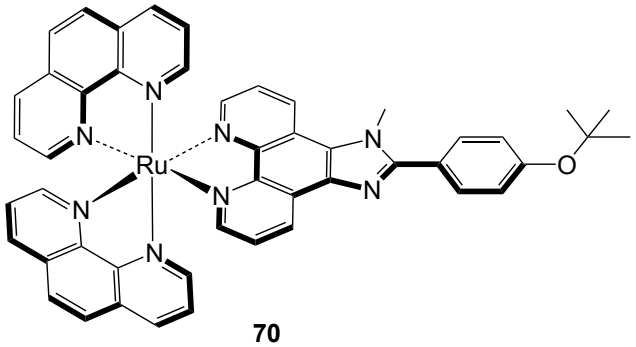

70

Figure 5.3: Structure of the Λ-enantiomer of $[Ru(phen)_2(p\text{-}MOPIP)]^{2+}$ **70**.

In light of these findings, we decided to design a molecule containing the key structural features discussed above, namely (a) a sapphyrin as a potential cancer-localizing core and (b) a 1,10-phenanthroline unit as a N-donor ligand that would allow for the stable complexation of ruthenium(II). Furthermore, while designing this sapphyrin species, particular consideration was devoted to finding a way to increase the relative absorption of the compound in the 700-800 nm region. Such a red shifting of the spectral features could allow for a more efficient use of excitation light energy in PDT applications.

5.3 Synthesis of 1,10-Phenanthroline Linked Sapphyrin

The synthesis of a phenanthroline-sapphyrin chimera is shown below. Briefly, it follows the "3+2" synthetic approach (3 = tripyrrane unit together with 2 = bipyrrole unit) for traditional sapphyrins as published previously.[6, 17] The synthesis of the diformyl bipyrrole unit **77** is shown in Scheme 5.1.[6] It follows a general procedure leading to diformyl-ß,ß,ß,ß-tetraalkylbipyrroles that is well established in the Sessler group.

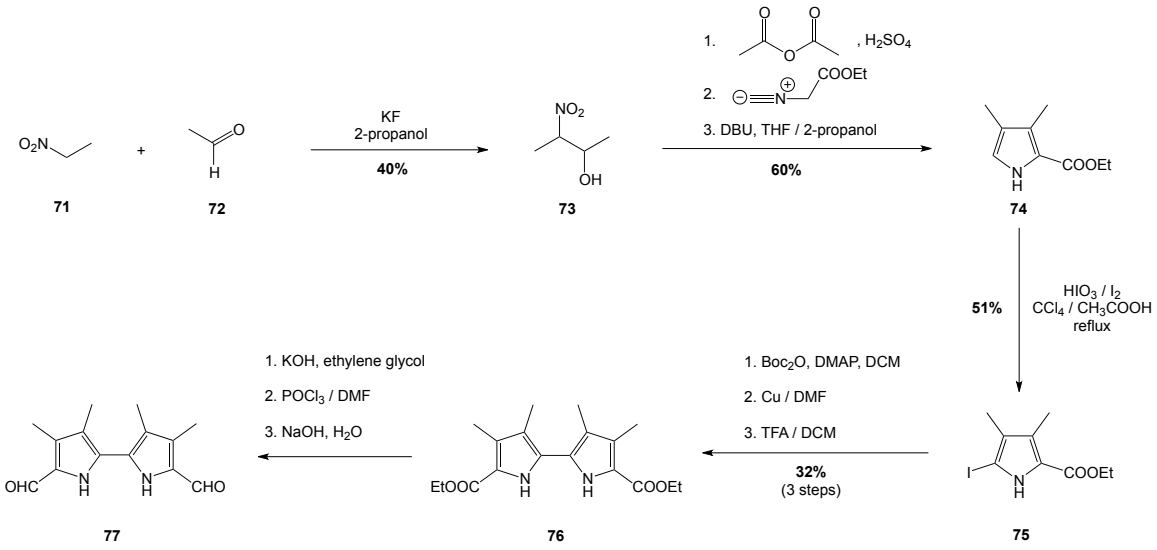

Scheme 5.1: Synthesis of diformyl bipyrrole unit **77**.

The synthetic route to obtain the tripyrrane precursor **83** is shown below. This procedure is a modified protocol reported by Lash *et al*.[18] The synthesis of compounds **14**[19] (via **81** and **82**) and **80**[18] have been reported previously.

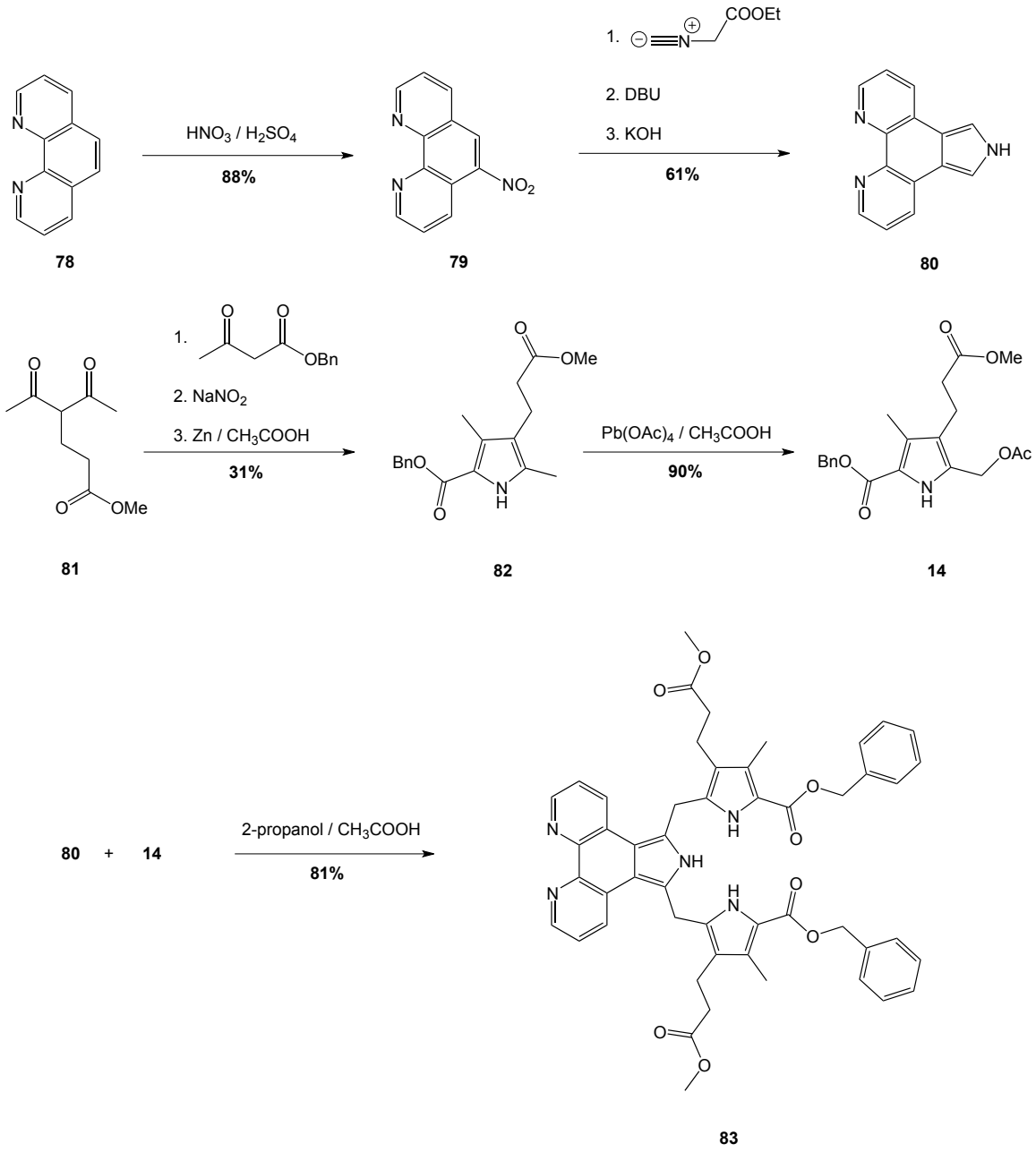

Scheme 5.2: Synthesis of tripyrrane unit **83**.

Commercially available 1,10-phenanthroline **78** was nitrated according to published procedures.[20] The resulting 5-nitro-1,10-phenanthroline **79** was subjected to

Barton-Zard conditions. Following saponification and decarboxylation, 1,10-phenanthrolinopyrrole **80** was obtained. Reaction of the latter species with the acetoxymethylpyrrole **14** (also used as a precursor for texaphyrin; see section 1.5.2.2) in 2-propanol under reflux in the presence of acetic acid yielded the tripyrrane unit **83**.

Single crystals suitable for X-ray diffraction analysis were obtained for **83** through slow evaporation of hexanes into a solution of **83** in chloroform containing 5% triethylamine. The addition of the latter base is important due to the fact that both nitrogen atoms on the phenanthroline moiety are basic and can be partially protonated by any proton source present in solution. This protonation, particularly if not complete, could lead to formation of non-crystalline species.

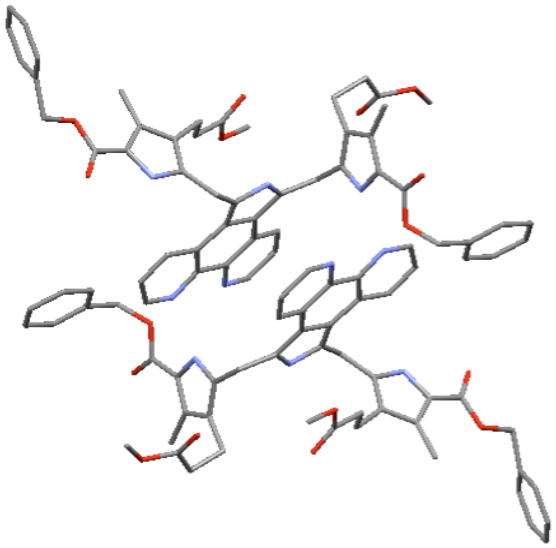

Figure 5.4: Single crystal X-ray structure of compound **83** (dimer shown).

The next step in the synthesis of the desired phenanthroline linked sapphyrin involves hydrogenolysis of the benzyl ester. However, attempts to cleave the benzyl esters of **83** with hydrogen over 10% palladium-charcoal or Pearlman's catalyst ($Pd(OH)_2$) were unsuccessful. Catalytic transfer hydrogenation reactions using cyclohexene, cyclohexadiene or ammonium formate also failed. The 1,10-phenanthroline unit appears to poison the catalyst through interaction with palladium. This renders the use of benzyl esters unsuitable as protective groups in this synthesis.

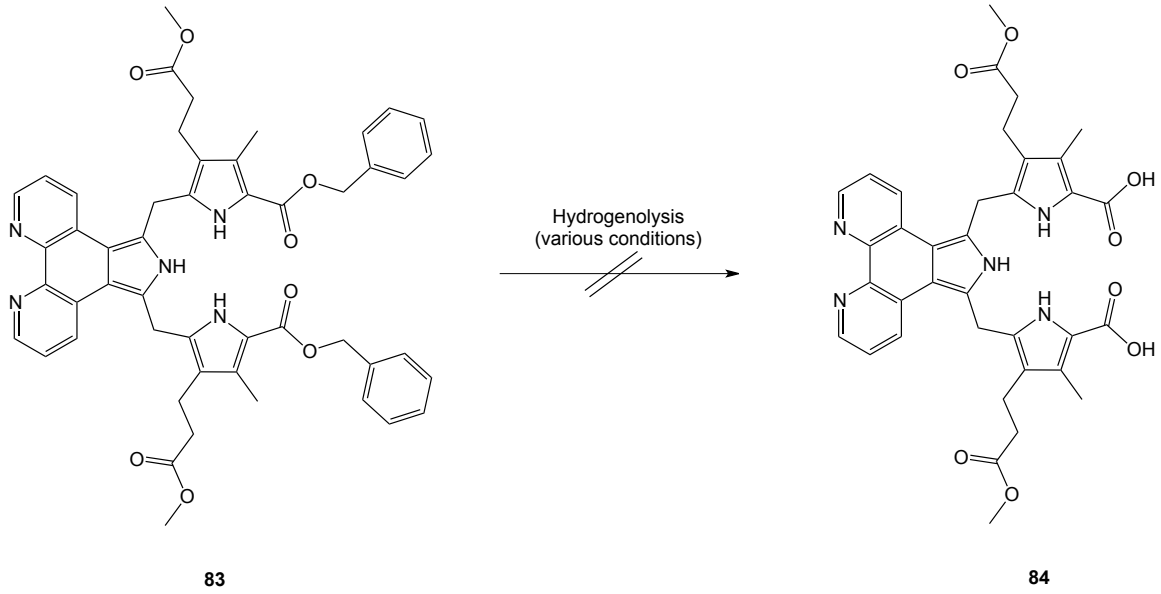

83 **84**

Scheme 5.3: Failed hydrogenolysis of compound **83**.

Given the above findings, the author decided to use tert-butyl esters as protecting groups for the tripyrrane unit instead of benzyl esters. The synthetic protocols for the synthesis of pyrrole precursor **84**[21] and **85**[22-24] have been published previously. The synthesis of the tripyrrane is shown in Scheme 5.4.

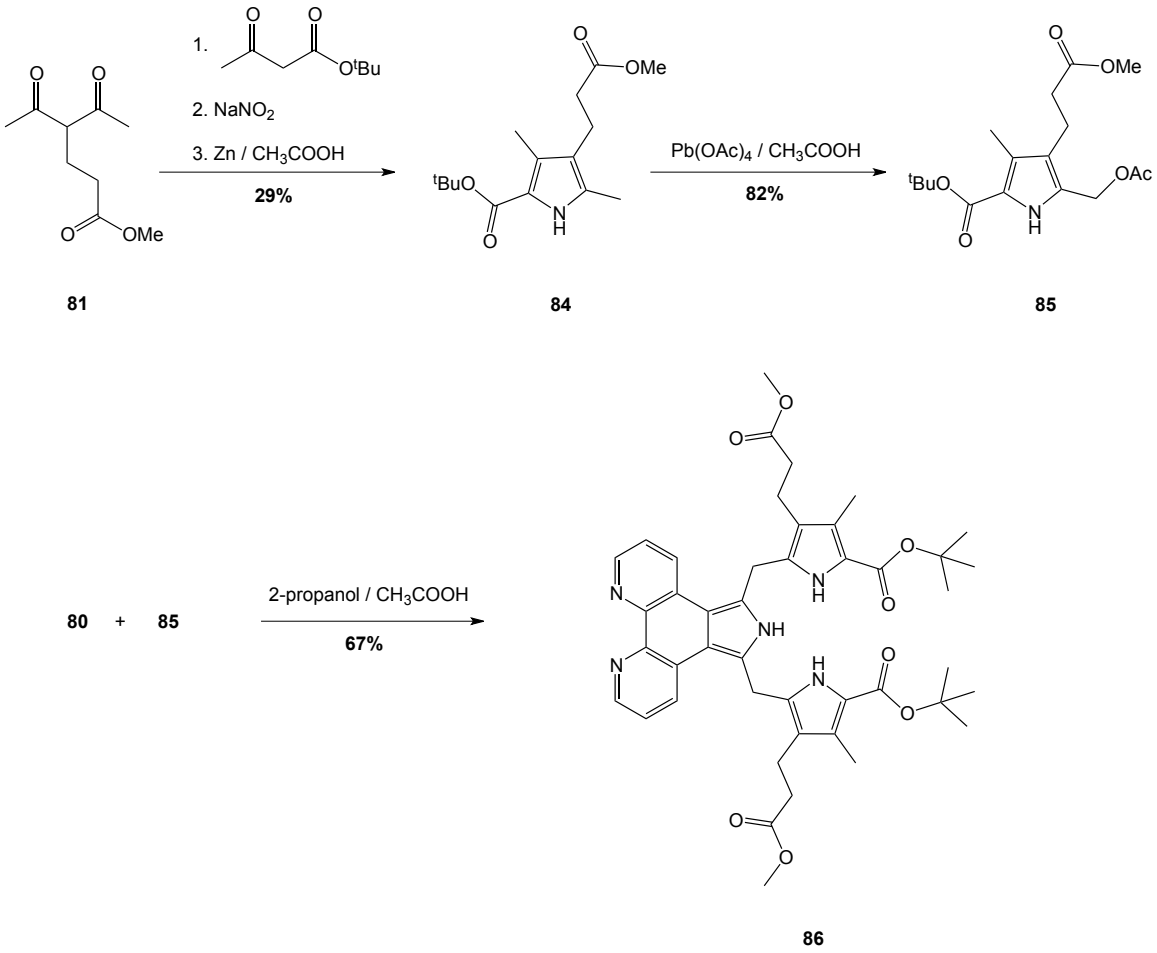

Scheme 5.4: Synthesis of tripyrrane unit **86**.

Single crystals of **86** suitable for X-ray diffraction were obtained through slow diffusion of diethyl ether into a solution of **86** in chloroform, methanol and 5% triethylamine.

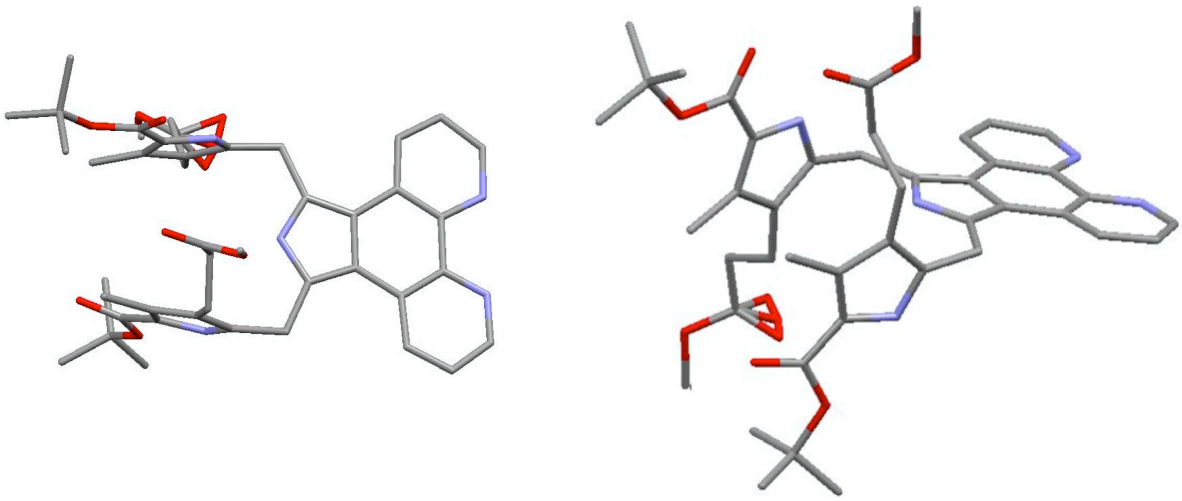

Figure 5.5: Top and side view of the single crystal X-ray structure of compound **86**.

Having precursors **77** and **86** in hand, the "3+2" synthesis of the desired sapphyrin could be completed. The cleavage of the tert-butyl esters in **86** and the subsequent decarboxylation reaction was achieved via the addition of trifluoroacetic acid (TFA, used as the solvent here) at 120 ºC. Then, addition of bipyrrole **77** dissolved in dichloromethane results in the formation of the sapphyrin.

Note that during cleavage of the tert-butyl ester and the decarboxylation reaction of the tripyrrane **86** in TFA, both methyl esters appear to be cleaved as well resulting in the formation of a tripyrrane dicarboxylate and eventually a sapphyrin dicarboxylate. Since column chromatographic purification of this highly polar species is not feasible, a final esterification step in ethanol with a catalytic amount of sulfuric acid is required.

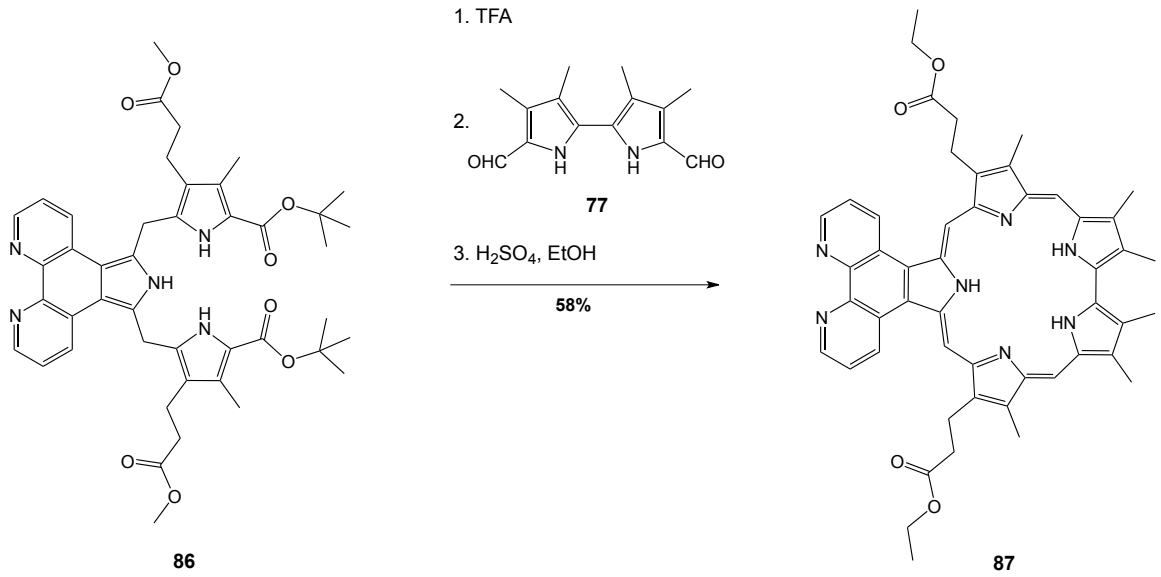

Scheme 5.5: Synthesis of 1,10-phenanthroline linked sapphyrin species **87**.

Single crystals suitable for X-ray diffraction were obtained for **87** through slow evaporation of hexanes into a solution in chloroform and. The sapphyrin scaffold proved to be highly planar, as expected for this aromatic expanded porphyrin. The phenanthroline moiety is slightly tilted (17.6º) out of the sapphyrin plane. One molecule of chloroform coordinates to the phenanthroline moiety in the solid state. Furthermore, one molecule of water resides inside the sapphyrin ring system.

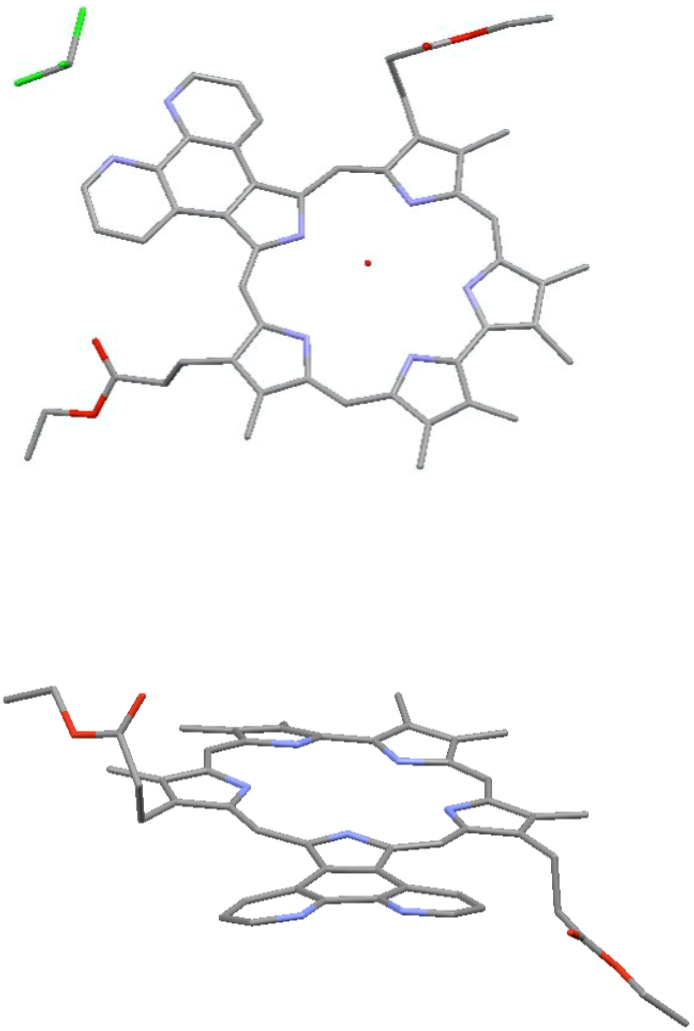

Figure 5.6: Top and side view of the single crystal X-ray structure of compound **87**.

After purification and characterization, compound **87** was reacted with $Ru(phen)_2Cl_2$ (compound **88**, synthesized from 1,10-phenanthroline as published previously[25]) in the presence of silver nitrate. This gave the Ru(II) complex of sapphyrin **89** (Scheme 5.6) in virtually quantitative yield.

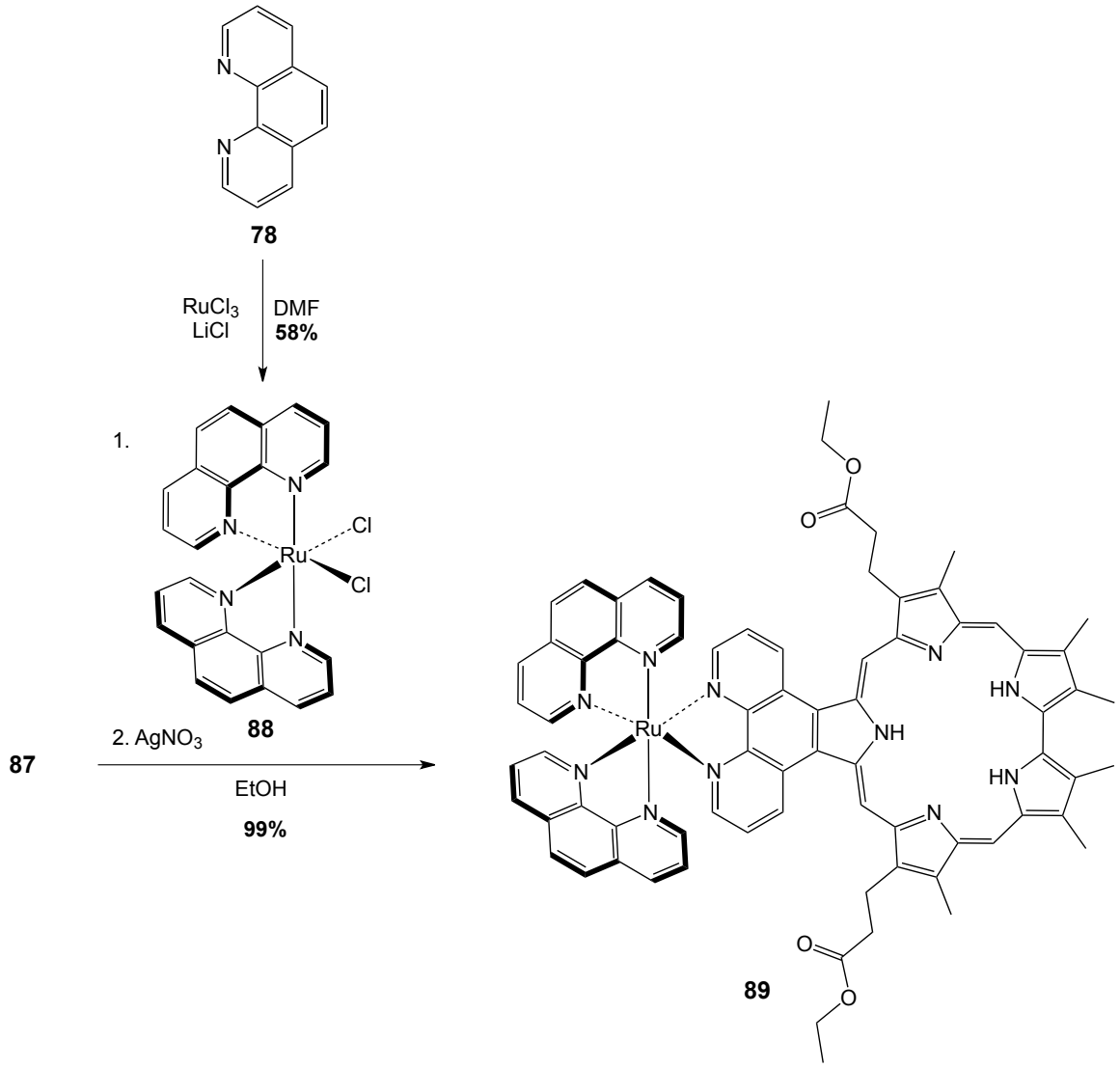

Scheme 5.6: Synthesis of $Ru(phen)_2Cl_2$ **88** and formation of complex **89**.

Interestingly, compound **89** proved to be water soluble, unlike the sapphyrin precursor **87**. Presumably, the two nitrate counteranions serve to improve water solubility of the complex drastically. Unfortunately, to date no crystals of complex **89** suitable for X-ray analysis in the solid state could be obtained.

In accord with the author's design expectations, the UV-Vis spectrum of complex **89** in comparison to the sapphyrin species **87** and the known, water soluble sapphyrin species **90** shows that the revealed intensity of the Q-band absorption centered around 715 nm is significantly increased. This low energy spectral feature is particularly important for potential photosensitizers since blood and membranes largely absorb in the blue-green area of the spectrum, which limits the penetration of visible photons with $\lambda_{max} \leq 650$ nm as noted earlier. Hence, an increased intensity for this is considered to be an attractive feature for potential photosensitizers (Figure 5.7).

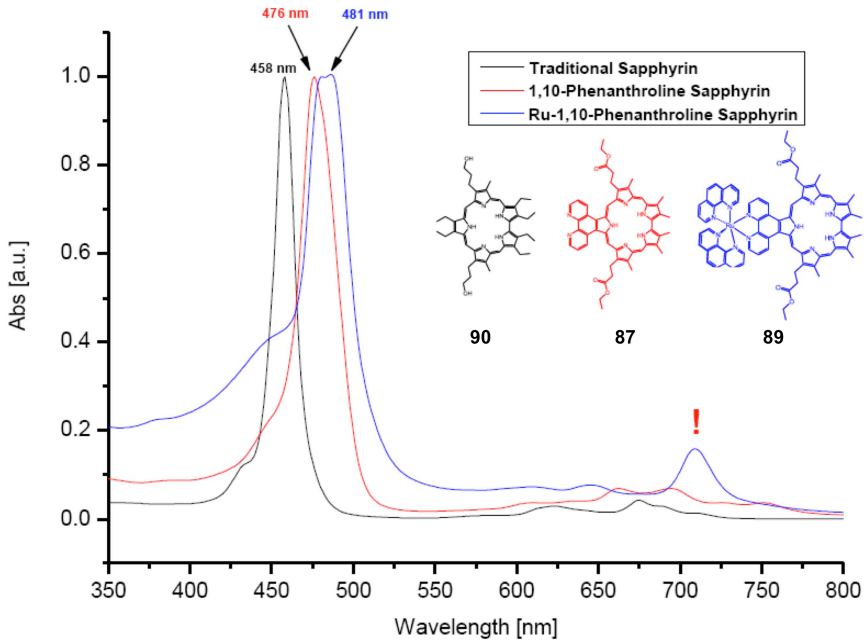

Figure 5.7: UV-Vis spectra of three structurally modified sapphyrins.

5.4 CONCLUSIONS

The findings described in this Chapter demonstrate a way to design and synthesize a sapphyrin compound that contains a N-donor ligand, namely 1,10-phenanthroline in its scaffold. This unit is able to stabilize a boud ruthenium(II) center which permits formation of a stable $[Ru(phen)_2(phenanthroline\text{-}sapphyrin)(NO_3)_2]$ complex **89**. Unfortunately, X-ray quality single crystals of compound **89** have not yet been obtained. Various methods including counteranion exchange (to, e.g., PF_6^-) were tried in an effort to improve crystallization, albeit without success. This inability to obtain diffraction grade crystals may reflect the fact that complex **89** is a mixture of both the Δ- and Λ-enantiomer. So far, attempts to isolate the individual enantiomers have proven unsuccessful.

Cell studies are now underway to examine the anticancer properties of compound **89** *in vitro*. If promising results are obtained, *in vivo* studies would follow.

References

(1) See reference (58) in Chapter 1.

(2) See reference (59) in Chapter 1.

(3) See reference (62) in Chapter 1.

(4) See reference (63) in Chapter 1.

(5) Sessler J. L.; Weghorn, S. J. In *Expanded, Contracted & Isomeric Porphyrins*, Elsevier Oxford, **1997**, Vol. 15.

(6) Bauer, V. J.; Clive, D. L. J.; Dolphin, D.; Paine III, J. B.; Harris, F. L.; King, M. M.; Loder, J.; Wang, S.-W. C.; Woodward, R. B. *J. Am. Chem. Soc.* **1983**, *105*, 6429-6436.

(7) Burell, A. K.; Sessler, J. L.; Cyr, M. J.; McGhee, E.; Ibers, J. A. *Angew. Chem. Int. Ed. Eng.* **1991**, *30*, 91-93.

(8) Sessler, J. L.; Gebauer, A.; Hoehner, M. C.; Lynch, V. *Chem. Commun.* **1998**, *17*, 1835-1836.

(9) Yan, Y. K.; Melchart, M.; Habtemariam, A.; Sadler, P. J. *Chem. Commun.* **2005**, *38*, 4764-4776.

(10) Ang, W. H.; Dyson, P. J. *Eur. J. Inorg. Chem.* **2006**, *20*, 4003-4018.

(11) Hartinger, C. G.; Zorbas-Seifried, S.; Jakupec, M. A.; Kynast, B.; Zorbas, H.; Kepper, B. K. *J. Inorg. Biochem.* **2006**, *100*, 891-904.

(12) Barton, J. K.; Danishefsky, A.; Goldberg, J. *J. Am. Chem. Soc.* **1984**, *106*, 2172-2176.

(13) Lincoln, P.; Nordén, B. *J. Phys. Chem. B* **1998**, *102*, 9583-9594.

(14) Hiort, C.; Linoln, P.; Nordén, B. *J. Am. Chem. Soc.* **1993**, *115*, 3448-3454.

(15) Nordell, P.; Westerlund, F.; Wilhelmsson, L. M.; Nordén, B.; Lincoln, P. *Angew. Chem. Int. Ed.* **2007**, *46*, 2203-2206.

(16) Chen, T. F.; Liu, Y. N.; Zheng, W. J.; Liu, J.; Wong, Y. S. Inorg. Chem. 2010, 49, 6366-6368.

(17) Sessler, J. L.; Cyr, M. J.; Lynch, V. M.; McGhee, E.; Ibers, J. A. *J. Am. Chem. Soc.* 1990, **112**, 2810-2813.

(18) Lash, T. D.; Lin, Y.; Novak, B. H.; Parikh, M. D. *Tetrahedron* **2005**, *61*, 11601-11614.

(19) Cyr, M. J., Ph.D. Dissertation, The University of Texas at Austin, 1991.

(20) Smith, G. F.; Cagle, F. Wm. *J. Org. Chem.* **1947**, *12*, 781-784.

(21) Schmuck, C.; Rupprecht, D.; Urban, C.; Walden, N. *Synthesis* **2006**, *1*, 89-96.

(22) Lightner, D. A.; McDonagh, A. F. *Acc. Chem. Res.* **1984**, *17*, 417-424.

(23) Smith, K. M.; Pandey, R. K. *J. Heterocycl. Chem.* **1983**, *20*, 1383-1388.

(24) Johnson, A. W.; Kay, I. T.; Markham, E.; Price, R.; Shaw, K. B. *J. Chem. Soc.* **1959**, 3416-3424.

(25) Sullivan, B. P.; Salmon, D. J.; Meyer, T. J. *Inorg. Chem.* **1978**, *17*, 3334-3341.

6. Synthetic Approaches to Antiaromatic Rosarins

As detailed in previous Chapters, expanded porphyrins, heteroannulenes with more than five pyrrolic subunits in the macrocyclic scaffold, have been thoroughly investigated in part due to their biological, anion recognition and coordination properties. Particularly intriguing is the interplay between the both concepts of aromaticity and antiaromaticity. This is especially true in the case of expanded porphyrins since many of the key properties of porphyrins reflect their unique electronic characteristics. Most expanded porphyrins reported to date are aromatic. This includes such classic species as the texaphyrins and sapphyrins described in previous Chapters. As detailed below, the author also explored another class of expanded porphyrins, namely rosarins. This work was undertaken in an effort to synthetically access structures that would exhibit Hückel antiaromaticity.

6.1 INTRODUCTION

Most reported expanded porphyrins are aromatic and characterized by well-defined π-conjugation pathways with absorption and emission features in the near-infrared (NIR) region.[1] However, a limited number of antiaromatic congeners are known. They are identified by featureless, broad absorption spectra, the nonfluorescent nature, relatively shortened excited state lifetimes, and small two-photon

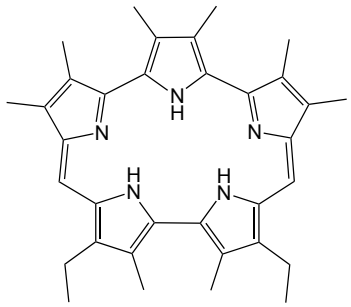

90

Figure 6.1: Structure of free base orangarin **90**.

absorption cross-section values.[2] An early example of an antiaromatic expanded porphyrin is orangarin (Figure 6.1). This pentaaza system contains 20 π-electrons in its core.[3] Osuka *et al*. also reported the gold(III) complex of hexaphyrin, another fully planar, antiaromatic expanded porphyrin.[4] More recently, amethyrin has been shown to display antiaromatic features.[5] Other fully planar antiaromatic porphyrinoids are extremely rare mostly due to the fact that expanded porphyrins often deviate from planarity when the number of pyrrole rings exceeds five. This distortion either makes them non-aromatic or allows them to adopt Möbius topologies and gain Möbius aromaticity.[6]

Meso-aryl hexaphyrins (1.0.1.0.1.0), termed *rosarins*, are a class of expanded porphyrinoids with a 4n π-electron conjugated electronic circuit in the ground state.[7, 8] According to Hückel's rule, the published β-dodecaalkyl substituted rosarin species **91** (shown in Figure 6.2) should be formally antiaromatic. However, the compound exhibits

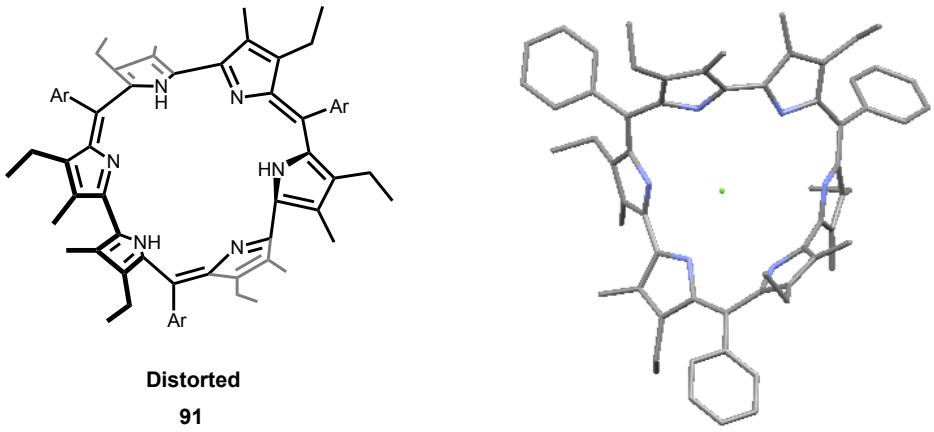

Figure 6.2: Distorted non-planar structure of rosarin species **91**.[7]

only weak antiaromaticity as judged from it spectral features. Presumably, this reflects the fact that it adopts non-planar conformations that minimize the effects of extended π-

conjugation as inferred from a single crystal X-ray diffraction analysis.[7] To test this rationale, we have designed and synthesized a new rosarin derivative named benzorosarin. This system differs from **91** in that it contains rigid ('fused') β,β'-phenylene bridges that serve to enforce planarity (Figure 6.2). As detailed below, the beonzorosarin displays spectroscopic and structural features expected for a 4n π-electron antiaromatic system.

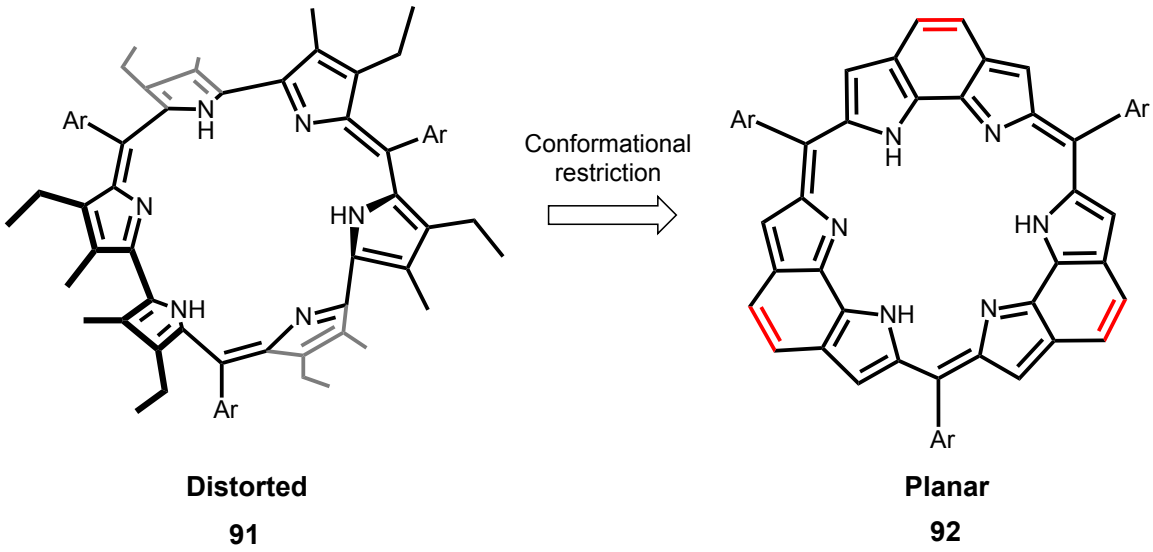

Distorted

91

Planar

92

Figure 6.3: Conformational restriction of rosarin derivatives by β,β'-phenylene bridges is expected to give a planar 24 π-electron conjugated porphyrinoid, **92**.

6.2 Synthesis and Characterization of Benzorosarin

The *β,β'*-fused rosarin derivative **92** was designed to contain a planar core geometry. To achieve this desired planarity, benzobipyrrole[9] would be a useful precursor since it would be expected to allow formation of the desired planar macrocycle. However, the use of unsubstituted benzobipyrrole (Scheme 6.1) did not yield any

macrocyclic products when reacted with benzaldehyde in the presence of trifluoroacetic acid. Instead, pyrrolic oligomers were formed. Presumably, substitution of both beta positions in the benzobipyrrole subunit is required to force reaction of the alpha positions of the bipyrrole.

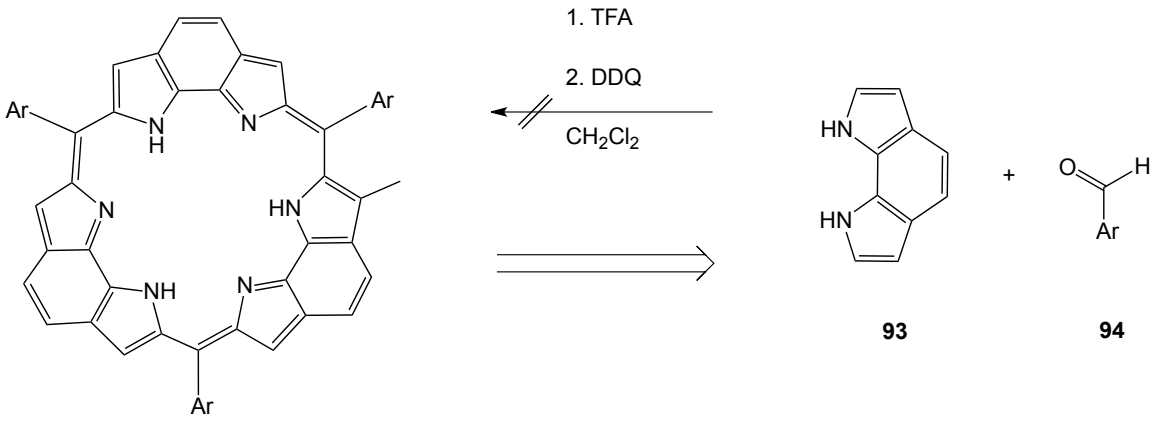

92 **93** **94**

Scheme 6.1: Failed synthetic procedure for the formation of benzorosarin species **92** from β-unsubstituted benzobipyrrole **93**.

Later it was found that β,β-dimethylbenzobipyrrole would indeed react in a productive fashion with a substituted benzaldehyde (either pentafluorobenzaldehyde or 4-tert-butyl benzaldehyde, see below) to form the desired expanded porphyrin, benzorosarin (Scheme 6.2).

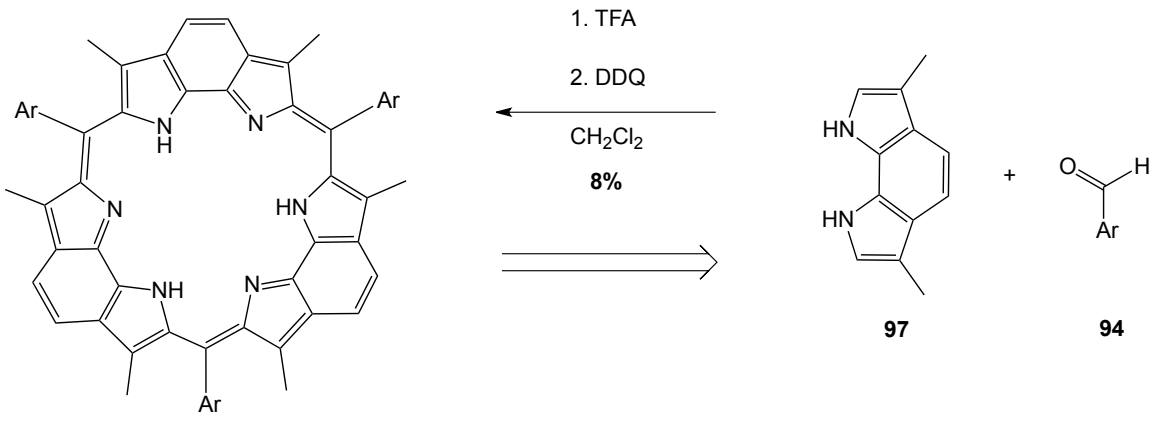

95, Ar = pentafluorophenyl

96, Ar = 4-tert.-butylphenyl

Scheme 6.2: Retrosynthetic analysis and synthetic procedure used to obtain the benzorosarin species **95** and **96** from β,β-dimethylbenzobipyrrole **97**.

The basic benzorosarin macrocycle was initially prepared via the acid catalyzed condensation of β,β-dimethylbenzobipyrrole with pentafluorobenzaldelhyde, followed by 2,3-dichloro-5,6-dicyano-*p*benzoquinone (DDQ) oxidation. However, the macrocycle demonstrated very low solubility in a variety of organic solvents and proved merely slightly soluble in DMSO. A complete and satisfactory characterization of the macrocycle was not possible. Therefore, 4-tert-butyl benzaldehyde was used instead of pentafluorobenzaldehyde as the condensation partner for the benzobipyrrole unit.

The synthesis of β,β-dimethylbenzobipyrrole **97** is shown in Scheme 6.3.

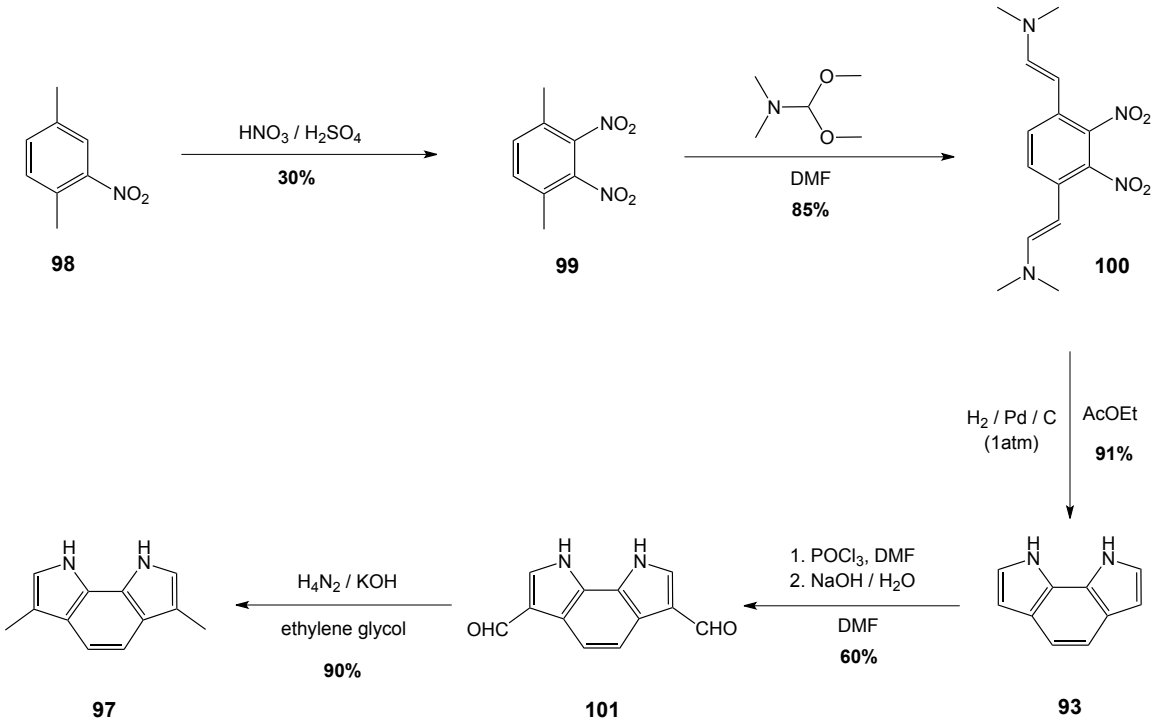

Scheme 6.3: Synthesis of β,β-dimethylbenzobipyrrole **97**.

Mononitration[10] of 1,4-dimethyl-2-nitrobenzene **98**, followed by double condensation of dimethylformamide diethyl acetal (DMFDEA) with 1,4-dimethyl-2,3-nitrobenzene **99**, results in the formation of the bis-enamine **100**. Catalytic hydrogenation of **100** directly affords benzobipyrrole **93**.[11]

3,6-Diformylbenzobipyrrole **101** was then obtained via a Vilsmeier-Haack formylation of benzobipyrrole **93**,[9] which upon Wolff-Kishner reduction using hydrazine and potassium hydroxide in ethylene glycol resulted in the formation of compound **96** in high yield. As has been noted for other structurally similar β-substituted α-free bipyrrole species, β,β-dimethylbenzobipyrrole proved to be highly unstable and decomposes quickly when exposed to ambient conditions. Therefore, it was used directly for the formation of both benzorosarin macrocycles **95** and **96.**

Addition of β,β-dimethylbenzobipyrrole **97** to a stoichiometric amount of 4-tert-butyl benzaldehyde in dichloromethane and addition of catalytic amounts trifluoroacetic acid (TFA) results in the formation of a nonaromatic porphyrinogen which is blue in color. Addition of DDQ then affords macrocycle **96** in 8% yield.

Compound **96** displays spectral features consistent with antiaromaticity, namely featureless, broad absorption spectra, a lack of appreciable fluorescence, and a vastly downfield shifted signal for the NH protons in the ^{1}H NMR (δ = 24.95 ppm, Figure 6.4). The π-conjugation pathway for rosarin **96** contains 24 π-electrons. It thus corresponds to a Hückel [4n]π antiaromatic species. Particular attention in this context is given to the inner NH protons. The published rosarin species. **91** does not show any substantial ring current effects and its NH protons resonate at ~12.3 ppm most likely due to its nonplanar structure. Hence, it is essentially considered to be nonaromatic.

On the other hand, the enforced molecular planarity by fusing the β-positions in the bipyrrole moieties and therefore rigidifying the rosarin macrocycle **96** results in a drastic downfield shift of the inner NH protons to 24.95 ppm. This may be an indication for a strong paratropic ring current in benzorosarin. Of a particular interest is the large change in the chemical shift value of NH protons of **91** upon rigidification to form **96**. The difference in chemical shift corresponds to a Δδ value of ~13 ppm.

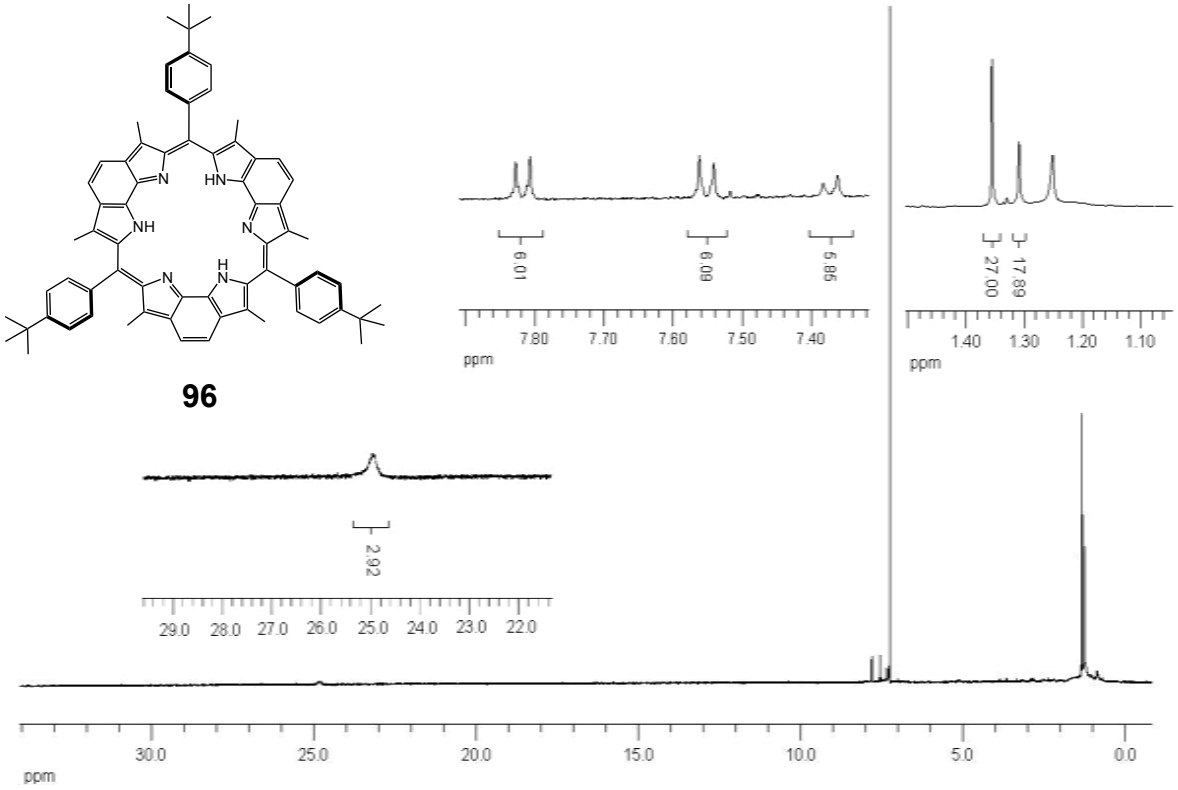

Figure 6.4: Structure and low-temperature ^{1}H NMR spectrum (400 MHz, $CDCl_3$, -40 °C) of compound **96**.

6.3 NAPHTHOROSARIN

Extensive efforts were devoted to experiments that would result in the generation of single crystals of macrocycle **96**. Unfortunately, to date no X-ray quality crystals of **96** could be obtained. This is could reflect the fact that compound **96** is fairly basic. It is thus easily protonated, even by solvent impurities. However, once protonated, compound **96** tends to decompose rapidly.

Because of this scientific drawback, we decided to focus crystallization efforts on a different rosarin macrocycle, synthesized by Prof. Chang Hee-Lee's group (Kangwon

National University, Chun-chon, Korea). In contrast to benzorosarin **96**, Prof. Lee's rosarin, termed naphthorosarin, **102**, proves to be chemically quite stable. X-ray quality crystals of the macrocycle were grown and the X-ray structure was solved by Dr. Jung-Su Park at The University of Texas at Austin. The valence bond structure of **102** together with its refined X-ray structure are shown below.

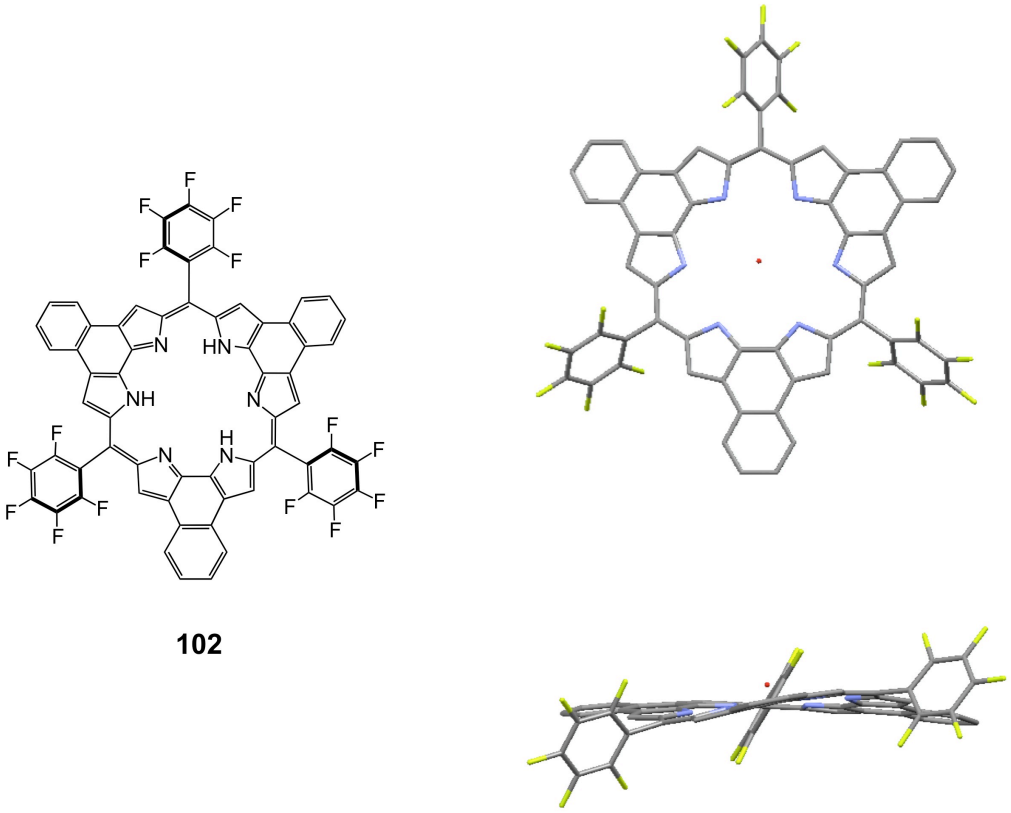

102

Figure 6.5: Valence bond structure and single crystal X-ray structure of naphtho-rosarin **102**. Hydrogen atoms have been omitted for clarity. Note that in the solid state one water molecule is found in the central core of the macrocycle.

As true for benzorosarin **96**, conformational restriction in the case of napthorosarin **102** results in the formation of a planar 24 π-electron conjugated

porphyrinoid. In accord with the Hückel rule, napthorosarin **102** displays featues that are consistent with a 4n (n = 6) antiaromatic electronic structure. Initial support for the assignment of **102** as an antiaromatic species came from ^{1}H NMR spectroscopic studies. For instance, in analogy to what was seen in the case of benzorosarin **96**, a dramatic downfield shift in the NH proton signal (δ = 26.22 ppm) was obtained in the ^{1}H NMR spectrum recorded at -60 ºC in CD_2Cl_2. Further evidence for the proposed antiaromaticity came from optical absorption studies. Specifially, the UV-Vis-NIR absorption spectrum of **102** (Figure 6.6) is characterized by a broad band at 462 nm along with an extremely weak and broad near-IR band in the 900-1600 nm spectral region. Similar near-IR spectral features are typically seen for other antiaromatic porphyrinoids.[12-14] However, the effect is particularly dramatic in the case of **102**.

In order to test whether the 4n π-electron napthorosarin **102** could be reduced to the corresponding 4n+2 π-electron congener (which was expected to exhibit Hückel aromaticity), it was exposed to sodium dithionite in water saturated dichloromethane. (Note: These studies were carried out in Prof. Dongho Kim's group at Yonsei university by postdoctoral fellow Dr. Masatoshi Ishida). The product of this reaction, presumably the 2-electron reduced form of **102**, demonstrates spectral features typical of aromatic porphyrinoids. For instance, a sharp Soret band at 612 nm and Q-bands with clear vibronic structure are seen in the absorption spectrum of the reduced

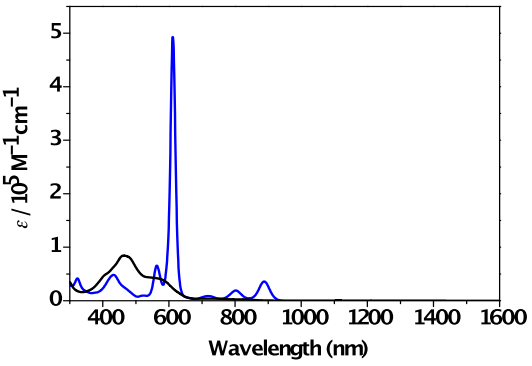

Figure 6.6:
Steady-state absorption spectra of **102** (black line), and **103** (blue line) in dichloromethane.

form, naphthorosarin **103**. This stands in clear contrast to the broad and featureless absorption spectrum of naphthorosarin **102**. In addition to dithionite, it was found that chloride anion could act as a reductant. In this case, conversion of the antiaromatic to the corresponding aromatic form takes place as the result of a proton-coupled electron transfer reaction.

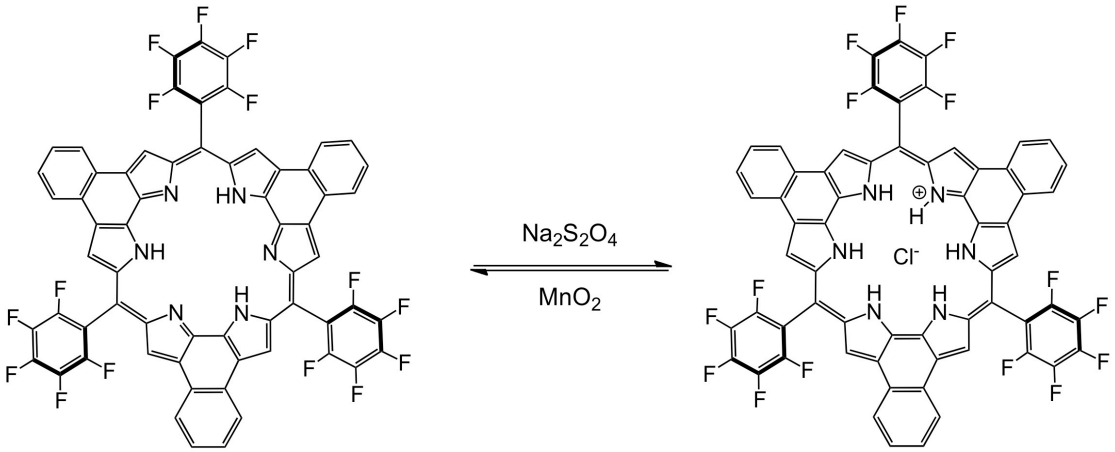

[24]-Naphthorosarin
brown solid, **purple** in solution

4n = Antiaromatic

102

[26]-Naphthorosarin
red solid, **blue** in solution

4n + 2 = Aromatic

103

Scheme 6.4: Reduction of napthrorosarin **102** using sodium dithionite. Also shown is the use of manganese(IV) oxide to effect reoxidation.

The author of this dissertation was able to grow X-ray diffraction quality single crystals of the reduced form of **102**, compound **103**. An X-ray diffraction structural analysis revealed that product **103** retains the initial quasi-planar geometry with a mean plane deviation of 0.235 Å being observed. A chloride counter anion (presumably from

free chloride present in the solvent) was found to be located inside the core and stabilized via multiple hydrogen bonding interactions involving the NH protons of the pyrrole rings.

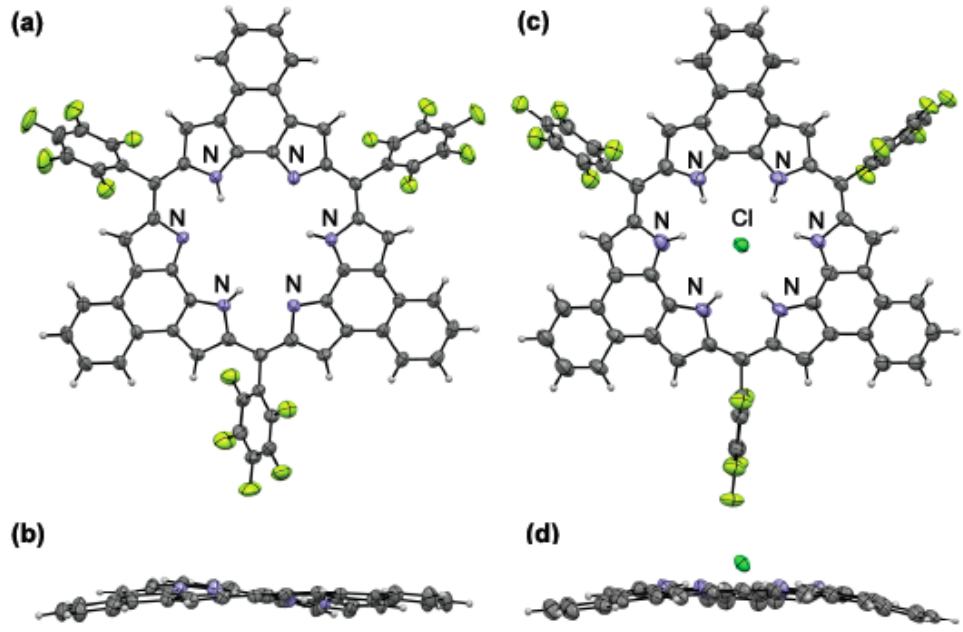

Figure 6.7: X-ray crystal structure showing (a) top and (b) side views of **102**, (c) top and (d) side views of **103**. *Meso*-aryl substituents are omitted for clarity in the side views. The thermal ellipsoids are scaled to the 50% probability level.

The ^{1}H NMR spectrum of **103** (recorded in CD_2Cl_2 at 25 ºC) revealed two pairs of deshielded outer C-H and β-H resonances (at 8.20, 9.90 and 11.00 ppm, respectively), as well as β-pyrrolic resonances at 11 ppm. A singlet at –5.30 ppm is also seen; it was assigned to the inner NH protons on the basis of D_2O exchange experiments. The distinct diatropic ring current observed in the case of **103** is as expected for a Hückel-type 4n+2 π-electron aromatic expanded porphyrin.[15-17]

6.4 CONCLUSIONS

We have synthesized and characterized a presumably coplanar benzorosarin. This new system was designed to allow the effect of enhanced molecular planarity on the electronic properties of potentially antiaromatic expanded porphyrins to be probed in detail. While X-ray crystallographic data support could not be obtained, we believe that by linking the beta positions on two adjacent pyrroles with phenylene linkers does serve to enforce rigidity. As a result, the molecular planarity and the paratropic ring current are enhanced. This assumption is supported by observations made from naphthorosarin, a related macrocycle synthesized in Prof. Chang-Hee Lee's group and further studied by Prof. Dongho Kim's group. Both β,β'-fused rosarins, benzorosarin **96** and naphthorosarin **102** exhibit a drastic downfield shift in the resonances for the inner NH protons. These signals appear at 24.95 ppm for benzorosarin **96** and 26.22 ppm for napthrorosarin **102**, respectively. Interestingly, naphthorosarin **102** can be reduced by addition of sodium dithionite; this forms an aromatic macrocycle **103** with a 4n + 2 π-electron periphery. X-ray diffraction analysis of the latter species (as the HCl salt) reveals a near-planar species. Detailed solution phase studies provided support for the notion that **103** is formed via a proton-coupled electron transfer process.

The author of this dissertation performed the synthesis of compound **96** and carried out X-ray diffraction analyses on the crystals under supervision of Dr. Jonathan L. Sessler and Dr. Vincent Lynch. Dr. Masatoshi Ishida carried out the bulk of the experimental work for compound **102** under supervision of Dr. Dongho Kim. All authors contributed to discussions. Sections of this Chapter were taken from Ishida, M.; Kim, S.-J.; Preihs, C.; Ohkubo, K.; Lim, J. M. Lee, B. S.; Park, J. S.; Lynch, V. M.; Roznyatovskiy, V. V.; Panda, P. K.; Lee, C.-H.; Fukuzumi, S.; Sessler, J. L. *Nature Chem*. **2012**, in press.

References

(1) See reference (5) in Chapter 5.

(2) Lim, J. M.; Yoon, Z. S.; Shin, J.-Y.; Kim, K. S.; Yoon, M.-C.; Kim, D. *Chem. Commun*. **2009**, 261-273.

(3) Yoon, Z. S.; Cho, D.-G.; Kim, K. S.; Sessler, J. L.; Kim, D. *J. Am. Chem. Soc*. **2008**, *130*, 6930-6931.

(4) Mori, S.; Osuka, A. *J. Am. Chem. Soc*. **2005**, *127*, 8030-8031.

(5) Cho, S.; Yoon, Z. S.; Kim, K. S.; Yoon, M.-C.; Cho, D.-G.; Sessler, J. L.; Kim, D. *J. Phys. Chem. Lett*. **2010**, 1, 895-900.

(6) Sessler, J. L.; Weghorn, S. J.; Morishima, T.; Rosingana, M.; Lynch, V.; Lee, V. *J. Am. Chem. Soc*. **1992**, *114*, 8306-8307. Figure 1 reprinted with permission from Sessler, J. L.; Weghorn, S. J.; Morishima, T.; Rosingana, M.; Lynch, V.; Lee, V. *J. Am. Chem. Soc*. **1992**, *114*, 8306-8307. Copyright 1992 American Chemical Society.

(7) Sessler, J. L.; Weghorn, S. J.; Morishima, T.; Rosingana, M.; Lynch, V.; Lee, V. *J. Am. Chem. Soc*. **1992**, *114*, 8306-8307.

(8) Setsune, J.; Katakami, Y.; Iizuka, N. *J. Am. Chem. Soc*. **1999**, *121*, 8957-8958.

(9) Panda, P. K.; Kang, Y.-J.; Lee, C.-H. *Angew. Chem. Int. Ed*. **2005**, *44*, 4053-4055.

(10) Kobe, K.; Herman, L. *J. Ind. Eng. Chem*. **1950**, *42*, 352-356.

(11) Berlin, A.; Bradamante, S.; Ferraccioli, R.; Pagani, G. A.; Sannicolò, F. *J. Chem. Soc., Chem. Commun*. **1987**, *15*, 1176-1177.

(12) Yoon, M.-C.; Cho, S.; Suzuki, M.; Osuka, A.; Kim, D. *J. Am. Chem. Soc*. **2009**, *131*, 7360-7367.

(13) Yoon, Z. S.; Kwon, J. H.; Yoon, M.-C.; Koh, M. K.; Noh, S. B.; Sesler, J. L.; Lee, J. T.; Seidel, D.; Aguilar, A.; Shimizu, S.; Suzuki, M.; Osuka, A.; Kim, D. *J. Am. Chem. Soc*. **2006**, *128*, 14128-14134.

(14) Mori, S.; Kim, K.. S.; Yoon, Z. S.; Noh, S. B.; Kim, D.; Osuka, A. *J. Am. Chem. Soc*. **2007**, *129*, 11344-11345.

(15) Sessler, J. L.; Seidel, D. *Angew. Chem. Int. Ed*. **2003**, *42*, 5134-5175.

(16) Saito, S.; Osuka, A. *Angew. Chem. Int. Ed*. **2011**, *50*, 4342-4373.

(17) Osuka, A.; Saito, S. *Chem. Commun*., **2011**, *47*, 4330-4339; and the references therein.

7. Experimental Procedures

7.1 General Procedures

All chemicals were obtained from commercial sources (Fisher Scientific, Acros Chemicals, Sigma-Aldrich or Strem Chemicals) and used as supplied unless otherwise noted. All solvents were of reagent grade quality. Fisher silica gel (230-400 mesh, Grade 60 Å) and Sorbent Technologies alumina (neutral, standard activity I, 50-200 μm) were used for column chromatography. Thin layer chromatography (TLC) analyses were either performed on silica gel (aluminum backed, 200 μm or glass backed, 250 μm) or alumina neutral TLC plates (polyester backed, 200 μm), both obtained from Sorbent Technologies. All NMR solvents were purchased from Cambridge Isotope Laboratories, Inc. ^{1}H NMR and ^{13}C NMR spectra used in the characterization of products were recorded on Varian Unity+ 300 MHz or Varian Mercury 400 MHz spectrometers. Chemical shifts are reported in units of δ (parts per million; ppm) and referenced to the residual solvent. Spectral splitting patterns are designated as s (singlet), d (doublet), t (triplet), q (quartet), m (multiplet) and br (broad). Low- and high-resolution ESI mass spectra were obtained at the Mass Spectrometry Facility of the Department of Chemistry and Biochemistry at The University of Texas at Austin using a Thermo Finnigan LTQ instrument and a Qq FTICR (7 Tesla) instrument, respectively. UV-Vis spectra were recorded either on a Beckman DU 640B spectrophotometer or a Varian Cary 5000 UV-visible spectrophotometer. HPLC spectra were taken on a Shimadzu High Performance Liquid Chromatograph (Fraction Collector Module FRC-10A, Auto Sampler SIL-20A, System Controller CBM-20A, UV-Vis Photodiode Array Detector SPD-M20A, Prominence).

The macrocyclic, methylene-bridged texaphyrin precursor used to prepare MGd (compound **56**, generally referred to as sp^3-Tex_{PEG}) and the so-called sp^3 form of the analogous texaphyrin precursor with appended methoxy functionalities (compound **57**, generally referred to as sp^3-Tex_{OMe}) were prepared as reported previously.[1-4]

The tripyrrane dialdehyde species **22** was provided by Pharmacyclics Inc. and synthesized as previously described.[5] The precursor 1,2-dimethoxy-4,5-dinitrobenzene **66** was synthesized as previously described.[6]

MGd **11** has been synthesized according to procedures previously described in the literature.[5]

7.2 Experimental Details for Chapter 2

7.2.1 Synthesis and Characterization of Complex 58

The hydrochloride salt of sp^3-Tex_{PEG} **56** (189.8 mg, 216.2 mmol) was dissolved in 20 ml methanol. Bismuth(III) nitrate pentahydrate (157.3 mg, 324.3 mmol, 1.5 equiv.) was added together with 1 ml triethylamine. The solution was stirred at 70 °C and gradually changed color from deep red to deep green. UV-Vis spectra were taken every two to four minutes (50 μL taken directly from the reaction mixture and diluted with 4 ml MeOH in the case of each sample). The insertion reaction was deemed complete after 34 minutes. No further increase in the intensity of the Soret band was observed after that time, a finding interpreted in terms of the formation of the stable, aromatic texaphyrin scaffold being complete. The solvent was removed *in vacuo* and the residue was subjected to column chromatography (silica gel, eluents: first 90% dichloromethane and 10% methanol, then 25% dichloromethane and 75% methanol). The deep green fraction

was collected and the solvent was removed *in vacuo* to give complex **58** as a deep green crystalline material (152.0 mg, 64%).

UV-Vis (MeOH, 25 °C): λ [nm] = 480 (Soret-type band); 723 (Q-type band); ^{1}H NMR (400 MHz, DMSO-d_6, 25 °C): δ[ppm] = 1.74 (t, J = 7.2 Hz, 6H); 2.24 (q, J = 6.8 Hz, 4H); 3.23 (s, 6H), 3.45 (m, 4H); 3.49 (s, 6H); 3.58 (m, 4H); 3.66 (m, 8H), 3.82 (m, 4H); 3.93 (m, 8H); 4.16 (br t, J = 4 Hz, 4H); 4.95 (br t, J = 4 Hz, 2H); 9.76 (s, 2H); 10.30 (s, 2H); 12.93 (s, 2H); ^{13}C NMR (125 MHz, DMSO-d_6, 25 °C): δ[ppm] = 4.6 (2 C); 15.4 (2 C); 22.0 (2 C); 32.2 (2 C); 37.8 (2 C); 55.2 (2 C); 59.5 (2 C); 69.0 (2 C); 70.1 (2 C); 71.3 (2 C); 100.1 (2 C); 116.7 (2 C); 117.1 (2 C); 118.0 (2 C); 128.4 (2 C); 150.1 (2 C); 150.9 (2 C); 151.4 (2 C); 155.5 (2 C); low resolution MS (ESI): 1098.47 (M^+, monomeric Bi(III)-texaphyrin with axial hydroxide ligand); high resolution MS (ESI): calculated for $C_{48}H_{67}N_5O_{11}Bi^{+1}$ = 1098.4641; found: 1098.46354 ($C_{48}H_{67}N_5O_{10}Bi^{+1}$, M^+); HPLC (tC18 reverse phase column, eluents: water (1% TFA) and acetonitrile) spectrum shows ≥96% purity;

7.2.2 Synthesis and Characterization of Complex 59

The hydrochloride salt of sp^3-Tex_{PEG} **56** (189.8 mg, 216.2 mmol) was dissolved in 20 ml methanol. Lead(II) nitrate (107.4 mg, 324.3 mmol, 1.5 equiv.) was added together with 1 ml triethylamine. The solution was stirred at 70 °C and gradually changed color from deep red to deep green. The mixture was stirred at that temperature for two hours. The solvent was removed *in vacuo* and the residue was then subjected to column chromatography (silica gel, eluents: first 90% dichloromethane and 10% methanol, then 25% dichloromethane and 75% methanol). The deep green fraction was collected and the

solvent was removed *in vacuo* to give complex **59** as a deep green crystalline material (109.8 mg, 47%).

UV-Vis (MeOH, 25 °C): λ [nm] = 471 (Soret-type band); 743 (Q-type band); ^{1}H NMR (400 MHz, CD_3OD, 25 °C): δ[ppm] = 1.57 (m, 6 H); 2.19 (br, 4 H); 3.27 (br, 6 H), 3.30 (m, 8 H); 3.50 (m, 4 H); 3.63 (m, 8 H); 3.74-3.95 (m, 16 H); 4.14 (br, 2H); 8.38 (s, 2 H); 8.98 (s, 2 H); 10.92 (br, 2 H); ^{13}C NMR (125 MHz, DMSO-d_6, 25 °C): δ[ppm] = 5.8 (2 C); 18.5 (2 C); 22.9 (2 C); 30.2 (2 C); 38.1 (2 C); 55.5 (2 C); 63.5 (2 C); 70.6 (2 C); 71.4 (2 C); 72.6 (2 C); 98.4 (2 C); 113.3 (2 C); 114.3 (2 C); 115.6 (2 C); 128.2 (2 C); 135.1 (2 C); 151.3 (2 C); 152.0 (2 C); 152.5 (2 C); 167.1 (2 C); low resolution MS (ESI): 1080.40 (M^+, monomeric Pb-Tx, no axial ligand); high resolution MS (ESI): calculated for $C_{48}H_{66}N_5O_{10}Pb^{+1}$ = 1080.4576; found: 1080.45706 ($C_{48}H_{66}N_5O_{10}Pb^{+1}$, M^+); HPLC (tC18 reverse phase column, eluents: water (1% TFA) and acetonitrile) spectrum shows ≥99% purity.

7.2.3 Synthesis and Characterization of 60

The hydrochloride salt of sp^3-Tex_{OMe} **57** (140.6 mg, 216.2 mmol) was dissolved in 20 ml methanol. Bismuth(III) nitrate pentahydrate (157.3 mg, 324.3 mmol, 1.5 equiv.) was added together with 1 ml triethylamine. The solution was stirred at 70 °C and gradually changed color from deep red to deep green. The mixture was stirred at that temperature for two hours. The solvent was removed in vacuo and the residue was then subjected to column chromatography (silica gel, eluents: first 95% dichloromethane and 5% methanol, then 60% dichloromethane and 40% methanol). The deep green fraction was collected and the solvent was removed *in vacuo* to give complex **60** as a deep green crystalline material (129.9 mg, 72%).

UV-Vis (MeOH, 25 °C): λ [nm] = 479 (Soret-type band); 722 (Q-type band); ^{1}H NMR (400 MHz, DMSO-d_6, 25 °C): δ[ppm] = 1.74 (t, J = 7.6 Hz, 6H); 2.25 (br t, J = 7.2 Hz, 4H); 3.16 (s, 2H), 3.51 (br s, 6H); 3.66 (t, J = 6 Hz, 4H); 3.95 (m, 6H); 4.45 (s, 6H); 9.77 (s, 2H); 10.35 (s, 2H); 13.01 (s, 2H); ^{13}C NMR (125 MHz, DMSO-d_6, 25 °C): δ[ppm] = 9.8 (2 C); 16.4 (2 C); 21.1 (2 C); 28.5 (2 C); 30.3 (2 C); 59.4 (2 C); 70.0 (2 C); 96.5 (2 C); 112.4 (2 C); 116.9 (2 C); 118.0 (2 C); 133.3 (2 C); 138.2 (2 C); 144.6 (2 C); 145.5 (2 C); 146.8 (2 C); 158.3 (2 C); low resolution MS (ESI): 834.27 (M^+, monomeric Bi(III)-texaphyrin with axial hydroxide ligand); high resolution MS (ESI): calculated for $C_{36}H_{43}N_5O_5Bi^{+1}$ = 834.3068; found: 834.30626 ($C_{48}H_{67}N_5O_{10}Bi^{+1}$, M^+);HPLC (tC18 reverse phase column, eluents: water (1% TFA) and acetonitrile) spectrum shows ≥98% purity.This complex was also characterized by X-ray diffraction analysis (see section 7.7 and Appendix section).

7.2.4 Synthesis and Characterization of Complex 61

The hydrochloride salt of sp^3-Tex$_{OMe}$ **57** (140.6 mg, 216.2 mmol) was dissolved in 20 ml methanol. Lead(II) nitrate (107.4 mg, 324.3 mmol, 1.5 equiv.) was added together with 1 ml triethylamine. The solution was stirred at 70 °C and gradually changed color from deep red to deep green. The mixture was stirred at that temperature for two hours. The solvent was removed in vacuo and the residue was subjected to column chromatography (silica gel, eluents: first 95% dichloromethane and 5% methanol, then 60% dichloromethane and 40% methanol). The deep green fraction was collected and the solvent was removed *in vacuo* to give complex **61** as a deep green crystalline material (123.6 mg, 70%).

UV-Vis (MeOH, 25 °C): λ [nm] = 479 (Soret-type band); 740 (Q-type band); ^{1}H NMR (300 MHz, CD_3OD, 25 °C): δ[ppm] = 1.62 (t, J = 7.2 Hz, 6 H); 2.19 (t, J = 6.8 Hz, 4 H); 3.66-3.92 (m, 12 H), 4.56 (s, 6 H); 8.58 (s, 2 H); 9.13 (s, 2 H); 11.12 (s, 2 H); ^{13}C NMR (125 MHz, DMSO-d_6, 25 °C): δ[ppm] = 6.0 (2 C); 17.1 (2 C); 22.7 (2 C); 26.6 (2 C); 32.8 (2 C); 58.3 (2 C); 66.2 (2 C); 97.2 (2 C); 108.3 (2 C); 119.5 (2 C); 120.2 (2 C); 135.5 (2 C); 140.8 (2 C); 148.8 (2 C); 149.9 (2 C); 150.4 (2 C); 159.9 (2 C); low resolution MS (ESI): 816.40 (M^+, monomeric Pb-Tx, no axial ligand); high resolution MS (ESI): calculated for $C_{36}H_{42}N_5O_4Pb^{+1}$ = 816.3003; found: 816.29977 ($C_{36}H_{42}N_5O_4Pb^{+1}$, M^+); HPLC (tC18 reverse phase column, eluents: water (1% TFA) and acetonitrile) spectrum shows ≥98% purity.

7.2.5 *In Vitro* Anti-Proliferative Activity of Complexes 58 (MBi) and 59 (MPb)

The proliferation of exponential phase cultures of A2780 cells was assessed by a dye reduction assay and assessing the formazan product.[7] Briefly, tumor cells were seeded in 96-well microtiter plates at 300 cells/well, respectively, and allowed to adhere overnight in RPMI 1640 medium supplemented with 2 mM L-glutamine, 10% heat inactivated fetal bovine serum, and antibiotics (200 U/cm^3 penicillin and 200 μg/cm^3 streptomycin). Stock solutions of MBi **58** and MPb **59** (30% v/v methanol/H_2O) were formulated in the indicated solvent for maximum stability and then diluted in medium for secondary stocks. Secondary stock solutions were serially diluted in medium and immediately added to wells to give the final concentrations indicated in the figures, whereupon plates were incubated at 37 ºC under a 5% CO_2 and 95% air atmosphere. After a total of five days, the tetrazolium dye, 3-(4,5-dimethylthiazol-2-yl)-2,5-diphenyltetrazolium bromide (MTT, Sigma Chemical) was added to each well, the plates

incubated at 37 ºC, whereupon the medium was removed, the formazan dissolved in 50 μM DMSO and absorbances measured at 560-650 nm using a microplate reader (Molecular Devices, Sunnyvale, CA). Absorbances were corrected for background and the values normalized to wells containing untreated cells to allow plate-to-plate comparison. The data are shown as mean inhibition of proliferation or growth as a % of control cells from eight to ten replicate values. Error bars represent the associated standard deviation.

7.3 EXPERIMENTAL DETAILS FOR CHAPTER 3

7.3.1 Synthesis of Double Effector Nanoparticles (GdTx-MNPs)

7.3.1.1 Synthesis of Complex *62*

This is a modified protocol of the synthetic procedures described previously[8]: To a dark green solution of MGd **11** (2.29 g, 2 mmol) in a mixture of 300 ml dry dichloromethane and 30 ml dry THF, diispropylethylamine (1.05 cm^3, 6 mmol) was added under argon at room temperature. Then, 4,4'-dimethoxytrityl chloride (1.7 g, 5 mmol) was added to the solution in one portion. The solution was stirred for 8-12 hours at room temperature. The reaction was monitored by HPLC. Three major peaks were seen: MGd (unfunctionalized), DMTO-MGd **62** (monofunctionalized) and $(DMTO)_2$-MGd (difunctionalized) in the HPLC-spectrum. When the integrated area of the peak corresponding to DMTO-MGd appeared to be maximal (around 40%), the reaction was quenched with 10 ml of methanol. At this point, a reverse-phase tC18 cartridge column was used for separation, with a mixture of acetonitrile and 0.1 M buffer (pH = 4.3, 0.1 M

ammonium acetate and 1% glacial acetic acid in water) being used as the eluent. MGd eluted first from the column with 25-30% acetonitrile-buffer, DMTO-MGd **62** with 50% acetonitrile-buffer and the doubly protected species $(DMTO)_2$-MGd with 70% acetonitrile-buffer. Compound **62** was desalted using a new tC18 column using deionized water. The product was eluted from the column with neat methanol and a deep green solid was obtained after evaporation and drying *in vacuo* (870 mg, 30%)

UV-Vis (MeOH, 25°C): λ [nm] = 475 (Soret-like band); 740 (Q-type band); low resolution MS (ESI): 1392 (M^+ - AcO); high resolution MS (ESI): calculated for $C_{71}H_{87}GdN_5O_{14}$ = 1391.5491; found: 1391.5502 ($C_{71}H_{87}GdN_5O_{14}$, M^+ - AcO); HPLC (tC18 reverse phase column, eluents: water (1% TFA) and acetonitrile) spectrum shows ≥ 94% purity.

7.3.1.2 Synthesis of Complex *63*

This complex was prepared using a modified version of the synthetic procedures described previously[8]: Complex **62** (530 mg, 0.37 mmol), phthalimide (269 mg, 1.83 mmol) and triphenylphosphine (479 mg, 1.83 mmol) were dried overnight using a vacuum pump. Dry DCM (50 mL, dried over calcium hydride and redistilled under argon) was added and to the resulting deep green solution, diethyl azodicarboxylate (287 mg, 1.65 mmol) was added dropwise at 0 ˚C and stirred for 5 hours. The solvent was removed *in vacuo* and hydrazine (24 mg, 0.75 mmol) in 20 mL methanol were slowly added to the flask. The turquoise solution was stirred for 4 hours under argon. Buffer (50 mL, pH = 4.3, 0.1 M ammonium acetate and 1% acetic acid in deionized water) was added and the solution was extracted with 3 x 50 mL chloroform. The organic layers were combined, dried over sodium sulfate and evaporated to dryness. The resulting crude

product was loaded onto a reverse-phase tC18 cartridge column. A mixture of acetonitrile and aqueous buffer was used to as the eluent. Finally, the material was subjected to further purification on a new tC18 column to remove excess ammonium salt. After evaporation of all solvents, the green solid was dissolved in 2 mL dichloromethane and 1 mL glacial acetic acid was added. The ensuing deprotection of the hydroxyl group was monitored by TLC and HPLC. After approximately three hours, the spot/peak corresponding to the starting material could no longer be observed. Dichloromethane was quickly removed using a vacuum pump. The resulting brownish liquid was immediately poured into 50 mL of the buffer described above and the resulting green solution was loaded onto a tC18 column. A mixture consisting of 30% acetonitrile/70% buffer was used to collect the green band. A pure green solid, corresponding to complex **63**, was obtained after removing the ammonium salt via passage through a new tC18 cartridge, washing with deionized water, eluting with neat methanol, and drying *in vacuo* (93 mg, 21%).

UV-Vis (MeOH, 25°C): λ [nm] = 478 (Soret-like band); 750 (Q-type band); lor resolution MS (ESI): 1148 (M^+ - AcO); high resolution MS (ESI): calculated for $C_{52}H_{74}GdN_6O_{13}$ = 1148.4264; found: 1148.4232 ($C_{71}H_{87}GdN_5O_{14}$, M^+ - AcO); HPLC (tC18 reverse phase column, eluents: water (1% TFA) and acetonitrile) spectrum shows ≥ 97% purity.

7.3.1.3 Synthesis of $Zn_{0.4}Fe_{2.6}O_4$ Nanoparticles and Surface Modification

Zinc doped iron oxide magnetic nanoparticles ($Zn_{0.4}Fe_{2.6}O_4$) were prepared as described previously[9] and redispersed in toluene. These nanoparticles were coated with a 16 nm SiO_2 shell using a modified base-catalyzed sol-gel process.[10] Briefly,

polyoxyethylene (5) nonylphenylether (1.95 mL, 4.40 mmol, also termed Igepal CO-520 containing 50 mol % hydrophilic groups) and 2.5 mg of the nanoparticles were dispersed in cyclohexane and subject to vortex mixing. Treatment with 30% aqueous ammonium hydroxide (0.26 mL) followed by tetraethyl orthosilicate (0.46 mL, 2.04 mmol, TEOS) provides silica coated nanoparticles. With these in hand, 3-aminopropyltrimethoxysilane (12.5 μL, 0.07 mmol, APTMS) was added to introduce the amine functional group. After 72 hours of aging at room temperature, the resulting amine functionalized nanoparticles were precipitated via addition of methanol. After collecting by centrifugation, the precipitates were treated with succinic anhydride (2.5 mg, 0.10 mmol, SA) in dimethyl sulfoxide (DMSO) and stirred for 24 hours. After filtration and rinsing, the carboxylate functionalized nanoparticles were redispersed in DMSO.

7.3.1.4 Synthesis of Gadolinium-Texaphyrin - $Zn_{0.4}Fe_{2.6}O_4$ Magnetic Nanoparticles (GdTx-MNPs)

1-Ethyl-3-(3-dimethylaminopropyl)carbodiimide hydrochloride (50 mM, EDC) and *N*-hydroxysulfosuccinimide (5 mM, Sulfo-NHS) were added to a solution of carboxylated $Zn_{0.4}Fe_{2.6}O_4$ nanoparticles in DMSO. Then, 3500 molecular weight poly(ethylene glycol) bis(amine) (50 mg, 0.03 mmol, PEG) was added to the reaction mixture. After stirring for two hours at room temperature, the PEGylated $Zn_{0.4}Fe_{2.6}O_4$ nanoparticles (MNPs) were isolated by centrifugation and redispersed in DMSO. Next, complex **63** (34.42 mg, 0.03 mmol, GdTx) and disuccinimidyl suberate (10 mg, 0.03 mmol, DSS) in anhydrous *N, N*-dimethyl-formamide (DMF) were stirred for four hours under argon. The above MNPs were then added to the mixture. After four hours, the GdTx-MNPs were precipitated by addition of acetone, and redispersed in DMSO. The GdTx-MNPs (as a dispersion in DMSO) were then transferred to an aqueous solution.

7.3.2 T_1 and T_2 MR Imaging of GdTx-MNPs, GdTx, and MNPs

MR imaging of the GdTx-MNPs of this study was performed using a 1.5 Tesla MRI instrument (Philips, Germany). T_1 scans were obtained using a standard sequence (TR = 625 ms, TE = 10 ms, FOV = 75 mm, matrix = 256 × 256, slice thickness = 0.7 mm, acquisition number = 1). T_2 scans were obtained by using fast spin-echo sequence (TR = 4000 ms, TE = 80 ms, FOV = 75 mm, matrix = 256 × 256, slice thickness = 0.7 mm, acquisition number = 1).

7.3.3 Measurement of Specific Loss Power

Magnetic heating of aqueous suspensions of GdTx-MNPs with a concentration of 0.2 mg/mL was performed under an alternating magnetic field (500 kHz at 30 kA/m, AC magnetic field), provided by a high-radiofrequency heating machine (HF 10K, Taeyang System Co., Korea). The temperature change was monitored by fiber optic thermometer (M602, Lumasense Technologies Inc., USA). The specific loss power (SLP) values (watt/g) for the samples are calculated using the following equation, where d*T*/d*t* is the initial slope of the graph (temperature change vs. time) in Figure 7.1.[10]

$$SLP = \frac{CV_s}{m}\frac{dT}{dt}$$

C: volumetric specific heat capacity of the sample solution ($JL^{-1}K^{-1}$)

V_s: sample volume (L)

m: mass of magnetic material in the sample (g)

dT/dt: initial slope of the change in temperature versus time curve (Ks^{-1})

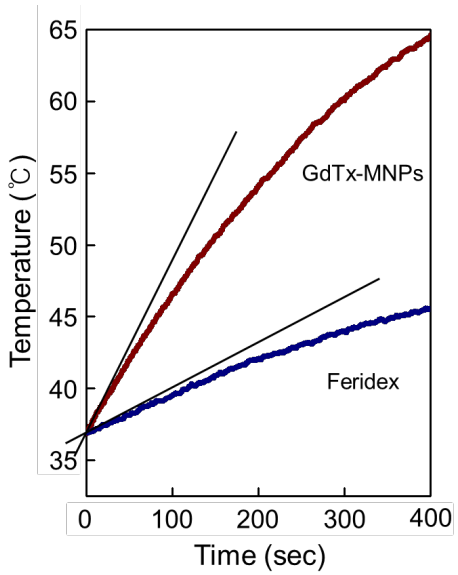

Figure 7.1: Temperature profile of GdTx-MNPs and Feridex subjected to an AC magnetic field. Each black linear line indicates the initial slope of GdTx-MNPs (red) or Feridex (blue). The fourfold increase in the initial slope for the GdTx-MNP experiments (0.12) compares favorably to the one produced by Feridex (0.03). The SLP values were 471 Wg^{-1} and 115 Wg^{-1} for GdTx-MNPs and Feridex, respectively.

7.3.4 Cytotoxicity Testing of MNPs

The breast cancer cells, MDA-MB-231, were cultured in culture media composed of minimal essential medium (MEM) supplemented with 10% fetal bovine serum (FBS), 25 mM HEPES buffer, and penicillin/streptomycin at 37 °C in a 5% CO_2 and 95% air atmosphere. The cytotoxicity of the MNPs was assessed using a cell counting kit-8 (CCK-8, Dojindo Molecular Technology). 1×10^5 MDA-MB-231 cells were seeded in a 24-well plate and incubated overnight. The cells were then incubated with 200 μL of a fresh media containing 12.5 – 300 μg/mL concentrations of MNPs for 24 hours. After the solution was replaced with a fresh media (OPTI-MEM), cells were incubated with 10 μL

of the CCK-8 solution for each well for two hours. Then, the absorbance of each sample was measured at 450 nm.

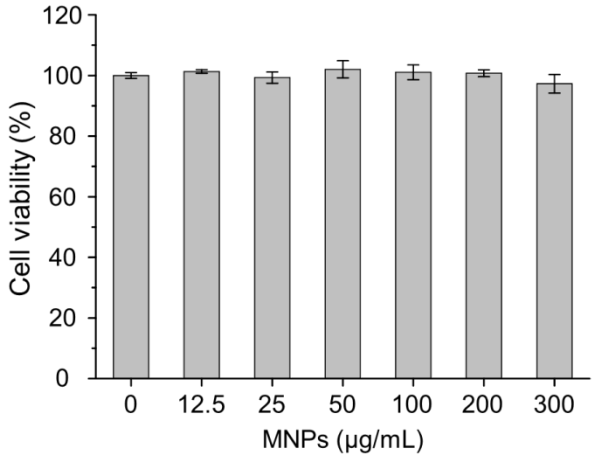

Figure 7.2: *In vitro* antiproliferative effect of MNPs on the MDA-MB-231 cancer cell line. The results provide support for the assumption that the inherent viability of these cells is not perturbed by the MNPs even at high (300 μg/ml) concentrations and in the absence of an applied magnetic field.

7.3.5 Cytotoxicity Testing of GdTx 63

The experiment was carried out in the same way described in section 3.5.4 but using complex **63** instead of the MNPs.

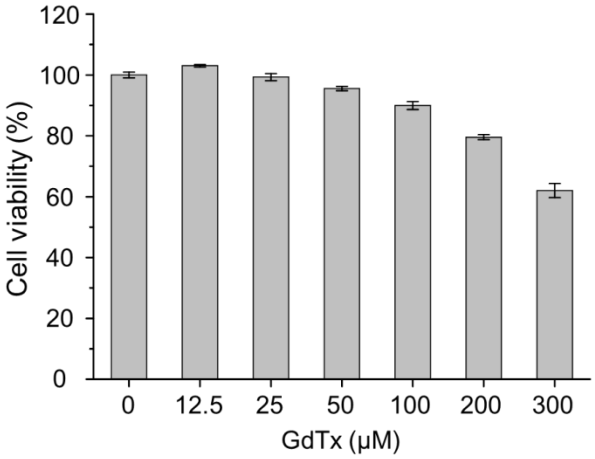

Figure 7.3: Anticancer effect of compound **63**. Note the decrease in cell viability as the concentration of compound **63** increases. At concentrations less than 25 μM, no cell death is observed.

7.3.6 Detection of Reactive Oxygen Species (ROS) in MDA-MB-231

ROS production was measured in live cells by monitoring the oxidation of 2′,7′-dichlorofluorescein diacetate (DCFA, Molecular Probes) and its ensuing conversion to 2′,7′-dichlorofluorescein (DCF).[11] In these experiments, 5 x 10^4 MDA-MB-231 cells/well were incubated in MEM supplemented with 10% FBS containing 0.2 mg/mL GdTx-MNPs and 100 μM ascorbate for 24 hours. After washing several times in PBS, the cells were incubated in 4 μM DCFA for 15 minutes at 37 °C in the dark. Cells were washed with PBS and imaged immediately using a FV1000 confocal microscope (Olympus).

7.3.7 Monitoring of Apoptosis Induced by Mild Hyperthermia in MDA-MB-231

To monitor the presumed apoptosis, the Annexin V-FITC Apoptosis Detection Kit (Biovision) was used. Here, MDA-MB-231 cells were incubated with 0.2 mg/mL of GdTx-MNPs for five hours and then subjected to an AC magnetic field for 30 min. At six

hours and 24 hours post treatment, 5 μL of Annexin V and PI in binding buffer were added to the cells. The treated cells were fixed with 4% paraformaldehyde at 4 ºC for 30 minutes and washed twice with cold PBS solution. At this junction, a mounting solution containing DAPI (4',6-diamidino-2-phenylindole) was added. The cells were observed using a FV1000 confocal microscope (Olympus).

7.3.8 Intracellular T_1-, T_2- MR images of GdTx-MNPs.

MDA-MB-231 cells were incubated with GdTx-MNPs for 24 hours and their T_1-, T_2-weighted MR images were obtained. Untreated cells served as control. Cells were incubated in OPTI-MEM containing 40 μg/mL of GdTx-MNPs and 1.6 μg/mL of poly L-lysine as a transfection agent for 24 hours. After rinsing several times with cold Phosphate buffered saline (PBS), the cells were fixed with 4% formaldehyde solution for 30 min at 4 ºC. After the cells were washed with cold PBS and resuspension in PBS, an aliquot of 1 x 10^5 cells was placed in a PCR tube. MR imaging of GdTx-MNPs incubated cells was performed by using a 1.5 Tesla MRI. T_1- and T_2-weighted MR scans were obtained by using the same method described in section 7.3.2 (*vide supra*).

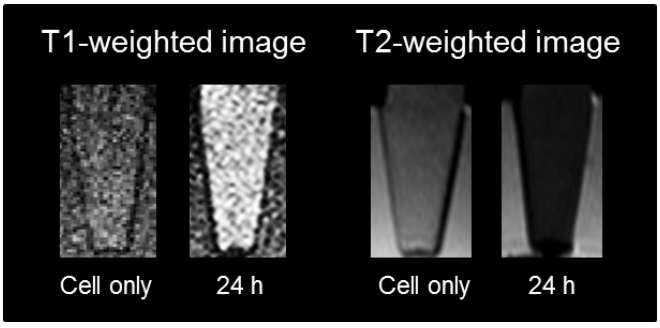

Figure 7.4: T_1- and T_2-weighted MR images of MDA-MB-231 cells incubated with GdTx-MNPs.

7.4 Experimental Details for Chapter 4

7.4.1 Synthesis and Characterization of Compound 67

1,2-dimethoxy-4,5-dinitrobenzene **66** (1 g, 4.38 mmol) was dissolved in 10 mL methanol and placed in a hydrogenation flask. The solution was purged with nitrogen for five minutes and palladium on activated carbon (10%, 0.1 g) was added. The mixture was degassed and allowed to react with hydrogen gas at 100 psi with agitation for 18 hours, filtered under Schlenk conditions through a minimal pad of Celite, and added instantly to a solution of **22** (2.11 g, 4.38 mmol) in 15 mL methanol under nitrogen at 70 ºC. Aqueous hydrochloric acid was added (2 mL, 0.5 M) and the resulting deep red reaction mixture was stirred for four hours. Next, gadolinium acetate tetrahydrate (2.67 g, 6.57 mmol, 1.5 equiv) was added together with 3 ml triethylamine and the solution was stirred at 70 °C for 16 hours, during which time the solution gradually changed color from deep red to deep green. The solvent was removed *in vacuo* and the residue was subjected to column chromatography (silica gel). To remove apolar impurities, the column was eluted with a mixture of 95% dichloromethane and 5% methanol. The product slowly starts to elute when a mixture of 60% dichloromethane and 40% methanol is used as the eluent. The deep green fraction isolated using this eluent mixture was collected and the solvent was removed in vacuo to give GdTx **67** as a deep green crystalline material (1.63 g, 42%). UV-Vis (MeOH, 25 °C): λ_{max} = 470 (Soret-type band); 739 (Q-type band); low resolution MS (ESI in MeOH): 797.25 (M^+ - 2OAc + OMe), 825.42 (M^+ - OAc); high resolution MS (ESI in MeOH): calculated for $[C_{38}H_{45}N_5O_6Gd^{+1}]^+$ = 825.2611; found: 825.2621 ($[C_{38}H_{45}N_5O_6Gd+1]^+$; M^+ - OAc); HPLC (tC18 reverse phase column, eluents: water (1% TFA) and acetonitrile) spectrum shows ≥98% purity.

7.4.2 Formulation and Stabilization of GdTx-Polymer Micelles

For targeted formulations, 5% of the targeted polymer and 95% of the untargeted polymer were used. The triblock polymer (750 mg) was dissolved in water (150 mL) at a concentration of 5 mg/mL and stirred with slight heating until fully dissolved. After cooling to room temperature, the polymer solution was placed in a sheer mixer and a solution of GdTx **67** (0.5% w/w in 380 μL dimethyl sulfoxide) was added. The resulting solution was then passed through a microfluidizer (Microfluidics, M-110Y) at 23,000 PSI, filtered through a 0.22 μm Steriflip-GP Filter Unit (Millipore) and lyophilized.

For stabilized formulations, the micelles were subjected to an Fe(III)-mediated crosslinking reaction.[12] $FeCl_3$ was prepared at a concentration of 1.35 g/mL in 20 mM Tris-Cl (pH = 7.4). The targeted and untargeted micelles were then dissolved in the Fe(III)-tris solution at a concentration of 20 mg/mL and the solution was adjusted to pH = 8 through dropwise addition of 0.1 – 1 M aqueous NaOH. The crosslinking reaction was stirred for 12 hours and the contents of the reaction vessel were then lyophilized.

7.4.3 Cell Culture

HCT116 (Human colon carcinoma) cells overexpressing hMC1R were engineered at Moffitt Cancer Center, Tampa, FL. HCT116 cells were transfected with the pCMV6-Entry Vector (Origene, RC 203218) using the Fugene 6 transfection reagent (Roche, 1814-443). Transfected cells were grown in a selection media containing 0.4 mg/ml geneticin (Life Technologies, 11811-031) and tested for the hMC1R cell surface expression by saturation binding assay.[13] Cells were maintained under standard conditions (37 °C and 5% CO_2) and were grown in Dulbecco's modified Eagle medium (DMEM) supplemented with 10% FBS and 5% penicillin/streptomycin. Geneticin

(G418S, 0.8%) was added to the media to ensure proper selection. Expression of hMC1R was verified through immunohistochemistry (Figure 7.5).

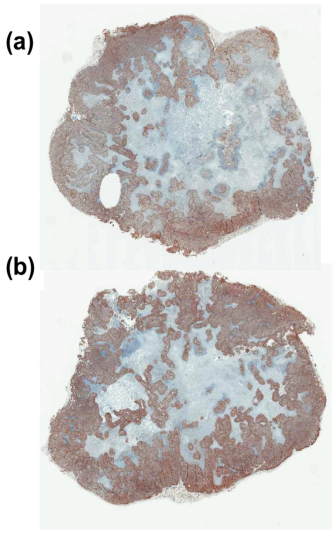

Figure 7.5: *In vivo* characterization of MC1R surface expression for HCT116/MC1R cells. (a-b) IHC staining of representative left (a) and right (b) tumors from a SCID mouse.

7.4.4 Europium Binding Assays

Europium binding assays were conducted as previously published.[14, 15]

7.4.5 *In Vivo* Murine Tumor Models

All animal experiments were carried out at The Moffitt Cancer Center (Tampa, FL). The studies were approved by the institution review board and conformed by guidelines on the care and use of animals in research. HCT116/hMC1R-expressing tumor models were studied in female SCID/beige mice obtained from Harlan

Laboratories at 6-8 weeks of age. HCT116/hMC1R cells were injected at concentrations of 3 X 10^6 – 10 X 10^6 cells per 0.1 mL of phosphate-buffered saline. Tumor volume measurements were made bi-weekly and calculated by multiplying the length by the width squared and dividing by two. Final volume measurements were determined through region of interest (ROI) analysis on the MRI.

7.4.6 MRI Imaging and Analysis

All imaging was completed at The Moffitt Imaging Center on a 7 Tesla, 30 cm horizontal bore Agilent magnetic resonance imaging (MRI) spectrometer ASR310 (Agilent Life Sciences Technologies, Santa Clara, CA). Once the tumors in the animals reached an average of ~ 500 mm^3, the animals were pair-matched by tumor size and sorted into four groups to receive the following micelles: TG-XL; UT-XL; T-UXL; or UT-UXL. Each animal was imaged the day before micelle injection for "pre" images. The following morning, each animal was individually administered 12 μmol/kg GdTx (as GdTx micelles) dissolved in 200 uL saline, via tail vein injection, and the time of injection was noted. Follow-up MRI images were taken at one hour, 4 hours, 12 hours, 24 hours and 48 hours post-injection of the micelles.

All animals were sedated using isoflurane and remained under anesthesia for the duration of the imaging. Animals were kept at body temperature (~37 ºC) using a warm air blower; the temperature of the air was adjusted to maintain the body temperature and was monitored using a fiber optic rectal probe. SCOUT images were taken to determine animal position within the magnet and setup the slices for the T_1 weighted spin echo multi slice (SEMS) images. The SEMS images were taken as coronal-90 images (read direction along the X-axis, phase-encode along the Z-axis), with data matrix of 128 X

128 and a FOV of 40 mm (read) X 90 mm (phase); 15 one-mm thick slices were taken with a 0.5 mm gap between slices; the TR was 180 ms, and TE was 8.62 ms; there were eight averages taken for each image, resulting in a total scan time of about three minutes per SEMS image.

Images were processed using MATLAB (Mathworks, Natick, MA) to draw regions of interest (ROI) in the tumors, kidney, liver and thigh muscle over multiple slices for each mouse at each time point. All intensities for each area of interest were averaged to determine a mean intensity. The mean intensity of each area was then normalized to the mean intensity of the thigh to generate a normalized intensity (NI):

$$NI = \frac{I_{tumor}}{I_{thigh}}$$

A percent change value was then calculated by comparing each normalized time point after injection to the normalized pre-injection intensity mean:

$$\%Change = \frac{NI_{12h}}{NI_{pre}} \text{ x } 100$$

Since the right and left tumors are histologically equivalent as judged by immunohistochemistry (Figure 7.5), the % change values for all tumors were averaged to obtain an "average tumor % change" at time points 1 – 24 hours. Percent change values were also averaged for R and L kidney to obtain an "average kidney % change" at time points 1 – 24 hours.

7.4.7 GdTx Micelle Stability

Crosslinked GdTx micelles were dissolved in PBS at the critical micelle concentration (CMC, 0.02 mg/mL) and dialyzed for six hours against PBS (pH = 8 and

pH = 3). HPLC analyses of the GdTx micelles pre- and post-dialysis indicated that the crosslinked micelles retained >95% of the encapsulated GdTx after dialysis at pH = 8 and 50% of the encapsulated GdTx at pH = 3.

7.4.8 Competitive Binding Assays

Time-resolved lanthanide fluorescence competitive binding assays[14, 15] were performed in an effort to optimize ligand loading for maximal avidity. In these assays, increasing concentrations of micelles were measured for their ability to displace competitively displace europium-labeled NDP-α-MSH **69**. The remaining europium was then measured using time resolved fluorescence. As gadolinium(III) cations can potentially interfere with the lanthanide-based TRF binding assays,[14] unloaded triblock polymer micelles (i.e., free of GdTx) targeted with 2.5% to 30% ligand **69** by weight loading were used. Micelles stabilized with Fe(III) crosslinking had the highest binding avidity at 5% ligand loading, as reflected in the lowest K_i (1.49 ± 0.12 nM; n = 4). It was also observed that XL micelles had significantly higher binding avidities at all ligand loading levels ($p < 0.001$). *In vitro* assays were also conducted with ligand **68**-targeted XL and UXL micelles at 5% ligand loading, as well as **68**-targeted monomers.[15] The K_i of the **68**-targeted XL micelles (2.9 ± 0.42 nM; n = 4) was four times lower than the corresponding UXL micelles (12 ± 2.6 nM; n = 4).[15] Control assays with untargeted micelles (XL and UXL) and untargeted polymer revealed no detectable interaction with the receptor.

7.4.9 *In Vitro* MR Imaging

In vitro imaging of GdTx micelle phantoms was completed using a SCOUT image for slice selection, and a multiple TR SEMS (TR = repetition time, SEMS = structural equation modeling) image was performed in order to calculate T_1 values. The TR calculation sequence consisted of TR values of 20, 10.99, 6.03, 3.31, 1.82, 1.00, 0.55, 0.30, 0.17, 0.09 and 0.05 s; the echo time (TE) was 8.62 ms, the data matrix was 128 x 128, 4 averages, two dummy scans, field of view (FOV) was 80 mm x 40 mm or 40 mm x 90 mm and the slice thickness was 1 - 2 mm (depending on the phantom). The T_1 values were calculated using the VnmrJ software (Agilent Life Sciences Technologies, Santa Clara, CA), and values were verified using MATLAB (Mathworks, Natick, MA).

To determine the MRI relaxivity of GdTx labeled micelles, phantoms were constructed in which each sample (T-XL, T-UXL, UT-XL, UT-UXL micelles) was prepared at the same GdTx concentration (0.01 mg/mL). T_1 values were determined by progressive saturation relaxation measurements using an Agilent seven Tesla small animal MRI spectrometer using a spin echo sequence, SEMS and T_1 values for each cohort of samples were averaged. There was no apparent T_1 effect attributable to the different micelle formulations, with coefficients of variation (CVs) ranging from 0.02 to 0.1 for each row of T_1 measurements. The phantom studies served to confirm the expectation that the observed T_1 values are positively correlated with GdTx weight loading, with 0.5% w/w encapsulated GdTx providing the lowest mean T_1 value (1.6 s).

7.4.10 *In Vivo* MR Imaging

Severe combined immunodeficiency (SCID) mice with subcutaneous MC1R-expressing tumors were injected with 0.5% w/w GdTx micelles (T-XL, T-UXL, UT-XL, UT-UXL) via tail vein at a dose of 12 μmol GdTx/kg. Targeted micelles (T-UXL and T-

XL) were formulated with 5% (w/w) of **69**-targeted polymer. Using an Agilent seven Tesla small animal MRI spectrometer, coronal T_1-weighted spin echo multi slice (SEMS) images were acquired of each animal prior to and 1, 4, 12, 24 and 48 hours after injection of the micelles. Following imaging, MC1R expression was confirmed in each tumor by immunohistochemistry staining (Figure 7.5).

To quantify enhancement due to tumor uptake of the micelles, intensity histograms for right (R) and left (L) whole tumors, kidneys and livers were prepared

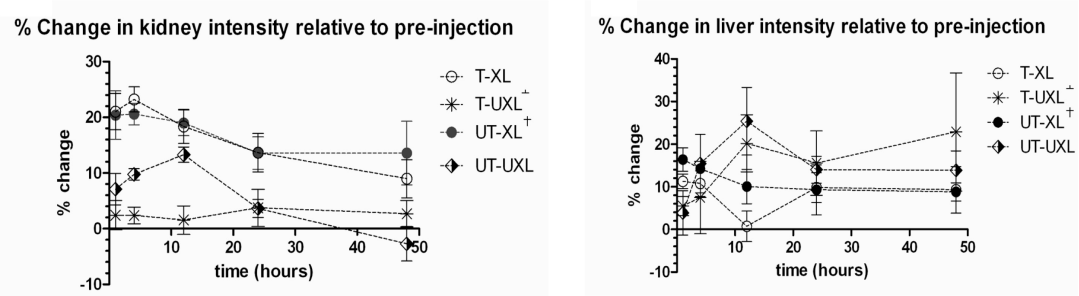

Figure 7.6: Clearance data for GdTx as inferred from contrast enhancement data recorded in the kidney and liver. All groups contained three mice except where noted.
⊥One mouse expired between the 24 hours and 48 hours time point.
†One mouse expired upon injection of the micelle agent.

using a MATLAB program (Mathworks) by drawing a region of interest (ROI) across all applicable slices for each time point. A mean intensity value was then calculated and normalized to thigh muscle. Figure 4.2 (section 4.3) shows the tumor uptake data for each 0.5% GdTx micelle group in the tumor.

The T-XL micelle group is the only one to show significant contrast enhancement in the tumors, with a peak accumulation occurring at 24 hours. The increased enhancement in the tumors of animals injected with the 0.5% GdTx T-XL micelles can be visualized in the post-injection MR images relative to tumors in all other animals

injected with the control formulation (UT-XL, T-UXL, UT-UXL). Again, no other micelle group displayed visible tumor uptake. The contrast enhancement for the T-XL micelles peaked in the kidneys at four hours and steadily decreased thereafter, whereas enhancement in the liver peaked at one hour (Figure 7.6).

To test whether the enhancement observed in the 0.5% GdTx, T-XL tumors was statistically different from the other groups, a one-way ANOVA analysis (Dunnett's Multiple Comparison Test) was carried out. While no significant difference was observed among the groups at one hour, the T-XL group was statistically different from all other groups at four hours to 48 hours ($p < 0.001$ for 4 – 24 hours; $p < 0.05$ at 48 hours). Additional analyses using the Student's *t*-test revealed that there are no statistical differences among the control groups (UT-XL, T-UXL or UT-UXL) at any time point.

7.5 Experimental Details for Chapter 5

7.5.1 Synthesis of Tripyrrane Precursor 83

A mixture of phenanthrolinopyrrole **80** (250 mg, 1.14 mmol) and benzyl 5-(acetoxymethyl)-4-(3-methoxy-3-oxopropyl)-3-methyl-1*H*-pyrrole-2-carboxylate **14** (894 mg, 2.39 mmol) was dissolved in 2-propanol (5 mL) and glacial acetic acid (5 mL). The mixture was heated at reflx under nitrogen overnight. The solvents were evaporated off under reduced pressure. Repeated recrystallization from triethylamine (10 mL) and ethanol (20 mL) yielded the tripyrrane (781 mg, 81%) as a yellow powder.

^{1}H NMR (400 MHz, DMSO-d_6, 25 °C): δ[ppm] = 1.74 (t, J = 7.2 Hz, 4H); 2.10 (s, 6H); 2.25 (t, J = 7.3 Hz, 4H); 4.47 (s, 4H); 5.24 (s, 4H); 7.31-7.45 (m, 10H); 8.40 (d, J = 7.6, 2H); 8.67 (d, J = 4.4, 2H); 11.41 (s, 2H); ^{13}C NMR (125 MHz, DMSO-d_6, 25 °C):

δ[ppm] = 10.8 (2 C); 19.8 (2 C); 23.0 (2 C); 35.1 (2 C); 52.0 (2 C); 65.4 (2 C); 117.0 (2 C); 119.5 (2 C); 121.4 (2 C); 125.9 (2 C); 127.3 (2 C); 128.0 (4 C); 129.7 (4 C); 130.6 (2 C); 131.1 (2 C); 132.8 (2 C); 135.6 (2 C); 136.1 (2 C); 144.5 (2 C); 150.2 (2 C); 161.4 (2 C); 173.5 (2 C); low resolution MS (EI): 846.3 (M^+ + H); high resolution MS (ESI): calculated for $C_{50}H_{47}N_5O_8^{+1}$ = 845.3425; found: 846.3426 ($C_{50}H_{47}N_5O_8$, M^+ + H);

7.5.2 Synthesis of Tripyrrane Precursor 86

A mixture of phenanthrolinopyrrole **80** (250 mg, 1.14 mmol) and *tert*-butyl 5-(acetoxymethyl)-4-(3-methoxy-3-oxopropyl)-3-methyl-1*H*-pyrrole-2-carboxylate **85** (811 mg, 2.39 mmol) was dissolved in 2-propanol (5 mL) and glacial acetic acid (5 mL). The mixture was heated at reflux under nitrogen overnight. The solvents were evaporated off under reduced pressure. Repeated recrystallization from triethylamine (10 mL) and ethanol (20 mL) yielded the tripyrrane (594 mg, 67%) as a yellow powder.

^{1}H NMR (400 MHz, DMSO-d_6, 25 °C): δ[ppm] = 1.44 (s, 18H); 2.21 (s, 6H); 2.40 (t, J = 7.2 Hz, 4H); 2.67 (t, J = 7.1 Hz, 4H); 3.53 (s, 6H); 4.45 (s, 4H); 7.42-7.45 (q, 2H); 8.23 (d, J = 8 Hz, 2H); 9.06 (br, 3H); ^{13}C NMR (125 MHz, DMSO-d_6, 25 °C): δ[ppm] = 10.6 (2 C); 19.6 (2 C); 22.9 (2 C); 29.2 (6C); 35.0 (2 C); 51.9 (2 C); 82.2 (2 C); 119.5 (2 C); 121.5 (2 C); 125.3 (2 C); 125.6 (2 C); 126.7 (4 C); 130.4 (4 C); 132.6 (2 C); 136.1 (2 C); 144.1 (2 C); 150.0 (2 C); 166.1 (2 C); 173.7 (2 C); low resolution MS (EI): 778.4 (M^+ + H); high resolution MS (ESI): calculated for $C_{44}H_{51}N_5O_8^{+1}$ = 777.3738; found: 778.3740 ($C_{50}H_{47}N_5O_8$, M^+ + H);

7.5.3 Synthesis of 1,10-Phenanthroline Linked Sapphyrin 87

Diformyl-ß,ß,ß,ß-tetramethylbipyrrole **77** was synthesized according to published procedures.[16]

The tripyrrane precursor **86** (200 mg, 0.26 mmol) was dissolved in neat trifluoroacetic acid (10 mL) and stirred under nitrogen for 15 minutes at 120 ºC. The reaction mixture was diluted with 100 mL dry dichloromethane. Then, diformyl-ß,ß,ß,ß-tetramethylbipyrrole **77** (62.81 mg, 0.26 mmol) was added in one portion and the resulting mixture was stirred under nitrogen for four hours at room temperature. Air was bubbled through the reaction mixture for 10 minutes and the resulting deep green solution was stirred for an additional 18 hours. After removal of the solvents *in vacuo*, the resulting green material was redissolved in ethanol. One drop of concentrated sulfuric acid was added and the reaction mixture was heated at reflux for two hours. All solvents were removed under reduced pressure. Column chromatography (neutral alumina, 95% chloroform, 5% methanol) afforded compound **87** as a blue-green powder with a metallic luster (122 mg, 58%).

^{1}H NMR (400 MHz, $CDCl_3$, 25 °C): δ[ppm] = 1.23 (t, J = 14.8 Hz, 6H); 2.11 (s, 6H); 2.23 (s, 6H); 2.47 (t, J = 7.5 Hz, 4H); 2.88 (t, J = 7.5 Hz, 4H); 4.27 (q, J = 7.2 Hz, 4H); 8.43 (br, 2H); 9.75 (s, 2H); 9.80 (br s, 2H); 10.2-10.5 (br, 3H); ^{13}C NMR (125 MHz, DMSO-d_6, 25 °C): δ[ppm] = 9.2 (2 C); 11.1 (2 C); 11.8 (2 C); 14.2 (2 C); 22.2 (2 C); 36.6 (2C); 62.0 (2 C); 85.7 (2 C); 115.2 (2 C); 120.5 (2 C); 121.6 (2 C); 126.7 (2 C); 127.2 (2 C); 126.7 (4 C); 128.6 (2 C); 133.1 (2 C); 136.4 (2 C); 144.3 (2 C); 148.2 (2 C); 148.4 (2 C); 149.7 (2 C); 151.2 (2 C); 173.4 (2 C); low resolution MS (EI): 812.4 (M^+ + H); high resolution MS (ESI): calculated for $C_{50}H_{49}N_7O_4^{+1}$ = 811.3846; found: 811.3851 ($C_{50}H_{49}N_7O_4$, M^{+1});

7.5.4 Synthesis of [Ru(phen)$_2$(phenanthroline-sapphyrin)(NO$_3$)$_2$] Complex 89

Compound **87** (50 mg, 61.6 mmol) was dissolved in ethanol (50 mL). Ru(phen)$_2$Cl$_2$ **88**[17] (32.8 mg, 61.6 mmol) was added together with silver nitrate (21 mg, 123.2 mmol). The resulting mixture was heated to reflux under nitrogen for 18 hours. The solvents were removed *in vacuo* and the resulting green-brown solid was subjected to column chromatography (neutral alumina, 98% chloroform, 2% methanol) to afford **89** as a green-brown solid that appears orange in solution (86 mg, quantitative).

^{1}H NMR (400 MHz, CDCl$_3$, 25 °C): δ[ppm] = 1.24 (t, J = 14.7 Hz, 6H); 2.12 (s, 6H); 2.24 (s, 6H); 2.49 (t, J = 7.6 Hz, 4H); 2.90 (t, J = 7.5 Hz, 4H); 4.29 (q, J = 7.3 Hz, 4H); 4.58 (br, 4H); 8.0-8.2 (br, 6H); 8.28 (br, 4H); 8.6-8.8 (br, 6H); 8.89 (br, 6H); 10.95 (br, 3H); ^{13}C NMR (125 MHz, DMSO-d_6, 25 °C): δ[ppm] = 9.3 (2 C); 11.2 (2 C); 11.9 (2 C); 14.3 (2 C); 22.4 (2 C); 36.7 (2C); 62.2 (2 C); 85.9 (2 C); 115.4 (2 C); 120.7 (2 C); 121.6 (8 C); 126.3 (2 C); 127.5 (4 C); 129.7 (4 C); 133.0 (2 C); 134.3 (2 C); 136.6 (8 C); 148.2 (6 C); 148.8 (6 C); 151.8 (2 C); 149.7 (2 C); 173.5 (2 C); low resolution MS (EI): 636.7 (M^{++}); high resolution MS (ESI): calculated for $C_{74}H_{65}N_{11}O_4Ru$, M^{++} = 1273.4492 (636.7246); found: 636.7137 ($C_{74}H_{65}N_{11}O_4Ru$, M^{++});

7.6 Experimental Details for Chapter 6

7.6.1 Synthesis of Benzobipyrrole 97

3,6-Diformylbenzobipyrrole **101**[18] (500 mg, 2.36 mmol) was dissolved in ethylene glycol (30 mL). Potassium hydroxide (1.06 g, 18.89 mmol) and hydrazine hydrate (945 mg, 18.89 mmol) were added and the resulting mixture was heated to reflux under nitrogen for two hours at 180 ºC. The brownish solution was poured into ice water (500

mL) and the precipitates were filtered off, washed multiple times with distilled water and dried *in vacuo*. The product was obtained as off-white prisms (391.3 mg, 90%) that quickly decompose upon standing.

^{1}H NMR (400 MHz, DMSO-d6, 25 ºC): δ[ppm] = 10.25 (s, 2H); 7.14 (s, 2H); 6.97 (m, 2H); 2.31 (s, 6H); ^{13}C NMR (125 MHz, DMSO-d6): δ[ppm] = 10.21 (2 C); 110.7 (2 C); 111.04 (2 C); 119.24 (2 C); 123.36 (2 C); 123.60 (2 C); low resolution MS (EI): 185.1 (M^+ + H); high resolution MS (ESI): calculated for $C_{12}H_{12}N_2^{+1}$ = 184.2371; found: 184.2374 ($C_{12}H_{12}N_4$, M^+);

7.6.2 Synthesis of Benzorosarin 96

Benzobipyrrole **97** (391.3 mg, 2.12 mmol) was dissolved in dry dichloromethane (600 mL). 4-tert-butyl benzaldehyde (343.9 mg, 2.12 mmol) was added together with trifluoroacetic acid (TFA, 0.25 mL). The mixture was stirred under nitrogen for 18 hours at room temperature. Then, 2,3-Dichloro-5,6-dicyano-1,4-benzoquinone (DDQ, 1.44 g, 6.36 mmol) was added and the reaction mixture was stirred for an additional two hours at room temperature. The reaction was stopped by addition of triethylamine (0.27 mL, 1.94 mmol). Then, the mixture was combined with 5% sodium hydroxide solution (100 mL) and extracted with CH_2Cl_2 (3 x 50 mL). The combined organic layers were dried over magnesium sulfate, filtered and the solvent was removed *in vacuo*. The remaining solid was purified by column chromatography (silica gel, 90% dichloromethane, 9% methanol, 1% triethylamine). The blue fraction was collected and repeated column chromatography was necessary in order to obtain reasonably pure product. Analytically pure product was obtained using preparative TLC (silica gel, 90% dichloromethane, 9% methanol, 1% triethylamine). The compound should be stored in solution (99% dry chloroform, 1% dry

triethylamine). If stored as a solid, protonation and eventually decomposition reactions can be observed (166 mg, 8%).

UV-Vis ($CHCl_3$, 25 °C): λ [nm] = 522 (broad); ^1H NMR (400 MHz, $CDCl_3$ -40 °C): δ[ppm] = 1.31 (s, 18H); 1.58 (s, 27H), 7.36 (d, J = 7.6 Hz, 6H); 7.55 (s, J = 7.8 Hz, 6H); 7.82 (d, J = 7.7 Hz, 6H); 24.95 (br s, 3H); ^{13}C NMR (125 MHz, $CDCl_3$, 25 °C): δ[ppm] = 12.7 (6 C); 32.5 (9 C); 34.1 (3 C); 113.2 (6 C); 121.3 (6 C); 122.0 (6 C); 123.6 (6 C); 125.5 (6 C); 129.1 (6 C); 130.1 (3 C); 132.0 (3 C); 140.2 (6 C); 156.6 (3 C); low resolution MS (MALDI): 979.6 (M^+ + H); high resolution MS (MALDI): calculated for $C_{69}H_{66}N_6^{+1}$ = 978.5349; found: 979.5453 ($C_{69}H_{66}N_6 + H^+$);

7.7 X-RAY EXPERIMENTAL

7.7.1 General Procedures

Details of crystal data, data collection and structure refinement are listed in the appendix section of this dissertation. Data reduction were performed using the Rigaku Americas Corporation's Crystal Clear version 1.40.[19] All structures were solved by direct methods using SIR97[20] and refined by full-matrix least-squares on F^2 with anisotropic displacement parameters for the non-H atoms using SHELXL-97.[21] The hydrogen atoms on carbon atoms were calculated in ideal positions with isotropic displacement parameters set to 1.2 x Ueq of the attached atom (1.5 x Ueq for methyl hydrogen atoms). The function, $\Sigma w(|F_o|^2 - |F_c|^2)^2$, was minimized, where $w = 1/[(s(F_o))^2 + (0.0789*P)^2 + (0.8963*P)]$ and $P = (|F_o|^2 + 2|F_c|^2)/3$. $R_W(F^2)$ refined to 0.134, with R(F) equal to 0.0479 and a goodness of fit, S = 1.094. Definitions used for calculating R(F), $R_W(F^2)$ and the goodness of fit, S, can be found in the reference section.[22] The data for each structure was checked for secondary extinction effects but no corrections was necessary. Neutral atom scattering factors and values used to calculate the linear absorption coefficient are from the International Tables for X-ray Crystallography (1992).[23] Tables summarizing the crystallographic data along with figures for all structure are included in the appendix section of this dissertation. All figures herein were generated using SHELXTL/PC.[24]

7.7.2 X-ray Experimental for Complex 60

Crystals grew as small, dark green prisms by slow evaporation from methanol. The data crystal had approximate dimensions; 0.18 x 0.13 x 0.04 mm. The data were

collected on a Rigaku AFC12 diffractometer with a Saturn 724+ CCD using a graphite monochromator with MoKa radiation (λ = 0.71069 Å). A total of 736 frames of data were collected using w-scans with a scan range of 0.5° and a counting time of 40 seconds per frame. The data were collected at 100 K using a Rigaku XStream low temperature device.

7.7.3 X-ray Experimental for Complex 67($2NO_3$)

Crystals suitable for X-ray diffraction were obtained by dissolving GdTx (2 mg, 2.26 μmol) in 1 mL methanol. Sodium nitrate (0.2 mg, 4 equiv) was added and the solution was heated to reflux at 60 °C for 24 hours. At this point, 0.25 mL chloroform was added and the solution was placed in a vial and diethyl ether was allowed to slowly diffuse into the solution at 5 °C.

The data crystal had approximate dimensions: 0.23 x 0.07 x 0.07 mm. The data were collected on a Nonius Kappa CCD diffractometer using a graphite monochromator with MoKa radiation (λ = 0.71073 Å). A total of 384 frames of data were collected using ω-scans with a scan range of 1.2° and a counting time of 144 seconds per frame. The data were collected at 153 K using an Oxford Cryostream low temperature device.

7.7.4 X-ray Experimental for Compound 83

Crystals grew as yellow prisms by slow diffusion of hexanes into a solution of compound **83** in acetone. The data crystal had approximate dimensions; 0.08 x 0.08 x 0.03 mm. The data were collected on a Nonius Kappa CCD diffractometer using a graphite monochromator with MoKα radiation (λ = 0.71073Å). A total of 208 frames of data were collected using ω-scans with a scan range of 2° and a counting time of 268

seconds per frame. The data were collected at 153 K using an Oxford Cryostream low temperature device.

A molecule of acetone was disordered. The molecule could not be adequately modeled. The contributions to the scattering factors due to this molecule were removed by use of the utility SQUEEZE.[25]

7.7.5 X-ray Experimental for Compound 86

Crystals grew as large, yellow plates by slow diffusion of diethyl ether into a solution of **86** in chloroform, methanol and 5% triethylamine. The data crystal was cut from a larger crystal and had approximate dimensions; 0.35 x 0.35 x 0.14 mm. The data were collected on a Rigaku SCX-Mini diffractometer with a Mercury CCD using a graphite monochromator with MoKa radiation (l = 0.71073Å). A total of 625 frames of data were collected using w-scans with a scan range of 1° and a counting time of 45 seconds per frame. The data were collected at 153 K using a Rigaku XStream low temperature device.

One of the ester groups was disordered. The disorder could be reasonably modeled for all atoms except the carbonyl oxygen atom, O3, which appeared to be dynamically disordered across a wide range of positions. With the exception of the carbonyl oxygen, O3, the remaining atoms were modeled by assigning the variable x to the site occupancy factor for atoms C34, C35, O4 and C36, with (1-x) set to the site occupancy for C34a, C35a, O4a and C36a. A common isotropic displacement parameter was refined for these eight atoms while refining x. The geometry of the two groups was restrained to be equivalent throughout the refinement process. An estimate for the site occupancy factors for O3 and O3a, which are the carbonyl oxygen atoms for these two

groups, were used from an earlier refinement. In this manner, the site occupancy for the major component consisting of atoms, C34, C35, O4 and C36 refined to 63(2)%. At this point in the refinement, there remained some fairly large peaks in the difference electron density map near the carbonyl oxygen atoms. These two big peaks were included in the refinement model to account for the position of the carbonyl oxygen atom. A refinement constraint was applied to the site occupancy factors for O3, O3a, O3b and O3c to sum to 1 using the SUMP instruction. The isotropic displacement parameters for the four atoms were refined using a single free variable in the final refinement model.

7.7.6 X-ray Experimental for Compound 87

Crystals grew as dark blue prisms by vapor diffusion of hexanes into a solution of macrocycle **87** in chloroform. The data crystal was had approximate dimensions; 0.13 x 0.06 x 0.04 mm. The data were collected on a Rigaku AFC12 diffractometer with a Saturn 724+ CCD using a graphite monochromator with MoKa radiation (l = 0.71073Å). A total of 714 frames of data were collected using w-scans with a scan range of 0.5° and a counting time of 70 seconds per frame. The data were collected at 100 K using a Rigaku XStream low temperature device.

The hydrogen atoms on the pyrrole nitrogen atoms and the water molecule were observed in a ΔF map and refined with isotropic displacement parameters.

One of the ethyl ester moieties was disordered. The disorder involved a rotation about the C46-C47 bond. The disorder was modeled by assigning the variable x to the site occupancy factors of one component of the disorder composed of atoms O1, O2, C48, C49 and C50. The variable 1-x) was assigned to the site occupancy factors of the alternate component composed of atoms, O1a, O2a, C48a, C49a and C50a. The geometry

of these two components was restrained to be comparable throughout the refinement. A common isotropic displacement parameter was refined for the atoms of the two groups. In this way, the major component of the disorder, O1, O2, C48, C49 and C50, had a site occupancy factor of 78(%). The atoms of the major component were refined anisotropically while restraining their displacement parameters to be approximately isotropic. The atoms of the minor component were refined isotropically.

7.7.7 X-ray Experimental for Compound 97

Crystals grew as black plates by vapor diffusion of pentane into a chloroform solution of the complex. The data crystal had approximate dimensions; 0.36 x 0.24 x 0.12 mm. The data were collected on a Rigaku AFC12 diffractometer with a Saturn 724+ CCD using a graphite monochromator with MoKα radiation (λ = 0.71075Å). A total of 1884 frames of data were collected using ω-scans with a scan range of 0.5° and a counting time of 23 seconds per frame. The data were collected at 100 K using a Rigaku XStream low temperature device.

What appeared to be three molecules of chloroform were disordered around a crystallographic inversion center at 0, 0, ½. The disorder could not be modeled satisfactorily. Therefore, the utility Squeeze[25] was used to remove the effects of the solvent disorder from the structure factors.

References

(1) See reference 68 in Chapter 1.

(2) Hannah, S.; Lynch, V.; Guldi, D. M.; Gerasimchuk, N.; Mac Donald, C. L. B.; Magda, D.; Sessler, J. L. *J. Am. Chem. Soc.* **2002**, *124*, 8416-8427.

(3) Sessler, J. L.; Hemmi, G. H.; Mody, T. D. *PCT Int. Appl.* **1993**, WO 9314093 A1 19939722.

(4) Sessler, J. L.; Mody, T. D.; Hemmi, G. W.; Kral, V. *U.S.* **1995**, US5457183 A 19951010.

(5) See reference (86) in Chapter 1.

(6) See reference (43) in Chapter 4.

(7) Mosmann, T. J. *Immunol. Methods* **1983**, *65*, 55-63.

(8) See reference (45) in Chapter 3.

(9) Lee, J.-H.; Huh, Y.-M.; Jun, Y.-w.; Seo, J.-w.; Jang, J.-t.; Song, H.-T.; Kim, S.; Cho, E.-J.; Yoon, H.-G.; Suh, J.-S.; Cheon, J. *Nature Medicine* **2007**, *13*, 95–99.

(10) Yi, D. K.; Lee, S. S.; Papaefthymiou, G. C.; Ying, J. Y. *Chem. Mater.* **2006**, *18*, 614–619.

(11) See reference (22) in Chapter 2.

(12) See reference (12) in Chapter 4.

(13) See reference (23) in Chapter 4.

(14) See reference (33) in Chapter 4.

(15) See reference (40) in Chapter 4.

(16) See reference (6) in Chapter 5.

(17) See reference (25) in Chapter 5.

(18) See reference (9) in Chapter 6.

(19) *CrystalClear Version 1.40* **2008**, Rigaku Americas Corportion, The Woodlands, TX, USA.

(20) *SIR97* **1999**, A program for crystal structure solution. Altomare, A.; Burla, M.C.; Camalli, M.; Cascarano, G.L.; Giacovazzo, C.; Guagliardi, A.; Moliterni, A. G. G.; Polidori, G.; Spagna, R. *J. Appl. Cryst.* **1999**, *32*, 115-119.

(21) Sheldrick, G. M. *SHELXL97* **1994**, Program for the Refinement of Crystal Structures, University of Göttingen, Germany.

(22) $(R_W(F^2) = \{Sw(|F_o|^2 - |F_c|^2)^2/Sw(|F_o|)^4\}^{1/2}$ where ω is the weight given each reflection. $R(F) = S(|F_o| - |F_c|)/S|F_o|\}$ for reflections with $F_o > 4(s(F_o))$. $S = [Sw(|F_o|^2 - |F_c|^2)^2/(n - p)]^{1/2}$, where n is the number of reflections and p is the number of refined parameters.

(23) In *International Tables for X-ray Crystallography* **1992**, Vol. C, Tables 4.2.6.8 and 6.1.1.4, A. J. C. Wilson, editor, Boston: Kluwer Academic Press.

(24) Sheldrick, G. M., *SHELXTL/PC* (Version 5.03) **1994**, Siemens Analytical X-ray Instruments, Inc., Madison, Wisconsin, USA.

(25) Sluis, P. v. d.; Spek, A. L. *Acta Cryst.* **1990**, *A46*, 194-201.

Appendix: X-ray Crystallographic Data

All crystals for X-ray crystallographic analyses described in this appendix were grown by the author. All crystal X-ray diffraction structures were solved and refined by Dr. Vincent Lynch of the Department of Chemistry and Biochemistry at The University of Texas at Austin. All structures have been deposited with the Cambridge Crystallographic Data Centre (CCDC) and can be obtained from that source by quoting the CCDC numbers given here. Relevant data tables for each structure as provided by Dr. Lynch follow.

Table A1: Crystallographic data and refinement for compound **60**.

CCDC Number	790736	
Empirical formula	C74 H100 Bi2 N12 O21	
Formula weight	1911.62	
Temperature	100(2) K	
Wavelength	0.71069 Å	
Crystal system	Triclinic	
Space group	P-1	
Unit cell dimensions	a = 10.9258(8) Å	a= 75.646(3)°.
	b = 12.9230(10) Å	b= 74.471(3)°.
	c = 15.3223(15) Å	g = 88.263(2)°.
Volume	2017.9(3) $Å^3$	
Z	1	
Density (calculated)	1.573 Mg/m^3	

Absorption coefficient	4.432 mm^{-1}
F(000)	962
Crystal size	0.18 x 0.13 x 0.04 mm
Theta range for data collection	3.08 to 27.48°.
Index ranges	-14<=h<=12, -10<=k<=16, -19<=l<=19
Reflections collected	16942
Independent reflections	9198 [R(int) = 0.0405]
Completeness to theta = 27.48°	99.4 %
Absorption correction	Semi-empirical from equivalents
Max. and min. transmission	0.84 and 0.66
Refinement method	Full-matrix least-squares on F^2
Data / restraints / parameters	9198 / 41 / 479
Goodness-of-fit on F^2	1.094
Final R indices [I>2sigma(I)]	R1 = 0.0479, wR2 = 0.1288
R indices (all data)	R1 = 0.0557, wR2 = 0.1341
Largest diff. peak and hole	1.893 and -2.670 e.$Å^{-3}$

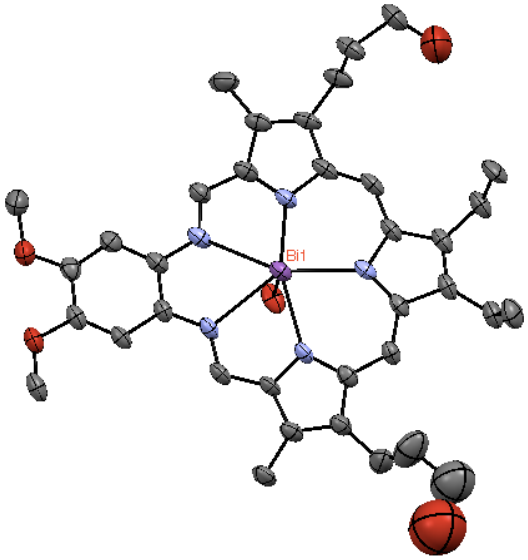

Figure A1: View of the Bi coordination to the macrocycle in complex **60** showing the atom labeling scheme. Displacement ellipsoids are scaled to the 50% probability level. Note that this structure shows only one individual texaphyrin subunit viewed form the top (ancillary ligands omitted). The complete structure is shown in Figure A2.

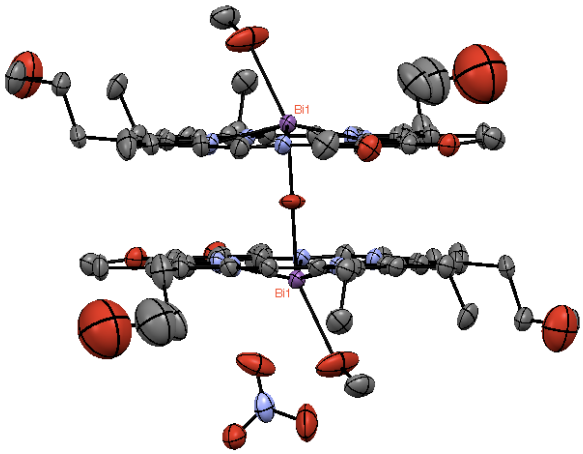

Figure A2: View of the dimer present in complex **60**. Displacement ellipsoids are scaled to the 50% probability level. The oxygen atom bridging the two Bi-cations resides on the crystallographic inversion center at ½, ½, O. The distance between the rings defined by the five nitrogen atoms of the macrocycle is 3.433(5) Å.

Table A2: Crystallographic data and refinement for compound **67**.

CCDC Number	859294	
Empirical formula	C37 H48 Gd N7 O12	
Formula weight	940.07	
Temperature	123(2) K	
Wavelength	0.71069 Å	
Crystal system	Monoclinic	
Space group	P21/c	
Unit cell dimensions	a = 15.3250(10) Å	a= 90°.
	b = 11.5950(8) Å	b= 99.592(2)°.
	c = 21.5387(15) Å	g = 90°.
Volume	3773.8(4) $Å^3$	
Z	4	
Density (calculated)	1.655 Mg/m^3	
Absorption coefficient	1.832 mm^{-1}	
F(000)	1916	
Crystal size	0.23 x 0.07 x 0.07 mm	
Theta range for data collection	2.00 to 25.00°.	
Index ranges	-18<=h<=18, -13<=k<=12, -25<=l<=25	
Reflections collected	11918	
Independent reflections	6623 [R(int) = 0.0816]	
Completeness to theta = 25.00°	99.9 %	
Absorption correction	Semi-empirical from equivalents	
Max. and min. transmission	1.00 and 0.869	
Refinement method	Full-matrix least-squares on F^2	
Data / restraints / parameters	6623 / 1 / 523	

Goodness-of-fit on F^2	1.171
Final R indices [I>2sigma(I)]	R1 = 0.0537, wR2 = 0.0838
R indices (all data)	R1 = 0.1176, wR2 = 0.1031
Largest diff. peak and hole	1.759 and -0.791 e.$Å^{-3}$

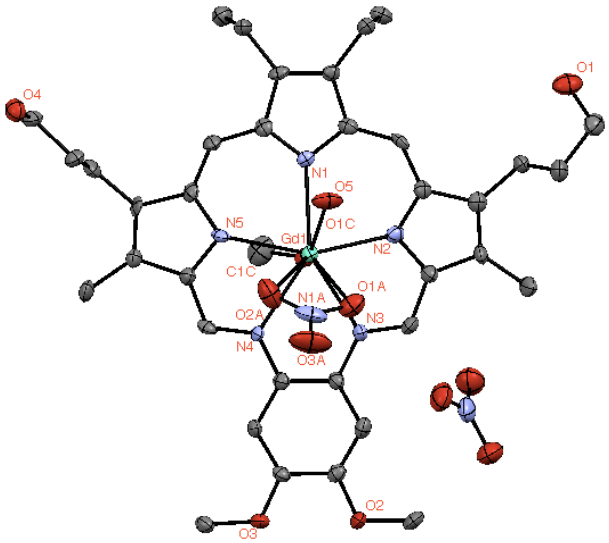

Figure A3: Top view of the GdTx complex **67** (after ligand exchange) showing a partial atom labeling scheme. Displacement ellipsoids are scaled to the 50% probability level. The hydrogen atoms were omitted for clarity.

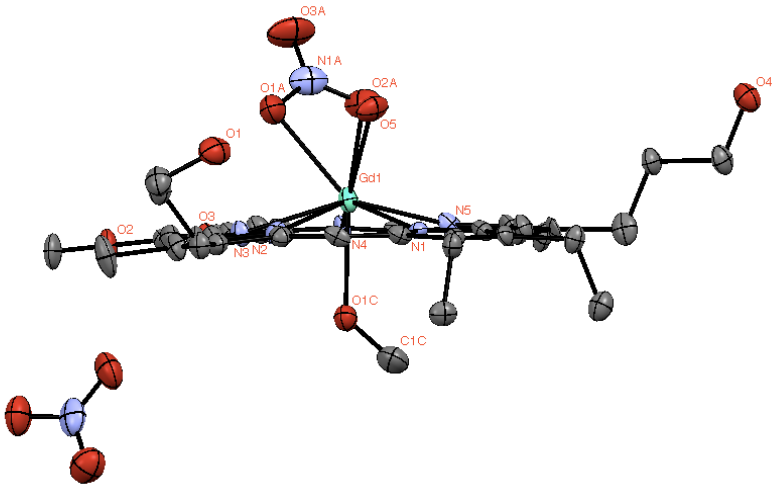

Figure A4: Side view of the GdTx complex **67** (after ligand exchange) showing a partial atom labeling scheme. Displacement ellipsoids are scaled to the 50% probability level. The hydrogen atoms have been omitted for clarity.

Table A3: Crystallographic data and refinement for compound **83**.

CCDC Number	907308	
Empirical formula	C50 H47 N5 O8	
Formula weight	904.00	
Temperature	153(2) K	
Wavelength	0.71070 Å	
Crystal system	Triclinic	
Space group	P-1	
Unit cell dimensions	a = 10.9910(6) Å	a= 65.252(2)°.
	b = 14.2970(8) Å	b= 79.553(3)°.
	c = 16.8010(9) Å	g = 86.157(2)°.
Volume	2357.7(2) $Å^3$	
Z	2	
Density (calculated)	1.273 Mg/m^3	
Absorption coefficient	0.088 mm^{-1}	
F(000)	956	
Crystal size	0.08 x 0.08 x 0.03 mm	
Theta range for data collection	1.57 to 24.98°.	
Index ranges	-13<=h<=12, -16<=k<=16, -19<=l<=19	
Reflections collected	14703	
Independent reflections	8152 [R(int) = 0.0761]	
Completeness to theta = 24.98°	98.6 %	
Absorption correction	None	
Refinement method	Full-matrix least-squares on F^2	
Data / restraints / parameters	8152 / 373 / 638	
Goodness-of-fit on F^2	1.045	

Final R indices [I>2sigma(I)]	R1 = 0.0650, wR2 = 0.1048
R indices (all data)	R1 = 0.1913, wR2 = 0.1230
Largest diff. peak and hole	0.251 and -0.229 e.Å^{-3}

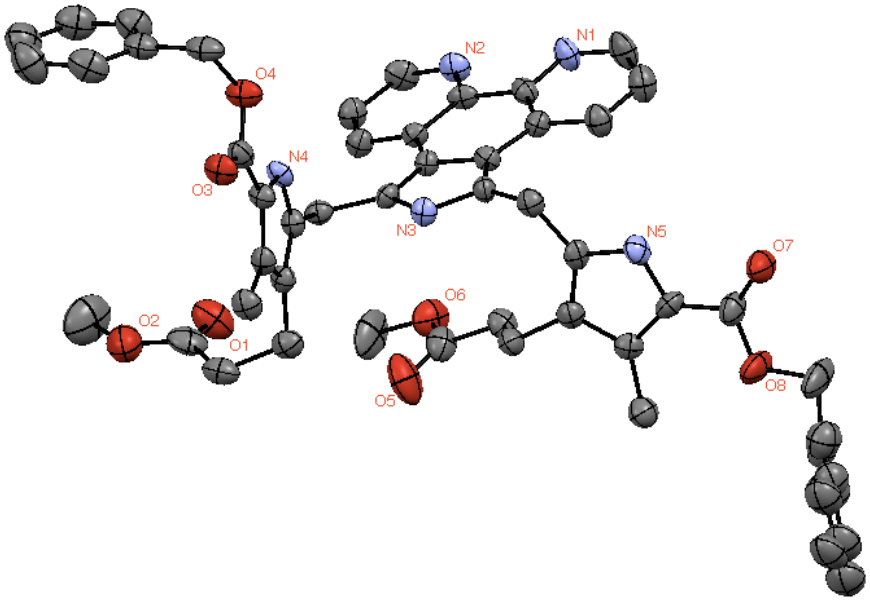

Figure A5: View of **83** showing a partial atom labeling scheme. Displacement ellipsoids are scaled to the 30% probability level.

Table A4: Crystallographic data and refinement for compound **86**.

CCDC Number	907306	
Empirical formula	C45 H52 Cl3 N5 O8	
Formula weight	897.27	
Temperature	153(2) K	
Wavelength	0.71075 Å	
Crystal system	Trilcinic	
Space group	P-1	
Unit cell dimensions	a = 13.5265(14) Å	a= 69.862(3)°.
	b = 14.2344(15) Å	b= 63.191(2)°.
	c = 14.841(2) Å	g = 64.576(3)°.
Volume	2262.8(5) $Å^3$	
Z	2	
Density (calculated)	1.317 Mg/m^3	
Absorption coefficient	0.260 mm^{-1}	
F(000)	944	
Crystal size	0.35 x 0.35 x 0.14 mm	
Theta range for data collection	3.00 to 27.48°.	
Index ranges	-17<=h<=17, -18<=k<=18, -19<=l<=19	
Reflections collected	27878	
Independent reflections	10344 [R(int) = 0.0526]	
Completeness to theta = 27.48°	99.5 %	
Absorption correction	Semi-empirical from equivalents	
Max. and min. transmission	1.00 and 0.705	
Refinement method	Full-matrix least-squares on F^2	
Data / restraints / parameters	10344 / 516 / 605	
Goodness-of-fit on F^2	1.021	

Final R indices [I>2sigma(I)]	R1 = 0.0581, wR2 = 0.1298
R indices (all data)	R1 = 0.0973, wR2 = 0.1517
Largest diff. peak and hole	0.347 and -0.408 e.Å^{-3}

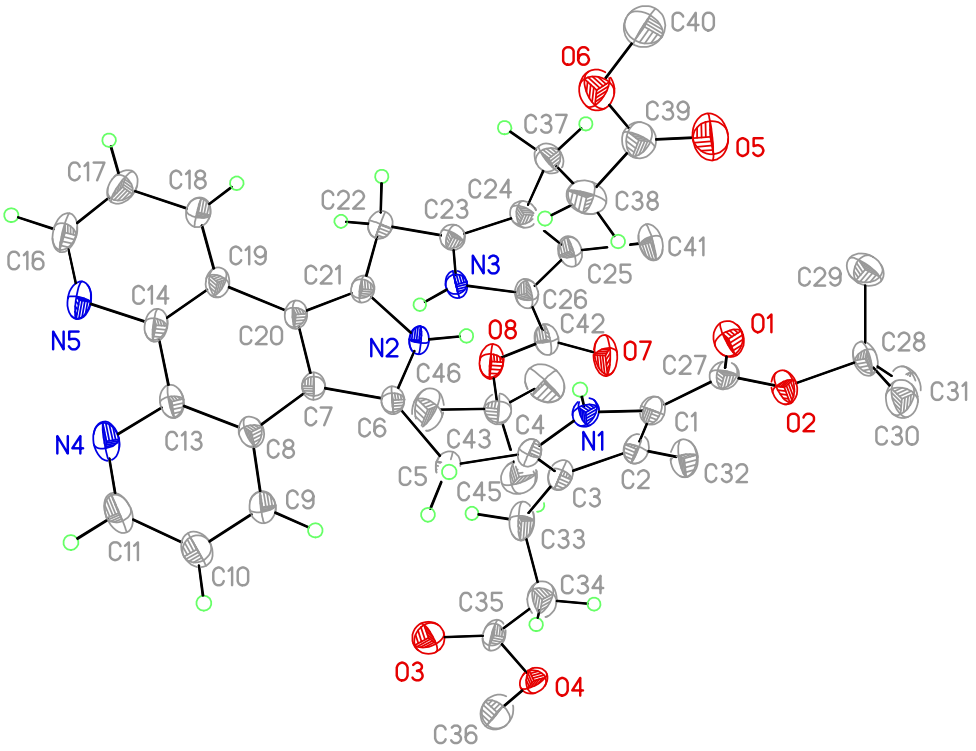

Figure A6: View of **86** showing the atom labeling scheme. Displacement ellipsoids are scaled to the 50% probability level. Only the major component of the disordered ester group is shown. Most hydrogen atoms have been omitted for clarity.

Table A5: Crystallographic data and refinement for compound **87**.

CCDC Number	907307	
Empirical formula	C51 H52 Cl3 N7 O5	
Formula weight	949.35	
Temperature	100(2) K	
Wavelength	0.71069 Å	
Crystal system	Triclinic	
Space group	P-1	
Unit cell dimensions	a = 11.2987(13) Å	a= 111.979(3)°.
	b = 13.8007(15) Å	b= 97.304(3)°.
	c = 16.639(2) Å	g = 101.968(2)°.
Volume	2292.9(5) $Å^3$	
Z	2	
Density (calculated)	1.375 Mg/m^3	
Absorption coefficient	0.258 mm^{-1}	
F(000)	996	
Crystal size	0.13 x 0.06 x 0.04 mm	
Theta range for data collection	3.02 to 27.48°.	
Index ranges	-14<=h<=14, -17<=k<=16, -19<=l<=21	
Reflections collected	18829	
Independent reflections	10172 [R(int) = 0.0479]	
Completeness to theta = 27.48°	96.7 %	
Absorption correction	None	
Refinement method	Full-matrix least-squares on F^2	
Data / restraints / parameters	10172 / 7 / 645	
Goodness-of-fit on F^2	1.001	
Final R indices [I>2sigma(I)]	R1 = 0.0642, wR2 = 0.1376	

R indices (all data)	R1 = 0.1147, wR2 = 0.1674
Largest diff. peak and hole	0.395 and -0.544 e.Å^{-3}

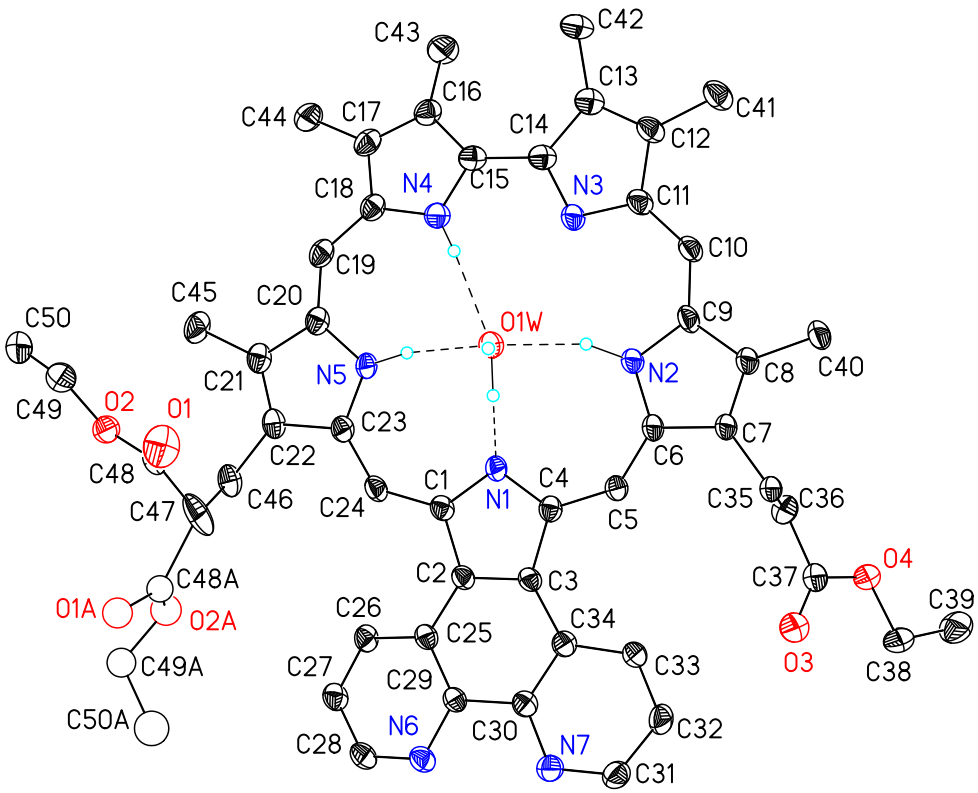

Figure A7: View of **87** showing the atom labeling scheme. Displacement ellipsoids are scaled to the 50% probability level. The minor component of the disordered ethyl acetate moiety is shown as open circles. Most hydrogen atoms have been omitted for clarity. The dashed lines are indicative of H-bonding interactions.

Table A6: Crystallographic data and refinement for compound **103**.

CCDC Number	889353	
Empirical formula	C66 H27 Cl5 F15 N6	
Formula weight	1366.19	
Temperature	100(2) K	
Wavelength	0.71075 Å	
Crystal system	Triclinic	
Space group	P-1	
Unit cell dimensions	a = 7.3095(9) Å	α= 88.785(3)°.
	b = 19.203(2) Å	β= 82.718(2)°.
	c = 21.986(2) Å	γ = 89.498(2)°.
Volume	3060.4(6) $Å^3$	
Z	2	
Density (calculated)	1.483 Mg/m^3	
Absorption coefficient	0.330 mm^{-1}	
F(000)	1370	
Crystal size	0.36 x 0.24 x 0.12 mm	
Theta range for data collection	3.00 to 27.48°.	
Index ranges	-9<=h<=9, -24<=k<=24, 0<=l<=28	
Reflections collected	62427	
Independent reflections	13819 [R(int) = 0.154]	
Completeness to theta = 27.48°	98.2 %	
Absorption correction	Semi-empirical from equivalents	
Max. and min. transmission	1.00 and 0.483	
Refinement method	Full-matrix least-squares on F^2	
Data / restraints / parameters	13819 / 0 / 766	

Goodness-of-fit on F^2	1.557
Final R indices [I>2sigma(I)]	R1 = 0.1173, wR2 = 0.2723
R indices (all data)	R1 = 0.1557, wR2 = 0.2849
Largest diff. peak and hole	0.557 and -0.481 e.$Å^{-3}$

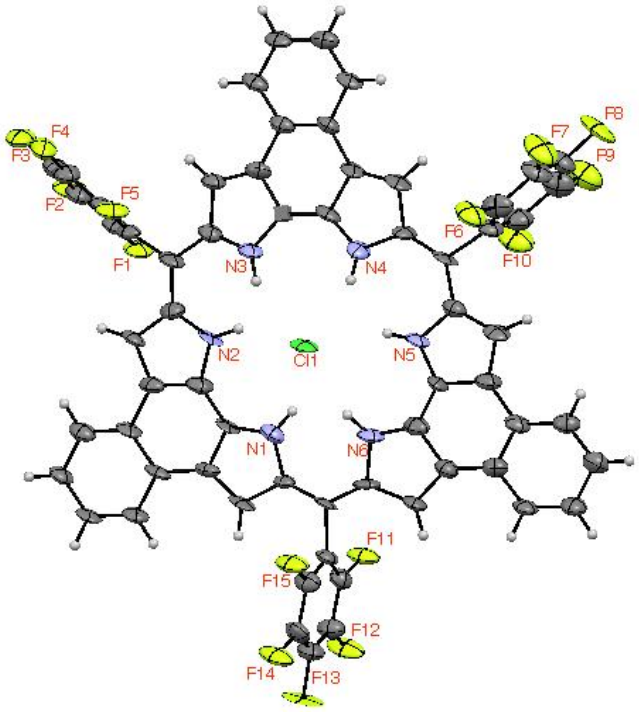

Figure A8: View of the chloride complex in **103** showing the atom labeling scheme. Displacement ellipsoids are scaled to the 50% probability level.

Comprehensive Bibliography

- Podsypanina, K.; Du, Y. C.; Jechlinger, M.; Beverly, L. J.; Hambardzumyan, D.; Varmus, H. *Science* **2008**, *321*, 1841-1844.
- Croce, C. M. *N. Engl.. J. Med.* **2008**, *358*, 502-511.
- Loeb, K. R.; Loeb, L. A. *Carcinogenesis* **2000**, *21*, 379-385.
- Merlo, L. M., Pepper, J. W.; Reid, B. J.; Maley, C. C. *Nat. Rev. Cancer* **2006**, 6, 924-935.
- Maruyama, K. In *Drug Delivery System*, CAS **1999**, Vol. 14, 433-447.
- Shayan, R.; Achen, M. G.; Stacker, S. A. *Carcinogenesis* **2006**, *27*, 1729-1738.
- Kunar, V.; Abbas, A. K.; Fausto, N.; Robbins, S. L.; Cotran, R. S. *Robbins and Cotran pathologic basis of disease*, 7th ed., Elsevier Saunders, Philadelphia, **2005**.
- Briasoulis, E.; Pavlidis, N. *Oncologist* **1997**, *2*, 142-152.
- American Cancer Society, Cancer Facts and Figures **2010**, American Cancer Society, Atlanta **2010**.
- Spalding, A. C.; Lawrence, T. S. *Cancer Investigation* **2006**, *24*, 444-456.
- Von Sonntag, C. In *The Chemical Basis of Radiation Biology*, Taylor and Francis, London **1987**.
- Feldmeier, J. J. In *Radiation Oncology*, G. R. Weiss, Ed., Appleton & Lange, Norwalk **1993**, 74-88.
- Petry, E. *Biochim. Z.* **1923**, *135*, 353-383.
- Thomlinson, R. H.; Gray, L. H. *British Journal of Cancer* **1955**, *9*, 539-549.
- Otto, S. E. In *Pocket guide to oncology nursing*, Mosby-Year Book, Inc., St. Louis **1995**.

- Gates, R. A.; Fink, R. M. In *Oncology nursing secrets*, Hanley and Belfus, Inc., Philadelphia **1997**.
- Longley, D. B.; Harkin, D. P.; Johnston, P. G. *Nat. Rev. Cancer* **2003**, *3*, 330-338.
- Thomas, D. M.; Zalcberg, J. R. *Clin. Exp. Pharmacol. Physiol.* **1998**, *25*, 887-895.
- Cerqueira, N. M. F. S. A.; Fernandes, P. A.; Ramos, M. J. *Chemistry: A European Journal* **2007**, *13*, 8507-8515.
- Guo, Z.; Sadler, P. J. *Angew. Chem. Int. Ed.* **1999**, *38*, 1512-1531.
- Turchi, J. J.; Henkels, K. M.; Hermanson, I. L.; Patrick, S. M. *J. Inorg. Biochem.* **1999**, *77*, 83-87.
- Rixe, O.; Ortuzar, W.; Alvarez, M.; Parker, R.; Reed, E. *Biochem. Pharmacol.* **1996**, *52*, 1855-1865.
- De Gramont, A.; Figer, A.; Seymour, M.; Homerin, M.; Hmissi, A. *J. Clin. Oncol.* **2000**, *18*, 2938-2947.
- Natarajan, G. et al. *Biochem. Pharmacol.* **1999**, *58*, 1625-1629.
- Jiang, X.; Pandey, R. K.; Smith, K. M. *Tetrahedron Letters* **1995**, *36*, 365-368.
- Ghiggino, K. P.; Bennett, L. E.; Henderson, R. W. *Photochemistry and Photobiology* **1988**, *47*, 65-72.
- Derat, E.; Cohen, S.; Shaik, S.; Altun, A.; Thies, W. *J. Am. Chem. Soc.* **2005**, *127*, 13611-136121.
- Benfrey, O. T.; Morris, P. J. T. Eds. *Robert Burns Woodward Artist and Architect in the World of Molecules*, Chemical Heritage Foundation, Philadelphia **2001**, 256-277, 302-242.
- Alberts, B.; Johnson, A.; Lewis, J.; Raff, M.; Roberts, K.; Walter, P. In *Molecular Biology of the Cell*, 4th Ed., Gardland Science, New York **2002**.

- Sanchez-Alcazar, J. A.; Khodjakov, A.; Schneider, E. *Cancer Research* **2001**, *61*, 1038-1044.
- Kalka, K.; Merk, H.; Mukhtar, H. *J. Am. Acad. Dermatol.* **2000**, *42*, 389-413.
- Luksiene, Z.; Juzenas, R.; Moan, J. *Cancer Letters* **2006**, *235*, 40-47.
- Hausmann, W. *Biochem. Z.* **1909**, *14*, 275-278.
- Schwartz, S.; Absolon, K.; Vermund, H. *Univ. Minnesota Med. Bull.* **1955**, *27*, 7-13.
- Schwartz, S.; Keprios, M.; Modelevsky, G.; Freyholtz, H.; Walters, R.; Larson, L. In *M. Doss (Ed.), Diagnosis and Therapy of Porphyrins and Lead Intoxication*, Springer, Berlin **1978**.
- Sternberg, E. D.; Dolphin, D. *Tetrahedron* **1998**, *54*, 4151-4202.
- Pandey, R. K.; Sihiau, F.-Y.; Dougherty, T. J.; Smith, K. M. *Tetrahedron* **1991**, *47*, 9571-9584.
- Lou, Y.; Chang, C. K.; Kessel, D. *Photochem. and Photobiol.* **1996**, *63*, 528-534.
- Dougherty, T. J.; Gomer, C. J.; Henderson, B. W.; Jori, G.; Kessel, D.; Korbelik, M.; Moan, J.; Peng, Q. *J. Nat. Cancer Inst.* **1998**, *90*, 889-905.
- Pandey, R. K.; Zheng, G. In *Porphyrin Handbook* **2000**, *6*, 157-230.
- Zhao, F.-Y.; Zhang, K.-H.; Huang, H.-N.; Sun, K.-H.; Ling, Q.-B.; Xu, B. *Lasers Med. Sci.* **1986**, *1*, 253-256.
- Chen, D. Y. *Treat. Laser* **1985**, *5*, 137.
- Bellnier, D. A.; Dougherty, T. J. *Int. J. Radiat. Biol.* **1986**, *50*, 659-664.
- Moan, J.; Pettersen, E. O. *Int. J. Radiat. Biol.* **1981**, *40*, 107-109.
- O´Hara, J.; Douple, E. B.; Abrams, M. J.; Picker, D. J.; Giandomenico, C. M.; Vollano, J. F. *Int. J. Radiat. Oncol. Biol. Phys.* **1989**, *16*, 1049-1052.
- James, B. R.; Meng, G. G.; Posakony, J. J.; Ravensbergen, J. A.; Ware, C. J.; Skov, K. A. *Metal-Based Drugs* **1996**, *3*, 85-89.

- Ali, H.; van Lier, J. E., *Chem. Rev.* **1999**, *99*, 2379-2450.
- Han, F. X. G.; Wheelhouse, R. T.; Hurley, L. H. *J. Am. Chem. Soc.* **1999**, *121*, 3561-3570.
- Yuasa, M.; Oyaizu, K.; Horiuchi, A.; Ogata, A.; Hatsugai, T.; Yamaguchi, A.; Kawakami, H. *Mol. Pharmaceutics* **200**4, *5*, 387-389.
- Rudat, V.; Stadler, P.; Becker, A.; Vanselow, B.; Dietz, A. *Strahlenther. Onkol.* **2001**, *177*, 462-468.
- Brizel, D. M.; Dodge, R. K.; Clough, R. W.; Dewhirst, M. W. *Radiother. Oncol.* **1999**, *53*, 113-117.
- Fyles, A. W.; Milosevic, M.; Pintilie, M.; Syed, A.; Hill, R. P. *Radiother. Oncol.* **2000**, *57*, 13-19.
- Bauer, V. J.; Clive, D. L. J.; Dolphin, D.; Paine III, J. B.; Harris, F. L.; King, M. M.; Loder, J.; Wang, S.-W. C.; Woodward, R. B. *J. Am. Chem. Soc.* **1983**, *105*, 6429-6436.
- Kral, V.; Davis, J.; Andrievsky, A.; Kralova, J.; Synytsya, A.; Pouckova, P.; Sessler, J. L. *J. Med. Chem.* **2002**, *45*, 1073-1078.
- Wang, Z.; Lecane, P.; Thiemann, P.; Fan, A.; Cortez, C.; Ma, X.; Tonev, D.; Miles, D.; Lin, A.; Hemmi, G.; Naumovski, L.; Miller, R. A.; Magda, D.; Cho, D.-G.; Sessler, J. L.; Pike, B. L.; Yeligar, S. M.; Karaman, M. W.; Hacia, J. G. *Mol. Cancer* **2007**, *6*, 9-20.
- Roitman, L.; Ehrenberg, B.; Nitzan, Y.; Kral, V.; Sessler, J. L. *Photochem. Photobiol.* **1994**, *60*, 421-426.
- van Gemert, M. G. C.; Welch, A. J.; Amin, A. P. *Lasers Surg. Med.* **1986**, *6*, 76-83.
- Wan, S.; Parrish, J. R.; Anderson, R. R.; Madden, M. *Photochem Photobiol.* **1981**, *34*, 679-681.

- Eichler, J.; Knop, J.; Lenz, H. *Radiat. Environ, Biophys*. **1977**, *14*, 239-242.
- Parmeswaran, D.; Pushpan, S. K.; Srinivasan, A.; Ravi, K. M.; Chandrashekar, T. K.; Ganesan, S. *Photochem. Photobiol*. **2003**, *78*, 487-495.
- Sessler, J. L.; Miller, R. A. *Biochem. Pharmacol*. **2000**, *59*, 733-739.
- Mehta, M. P.; Shapiro, W. R.; Phan, S. C.; Gervais, R.; Carrie, C.; Chabot, P.; Patchell, R. A.; Glantz, M. J.; Recht, L.; Langer, C.; Sur, R. K.; Roa, W. H.; Mahe, M. A.; Fortin, A.; Nieder, C.; Meyers, C. A.; Smith, J. A.; Miller, R. A.; Renschler, M. F. *Int. J. Radiat. Oncol. Biol. Phys*. **2009**, *73*, 1069-1076.
- Patel, H.; Mick, R.; Finlay, J.; Zhu, T. C.; Rickter, E.; Cengel, K. A.; Malkowicz, S. B.; Hahn, S. M.; Busch, T. M. *Clin. Cancer Res*. **2008**, *14*, 4869-4876.
- Sessler, J. L.; Hemmi, G.; Mody, T. D.; Murai, T.; Burrell, A.; Young, S. W. *Acc. Chem. Res*. **1994**, *27*, 43-50.
- Magda, D.; Lepp, C.; Gerasimchuk, N.; Lee, I.; Sessler, J. L.; Lin, A.; Biaglow, J.; Miller, R. A. *Int. J. Radiat. Biol. Oncol. Phys*. **2001**, *51*, 1025-1036.
- Sessler, J. L.; Tvermoes, N. A.; Guldi, D. M.; Hug, G. L.; Mody, T. D.; Magda, D. *J. Phys. Chem. B* **2001**, *105*, 1452-1457.
- Rockwell, S.; Donnelly, E. T.; Liu, Y.; Tang, L.-Q. *Int. J. Radiat. Oncol. Biol. Phys*. **2002**, *54*, 536.
- Young, S. W.; Sidhu, M. K.; Qing, F. *Invest. Radiol*. **1994**, *29*, 330-338.
- Rosenthal, D. I.; Nurenberg, P.; Becerra, C. R.; Frenkel, E. P.; Carbonne, D. P.; Lum, B. L.; Miller, R.; Engel, J.; Young, S.; Miles, D.; Renschler, M. F. *Clin. Cancer Res*. **1999**, *5*, 739-745.
- Carde, P.; Timmerman, R.; Mehta, M. P.; Koprowski, C. D.; Ford, J.; Tishler, R. B.; Miles, D.; Miller, R. A.; Renschler, M. F. *J. Clin. Oncol*. **2001**, *19*, 2074-2083.

- Viala, J.; Vanel, D.; Meingau, P.; Lartigau, E.; Carde, P.; Renschler, M. F. *Radiology* **1999**, *3*, 755-759.
- Miller, R. A.; Woodburn, K.; Fan, Q.; Renschler, M. F.; Sessler, J. L.; Koutcher, J. A. *Int. J. Radiation Oncology Biol. Phys.* **1999**, *45*, 981-989.
- Mehta, M. P.; Shapiro, W. R.; Glantz, M. J.; Patchell, R. A.; Weitzner, M. A.; Meyers, C. A.; Schultz, C. J.; Roa, W. H.; Leibenhout, M.; Ford, J.; Curran, W.; Phan, S.; Smith, J. A.; Miller, R. A.; Renschler, M. F. *J. Clin. Oncol.* **2002**, *20*, 3445-3453.
- Sessler, J. L.; Burrel, A. K. *Top. Curr. Chem.* **1991**, *161*, 177.
- Acholla, F. V.; Mertes, K. B. *Tetrahedron Lett.* **1984**, *25*, 3269-3270.
- Acholla, F. V.; Takusagawa, F.; Mertes, K. B. *J. Am. Chem. Soc.* **1985**, *107*, 6902-6908.
- Curtis, N. F. *Coord. Chem. Rev.* **1968**, *3*, 3-47.
- Sessler, J. L.; Johnson, M. R.; Lynch, V. *J. Org. Chem.* **1987**, *52*, 4394-4397.
- Sessler, J. L.; Hemmi, G. W.; Mody, T. D.; Murai, T.; Burrell, A. *Acc. Chem. Res.* **1994**, *27*, 43-50.
- Mody, T. D.; Sessler, J. L. In *Supramolecular Materials and Technologies*, Reinhoudt DN (ed) Wiley: Chichester **1999**, *Vol. 4*, 245-299.
- Mody, T. D.; Fu, L.; Sessler, J. L. In *Progress Inorganic Chemistry*, Karlin KJ (ed) Wiley: Chichester **2001**, *Vol. 49*, 551.
- Sessler, J. L.; Mody, T. D.; Hemmi, G. W.; Lynch, V. *Inorg. Chem.* **1993**, *32*, 3175-3187.
- Sessler, J. L.; Tvermoes, N. A.; Guldi, D. M.; Mody, T. D. *Phys. Chem.* **1999**, *103*, 787-794.
- Mody, T. D.; Sessler, J. L. *J. Porphy. Phthalocy.* **2001**, *5*, 134-142.
- Clezy, P. S.; Liepa, A. J. *Aust. J. Chem.* **1972**, *25*, 1979-1990.

- Jasat, A.; Dolphin, D. *Chem. Rev.* **1997**, *97*, 2267-2340.
- Sessler, J. L.; Murai, T.; Lynch, V.; Cyr, M. *J. Am. Chem. Soc.* **1988**, *110*, 5586-5588.
- Sessler, J. L.; Murai, T.; Lynch, V. *Inorg. Chem.* **1989**, *28*, 1333-1341.
- Sessler, J. L.; Johnson, M. R.; Lynch, V.; Murai, T. *J. Coord. Chem.* **1988**, *18*, 99-104.
- Cotton, F. A.; Wilkinson, G. In *Advanced Inorganic Chemistry*, John Wiley: New York **1980**, *4th ed.,* pp 589, 982.
- Maiya, B. G.; Mallouk, T. E.; Hemmi, G. W.; Sessler, J. L. *Inorg. Chem.* **1990**, *29*, 3738-3745.
- Sessler, J. L.; Mody, T. D.; Ramasamy, R.; Sherry, A. D. *New J. Chem.* **1992**, *16*, 541-544.
- Sessler, J. L.; Dow, W. C.; O'Connor, D.; Harriman, A.; Hemmi, G. W.; Mody, T. D.; Miller, R. A.; Qing, F.; Springs, S.; Woodburn, K. *J. Alloys and Compounds* **1997**, *249*, 146-152.
- Harriman, A.; Majya, B. G.; Murai, T. D.; Hemmi, G. W.; Sessler, J. L.; Mallouk, T. E. *J. Chem. Soc., Chem. Commun.* **1989**, 314-316.
- Hemmi, G. W. *Dissertation (Ph.D.)*, The University of Texas at Austin **1992**, 41-43.
- Baxter, G. F. *Chem. Ber.* **1992**, *28*, 445-448.
- Kozak, R. W.; Waldmann, T. A.; Atcher, R. W.; Gansow, O. A. *Trends Biotechnol.* **1985**, *4*, 259-264.
- Kumar, K.; Magerstädt, M.; Gansow, O. A. *J. Am. Chem. Soc., Chem. Commun.* **1989**, 145-146.
- Hancock, R. D.; Cukrowski, I.; Baloyi, J.; Mashishi, J. *J. Chem. Soc., Dalton Trans.* **1993**, 2895-2899.
- Luckay, R.; Reibenspies, J. H.; Hancock, R. D. *J. Chem. Soc., Chem. Commun.* **1995**, 2365-2366.

- Hancock, R. D.; Maumela, H.; de Sousa, A. S. *Coord. Chem. Rev.* **1996**, *148*, 315-347.
- Wullens, H.; Devillers, M.; Tinant, B.; Declercq, J.-P. *J. Chem. Soc., Dalton Trans.* **1996**, 2023-2029.
- Brechbiel, M. W.; Pippin, C. G.; McMurry, T. J.; Milenic, D.; Roselli, M.; Colcher, D.; Gansow, O. A. *J. Chem. Soc., Chem. Commun.* **1991**, 1169-1170.
- Treibs, A. *Justus Liebigs Ann. Chem.* **1969**, *728*, 115-148.
- Buchler, J. W.; Lay, K. L. *Inorg. Nucl. Chem. Lett.* **1974**, *10*, 297-300.
- Barbour, J.; Belcher, W. J.; Brothers, P. J.; Rickard, C. E. F.; Ware, D. C. *Inorg. Chem.* **1992**, *31*, 746-754.
- Michaudet, L.; Fasseur, D.; Guilard, R.; Ou, Z.; Kadish, K. M.; Dahoui, S.; Lecomte, C. *J. Porphyrins Phthalocyanins* **2000**, *4*, 261-270.
- Chacko, G.-P.; Hambright, P. *Inorg. Chem.* **1994**, *33*, 5595-5597.
- Boitrel, B.; Breede, M.; Brothers, P. J.; Hodgson, M.; Michaudet, L.; Rickard, C. E. F.; Al Salim, N. *Dalton Trans.* **2003**, 1803-1807.
- Halime, Z.; Lachkar, M.; Furet, E.; Halet, J.-F.; Boitrel, B. *Inorg. Chem.* **2006**, *45*, 10661-10669.
- Halime, Z.; Lachkar, M.; Roisnel, R.; Furet, E.; Halet, J.-F.; Boitrel, B. *Angew. Chem. Int. Ed.* **2007**, *46*, 5120-5124. *46*, 5120-5124.
- Barkigia, K. M.; Fajer, J.; Adler, A. D.; Williams, G. J. B. *Inorg. Chem.* **1980**, *19*, 2057-2061.
- Sayer, P.; Gouterman, M.; Connell, C. R. *Acc. Chem. Res.* **1982**, *15*, 73-79.
- Arambula, J. F.; Sessler, J. L.; Fountain, M. E.; Wei, W.; Magda, D.; Siddik, Z. H. *Dalton Trans.* **2009**, *48*, 10834–10840.

- Magda, D.; Sessler, J. L.; Gerasimchuk, N.; Miller, R. A. In *Medicinal Inorganic Chemistry*, Sessler, J. L.; Doctrow, S.; McMurry, T.; Lippard, S. J. Eds. American Chemical Society Symposium Series 903, Oxford University Press, **2005**.
- Evens, A. M.; Lecane, P.; Magda, D.; Prachand, S.; Singhal, S.; Nelson, J.; Miller, R. A.; Gartenhaus, R. B.; Gordon, L. I. *Blood*, **2005**, *105*, 1265–1273.
- Lauffer, R. E. *Chem. Rev.* **1987**, *87*, 901-927.
- Na, H. B.; Song, I. C.; Hyeon, T. *Adv. Mater.* **2009**, *21*, 2133-2148.
- Arbab, A. S.; Liu, W.; Frank, J. A. *Expert Rev. Med. Devices* **2006**, *3*, 427-439.
- Jun, Y.-w.; Lee, J.-H.; Cheon, J. *Angew. Chem., Int. Ed.* **2008**, *47*, 5122-5135.
- Caravan, P. *Chem. Soc. Rev.* **2006**, *35*, 512-523.
- Bulte, D. L.; Kraitchman, W. M. *NMR Biomed.* **2004**, *17*, 484-499.
- Massoud, T. F.; Gambhir, S. S. *Gene. Dev.* **2003**, *17*, 545-580
- Nahrendorf, M.; Zhang, H.; Hembrador, S.; Panizzi, P.; Sosnovik, D. E.; Aikawa, E.; Libby, P.; Swirski, F. K.; Weissleder, R. *Circulation* **2008**, *117*, 379-387.
- Cheon, J.; Lee, J.-H. *Acc. Chem. Res.* **2008**, *41*, 1630-1640.
- Gao, J. H.; Gu, H. W.; Xu, B. *Acc. Chem. Res.* **2009**, *42*, 1097-1107.
- Mosley, M.; Donnan, G. *Stroke* **2004**, *35*, 2632-2634.
- Choi, J.-s.; Lee, J.-H.; Shin, T.-H.; Song, H.-T.; Kim, E. Y.; Cheon, J. *J. Am. Chem. Soc.* **2010**, *132*, 11015-11017.
- Raison, C. L.; Miller, A. H. *Mol. Psychiatry* **2012**, 1–23, *and references therein*.
- Kluger, M. J. In *Fever: Its Biology, Evolution, and Function*, Princeton University Press, Princeton **1979**.
- Su, Y.; Wei, X.; Peng, F.; Zhong, Y.; Lu, Y.; Su, S.; Xu, T.; Lee, S.-T.; He, Y. *Nano Lett.* **2012**, *12*, 1845-1850.

- Barreto, J. A.; O'Malley, W.; Kubeil, M.; Graham, B.; Stephan, H.; Spiccia, L. *Adv. Mater*. **2011**, *23*, H18-H40.
- Kuo, W.-S.; Chang, C.-N.; Chang, Y.-T.; Yang, M.-H.; Chien, Y.-H.; Chen, S.-J.; Yeh, C.-S. *Angew. Chem., Int. Ed*. **2010**, *49*, 2711-2715.
- Hu, K.-W.; Liu, T.-M.; Chung, K.-Y.; Huang, K.-S.; Hsieh, C.-T.; Sun, C.-K.; Yeh, C.-S. *J. Am. Chem. Soc*. **2009**, *131*, 14186-14187.
- Fortin, J.-P.; Wilhelm, C.; Servais, J.; Ménager, C.; Bacri, J.-C.; Gazeau, F. *J. Am. Chem. Soc*. **2007**, *129*, 2628-2635.
- Hiraoka, M.; Nagata, Y.; Mitsumori, M.; Sakamoto, M.; Masunaga, S. *AIP Conf. Proc*. **2004**, *716*, 102-105.
- Ito, A.; Shinkai, M.; Honda, H.; Kobayashi, T. *J. Biosci. Bioeng*. **2005**, *100*, 1-11.
- Colombo, M.; Carregal-Romero, S.; Casula, M. F.; Gutiérrez, L.; Morales, M. P.; Böhm, I. B.; Heverhagen, J. T.; Prosperi, D.; Parak, W. *J. Chem. Soc. Rev*. **2012**, *41*, 4306-4334.
- Noh, S.-h.; Na, W.; Jang, J.-t.; Lee, J.-H.; Lee, E. J.; Moon, S. H.; Lim, Y.; Shin, J.-S.; Cheon, *J. Nano Lett*. **2012**, *12*, 3716-3721.
- Bae, K. H.; Park, M.; Do, M. J.; Lee, N.; Ryu, J. H.; Kim, G. W.; Kim, C.; Park, T. G.; Hyeon, T. *ACS Nano* **2012**, *6*, 5266-5273.
- Guardia, P.; Di Corato, R.; Lartigue, L.; Wilhelm, C.; Espinosa, A.; Garcia-Hernandez, M.; Gazeau, F.; Manna, L.; Pellegrino, T. *ACS Nano* **2012**, *6*, 3080-3091.
- Lartigue, L.; Innocenti, C.; Kalaivani, T.; Awwad, A.; del Mar Sanchez Duque, M.; Guari, Y.; Larionova, J.; Guerin, C.; Montero, J.-L. G.; Barragan-Montero, V.; Arosio, P.; Lascialfari, A.; Gatteschi, D.; Sangregorio, C. *J. Am. Chem. Soc*. **2011**, *133*, 10459-10472.

- Lee, J.-H.; Jang, J.-t.; Choi, J.-s.; Moon, S. H.; Noh, S.-h.; Kim, J.-w.; Kim, J.-G.; Kim, I. S.; Park, K. I.; Cheon, *J. Nature Nanotechnol*. **2011**, *6*, 418-422.
- Ho, D.; Sun, X.-L.; Sun, S.-H. *Acc. Chem. Res*. **2011**, *44*, 875-882.
- Yoo, D.; Lee, J.-H.; Shin, T.-H.; Cheon, J. *Acc. Chem. Res*. **2011**, *44*, 863-874.
- Cole, A. J.; Yang, V. C.; David, A. E. *Trends Biotechnol*. **2011**, *29*, 323-332.
- Riehemann, K.; Schneider, S. W.; Luger, T. A.; Godin, B.; Ferraro, M.; Fuchs, H. *Angew. Chem., Int. Ed*. **2009**, *48*, 872-897.
- Shi, D.; Cho, H. S.; Chen, Y.; Xu, H.; Gu, H.; Lian, J.; Wang, W.; Liu, G.; Huth, C.; Wang, L.; Ewing, R. C.; Budko, S.; Pauletti, G. M.; Dong, Z. *Adv. Mater*. **2009**, *21*, 2170-2173.
- Sonvico, F.; Mornet, S.; Vasseur, S.; Dubernet, C.; Jaillard, D.; Degrouard, J.; Hoebeke, J.; Duguet, E.; Colombo, P.; Couvreur, P. *Bioconjugate Chem*. **2005**, *16*, 1181-1188.
- O'Neill, K. L.; Fairbairn, D. W.; Smith, M. J.; Poe, B. S. *Apoptosis* **1998**, *3*, 369-375.
- Harmon, B. V.; Corder, A. M.; Collins, R. J.; Gobé, G. C.; Allen, J.; Allan, D. J. Kerr, J. F. R. *Int. J. Radiat. Biol*. **1990**, *58*, 845-858.
- Kanduc, D.; Mittelman, A.; Serpico, R.; Sinigaglia, E.; Sinha, A. A.; Natale, C.; Santaroce, R.; Di Corcia, M. G.; Lucchese, A.; Dini, L.; Pani, P.; Santacroce, S.; Simone, S.; Bucci, R.; Farber, E. *Int. J. Oncol*. **2002**, *21*, 165-170.
- Golstein, P.; Kroemer, G. *Trends Biochem. Sci*. **2007**, *32*, 37-43.
- Bonfil, R. D.; Bustuoabad, O. D.; Ruggiero, R. A.; Meiss, R. P.; Pasqualini, C. D. *Clin. Expl. Metastasis* **1998**, *6*, 121-129.
- Beckham, J. T.; Wilmink, G. J.; Opalenik, S. R.; Mackanos, M. A.; Abraham, A. A.; Takahashi, K.; Contag, C. H.; Takahashi, T.; Jansen, E. D. *Laser Surg. Med*. **2010**, *42*, 752-765.

- Huang, L.; Mivechi, N. F.; Moskophidis, D. *Mol. Cell. Biol.* **2001**, *21*, 8575-8591.
- Nollen, E. A. A.; Brunsting, J. F.; Roelofsen, H.; Weber, L. A.; Kampinga, H. H. *Mol. Cell. Biol.* **1999**, *19*, 2069-2079.
- Van der Zee, J. *Ann. Oncol.* **2002**, *13*, 1173-1184.
- Fajardo, L. F. *Cancer Res.* **1984**, *44*, 4826-4835.
- Wei, W.-H.; Fountain, M.; Magda, D.; Wang, Z.; Lecane, P.; Mesfin, M.; Miles, D.; Sessler, J. L. *Org. Biomol. Chem.* **2005**, *3*, 3290-3296.
- Wondrak, G. T. *Antioxid. Redox Signaling* **2009**, *11*, 3013–3069.
- Yokoyama, M. J. *Exp. Clin. Med.* **2011**, *3*, 151-158.
- Oerlemans, C.; Bult, W.; Bos, M.; Storm, G.; Nijsen, J. F. W.; Hennik, W. E. *Pharm. Res.* **2010**, *27*, 2569-2589.
- Kedar, U.; Phutane, P.; Shidhaye, S.; Kadm, V. *Nanomed.: Nanotech., Biology and Medicine* **2010**, *6*, 714-729.
- Kim, S.; Shi, Y.; Kim, J. Y.; Chen, K. P. & J.-X. *Expert Opin. Drug Deliv.* **2010**, *7*, 49-62.
- Shiraishi, K.; Kawano, K.; Maitani, Y.; Yokoyama, M. *J. Controlled Release* **2010**, *148*, 160-167.
- Li, J.; Huo, M.; Wang, J.; Zhou, J.; Mohammad, J. M. Zhang, Y.; Zhu, Q.; Waddad, Z. Y.; Zhang, Q. *Biomaterials* **2012**, *33*, 2310-2320.
- Lee, H.; Hoang, B. Fonge, H.; Reilly, R.; Allen, C. *Pharmaceutical Research* **2010**, *27*, 2343-2355.
- Kim, T.; Chen, Y.; Mount, C.; Gambotz, W.; Li, X.; Pun, S. *Pharm. Res.* **2010**, *27*, 1900-1913.
- Jia, Z.; Wong, L.; Davis, T. P.; Bulmus, V. *Biomacromolecules* **2008**, *9*, 3106-3113.

- Yang, X.; Grailer, J. J.; Pilla, S.; Steebe, D. A.; Dong, S. *Bioconjugate Chem*. **2010**, *21*, 496-504.
- Li, Y.; Xiao, W.; Xiao, K.; Berti, L.; Luo, J.; Tseng, H. P.; Fung, G.; Lam, K. S. *Angew. Chem., Int. Ed*. **2012**, *51*, 2864-2869.
- Cannan, R. K.; Kibrick, A. *J. Am. Chem. Soc*. **1938**, *60*, 2314-2320.
- Rios-Doria, J.; Carie, A.; Costich, T.; Burke, B.; Skaff, H.; Panicucci, R.; Sill, K. *J. Drug Delivery* **2012**, Article ID 951741, 1-8.
- Sun, T.-M.; Du, J.-Z.; Yao, Y.-D.; Mao, C. Q.; Dou, S.; Huang, S. Y.; Zhang, P. Z.; Leong, K. W.; Song, E. W.; Wang, J. *ACS Nano* **2011**, *5*, 1483-1494.
- Koo, H.; Huh, M.; Sun, I.-C.; Yuk, S. H.; Choi, K.; Kim, K.; Kwon, I. C. *Acc. Chem. Res*. **2011**, *44*, 1018-1028.
- Tang, N.; Dy, G.; Wang, N.; Liu, C.; Hang, H.; Liang, W. J. *Natl. Cancer Inst*. **2007**, *99*, 1004-1015.
- Christina, A.; Massey, K. A.; Schnitzer, J. E. *Interdisciplinary Reviews: Nanomedicine and Nanobiotechnology* **2011**, *3*, 421-437.
- Kessinger, C.; Khemtong, C.; Togao, O.; Tajahashi, M.; Sumer, B.; Gao, J. *Experim. Biol. Med*. **2010**, *235*, 957-965.
- Poon, Z.; Lee, J.; Huang, S.; Prevost, R.; Hammond, P. *Nanomedicine* **2010**, *7*, 201-209.
- Lee, H.; Fonge, H.; Hoang, B.; Reilly, R.; Allen, C. *Mol. Pharm*. **2010**, *7*, 1195-1208.
- Hu, J.; Qian, Y.; Wang, X.; Liu, W.; Liu, S. *Langmuir* **2012**, *28*, 2073-2082.
- Liu, T.; Liu, X.; Qian, Y.; Hu, X.; Liu, S. *Biomaterials* **2012**, *33*, 2521-2531.
- Xiong, X.-B.; Lavasanifar, A. *ACS Nano* **2011**, *5*, 5202-5213.
- Yang, R.; Meng, F.; Ma, S.; Huang, F.; Liu, H.; Zhong, Z. *Biomacromolecules* **2011**, *12*, 3047-3055.

- Siegrist W.; Solca, F.; Stutz S.; Giuffrè, L.; Carrel, S.; Girard, J.; Eberle, A. N. *Cancer Res*. **1989**, *49*, 6352-6358.
- Cai, M.; Varga, E. V.; Stankova, M.; Mayorov, A.; Perry, J. W.; Yamamura, H. I.; Trivedi, D.; Hruby, V. *J. Chem. Biol. Drug Des*. **2006**, *68*, 183-193.
- Mayorov, A. V.; Han, S. Y.; Cai, M.; Hammer, M. R.; Trivedi, D.; Hruby, V. *J. Chem. Biol. Drug Design* **2006**, *67*, 329-335.
- Koikov, L. N.; Ebertino, F. H.; Solinsky, M. G. *Bioorg. Med. Chem. Lett*. **2003**, *13*, 2647-2650.
- Chen, J.; Giblin, M. F.; Wang, N.; Jurisson, S. S.; Quinn, T. P. *Nucl. Med. Biol*. **1999**, *26*, 687-693.
- Sawyer, T.; Sanfilippo, P.; Hruby, V.; Engel, M. H.; Heward, C. B.; Burnett, J. B.; Hadley, M. E. *Procl. Natl. Acad. Sci*. USA **1980**, *77*, 5754-5758.
- Chen, J.; Cheng, Z.; Hoffman, T. J.; Jurisson, S. S.; Quinn, T. P. *Cancer Res*. **2000**, *60*, 5649-5658.
- Cai, M.; Mayorov, A. V.; Cabello, C.; Stankova, M.; Trivedi, D.; Hruby, V. J. *J. Med. Chem*. **2005**, *48*, 1839-1848.
- Handl, H. L.; Vagner, J.; Yamamura, H. I.; Hruby, V. J.; Gillies, R. *J. Anal. Biochem*. **2004**, *330*, 242-250.
- Yang, Y.; Hruby, V. J.; Chen, M.; Crasto, C.; Cai, M.; Harmon, C. M. *Biochemistry* **2009**, *48*, 9775-9784.
- Rodrigues, A. R.; Pignatelli, D.; Almeida, H.; Gouveiaa, A. M. *J. Mol. Cell. Endocrinol*. **2009**, *303*, 74-81.
- Webb, T. R.; Clark, A. J. L. *J. Mol. Endocrinol*. **2009**, *24*, 475-484.
- Van der Ploeg, L. H. T.; Martin, W. J.; Howard, A. D.; Nargund, R. P.; Austin, C. P.; Guan, X.; Drisko, J.; Cashen, D.; Sebhat, I.; Patchett, A. A.; Figueroa, D. J.; DiLella,

A. G.; Connolly, B. M.; Weinberg, D. H.; Tan, C. P.; Palysha, O. C.; Pong, S.-S.; MacNeil, T.; Rosenblum, C.; Vongs, A.; Tang, R.; Yu, H.; Sailer, A. W.; Fong, T. M.; Huang, C.; Tota, M. R.; Chang, R. S.; Stearns, R.; Tamvakopoulos, C.; Christ, G.; Drazen, D. L.; Spar, B. D.; Nelson, R. J.; MacIntyre, D. E. *PNAS* **2002**, *99*, 11381-11386.

- Hall, J. E.; da Silva, A. A.; do Carmo, J. M.; Dubinion, J.; Hamza, S.; Munusmy, S.; Smith, G.; Stec, D. E. *J. Biol. Chem.* **2010**, *285*, 17271-17276.
- Jun, D.-J.; Na, K.-Y.; Kim, W.; Kwak, D.; Kwon, E. J.; Yoon, J. H.; Yea, K.; Lee, H.; Kim, J.; Suh, P. G.; Ryu, S. H.; Kim, K. T. *J. Mol. Endocrinol.* **2010**, *44*, 225-236.
- Barkey, N. M.; Tafreshi, N. K.; Josan, J. S.; De Silva, C. R.; Sill, K. N.; Hruby, V. J.; Gillies, R. J.; Morse, D. L.; Vagner, J. *J. Med. Chem.* **2011**, *54*, 8078-8084.
- Ehrlich, J.; Bogert, M. T. *J. Org. Chem.* **1947**, *12*, 522-534.
- Sessler J. L.; Weghorn, S. J. In *Expanded, Contracted & Isomeric Porphyrins*, Elsevier Oxford, **1997**, Vol. 15.
- Bauer, V. J.; Clive, D. L. J.; Dolphin, D.; Paine III, J. B.; Harris, F. L.; King, M. M.; Loder, J.; Wang, S.-W. C.; Woodward, R. B. *J. Am. Chem. Soc.* **1983**, *105*, 6429-6436.
- Burell, A. K.; Sessler, J. L.; Cyr, M. J.; McGhee, E.; Ibers, J. A. *Angew. Chem. Int. Ed. Eng.* **1991**, *30*, 91-93.
- Sessler, J. L.; Gebauer, A.; Hoehner, M. C.; Lynch, V. *Chem. Commun.* **1998**, *17*, 1835-1836.
- Yan, Y. K.; Melchart, M.; Habtemariam, A.; Sadler, P. J. *Chem. Commun.* **2005**, *38*, 4764-4776.
- Ang, W. H.; Dyson, P. J. *Eur. J. Inorg. Chem.* **2006**, *20*, 4003-4018.

- Hartinger, C. G.; Zorbas-Seifried, S.; Jakupec, M. A.; Kynast, B.; Zorbas, H.; Kepper, B. K. *J. Inorg. Biochem.* **2006**, *100*, 891-904.
- Barton, J. K.; Danishefsky, A.; Goldberg, J. *J. Am. Chem. Soc.* **1984**, *106*, 2172-2176.
- Lincoln, P.; Nordén, B. *J. Phys. Chem. B* **1998**, *102*, 9583-9594.
- Hiort, C.; Linoln, P.; Nordén, B. *J. Am. Chem. Soc.* **1993**, *115*, 3448-3454.
- Nordell, P.; Westerlund, F.; Wilhelmsson, L. M.; Nordén, B.; Lincoln, P. *Angew. Chem. Int. Ed.* **2007**, *46*, 2203-2206.
- Chen, T. F.; Liu, Y. N.; Zheng, W. J.; Liu, J.; Wong, Y. S. Inorg. Chem. 2010, 49, 6366-6368.
- Sessler, J. L.; Cyr, M. J.; Lynch, V. M.; McGhee, E.; Ibers, J. A. *J. Am. Chem. Soc.* 1990, **112**, 2810-2813.
- Lash, T. D.; Lin, Y.; Novak, B. H.; Parikh, M. D. *Tetrahedron* **2005**, *61*, 11601-11614.
- Cyr, M. J., Ph.D. Dissertation, The University of Texas at Austin, 1991.
- Smith, G. F.; Cagle, F. Wm. *J. Org. Chem.* **1947**, *12*, 781-784.
- Schmuck, C.; Rupprecht, D.; Urban, C.; Walden, N. *Synthesis* **2006**, *1*, 89-96.
- Lightner, D. A.; McDonagh, A. F. *Acc. Chem. Res.* **1984**, *17*, 417-424.
- Smith, K. M.; Pandey, R. K. *J. Heterocycl. Chem.* **1983**, *20*, 1383-1388.
- Johnson, A. W.; Kay, I. T.; Markham, E.; Price, R.; Shaw, K. B. *J. Chem. Soc.* **1959**, 3416-3424.
- Sullivan, B. P.; Salmon, D. J.; Meyer, T. J. *Inorg. Chem.* **1978**, *17*, 3334-3341.
- Lim, J. M.; Yoon, Z. S.; Shin, J.-Y.; Kim, K. S.; Yoon, M.-C.; Kim, D. *Chem. Commun.* **2009**, 261-273.
- Yoon, Z. S.; Cho, D.-G.; Kim, K. S.; Sessler, J. L.; Kim, D. *J. Am. Chem. Soc.* **2008**, *130*, 6930-6931.
- Mori, S.; Osuka, A. *J. Am. Chem. Soc.* **2005**, *127*, 8030-8031.

- Cho, S.; Yoon, Z. S.; Kim, K. S.; Yoon, M.-C.; Cho, D.-G.; Sessler, J. L.; Kim, D. *J. Phys. Chem. Lett.* **2010**, 1, 895-900.
- Sessler, J. L.; Weghorn, S. J.; Morishima, T.; Rosingana, M.; Lynch, V.; Lee, V. *J. Am. Chem. Soc.* **1992**, *114*, 8306-8307.
- Sessler, J. L.; Weghorn, S. J.; Morishima, T.; Rosingana, M.; Lynch, V.; Lee, V. *J. Am. Chem. Soc.* **1992**, *114*, 8306-8307.
- Setsune, J.; Katakami, Y.; Iizuka, N. *J. Am. Chem. Soc.* **1999**, *121*, 8957-8958.
- Panda, P. K.; Kang, Y.-J.; Lee, C.-H. *Angew. Chem. Int. Ed.* **2005**, *44*, 4053-4055.
- Kobe, K.; Herman, L. *J. Ind. Eng. Chem.* **1950**, *42*, 352-356.
- Berlin, A.; Bradamante, S.; Ferraccioli, R.; Pagani, G. A.; Sannicolò, F. *J. Chem. Soc., Chem. Commun.* **1987**, *15*, 1176-1177.
- Yoon, M.-C.; Cho, S.; Suzuki, M.; Osuka, A.; Kim, D. *J. Am. Chem. Soc.* **2009**, *131*, 7360-7367.
- Yoon, Z. S.; Kwon, J. H.; Yoon, M.-C.; Koh, M. K.; Noh, S. B.; Sesler, J. L.; Lee, J. T.; Seidel, D.; Aguilar, A.; Shimizu, S.; Suzuki, M.; Osuka, A.; Kim, D. *J. Am. Chem. Soc.* **2006**, *128*, 14128-14134.
- Mori, S.; Kim, K.. S.; Yoon, Z. S.; Noh, S. B.; Kim, D.; Osuka, A. *J. Am. Chem. Soc.* **2007**, *129*, 11344-11345.
- Sessler, J. L.; Seidel, D. *Angew. Chem. Int. Ed.* **2003**, *42*, 5134-5175.
- Saito, S.; Osuka, A. *Angew. Chem. Int. Ed.* **2011**, *50*, 4342-4373.
- Osuka, A.; Saito, S. *Chem. Commun.*, **2011**, *47*, 4330-4339; and the references therein.
- Hannah, S.; Lynch, V.; Guldi, D. M.; Gerasimchuk, N.; Mac Donald, C. L. B.; Magda, D.; Sessler, J. L. *J. Am. Chem. Soc.* **2002**, *124*, 8416-8427.
- Sessler, J. L.; Hemmi, G. H.; Mody, T. D. *PCT Int. Appl.* **1993**, WO 9314093 A1 19939722.

- Sessler, J. L.; Mody, T. D.; Hemmi, G. W.; Kral, V. *U.S.* **1995**, US5457183 A 19951010.
- Mosmann, T. J. *Immunol. Methods* **1983**, *65*, 55-63.
- Lee, J.-H.; Huh, Y.-M.; Jun, Y.-w.; Seo, J.-w.; Jang, J.-t.; Song, H.-T.; Kim, S.; Cho, E.-J.; Yoon, H.-G.; Suh, J.-S.; Cheon, J. *Nature Medicine* **2007**, *13*, 95–99.
- Yi, D. K.; Lee, S. S.; Papaefthymiou, G. C.; Ying, J. Y. *Chem. Mater.* **2006**, *18*, 614–619.
- *CrystalClear Version 1.40* **2008**, Rigaku Americas Corportion, The Woodlands, TX, USA.
- *SIR97* **1999**, A program for crystal structure solution. Altomare, A.; Burla, M.C.; Camalli, M.; Cascarano, G.L.; Giacovazzo, C.; Guagliardi, A.; Moliterni, A. G. G.; Polidori, G.; Spagna, R. *J. Appl. Cryst.* **1999**, *32*, 115-119.
- Sheldrick, G. M. *SHELXL97* **1994**, Program for the Refinement of Crystal Structures, University of Göttingen, Germany.
- In *International Tables for X-ray Crystallography* **1992**, Vol. C, Tables 4.2.6.8 and 6.1.1.4, A. J. C. Wilson, editor, Boston: Kluwer Academic Press.
- Sheldrick, G. M., *SHELXTL/PC* (Version 5.03) **1994**, Siemens Analytical X-ray Instruments, Inc., Madison, Wisconsin, USA.
- Sluis, P. v. d.; Spek, A. L. *Acta Cryst.* **1990**, *A46*, 194-201.